

**SCDAP/RELAP5 Thermal-Hydraulic
Evaluations of the Potential for
Containment Bypass During
Extended Station Blackout
Severe Accident Sequences in a
Westinghouse Four-Loop PWR**

**AVAILABILITY OF REFERENCE MATERIALS
IN NRC PUBLICATIONS**

NRC Reference Material

As of November 1999, you may electronically access NUREG-series publications and other NRC records at NRC's Public Electronic Reading Room at <http://www.nrc.gov/reading-rm.html>. Publicly released records include, to name a few, NUREG-series publications; *Federal Register* notices; applicant, licensee, and vendor documents and correspondence; NRC correspondence and internal memoranda; bulletins and information notices; inspection and investigative reports; licensee event reports; and Commission papers and their attachments.

NRC publications in the NUREG series, NRC regulations, and *Title 10, Energy*, in the Code of *Federal Regulations* may also be purchased from one of these two sources.

1. The Superintendent of Documents
U.S. Government Printing Office
Mail Stop SSOP
Washington, DC 20402-0001
Internet: bookstore.gpo.gov
Telephone: 202-512-1800
Fax: 202-512-2250
2. The National Technical Information Service
Springfield, VA 22161-0002
www.ntis.gov
1-800-553-6847 or, locally, 703-605-6000

A single copy of each NRC draft report for comment is available free, to the extent of supply, upon written request as follows:

Address: Office of Administration
Reproduction and Mail Services Branch
U.S. Nuclear Regulatory Commission
Washington, DC 20555-0001

E-mail: DISTRIBUTION@nrc.gov
Facsimile: 301-415-2289

Some publications in the NUREG series that are posted at NRC's Web site address <http://www.nrc.gov/reading-rm/doc-collections/nuregs> are updated periodically and may differ from the last printed version. Although references to material found on a Web site bear the date the material was accessed, the material available on the date cited may subsequently be removed from the site.

Non-NRC Reference Material

Documents available from public and special technical libraries include all open literature items, such as books, journal articles, and transactions, *Federal Register* notices, Federal and State legislation, and congressional reports. Such documents as theses, dissertations, foreign reports and translations, and non-NRC conference proceedings may be purchased from their sponsoring organization.

Copies of industry codes and standards used in a substantive manner in the NRC regulatory process are maintained at—

The NRC Technical Library
Two White Flint North
11545 Rockville Pike
Rockville, MD 20852-2738

These standards are available in the library for reference use by the public. Codes and standards are usually copyrighted and may be purchased from the originating organization or, if they are American National Standards, from—

American National Standards Institute
11 West 42nd Street
New York, NY 10036-8002
www.ansi.org
212-642-4900

Legally binding regulatory requirements are stated only in laws; NRC regulations; licenses, including technical specifications; or orders, not in NUREG-series publications. The views expressed in contractor-prepared publications in this series are not necessarily those of the NRC.

The NUREG series comprises (1) technical and administrative reports and books prepared by the staff (NUREG-XXXX) or agency contractors (NUREG/CR-XXXX), (2) proceedings of conferences (NUREG/CP-XXXX), (3) reports resulting from international agreements (NUREG/IA-XXXX), (4) brochures (NUREG/BR-XXXX), and (5) compilations of legal decisions and orders of the Commission and Atomic and Safety Licensing Boards and of Directors' decisions under Section 2.206 of NRC's regulations (NUREG-0750).

DISCLAIMER: This report was prepared as an account of work sponsored by an agency of the U.S. Government. Neither the U.S. Government nor any agency thereof, nor any employee, makes any warranty, expressed or implied, or assumes any legal liability or responsibility for any third party's use, or the results of such use, of any information, apparatus, product, or process disclosed in this publication, or represents that its use by such third party would not infringe privately owned rights.



United States Nuclear Regulatory Commission

Protecting People and the Environment

NUREG/CR-6995

SCDAP/RELAP5 Thermal-Hydraulic Evaluations of the Potential for Containment Bypass During Extended Station Blackout Severe Accident Sequences in a Westinghouse Four-Loop PWR

Manuscript Completed: February 2010

Date Published: March 2010

Prepared by

C.D. Fletcher, R.M. Beaton, V. V. Palazov, and D.L. Caraher

R.W. Shumway (Consultant)

Information Systems Laboratories, Inc.

10070 Barnes Canyon Road

San Diego, CA 92121

C. Boyd, NRC Point of Contact

NRC Job Code Y6198

Office of Nuclear Regulatory Research

ABSTRACT

The U.S. Nuclear Regulatory Commission has been conducting studies to evaluate the risk associated with steam generator tube failure during low probability severe accidents in pressurized-water reactors (PWRs) employing U-tube-type steam generators as part of the agency's Steam Generator Action Plan (ML 011300073). The evaluations focus on station blackout events that include a series of unlikely events and conditions that result in a "high-dry-low" plant condition. The high-dry-low condition refers to high primary side pressure along with a dried-out steam generator that is at low pressure. Failures of hot leg piping, pressurizer surge-line piping, and the reactor vessel lead to discharge of fission products into the containment. Failure of steam generator tubes prior to the failure of one of these other components leads to discharge of some fission products into the steam generator secondary system from where they may be discharged to the environment through the pressure-relief valves. This latter sequence is potentially more risk-significant since it involves a containment bypass scenario. The relative timing of these structural failures therefore affects the event sequence and whether the containment is bypassed.

This report summarizes thermal-hydraulic evaluations performed using the SCDAP/RELAP5 systems analysis code and a model representing a Westinghouse four-loop PWR. An assessment is made of the SCDAP/RELAP5 capabilities for predicting the phenomena and behavior important for this application. The plant model has benefitted from (1) extensive iterative comparisons with evaluations of natural circulation flows and turbulent mixing using a computational fluid dynamics code and (2) from comparison with experimental data for pertinent fluid-mixing behavior. This report documents the recent history of SCDAP/RELAP5 model improvements for this application, numerous sensitivity evaluations, estimates of the uncertainties in the calculated results, analyses of extended station blackout accident event sequences in a Westinghouse four-loop PWR, and a categorization of those event sequences based on containment bypass outcome.

FOREWORD

Steam generator tubes comprise a majority of the reactor coolant system pressure boundary and therefore their integrity is important to ensuring safe operation of the plants. During November 2000, after the Indian Point 2 steam generator leakage event, NRC developed a Steam Generator Action Plan (ML 011300073) to consolidate activities related to steam generators and to ensure that issues are appropriately tracked and resolved. In May 2001, this plan was revised to address a differing professional opinion on steam generator tube integrity. This plan is one facet of NRC's strategy to maintain safe operation of nuclear power plants and to increase public confidence in agency regulatory actions.

One aspect of the Steam Generator Action Plan is the analysis of the risk of low probability severe accident-induced tube failures. Tube failure during a severe accident has the potential for radioactive release that bypasses containment. An important aspect of this analysis is the prediction of the thermal-hydraulic response of the reactor coolant system during postulated severe accident conditions as well as the prediction of the thermal-hydraulic loads that challenge specific reactor coolant system (RCS) components. This report describes the completion of a series of analyses involving hypothetical station blackout event sequences that lead to severe accidents.

The sequences are set up by assuming multiple concurrent failures of systems and components. These assumptions are selected to cover the range of "high-dry-low" conditions (which refer to high reactor coolant system pressure and dry steam generators at low pressure) that challenge the integrity of the steam generator tubes. The analyses do not represent best-estimate plant behavior, nor do the results indicate the most-likely outcomes of the event sequences because several systems or operator actions can eliminate one or more of the high, dry, or low conditions. For example, high reactor coolant pump shaft seal leakage rates can eliminate the high reactor coolant system pressure condition, operation of the turbine-driven auxiliary feedwater system can eliminate the dry steam generator condition, and maintenance of the steam generator secondary pressure boundary can eliminate the low steam generator pressure condition. Considerations such as these are ultimately accounted for in an integrated probabilistic risk assessment of severe accident-induced steam generator tube failures currently being performed by the Office of Nuclear Regulatory Research, Division of Risk Analysis.

The predictions provide a screening tool for the potential of severe accident induced tube failures and some conservatism is applied to ensure that potential scenarios are considered. The predictions provide valuable insights into what variables or factors affect the timing of induced failures for the steam generator tubes as well as other RCS components. In addition to providing a more complete perspective on the potential for consequential steam generator tube rupture, these predictions demonstrate the effectiveness of operator actions and safety systems to reduce or eliminate the risk of induced tube failures.

TABLE OF CONTENTS

ABSTRACT.....	iii
FOREWORD.....	v
EXECUTIVE SUMMARY	xv
ACKNOWLEDGEMENTS	xxi
NOMENCLATURE.....	xxiii
1. INTRODUCTION.....	1
1.1 Objective of This Report.....	3
1.2 Description of a Base Case Station Blackout Accident Scenario.....	3
1.3 Plant Behavior During the Base Case Accident Scenario.....	4
1.4 Definition of SG Tube Failure Margin and Criteria for Judging Occurrence of Containment Bypass	6
1.5 Organization of This Report	7
2. BACKGROUND	9
2.1 NUREG-1570 Analyses, 1998-2000	9
2.2 NUREG-1740 Independent Review and Steam Generator Action Plan, 2000-2001	9
2.3 Revised Station Blackout Base Case Event Sequence and Analysis, 2000-2003.....	11
2.4 Sensitivity Analyses, 2004.....	14
2.5 ACRS Review Meeting, 2004.....	16
2.6 Analyses to Support PRA, 2004-2005.....	17
2.7 NRC and Consultant PIRT Evaluation and Peer Review, 2005	19
2.7.1 Independent Technical Review Issues.....	19
2.7.2 Identification of Dependent Variables for the Uncertainty Evaluation	20
2.7.3 Identification of Independent Variables for the Uncertainty Evaluation	20
2.8 Revised Base Case Calculation and Evaluation of Primary Coolant System Energy Flow, 2006.....	25
2.9 Evaluation of Uncertainties in SCDAP/RELAP5 Simulations, 2006.....	26
2.10 Public Peer Review Meeting, 2007	27
3. DESCRIPTION OF ANALYSIS METHODS	31
3.1 SCDAP/RELAP5 Code Description.....	31
3.2 RELAP5 Assessments Pertinent for the Containment Bypass Application.....	32
3.2.1 Loop Seal Behavior.....	32
3.2.2 Pressurizer Filling, Draining and Relief Valve Behavior.....	37
3.3 SCDAP Assessments Pertinent for the Containment Bypass Application	42
3.3.1 Models for PWR Fuel Assembly Heat-Up Behavior	42
3.3.2 Models for Fuel Rod Cladding Oxidation.....	44
3.3.3 Models for Fuel Rod Ballooning and Rupture	46
3.4 Description of SCDAP/RELAP5 Westinghouse Four-Loop Plant Model, Including Features Benefitting from Supporting CFD Analyses.....	46
4. WESTINGHOUSE FOUR-LOOP PLANT STATION BLACKOUT BASE CASE ANALYSIS.....	57
4.1 Full-Power Steady State Calculation.....	57

4.2	Transient Station Blackout Calculation.....	58
5.	KEY SENSITIVITIES.....	77
5.1	RCP Shaft Seal Leakage Behavior	77
5.1.1	Leakage Rate Increases Due to Seal Failures at 13 Minutes	78
5.1.2	Leakage Rate Increases Due to Seal Failures When RCPs Experience Saturated Fluid Conditions.....	80
5.2	Effect of Variations in Turbine-Driven Auxiliary Feedwater Operation and SG Steam Leakage	80
5.3	Mitigative Operator Intervention	86
5.3.1	Pre-Core Damage Operator Action	86
5.3.2	Post-Core Damage Operator Action	101
5.4	Sensitivity of Results to Assumed Split of SG Tubes into Hot and Cold Sections	103
5.5	Effects Related to Opening SG Tube and HL Rupture Flow Paths.....	103
6.	GROUPING OF EXTENDED SBO EVENT SEQUENCES INTO CONTAINMENT BYPASS, POTENTIAL FOR CONTAINMENT BYPASS, AND NO CONTAINMENT BYPASS CATEGORIES	109
6.1	Categorization of Event Sequences Without Operator Intervention.....	111
6.2	Categorization of Event Sequences with Operator Intervention.....	119
7.	CONCLUSIONS.....	123
8.	REFERENCES.....	127
	APPENDIX A – RESULTS OF 2004 SENSITIVITY ANALYSES	A-1
	APPENDIX B – ANALYSES TO SUPPORT PRA.....	B-1
	APPENDIX C – EVALUATION OF PRIMARY COOLANT SYSTEM ENERGY FLOW	C-1
	APPENDIX D - ESTIMATES OF UNCERTAINTIES IN THE SCDAP/RELAP5 SIMULATIONS	D-1
	APPENDIX E – EFFECT OF MODELING REACTOR VESSEL OUTLET NOZZLE CARBON STEEL SAFE END.....	E-1

LIST OF FIGURES

Figure 1.1	Schematic of Westinghouse Four-Loop Pressurized Water Reactor	2
Figure 1.2	Potential Coolant Loop Natural Circulation Flow Patterns During System Heat-Up	5
Figure 3.1	Steam Emissivity as a Function of Temperature and Optical Depth	35
Figure 3.2	Break Flow for ROSA-IV Test SB-CL-18	35
Figure 3.3	Hot Leg Loop Seal Collapsed Levels for the PMK CAMP-CLB Experiment.....	36
Figure 3.4	Cold Leg Loop Seal Collapsed Levels for the PMK CAMP-CLB Experiment	36
Figure 3.5	Pressurizer Level for MIT ST4 Pressurizer Insurge Experiment	39
Figure 3.6	RCS Pressure for APEX-CE-13 Stuck-Open Pressurizer SRV Experiment.....	39
Figure 3.7	Pressurizer Level for APEX-CE-13 Stuck-Open Pressurizer SRV Experiment	40
Figure 3.8	Pressurizer PORV Flow for MIST 360499 Feed-and-Bleed Cooling Experiment	41
Figure 3.9	RCS Pressure for MIST 360499 Feed-and-Bleed Cooling Experiment.....	41
Figure 3.10	RCS Pressure for LOBI BT-56 Loss-of-Feedwater Experiment	43
Figure 3.11	Pressurizer Surge Line Flow for LOBI BT-56 Loss-of-Feedwater Experiment	43
Figure 3.12	Intact Loop Cold Leg Density for LOBI BT-56 Loss-of-Feedwater Experiment	44
Figure 3.13	Fuel Rod Temperature at the 0.75-m Elevation for CORA-7 Test.....	45
Figure 3.14	Reactor Vessel Nodalization	48
Figure 3.15	Coolant Loop Nodalization Excluding Provisions for Countercurrent Natural Circulation	49
Figure 3.16	Coolant Loop Nodalization With Provisions for Countercurrent Natural Circulation	50
Figure 3.17	Surge Line Connections to the Split Hot Leg During Countercurrent Natural Circulation	51
Figure 4.1	Reactor Coolant System Pressure	60
Figure 4.2	Steam Generator Secondary Pressures.....	60
Figure 4.3	Reactor Coolant Pump Shaft Seal Leakage Flows	61
Figure 4.4	Steam Generator Secondary Liquid Masses.....	61
Figure 4.5	Total Pressurizer PORV Flow.....	62
Figure 4.6	Pressurizer SRV Flow	62
Figure 4.7	Pressurizer Level.....	63
Figure 4.8	Reactor Coolant Pump Loop Seal Void Fractions	63
Figure 4.9	SG 1 Hot and Cold Average Tube Flows	65
Figure 4.10	Hot Leg 1 Upper and Lower Section Flows	65
Figure 4.11	Vessel Circulation Flows	67
Figure 4.12	Hot Leg Discharge Coefficients	67
Figure 4.13	Recirculation Ratios	68
Figure 4.14	Hot Mixing Fractions.....	68
Figure 4.15	Cold Mixing Fractions.....	69
Figure 4.16	SG Power Fractions	69
Figure 4.17	Hydrogen Generation Rate	71
Figure 4.18	Loop 1 Structure Temperatures	71

Figure 4.19	Correspondence Between Loop 1 Structure Temperatures and Failure Times.....	73
Figure 4.20	Hot Leg and Pressurizer Surge Line Creep Rupture Damage Indexes.....	73
Figure 4.21	SG 1 Average Tube and Hot Leg 1 Creep Rupture Damage Indexes	74
Figure 4.22	SG 1 Hottest Tube and Hot Leg 1 Creep Rupture Damage Indexes	74
Figure 5.1	Case 153 SG Secondary Pressures.....	89
Figure 5.2	Case 153 SG Water Masses	90
Figure 5.3	Case 153 RCS Pressure	90
Figure 5.4	Case 153A SG Pressures	92
Figure 5.5	Case 153A SG Water Masses.....	92
Figure 5.6	Case 153A RCS Pressure.....	93
Figure 5.7	Case 161 RCS Pressure	95
Figure 5.8	Case 161 SG Secondary Pressures.....	95
Figure 5.9	Case 161m and Case 161mA HL Vapor Temperatures.....	98
Figure 5.10	Case 161m and Case 161mA RCS Pressures.....	98
Figure 5.11	Case 165m and Case 161m RCS Pressures	99
Figure 5.12	Case 165m and Case 161m SG 2 Pressures	99
Figure 6.1	Map of Containment Bypass Outcome for No Operator Intervention and Variations in SG Steam Leakage and RCP Shaft Seal Leakage Which Increases at 13 Minutes	115
Figure 6.2	Map of Containment Bypass Outcome for No Operator Intervention and Variations in SG Steam Leakage and RCP Shaft Seal Leakage Which Increases When the RCP Fluid Reaches the Saturation Temperature	115
Figure 6.3	Map of Containment Bypass Outcome for No Operator Intervention and Variations in Temporary TDAFW System Operation and RCP Shaft Seal Leakage Which Increases at 13 Minutes.....	118
Figure 6.4	Map of Containment Bypass Outcome for No Operator Intervention and Variations in Temporary TDAFW System Operation and RCP Shaft Seal Leakage Which Increases When the RCP Fluid Reaches the Saturation Temperature	118
Figure 6.5	Map of Containment Bypass Outcome for No Operator Intervention and Variations in Temporary TDAFW System Operation and SG Steam Leakage.....	119
Figure 6.6	Map of Containment Bypass Outcome for Pre-Core Damage Operator Intervention.....	122
Figure 6.7	Map of Containment Bypass Outcome for Post-Core Damage Operator Intervention.....	122
Figure C.1	Control Volume Arrangement for the Energy Balance Analysis	C-2
Figure C.2	Average Total Core Power Generated During the Five Phases of the SBO Accident Heat-Up Period	C-6
Figure C.3	Portion of the Integrated Core Power Retained in the Fuel During the Five Phases of the SBO Accident Heat-Up Period	C-6
Figure C.4	Portion of the Integrated Core Power Transferred to the Core Fluid During the Five Phases of the SBO Accident Heat-Up Period.....	C-7
Figure C.5	Change in Reactor Vessel Fluid Energy During the Five Phases of the SBO Accident Heat-Up Period	C-7
Figure C.6	Change in Pressurizer Fluid Energy During the Five Phases of the SBO Accident Heat-Up Period	C-8
Figure C.7	Change in Fluid Energy in RCS Regions Other Than the Reactor Vessel and Pressurizer During the Five Phases of the SBO Accident Heat-Up Period	C-8

Figure C.8	Integrated Flow of Energy Through the Pressurizer PORVs and Reactor Coolant Pump Shaft Seal Leaks During the Five Phases of the SBO Accident Heat-Up Period	C-9
Figure C.9	Integrated Heat Transfer Rate from SG Tubes to Fluid During the Five Phases of the SBO Accident Heat-Up Period	C-11
Figure C.10	Integrated Heat Transfer Rate from All Structures (Except SG Tubes) to Fluid During the Five Phases of the SBO Accident Heat-Up Period	C-11
Figure D.1	Mass Flow Rates Through One of the Two Pressurizer PORVs for the Relief Valve Flow Area Sensitivity Cases.....	D-18
Figure D.2	RCS Pressures for the Relief Valve Flow Area Sensitivity Cases.....	D-18
Figure D.3	Hot Leg 1 Discharge Coefficient Responses for the Hot Leg Discharge Coefficient Sensitivity Cases	D-20
Figure D.4	Hot Leg 1 Upper Section Flow Rates for the Hot Leg Discharge Coefficient Sensitivity Cases	D-20
Figure D.5	Integrated SG Power Fractions for the Hot Leg Discharge Coefficient Sensitivity Cases	D-21
Figure D.6	Loop 1 Recirculation Ratio Responses for the Recirculation Ratio Sensitivity Cases	D-21
Figure D.7	Loop 1 Integrated SG Power Fractions for the Recirculation Ratio Sensitivity Cases	D-22
Figure D.8	Loop 1 Hot Mixing Fraction Responses for the Mixing Fraction Sensitivity Cases	D-23
Figure D.9	Loop 1 Cold Mixing Fraction Responses for the Mixing Fraction Sensitivity Cases	D-24
Figure D.10	Integrated SG 1 Power Fractions for the Mixing Fraction Sensitivity Cases ...	D-24
Figure D.11	Mass Flow Rates in SG 1 Hot Average Tube for the Tube Split Sensitivity Cases	D-25
Figure D.12	Fluid Velocities in SG 1 Hot Average Tube for the Tube Split Sensitivity Cases	D-25
Figure D.13	SG 1 Hot Average Tube Wall Inside Surface Heat Transfer Coefficients for the Tube Split Sensitivity Cases.....	D-27
Figure D.14	Tube Wall Temperatures in SG 1 Hot Average Tube for the Tube Split Sensitivity Cases	D-27
Figure D.15	SG 1 Hot Average Tube Outer Surface Heat Transfer Coefficients for the Tube Outer Wall Heat Transfer Sensitivity Cases.....	D-28
Figure D.16	SG 1 Hot Average Tube Wall Temperatures for the Tube Outer Wall Heat Transfer Sensitivity Cases.....	D-28
Figure D.17	Fuel Rod Cladding Oxidation Powers for the Oxidation Sensitivity Cases.....	D-30
Figure D.18	Hot Leg 1 Upper Section Fluid Temperatures for the Oxidation Sensitivity Cases	D-30
Figure D.19	Flow Rates at Top of Central Core Region for the Vessel Circulation Sensitivity Cases	D-31
Figure D.20	Total Fuel Rod Cladding Oxidation Power for the Vessel Circulation Sensitivity Cases	D-32
Figure D.21	Hot Leg 1 Upper Section Fluid Temperatures for the Vessel Circulation Sensitivity Cases	D-32
Figure D.22	Hot Leg 1 Upper Section Average Wall Temperatures for the Vessel Circulation Sensitivity Cases	D-33
Figure D.23	Heat Fluxes from Outer Surface of Reactor Vessel to Containment for the RCS Heat Loss Sensitivity Cases	D-34
Figure D.24	Pressurizer Level Responses for the RCS Heat Loss Sensitivity Cases	D-34

Figure D.25	Pump 1 Leakage Rates for the Symmetric Pump Shaft Seal Leak Sensitivity Cases	D-35
Figure D.26	RCS Pressures for the Symmetric Pump Shaft Seal Leak Sensitivity Cases	D-37
Figure D.27	Hot Leg 1 Fluid Temperatures for the Symmetric Pump Shaft Seal Leak Sensitivity Cases	D-37
Figure D.28	Single-Pump Leakage Rates for the Unsymmetrical Pump Shaft Seal Leak Sensitivity Cases	D-38
Figure D.29	RCS Pressures for the Unsymmetrical Pump Shaft Seal Leak Sensitivity Cases	D-38
Figure D.30	Hot Leg 1 Fluid Temperatures for the Unsymmetrical Pump Shaft Seal Leak Sensitivity Cases	D-39
Figure D.31	Pressurizer Surge Line Fluid Temperature for the Top Mounted Surge Line Sensitivity Case	D-41
Figure D.32	SG 1 Pressure for the Stuck-Open SG Safety Relief Valve Sensitivity Case	D-41
Figure D.33	SG 2 Pressure for the Stuck-Open SG Safety Relief Valve Sensitivity Case	D-42
Figure D.34	Hot Leg 1 Fluid Temperature for the Stuck-Open SG Safety Relief Valve Sensitivity Case	D-42
Figure D.35	SG Secondary Pressures for the SG Secondary Leakage Sensitivity Cases	D-44
Figure D.36	Hot Leg 1 Inside Surface Heat Transfer Coefficient for the Hot Leg and Surge Line Heat Transfer Sensitivity Cases	D-44
Figure D.37	Hot Leg 1 Wall Temperature for the Hot Leg and Surge Line Heat Transfer Sensitivity Cases	D-45
Figure D.38	SG 1 Hot Average Tube Wall Temperature for the Hot Leg and Surge Line Heat Transfer Sensitivity Cases	D-45
Figure D.39	SG 1 Tubesheet Heat Transfer Coefficient for the Tubesheet Heat Transfer Sensitivity Cases	D-47
Figure D.40	SG 1 Tubesheet Wall Temperature for the Tubesheet Heat Transfer Sensitivity Cases	D-47
Figure D.42	Tube Leak Rate for the SG Tube Leakage Sensitivity Case	D-49
Figure D.43	Hot Leg 1 Upper Section Wall Temperature for the SG Tube Leakage Sensitivity Case	D-50
Figure D.44	SG 1 Average Tube Wall Temperature for the SG Tube Leakage Sensitivity Case	D-50
Figure D.45	Hot Leg Pressure for the SG Tube Leakage Sensitivity Case	D-51
Figure D.46	SG 1 Secondary Pressure for the SG Tube Leakage Sensitivity Case	D-51

LIST OF TABLES

Table 2.1	Ranking Table of Items Important for the Containment Bypass Issue During SBO Severe Accident Scenarios in a Westinghouse Four-Loop PWR	21
Table 2.2	Base Case Values and Standard Deviations for the Dependent Variables.....	26
Table 3.1	Summary of Measured and SCDAP-Calculated Hydrogen Production During Severe Accident Experiments.....	45
Table 3.2	Summary of Measured and SCDAP-Calculated Fuel Rod Rupture Behavior During Severe Accident Experiments.....	46
Table 4.1	SCDAP/RELAP5 Full-Power Steady State Results.....	57
Table 4.2	Sequence of Events from the SCDAP/RELAP5 SBO Base Case Calculation.....	59
Table 4.3	Comparison of Target and SCDAP/RELAP5-Calculated SG Inlet Plenum Fluid Mixing and Flow Parameters	70
Table 4.4	Summary of Calculated Creep Rupture Failure Times from the Base Case Calculation.....	75
Table 5.1	Sensitivity of Results to Increased RCP Shaft Seal Leakage After 13 Minutes.....	79
Table 5.2	Sensitivity of Results to Increased Shaft Seal Leakage After Transition of RCP Fluid from Liquid to Steam	81
Table 5.3	Results of Sensitivity Calculations Evaluating Variations in TDAFW System Operation and SG Secondary System Steam Leakage	83
Table 5.4	Results of Sensitivity Calculations Evaluating Pre-Core Damage Mitigative Operator Intervention	88
Table 5.5	Results of Sensitivity Calculations Evaluating Post-Core Damage Mitigative Operator Intervention	102
Table 5.6	Results of Sensitivity Calculations Evaluating the Effects of Opening SG Tube Rupture and HL Rupture Flow Paths	104
Table 6.1	Characterization of Plant Fluid Conditions During Typical Non-LOCA Accident Sequences with Normal Operation of Safety Systems	110
Table 6.2	Characterization of Plant Fluid Conditions During an Extended Station Blackout Accident Sequence.....	110
Table 6.3	Major Considerations and Influences on the Containment Bypass Outcome for Event Sequences Without Operator Intervention	113
Table 6.4	Pre-Core Damage Mitigative Operator Intervention Strategy.....	121
Table 6.5	Post-Core Damage Mitigative Operator Intervention Strategy	121
Table B.1	Summary of Assumptions for the Task 8 PRA Event Sequences, September 2004	B-2
Table B.2	Summary of SG Tube Failure Margin Results for the Task 8 PRA Event Sequences	B-4
Table B.3	Summary of Assumptions for the Phase 3 PRA Event Sequences, January 2005.....	B-6
Table B.4	Summary of SG Tube Failure Margin Results for the Phase 3 PRA Event Sequences	B-8
Table C.1	Description of Control Volumes for the Energy Balance Analysis	C-3
Table D.1	Summary of Sensitivity Runs Implementing Variations in the Uncertainty Study Independent Variables	D-4
Table D.2	List of Sensitivity Calculations	D-8

Table D.3	Comparison of SCDAP/RELAP5-Calculated Results for Failure Times and Margins for the Cases Used in the Uncertainty Analysis.....	D-16
Table D.4	Comparison of SCDAP/RELAP5-Calculated Results for Temperatures and Wall Heat Transfer Coefficients for the Cases Used in the Uncertainty Analysis	D-17
Table D.5	SCDAP/RELAP5-Calculated Results for Case 8G, Evaluating Sensitivity to SG Secondary Steam Leak Flow Area Assumptions	D-46
Table D.6	Compilation of Differences Between the SCDAP/RELAP5-Calculated Results from the Sensitivity and Base Case Runs for the SG Tube Failure Margin and SG Tube Temperature Dependent Variables	D-56
Table D.7	Compilation of Differences Between the SCDAP/RELAP5-Calculated Results from the Sensitivity and Base Case Runs for the Hot Leg and Surge Line Temperature and Heat Transfer Coefficient Dependent Variables	D-57
Table D.8	Standard Deviations for the Dependent Variables Calculated Using Four Methods.....	D-59
Table D.9	Base Case Values and Recommended Standard Deviations for the Dependent Variables	D-60

EXECUTIVE SUMMARY

The U.S. Nuclear Regulatory Commission (NRC) has been sponsoring research to evaluate the risks associated with steam generator (SG) tube failure during severe accidents in pressurized-water reactors (PWRs) as part of the agency's Steam Generator Action Plan. For PWRs with U-tube SGs, the natural circulation of superheated steam in the loop piping during specific low probability severe accident conditions could result in sufficient heating of the SG tubes to induce creep rupture failure under certain scenarios. To support an overall examination of the risk impacts of induced tube failure, thermal-hydraulic analyses have been performed. The analyses used the SCDAP/RELAP5 systems analysis computer code, aided by computational fluid dynamics (CFD) simulations, to examine the pressure and temperature conditions that challenge the integrity of the reactor coolant system pressure boundary and to estimate the timing of specific reactor coolant system component failures.

These evaluations have focused on station blackout (SBO) severe accident scenarios in Westinghouse four-loop PWRs. The scenarios that challenge the tubes primarily involve a counter-current natural circulation flow pattern during conditions referred to as high-dry-low. The high-dry-low scenario refers to a set of conditions that includes a high pressure in the reactor coolant system (RCS), a loss of SG water inventory and a failure to provide a source of feedwater (dry), and a significant leak from the SG secondary side boundary that results in a low pressure on the secondary side of the SG tubes. Another condition posing a challenge to steam generator tubes is associated with full-loop natural circulation flows that are possible if the water in the loop seal is cleared and the reactor vessel downcomer is cleared. Based on our recent SCDAP/RELAP5 analysis, this condition is considered to be much less likely than the condition of counter-current natural circulation flow.

During an SBO that results in the counter-current natural circulation flows, hot steam from the upper plenum of the reactor vessel (RV) enters the hot leg (HL) and flows toward the SG. This hot steam flows along the upper half of the HL and enters the SG inlet plenum (forming a hot rising plume) where it mixes with cooler steam. After significant mixing and entrainment of cooler steam, the forward-flowing steam enters a portion of the SG tubes and flows to the SG outlet plenum. With the loop seals filled with water, this steam cannot continue in the forward loop direction and must turn around in the SG outlet plenum and flow back to the inlet plenum and ultimately back through the lower half of the HL to the vessel upper plenum. This returning steam flow, which has passed through SG tubes in both directions, is significantly cooler than the flow leaving the vessel. Through mixing and entrainment, this steam flow helps to reduce the temperature of the hottest steam that enters the SG tubes. These natural-circulation-driven counter-current flow patterns carry the energy away from the RV and out into the loops where it heats up the RCS piping and SG tubes. The overall mass flow and heat-transfer rates, along with the amount of mixing and entrainment between the hottest and cooler flows, are significant factors in determining the timing of the RCS failures.

A severe accident-induced failure of a SG tube releases radioactivity from the RCS into the SG secondary coolant system from where it may escape to the environment through the pressure relief valves. An environmental release in this manner is called "containment bypass," which contrasts with releases into the containment that result from failures of HL piping, pressurizer surge-line piping, or the lower head of the RV. The potential for steam generator tube failure by creep rupture and containment bypass under the high-dry-low conditions is effectively eliminated if (1) the RCS pressure is reduced because of operator actions to intentionally

depressurize the RCS or primary system leakage (eliminating the high-pressure condition), (2) feedwater flow is maintained (eliminating the dry condition and reducing RCS pressure), or (3) the SG secondary system retains pressure (eliminating the low-pressure condition on the secondary side).

The clearing of a loop seal eliminates the counter-current flow pattern described above and creates a challenging environment for SG tubes. Loop seal clearing (along with a clearing of the fluid in the RV lower downcomer region) results in a direct natural circulation path around the coolant loop (RV, HL, SG, cold leg). Loop seals are more likely to clear when the water in the loop seals is heated and a rapid depressurization occurs. If loop seals are cleared and full loop natural circulation is established, the hot steam from the RV challenges the integrity of the SG tubes.

The timing of the failure of the system components is significant. If a SG tube or tubes are predicted to fail prior to the HL or other RCS components, steam and radioactive fission products (released during core degradation) pass into the SG secondary system and provide a potential for containment bypass. Predictions indicate that a HL or other RCS component will fail shortly after a SG tube fails because the SG tube failures do not immediately depressurize the system. The subsequent failure of the RCS boundary significantly reduces the rate of mass flow from the primary system into the SG secondary system. Alternatively, if a HL or other RCS component of significant size fails prior to an SG tube, the release of contaminated steam would be completely into the containment because the resulting rapid RCS depressurization prevents subsequent failures of SG tubes and the associated containment bypass.

Some previous NRC analysis indicated that an unflawed tube in the hottest region of the SG could fail just prior to the HL for certain high-dry-low conditions. After further review of the SCDAP/RELAP5 modeling approach, it was found that the HL radiation model was not appropriate under these conditions and also that the hottest tube prediction was biased toward higher temperatures. NRC addressed these issues with updated models as described in this report. The improved models predict HL failure prior to an unflawed tube in the hottest region of the SG. The updated predictions indicate that it requires the addition of a stress multiplier in the range of 1.5 to 2.0 to predict a hottest SG tube failure just prior to the HL failure under the base case high-dry-low conditions. The stress multiplier is used as a means to account for tubes with flaws or other degradation in the tube bundle. The stress multiplier of 2.0 is considered bounding for tube flaws in a typical steam generator. The hottest temperatures in the SG tube bundle are estimated based on CFD predictions of the natural circulation flows from the inlet plenum to the tube bundle. These current predictions have some identifiable conservatisms. First, the tube modeling assumes the potential flaws are just above the tube sheet in the hottest section of the tube bundle. In addition, the SCDAP/RELAP5 predictions use a simplified one-dimensional HL failure model. Simulations that have accounted for the multidimensional aspects of the HL structure and thermal boundary conditions (ABAQUS calculations) have indicated earlier HL failure times. For the purposes of this report, the failure times for the hottest tube and the HL are reported directly from the SCDAP/RELAP5 model, and these provide a means of screening scenarios and evaluating sensitivities and uncertainties in the thermal-hydraulic modeling. Best-estimate modeling of HL failure time should include the full impact of the thermal entrance effects on the heat-transfer coefficient and the details of the junction between the carbon steel material in the vessel outlet and the stainless steel HL.

Event sequence scenario assumptions and modeling methods have significantly evolved over the years of research described in this report. This report documents the current predictions for system behavior during extended SBO scenarios. The objective of this report is to combine the

findings from prior evaluations and selected new evaluations into a view of the Westinghouse four-loop PWR extended SBO severe accident event sequences that fall into the following three categories:

1. Sequences resulting in containment bypass.
2. Sequences providing a potential for containment bypass for which an outcome may be determined by initially comparing the degradation of tube strengths in a prototype SG against the SCDAP/RELAP5-predicted tube-failure margins.
3. Sequences not resulting in containment bypass.

This categorization of event sequences provides information that—when combined with results from RCS component analyses, probabilistic risk assessments, and environmental release evaluations—will permit an evaluation of risks due to containment bypass for Westinghouse four-loop plants.

A model of a Westinghouse four-loop plant is developed for use with the SCDAP/RELAP5 thermal-hydraulic system code and employed to perform simulations of accident-event sequences pertinent for the containment bypass issue. The SCDAP/RELAP5 code calculates fluid and structure conditions, such as pressures and temperatures, throughout the regions of a plant model. In addition, the code includes models for calculating the progression of core-damage behavior during severe accidents and simplified models for creep rupture behavior of RCS components. In the Westinghouse four-loop plant model, creep-rupture behavior is evaluated with SCDAP/RELAP5 to predict failure times for the HLs, pressurizer surge line, and SG tubes. The creep-rupture model allows one to specify a “stress multiplier.” A multiplier of 1.0 provides a creep rupture failure prediction based on no degradation of the structural strength of the material. Multipliers greater than 1.0 represent degraded structural strengths associated with preexisting tube flaws or degradation that may exist. A stress multiplier of 2.0, for example, represents a degraded-strength condition for which the creep-rupture failure of a structure is predicted when the stress applied is only 50 percent of that required to fail the undegraded structure. The term “SG tube failure margin” as used in this report refers to the tube-stress multiplier in the model that results in prediction of SG tube creep-rupture failure coincident with the earliest failure of another RCS pressure boundary component, typically a HL. Therefore, tubes with higher stress multipliers are predicted to be the first RCS pressure-boundary components to fail, in which case containment bypass occurs. Two SG tube failure margins—one for the average tube and another for a tube in the hottest region of the SG—represent the key output from the SCDAP/RELAP5 event sequence simulations.

Assessments are made of SCDAP/RELAP5 code capabilities for predicting the plant behavior during an SBO event. In these assessments, particular attention is paid to code capabilities for predicting phenomena important to these scenarios and for predicting the behavior deemed to be the most significant with respect to the timing of SG tube failures. In addition, estimates are made of the uncertainties associated with the SCDAP/RELAP5 predictions for key fluid and component conditions and for the SG tube failure margins.

A base case SBO accident event sequence is defined to serve as a reference case from which sensitivity evaluations may be made to determine the event sequence, plant configuration, and plant condition parameters that have the most important influence on the SG tube failure margins. The base case event sequence was selected to ensure that the plant quickly entered the high-dry-low state so that this specific condition could be studied efficiently (i.e., the

calculation transient time was shortest, in a bounding way). It is noted that this approach requires a significant number of assumptions that are conservative and are of low probability. The base case assumptions are listed below:

- The accident is initiated by a loss of offsite alternating current (AC) power, which immediately results in reactor and turbine trips and the coast-down of the four reactor coolant pumps (RCPs). The diesel-electric generators fail to start and, as a result, all AC power sources are lost. Letdown flow is isolated, and the pressurizer level control and RCP seal injection functions of the charging system are lost. The high-pressure and low-pressure safety injection systems and RCP seal cooling are unavailable as a result of the AC power loss.
- The accumulator systems are available for injecting coolant into the cold legs should the RCS pressure fall below the initial accumulator pressure. The main feedwater (MFW) flow stops and the motor-driven auxiliary feedwater (MDAFW) system is unavailable as a result of the AC power loss. The turbine-driven auxiliary feedwater (TDAFW) system is assumed to independently fail immediately, so no main or auxiliary feedwater system is operable.
- A station battery life of 4 hours is assumed; after that time, all automatic and operator control over the pressurizer power operated relief valves (PORVs) and SG secondary system PORVs is lost.
- A steam leak path, with a flow area of 3.23 cm^2 [0.5 in^2], is assumed to be present in each of the four SGs; leakage through these paths into the turbine system depressurizes the SGs prior to core heatup.
- The loss of RCP seal injection cooling flow is assumed to result in leakage of RCS coolant through shaft seals into the containment at 1.325-L/s [21.0-gpm] in each of the four RCPs.
- No operator intervention is assumed to occur, whether by emergency procedures, severe accident management guidelines, or recent security-related mitigation measures.

Beyond the SCDAP/RELAP5 base case event sequence simulation, many additional SCDAP/RELAP5 simulations are performed to evaluate the effects of variations in the event sequence assumptions, the plant configuration, the system operation, and mitigative operator intervention. Of particular interest are variations in the event sequence assumptions deemed to be most important for the containment bypass outcome—the RCP shaft seal leakage rate and the timing of seal failures, the size of the SG steam leakage flow paths, and the startup and continued operation of the TDAFW system or alternate feedwater makeup.

Event sequences are categorized relative to the potential for containment bypass using the following criteria based on the SCDAP/RELAP5-predicted hottest SG tube failure margin:

- Containment bypass is assumed if the 1.0-stress multiplier (i.e., undegraded) hottest SG tube is predicted to fail prior to the HL, pressurizer surge line, or RV.
- A potential for containment bypass is assumed if the hottest SG tube failure margin is between 1.0 and 3.0. In this case, data for the actual SG tube strengths and their distribution resident in a prototype SG are needed to determine the outcome.

- Containment bypass is not indicated if the hottest SG tube failure margin is 3.0 or higher.

The major findings of the extended SBO event sequence categorization for Westinghouse four-loop PWRs are summarized as follows.

For situations where the operators are assumed to take no action:

- Event sequences that do not involve secondary side depressurization (i.e., leakage from the secondary system of 0.64 cm²/SG [0.1 in²/SG] and smaller) generally do not result in containment bypass. The reduced SG tube stresses resulting from the SG secondary pressures remaining elevated prevent SG tubes from failing prior to the HL, surge line, or RV.
- Event sequences that assume RCP shaft seal leakage rates lower than 11.36 L/s [180 gpm] per pump generally provide a potential for containment bypass. Event sequences that assume RCP shaft seal leakage rates of 11.36 L/s [180 gpm] per pump and higher generally do not result in containment bypass. A high leak rate leads to lower RCS pressures, and the reduced SG tube stresses prevent SG tubes from failing prior to the HL, surge line, or RV. However, exceptions exist related to the time when RCP shaft seal failures are assumed to occur. For RCP shaft seal failures that occur late in the event sequences, loop seal clearing and, therefore, containment bypass can occur for leakage rates above 25.23 L/s [400 gpm] per pump.
- Event sequences in which the TDAFW system operates and continues operating (or alternate feedwater is available) do not result in containment bypass. The outer surfaces of the SG tubes remain wet, and the RCS heat removal provided prevents system heatup.
- For event sequences in which the TDAFW system is assumed to initially operate and later fail, the likelihood of tube rupture is predicted to be very similar to scenarios where the TDAFW does not operate at all because eventually, without other mitigation, the system may reach the high-dry-low condition. However, the timing of potential tube failures is significantly delayed by the initial operation of the TDAFW system. Challenges to continued TDAFW operation are a result of depletion of the station batteries or the depletion of the condensate storage tank inventory. Probabilistically, additional mitigation should be considered as well as the likelihood that auxiliary feedwater may not be maintained.

For situations where the operators take mitigative action:

- An evaluation was performed for a strategy in which operators implement SG feed-and-bleed cooling at 30 minutes into the event sequence (using the TDAFW system and opening the SG PORVs). The evaluation shows that this strategy is effective in the short term for preventing containment bypass. At a minimum, the onset of the RCS heatup is significantly delayed, thereby providing additional time for other plant recovery opportunities to be considered and implemented. In the long term, the SG PORVs fail closed when the batteries are depleted, and continued success of this strategy requires that a TDAFW water source remains available along with some capability for delivering the water into the SGs. For sequences in which the TDAFW system initially operates but later fails, no large changes in SG tube failure margins (relative to the no-intervention case) were predicted.

- An evaluation was also performed for a post-core damage strategy in which the operators depressurize the RCS by opening one or two pressurizer PORVs after plant instrumentation indicates that core cooling is inadequate. PORVs are opened at the time when the core exit temperature reaches 922 K (1,200 °F) or 12 minutes later. The evaluation shows that opening only one PORV limits the cooling afforded to the RCS, the core fails early (prior to battery depletion), and containment bypass is avoided for both operator action times. The evaluations also show that the greater RCS cooling afforded by opening two PORVs prevents early core damage and also prevents early failure of the HL and SG tube structures. When the PORVs fail closed after battery depletion, the RCS begins repressurizing and reheating, and this subsequently leads to HL and SG tube failures. The SG tube failure margins seen for the operator intervention cases are significantly improved (relative to the no-intervention cases), and containment bypass is seen to be avoided for both of the post-core damage operator action times.

ACKNOWLEDGEMENTS

The authors wish to acknowledge James Han and Osvaldo Font of NRC for their technical direction of the work described here.

The authors wish to acknowledge David Bessette and Steve Long of NRC and consultants Marino DiMarzo and Peter Griffith for their helpful suggestions during reviews of the work described here.

The authors wish to acknowledge the efforts of Colleen Amoruso of ISL for technical editing and other support needed to publish this report.

NOMENCLATURE

AC	alternating current
ACRS	Advisory Committee on Reactor Safeguards
AFW	auxiliary feedwater
CCFL	counter-current flow limiting
C_D	hot leg discharge coefficient
CE	Combustion Engineering
CFD	computational fluid dynamics
CST	condensate storage tank
ECC	emergency core cooling
EPRI	Electric Power Research Institute
FW	feedwater
HL	hot leg
HPI	high-pressure injection
INEL	Idaho National Engineering Laboratory
ISL	Information Systems Laboratories, Inc.
MDAFW	motor-driven auxiliary feedwater
MFW	main feedwater
MIT	Massachusetts Institute of Technology
NTR	normalized temperature ratio
NRC	U. S. Nuclear Regulatory Commission
NRR	NRC Office of Nuclear Reactor Regulation
PIRT	phenomena identification and ranking table
PORV	power-operated relief valve
PRA	probabilistic risk assessment
PWR	pressurized-water reactor
RCP	reactor coolant pump
RCS	reactor coolant system
RES	NRC Office of Nuclear Regulatory Research
RV	reactor vessel
SOARCA	State-of-the-Art Reactor Consequences Analyses Project
SBLOCA	small break loss-of-coolant accident
SBO	station blackout
SG	steam generator
SGAP	Steam Generator Action Plan
SL	surge line
SRV	safety relief valve
TDAFW	turbine-driven auxiliary feedwater

1. INTRODUCTION

The U. S. Nuclear Regulatory Commission (NRC) has been conducting studies to evaluate the risks associated with steam generator (SG) tube failure following low probability severe accidents in pressurized water reactors (PWRs). For PWRs with U-tube SGs, the natural circulation of superheated steam in the loop piping during severe accidents could result in sufficient heating of the SG tubes to induce creep rupture failure prior to hot leg (HL) or pressurizer surge line failure. To examine the risk impacts of induced SG tube rupture, severe accident thermal-hydraulic analyses have been performed. The analyses use the SCDAP/RELAP5 systems computer code, aided by computational fluid dynamics (CFD) simulations, to examine the pressure and temperature conditions imposed on the SG tubes and system piping.

These evaluations have focused on tube integrity during station blackout (SBO) severe accident scenarios in Westinghouse four-loop PWRs. A schematic of a Westinghouse four-loop plant is shown in Figure 1.1. During these hypothetical accident scenarios a set of "high-dry-low" conditions is experienced. The reactor coolant system (RCS) loses its cooling water and remains at "high" pressure, the SG water inventory is lost and no source of feedwater is assumed available causing "dry" SG conditions. This type of event exposes the SG tubes to highly-superheated steam at the high RCS pressures associated with the opening set-point pressures of the pressurizer power operated relief valves (PORVs) and safety relief valves (SRVs). In the event the secondary coolant system is depressurized due to leaking relief valves or other system steam leaks, leading to "low" SG secondary pressures, this hypothetical event sequence provides a potential for SG tubes to contain high-pressure steam on the inside and low-pressure steam on the outside. This pressure differential, coupled with rapidly-increasing system temperatures caused by the uncovering and heat-up of the reactor core provide a potential for SG tube failure.

A failure of a SG tube releases radioactivity from the RCS into the SG secondary coolant system, from where it has the potential to escape to the environment through the secondary coolant system pressure relief valves. An environmental release in this manner is called "containment bypass" which contrasts with releases into the containment that result from failure of HL or pressurizer surge line piping or of the reactor vessel (RV).

The sequential order in which the system components fail is therefore of importance because (1) it affects the destination of the radioactive release and (2) it affects the thermal-hydraulic and stress conditions in the other components, and therefore their likelihood of subsequently failing. If a SG tube is the first component to fail, the release into the SG secondary system provides a potential for containment bypass but if a HL, the pressurizer surge line, or the RV is the first component to fail the release is instead made into the containment and the depressurization of the RCS prevents subsequent failures of SG tubes. However, analysis demonstrates that even if a SG tube is the first component predicted to fail, the HL is predicted to subsequently fail shortly thereafter, thereby mitigating the release of radioactivity into the secondary side and directing most of the radioactive release into the containment.

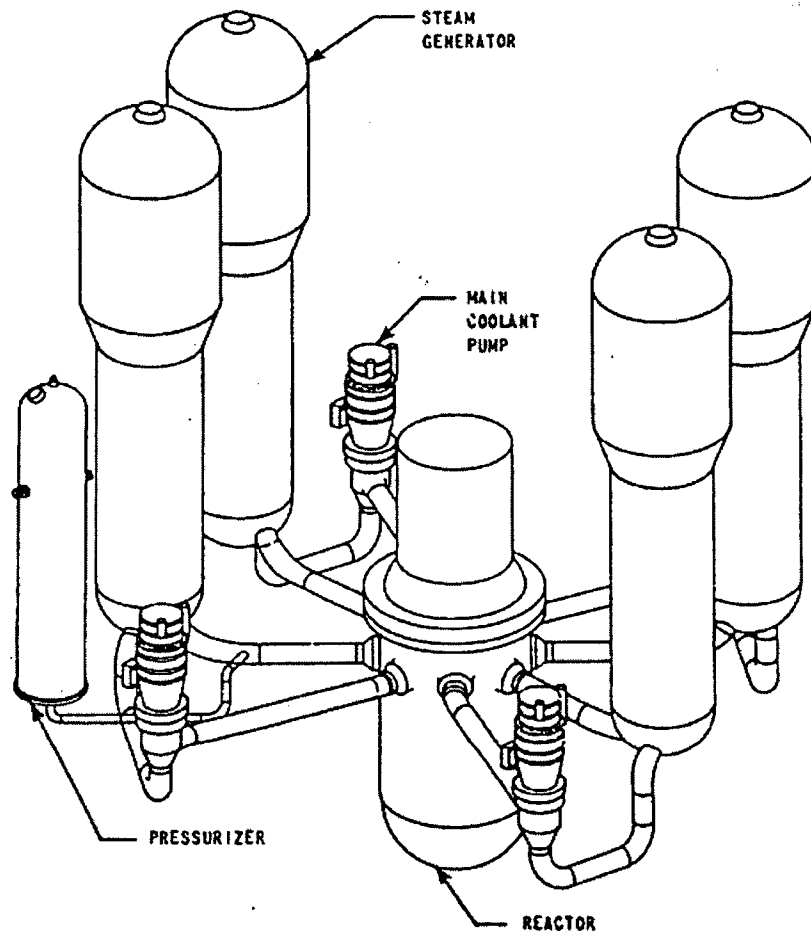


Figure 1.1 Schematic of Westinghouse Four-Loop Pressurized Water Reactor

1.1 Objective of This Report

Extensive evaluations of the containment bypass issue for Westinghouse four-loop plants have been performed over the past 12 years. The objective of this report is to coalesce the findings from those former evaluations, along with selected additional evaluations, into a view of the SBO severe accident event sequences that fall into each of the following three categories:

- Sequences resulting in containment bypass.
- Sequences with a potential to result in containment bypass, for which an outcome may be determined by comparing the degradation of tube strengths in a prototype SG against the SCDAP/RELAP5-predicted tube failure margins.
- Sequences not resulting in containment bypass.

This categorization of event sequences provides information that (when combined with results from pertinent SG tube structural analyses, probabilistic risk assessments and environmental release evaluations) permits an evaluation of risks due to containment bypass for Westinghouse four-loop plants. This work is currently underway within the Office of Nuclear Regulatory Research, Division of Risk Analysis.

To explain the process by which the event sequence categorization is performed, a base case SBO accident scenario is first defined for the purpose of illustrating the thermal hydraulic technical issues associated with the containment bypass issue. The base case event sequence is not considered a most-likely accident scenario. The expected plant behavior during the base case event sequence is discussed in order to explain the relevant technical issues and describe criteria by which an event-sequence outcome relative to the three above categories can be judged.

1.2 Description of a Base Case Station Blackout Accident Scenario

The Westinghouse four-loop plant conditions at the start of the base case accident scenario represent full-power operation of the plant with 10% of the 3,388, 1.97-cm [0.775-in] inner diameter, tubes plugged in each SG: a reactor power of 3,250 MW, a RCS pressure of 15.51 MPa [2,250 psia], an average RCS temperature of 567.7 K [562.2°F], a total coolant loop flow rate of 17,010 kg/s [135 Mlbm/hr] and a SG secondary system pressure of 4.964 MPa [720 psia].

The accident event is initiated by a loss of off-site alternating current (AC) power, which immediately results in reactor and turbine trips and the coast-down of the four reactor coolant pumps (RCPs). The diesel-electric generators fail to start and as a result all AC power sources are lost. Letdown flow is isolated and the pressurizer level control and RCP seal injection functions of the charging system are lost. The high-pressure and low-pressure safety injection systems are unavailable as a result of the AC power loss. The accumulator systems are available for injecting coolant into the cold legs should the RCS pressure fall below the initial accumulator pressure, 4.24 MPa [615 psia]. The main feedwater (MFW) flow stops and the motor-driven auxiliary feedwater (MDAFW) system is unavailable as a result of the AC power loss. The turbine-driven auxiliary feedwater (TDAFW) system is assumed to independently fail, so no MFW or auxiliary feedwater (AFW) system is available. A station battery life of four hours

is assumed; after that time all automatic and operator control of the pressurizer PORVs and SG secondary system PORVs is lost.

Because the feedwater and steam flow paths are isolated at the beginning of the event sequence, the SG secondary system pressures initially rise. The SG secondary water inventory boils and the SG PORVs open to limit the SG secondary system pressure increase. Minor steam leak paths from the SGs are assumed to be present. Constant steam leak flow areas of 3.23 cm² [0.5 in²] are assumed in each SG, resulting in a leakage rate that is about 0.7% of the full-power steam flow rate. The effect of these steam leaks is to slowly depressurize the SGs over a period of about two hours following the time when the SG water inventories have been completely boiled away.

The loss of RCP seal injection cooling flow is assumed to result in leakage of RCS coolant through the RCP shaft seals and into the containment starting at the beginning of the SBO event sequence. An initial 1.325-L/s [21.0-gpm] shaft seal leak rate is assumed in each of the four RCPs. This rate is considered to be a postulated minimum flow rate under conditions where RCP seal cooling is lost and not recovered. The seal leak path characteristics and flow areas are assumed not to change over the course of the event sequence and the leak flow rates are therefore subsequently determined by the transient fluid conditions in the RCPs and containment. It is noted that this shaft seal leakage rate is considered to be the postulated minimum flow following a loss of seal injection flow. Other higher shaft seal leak rates may also be experienced as a result of various possible seal hardware failures.

1.3 Plant Behavior During the Base Case Accident Scenario

The low-probability SBO base case accident event scenario described in Section 1.2 results in a severe accident because none of the systems that normally provide core cooling are assumed to be operable nor is any alternate equipment (e.g., security-related mitigation methods) assumed to be available. During the initial portion of the accident scenario, buoyancy-driven coolant-loop natural circulation carries hot water from the core through the SGs, transferring heat to the SG secondary water inventory. The SG water inventory is boiled and the steam is released through the SG PORVs. Since the MFW and AFW systems are not operative, the secondary water inventory declines and is eventually fully depleted. After that time, the core decay power heats and swells the RCS water, increasing its temperature and pressure. During this process, the RCS pressure increase is limited by the opening of the pressurizer PORVs and SRVs. However, the RCS fluid lost through those valves (as well as through the RCP shaft seals) is not recoverable and the RCS coolant inventory continuously declines. Eventually, the RCS inventory loss becomes extreme, the core uncovers and the fuel starts to heat up. The fuel heat-up leads to an exothermic oxidation reaction between the steam and the fuel rod cladding that adds heat to the fuel in addition to the heat generated from the fission product decay process.

The basic physical processes of this event sequence during the period when the steam temperatures are rising regard the transport of hot steam from the core outward into the other regions of the RV and coolant loops. Figure 1.2 shows two coolant loop natural circulation flow patterns that may be encountered subsequent to the uncovering and heat-up of the reactor core. The flow patterns differ based upon whether or not the loop seals (the cold leg piping connecting the outlets of the SGs to the inlets of the RCPs) remain liquid-plugged.

If liquid is cleared from a loop seal (along with the region of the RV lower plenum that extends above the bottom of the core barrel, the "downcomer skirt"), the loop natural circulation flow

pattern on the left side of Figure 1.2 develops. Hot steam is transported from the core through the HLs, SG tubes and cold legs in the normal direction of flow (i.e., that seen during plant operation). This flow pattern transports the hot steam directly (without benefit of mixing) through all of the SG tubes, leading to SG tube failure prior to HL or pressurizer surge line failure.

However, if a loop seal remains liquid-plugged, the more complex flow pattern shown on the right side of Figure 1.2 develops instead. Hot steam is transported through the upper portion of the HL cross section to the SG inlet plenum, where it is mixed with cooler steam emanating from circulations set up as shown within the SGs, with some of the tubes flowing in the normal direction and the remaining tubes flowing in the reverse direction. The mixing process within the SG inlet plenum determines the temperatures of the steam entering the SG tubes and the steam that is returned to the RV through the lower portion of the HL cross section. Fluid mixing in the SG inlet plenum buffers the entry of hot steam into the SG tubes, thus delaying SG tube failure and making it more likely that some other component (HL, pressurizer surge line or RV) will be the first to fail.

The issues of primary interest for containment bypass are: (1) do the loop seals in all coolant loops remain liquid plugged and if so (2) does the fluid mixing in the SG inlet plenum sufficiently slow the SG tube heat-up process so that the HL, pressurizer surge line or RV will fail prior to a SG tube? The analyses in this report address these issues, evaluating them for the base case and other accident event sequences.

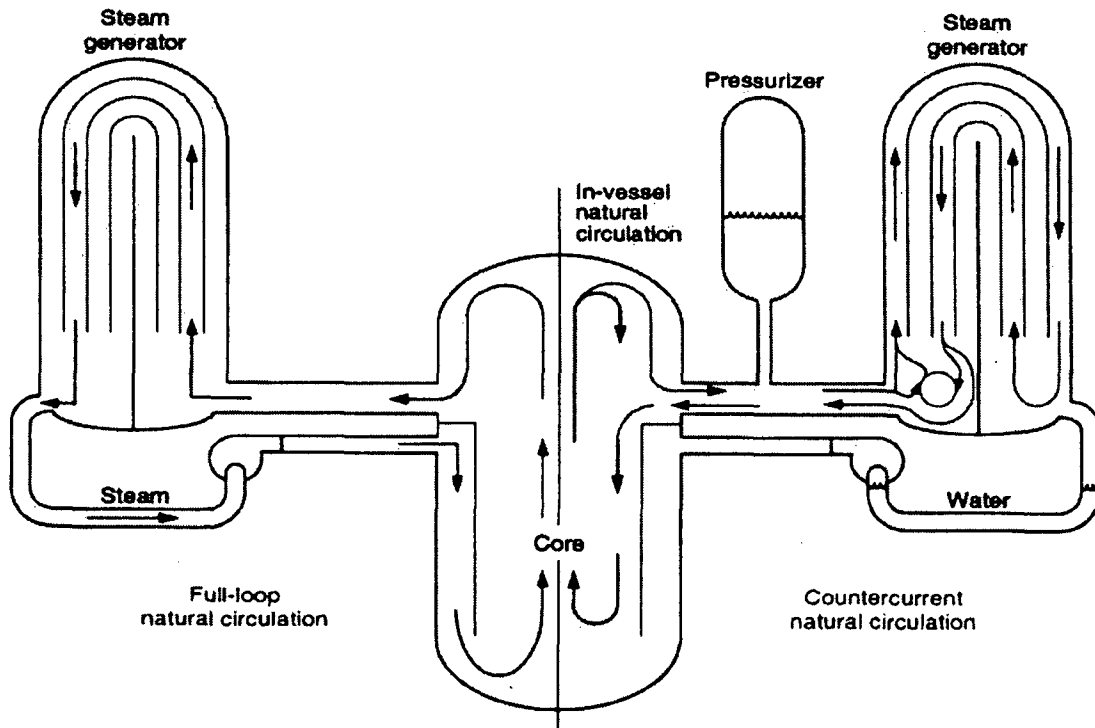


Figure 1.2 Potential Coolant Loop Natural Circulation Flow Patterns During System Heat-Up

1.4 Definition of SG Tube Failure Margin and Criteria for Judging Occurrence of Containment Bypass

Predictions of structural failure are made based on the structure configuration, its material properties and the fluid conditions that are locally present. The SCDAP/RELAP5 thermal-hydraulic system code calculates the local fluid conditions, such as pressures and temperatures, throughout the fluid regions of a model which represents a power plant. The code also includes models for calculating the creep rupture failure of structural components and these are used to predict failure times for the HLs, pressurizer surge line, and SG tubes for the Westinghouse four-loop plant model. It is noted that the SCDAP/RELAP5-calculated predictions of structural failures are intended to provide a screening tool to assess structural failure issues. These predictions are not intended to supplant failure evaluations using more detailed analysis tools.

The SCDAP/RELAP5 creep rupture model allows one to specify a "stress multiplier." A multiplier of 1.0 provides a creep rupture failure prediction based on no degradation of the structural strength of the material. Multipliers greater than 1.0 represent degraded structural strengths. A stress multiplier of 3.0, for example, represents a degraded-strength condition for which the creep-rupture failure of a structure is predicted when the stress applied is only 33.3% of that required to fail the undegraded structure. A stress multiplier of 3.0 is considered to be a conservative upper bound for screening the steam generator tube failures. (The meaning of "stress multiplier" as used in this report is the same as "stress magnification factor" as used in the previous NUREG-1570 analysis described in Section 2.1). In the SCDAP/RELAP5 Westinghouse plant model, creep rupture failure calculations are performed for the "average" SG tubes and HLs in all four coolant loops, and for the pressurizer surge line and "hottest" SG tube in the pressurizer-loop SG. The terms average and hottest SG tubes, respectively, refer to tube models which transport fluids that are at the average and highest temperatures among all of the SG tubes.

For the Westinghouse four-loop plant model, a stress multiplier of 1.0 is used for the HL and pressurizer surge line structure calculations while stress multipliers from 1.0 to 7.5 (in increments of 0.5) are used for the SG tube calculations. Therefore creep rupture predictions for the HL and pressurizer surge line structures are based on undegraded material strengths while the creep rupture predictions for the SG tubes are based on a spectrum of material strengths, from undegraded to highly-degraded. The purpose of evaluating a spectrum of SG tube strengths is to consider parametrically in the analysis a distribution of SG tube material strengths. Stress multipliers up to 7.5 are not realistic for any steam generator but these values are tracked so that sensitivities to various modeling parameters could be established. The actual distributions vary from plant to plant, as functions of the tube material specifications, time in service, and other factors.

The term "SG tube failure margin" as used in this report refers to the tube stress multiplier in the model which results in prediction of SG tube creep rupture failure coincident with the earliest failure of another RCS pressure boundary component (HL, pressurizer surge line, or RV).

Tubes with higher stress multipliers are therefore predicted to be the first RCS pressure boundary component to fail, in which case RCS fluid flows into the SG secondary system, leading to containment bypass. Two SG tube failure margins, one for the average tube and another for the hottest tube, are the key results of the event sequence simulations.

In the more recent SCDAP/RELAP5 analyses described in this report, a HL is typically predicted to fail prior to the pressurizer surge line. In some of the SCDAP/RELAP5 simulations, the core damage process is accelerated and core fuel rod melting and refreezing, core flow blockage and relocation of molten core materials to the lower head of the RV are predicted prior to HL, pressurizer surge line or SG tube failures. The prediction of core damage that significantly alters the configuration of the core is taken as a proxy for RV failure. The challenge to SG tubes integrity is removed if core fuel damage is sufficient to entirely block the flow of steam through the core (thereby stopping the robust flow of hot steam to the SGs) or sufficient to convert the core into an uncoolable molten mass that slumps into the lower head region of the RV (in which case the flow of core heat into the steam virtually ceases).

Criteria are needed in order to judge whether or not containment bypass is predicted to occur for a particular event sequence. The criteria used in this report are based on the SCDAP/RELAP5 predicted hottest SG tube failure margin:

- **Containment bypass is indicated if the 1.0-stress multiplier (i.e., undegraded) hottest SG tube is predicted to fail prior to the HL. (For these challenging event sequences the definition for the “SG tube failure margin” is changed to instead indicate the time in seconds by which the hottest SG tube failure precedes the HL failure).**
- **A potential for containment bypass is indicated if the hottest SG tube failure margin is between 1.0 and 3.0. In this case, data for the actual SG tube strengths and their distribution resident in a prototype SG is needed in order to determine the outcome.**
- **Containment bypass is not indicated if the hottest SG tube failure margin is 3.0 or higher.**

These criteria and the results of SCDAP/RELAP5 simulations for SBO event sequences are used to group the event sequences into the three categories of containment bypass behavior described in Section 1.1. It is noted that the criteria are somewhat arbitrary and are necessarily subject to uncertainties related to the characteristics of SG tubes actually resident in a specific SGs, as well as uncertainties in SCDAP/RELAP5 modeling such as are described in Sections 2.9 and 5.4 of this report.

1.5 Organization of This Report

Section 2 of this report provides background on prior thermal-hydraulic containment bypass evaluations. Section 3 describes the thermal-hydraulic analysis methods used, including descriptions of the SCDAP/RELAP5 computer code, assessments of its capabilities pertinent for the containment bypass application and aspects of the modeling which have benefitted from ongoing CFD analyses. Section 4 summarizes the SCDAP/RELAP5 model of the Westinghouse four-loop plant and the detailed results from the base case SBO accident calculation. Section 5 describes key sensitivity analyses performed to evaluate variations in the event sequence assumptions, plant configuration, system operation and mitigative operator intervention. The categorization of event sequences into the three above categories is performed in Section 6; the information provided in this section is considered to be the main product of the detailed research summarized in this report. Conclusions are presented in

Section 7 and references are provided in Section 8. Details of supporting analyses are provided in the appendixes of this report.

2. BACKGROUND

This section describes background studies, reviews and preliminary SCDAP/RELAP5 sensitivity evaluations into the containment bypass issue performed over the period from 1995 through 2007. The material presented here is intended to provide a historical perspective on the SCDAP/RELAP5 containment bypass systems analysis research. This perspective is useful both for understanding the evolution of the SCDAP/RELAP5 model and for summarizing the results from prior sensitivity evaluations, many of which remain pertinent today.

2.1 NUREG-1570 Analyses, 1998-2000

An assessment of PWR containment bypass potential attributable to SG tube rupture induced by severe accidents was first made by an *ad hoc* NRC working group. This group began work in 1995 and published its findings in NUREG-1570, March 1998 (Reference 2.1). The study drew upon risk and thermal-hydraulic analyses for various core damage sequences and concluded that the primary accident sequence of interest for containment bypass was a SBO event, coupled with a failure of AFW, the depressurization of at least one SG secondary system and no operator intervention.

The containment bypass susceptibility for this type of event sequence was found to be limited to plants that employ U-tube type SGs, plants of Westinghouse and Combustion Engineering (CE) design. Experimental evidence (Reference 2.2) demonstrated that during this type of event sequence in Babcock and Wilcox design plants, which employ once-through type SGs, a flow of superheated gas does not reach the SG tube bundles and a heat-up of the SG tubes producing creep rupture tube failure is not encountered.

The thermal-hydraulic analyses documented in NUREG-1570 were principally performed at the INEL using the SCDAP/RELAP5/MOD3.1 system code (Reference 2.3) and models of a Westinghouse three-loop plant and a CE plant. The purpose of these analyses was to provide the HL, pressurizer surge line and SG tube thermal-hydraulic conditions expected during SBO severe accident event sequences. Thermal-hydraulic calculations and analyses were performed for accident sequences identified by a Probabilistic Risk Assessment (PRA). Additional calculations and analyses were performed to address numerous other issues, such as variations in the accident sequence description, uncertainties in modeling the plant behavior and uncertainties in the boundary and initial conditions.

The NUREG-1570 analyses also investigated the potential for loop seal clearing, which is of significance for the containment bypass issue as explained in Section 1.3. The analyses for both plants indicated: (1) loop seal clearing is not encountered prior to HL or pressurizer surge line failure when nominal 1.32 L/s [21 gpm] per pump RCP shaft seal leakage rates are assumed, and (2) loop seal clearing prior to HL or surge line failure is encountered when much larger RCP shaft seal leakage rates are assumed (15.8 L/s [250 gpm] for the Westinghouse plant and 13.9 L/s [220 gpm] for the CE plant).

2.2 NUREG-1740 Independent Review and Steam Generator Action Plan, 2000-2001

The Advisory Committee on Reactor Safeguards (ACRS) undertook an independent examination of the technical issues associated with voltage-based alternative repair criteria for SG tubes. The purpose of this examination was to provide comments and recommendations to

the NRC for resolving a differing professional opinion concerning the adequacy of the repair approach documented in Generic Letter 95-05, Reference 2.4. This independent review was performed by an *ad hoc* subcommittee composed of ACRS members and consultants to assess the containment bypass potential attributable to SG tube rupture induced by severe accidents as documented in NUREG-1570. The ACRS subcommittee review was documented in NUREG-1740, Reference 2.5. The review findings related to thermal-hydraulic analysis of the containment bypass issue are summarized as follows:

The reviewers reiterated the significance of loop seal behavior for the outcome of the analyses that was noted in NUREG-1570, adding that loop seal clearing considerations (including the potential for periodic clearing and refilling) increase the expected complexity of the plant response.

The reviewers noted that the system computer codes (such as SCDAP/RELAP5) used for the analyses are lumped-parameter codes and do not make reliable predictions of natural circulation behavior or local phenomena involving fluid momentum.

The reviewers noted that the system code input decks are "tuned" by benchmarking against experimental results, such as the Westinghouse one-seventh scale PWR model (Reference 2.6). They noted that such test results have been criticized because of improper scaling of the SG region of the test rig to the full-scale PWR SG. It was mentioned that one consequence of this scaling shortcoming could be overestimation of the mixing occurring in the SG inlet plenum, which would lead to delays in the heat-up and creep rupture failure of the SG tubes. They noted that the sensitivity studies regarding SG inlet plenum mixing performed as a part of the analyses have not evaluated the plausible ranges of parameter variations nor considered simultaneous variations of multiple parameters.

Finally, the reviewers noted that the experiments did not consider the effects SG tube leakage and that related sensitivity studies have not considered the plausible range of variations in that parameter.

In February, 2000 the NRC Office of Nuclear Reactor Regulation (NRR) provided a user need letter (Reference 2.7) to NRC Office of Nuclear Regulatory Research (RES) requesting that RES develop a confirmatory research program to address the thermal-hydraulic, dose-consequence and structural behavior of PWRs during postulated severe accidents. The letter included a request to develop models and methods that provide improved understanding of transient thermal-hydraulic conditions in the primary piping and SG tube regions of the reactor coolant system.

The RES response to NRR, Reference 2.8, came in September 2000. The RES research plan built on the prior work performed in support of the NUREG-1570 assessment of containment bypass and included new work in the following areas: accident sequence variations, plant design differences, fluid mixing in the SG inlet plenum, tube-to-tube variation of the fluid conditions and the effects of variations in the core melt progression. The research plan included continued refinement and improvement of SCDAP/RELAP5 plant system models and accident sequence analysis performed with the upgraded models. The system analyses were to be complemented and enhanced with CFD models and analyses. The CFD models are employed to simulate local thermal-hydraulic behavior which is beyond the capabilities of the lumped-

parameter system models. The results of the CFD analyses also are employed to generate correlations and mixing parameters for the system model, thereby incorporating effects of the more-physical behavior generated with CFD into the system model.

In May 2001, RES and NRR jointly developed a Steam Generator Action Plan (SGAP, Reference 2.9) to address the conclusions and recommendations contained in the NUREG-1740 ACRS review. The SGAP included thermal-hydraulic tasks to: perform system level analyses assessing the impact of plant sequence variations (Task 3.4a), re-evaluate existing system level code assumptions and simplifications (Task 3.4b), examine the one-seventh scale data to assess tube-to-tube variations and estimate those variations at the plant scale (Task 3.4c), perform a more rigorous uncertainty analysis regarding inlet plenum mixing behavior (Task 3.4d), examine the uncertainties related to the progression of the core melt process (Task 3.4f), and examine SG tube severe accident conditions using CFD methods including benchmarking of the model with the one-seventh scale test data, performing analysis of the local HL and SG behavior and addressing inlet plenum mixing effects of tube leakage and the HL-inlet plenum geometrical configuration (Task 3.4e).

2.3 Revised Station Blackout Base Case Event Sequence and Analysis, 2000-2003

Subsequent to the release of NUREG-1570, Idaho National Engineering Laboratory (INEL) performed SCDAP/RELAP5 analyses to support the SGAP. INEL evaluated SBO event sequence variations and modeling assumptions and the focus of the analysis was switched to Westinghouse four-loop plants. That switch was made because the four-loop plant is representative of a large number of PWRs; the understanding of the overall SGTR risk for the fleet of U. S. operating plants was thus broadened.

INEL refined the SCDAP/RELAP5 Westinghouse four-loop plant model for simulating the SBO accident sequence, including benchmarking of SG inlet plenum fluid mixing behavior to the Westinghouse one-seventh scale natural circulation experiments (Reference 2.6) and implementing model features to switch between normal and recirculating natural circulation modes based on the status (open or water-plugged) of the loop seals and at the bottom of the RV downcomer skirt. INEL also introduced stress multipliers in the SCDAP/RELAP5 modeling of the creep rupture structural failures, allowing various extents of tube strength degradation to be parametrically included in the SCDAP/RELAP5 calculation results.

In Reference 2.10 INEL used the refined Westinghouse four-loop plant model to evaluate behavior for a base case SBO accident scenario that included: loss of all on-site and off-site AC power, failure to start all diesel-electric generators, loss of all main and auxiliary feedwater, 15% tube plugging in all SGs, and a stuck-open PORV on the secondary side of the pressurizer-loop SG. INEL also evaluated the sensitivity of results to differences in design between the Westinghouse three-loop and four-loop plants, including the configuration of the HL-to-surge line connection, the loop seal geometry and the core bypass. INEL concluded that for the base case accident scenario in the Westinghouse four-loop plant the creep rupture failure of unflawed SG tubes will occur subsequent to the failure of the pressurizer surge line. However the margin was relatively small and SG tubes with stress multipliers greater than 2.0 were predicted to fail prior to the surge line. INEL also concluded that the plant behavior may be sensitive to the modeling of the fuel rod oxidation process, the modeling of the surge line-to-HL connection and the assumptions made regarding SG tube plugging and core bypass.

After 2000, SCDAP/RELAP5 thermal-hydraulic analyses supporting the containment bypass project SGAP were performed by Information Systems Laboratories, Inc. (ISL) and were based on further refinements and improvements upon the INEL SCDAP/RELAP5 Westinghouse four-loop plant model from Reference 2.10.

In Reference 2.11 ISL investigated additional variations in the accident sequence assumptions to look for changes in assumptions that could result in more limiting SG tube failure margins than were previously predicted. The effects of leakage through a pressurizer SRV (equivalent to 13% of the valve flow area) and leakage through the RCP shaft seals (leakage rates up to 15.8 L/s [250 gpm] per pump) were investigated. The results indicated that these RCS leakages increased the SG tube failure margin and did not result in clearing of loop seals. The margin improvements were seen to result from the reduction of the RCS pressure caused by including the RCS leakages in the model. The effects of reducing SG tube plugging from 15% (assumed in the base case at that time) to 0% were investigated. As expected, decreasing the assumed number of plugged tubes was found to reduce tube temperatures and increase the SG tube failure margin, although the margin change was small. As a result of the evaluations in Reference 2.11, no changes were recommended for the base case accident sequence assumptions or for the SCDAP/RELAP5 modeling approach.

In Reference 2.12 ISL investigated potential conservatisms in SCDAP/RELAP5 modeling of the Westinghouse four-loop SBO base case accident sequence. The effect of changes in the time step size and heat structure mesh size on the calculated base case results were independently investigated. The maximum time step size was reduced from 0.075 s to 0.005 s. The number of mesh intervals across the thickness of the HL wall was doubled. Neither the time-step size nor mesh-size variations were seen to significantly impact the calculation results. Another sensitivity run was made to determine the impact of increasing the heat transfer coefficient from the SG tube outer wall surface to the fluid in the SG boiler region by a factor of 5.0. This increase was intended to represent an upper bound for the heat transfer through this path, including effects due to steam-to-wall thermal radiation and tube-bundle induced turbulence not modeled with SCDAP/RELAP5. In the sensitivity run, coupling between the SG tube outer wall and the cooler steam in the SG boiler region was shown to significantly increase the SG tube failure margin (the stress multiplier required for tube failure to precede surge line failure increased from about 2.0 in the base case run to about 3.0 in the sensitivity run). Based on this result, it was concluded that steam-to-wall and wall-to-wall thermal radiation processes could in general affect the heat-up of structures and that the SCDAP/RELAP5 code should be upgraded to represent those processes.

In Reference 2.13 ISL performed initial evaluations into expected tube-to-tube variations, the manner in which hot steam entering the SG inlet plenum from the HL is distributed among the inlets of the SG tubes. The buoyant hot steam rises as it emerges from the HL, flowing toward the bottom face of the tubesheet. Flow enters the hot SG tubes (i.e., those tubes through which flow is traveling in the upward direction). The issue relates both to the spreading of the hot steam region as it rises and to the mixing it encounters with cooler steam along the way. The cooler steam enters the SG inlet plenum through the cold SG tubes (i.e., those through which flow is traveling in the downward direction). Of specific interest is the hottest steam temperature that is expected to enter the hot tubes and the number of tubes that experience that hottest steam temperature. Up to this time, SCDAP/RELAP5 plant models had separated the SG tube bundle into hot and cold tube sections which were assumed to be passing steam of an average, not maximum, temperature.

The evaluation of the tube-to-tube variation issue concluded, based on a review of the Westinghouse one-seventh scale test data (Reference 2.6), that mixing between the hot and cold steam flows primarily occurs locally near the connection between the HL and SG inlet plenum and little further decline in the steam temperature is seen from this point of mixing upward toward the tubesheet. A review of the literature showed that plume models predict a decay in temperature with distance from the source position and therefore a plume modeling approach does not appear to represent the mixing process in the SG inlet plenum. The mixing behavior in the SG inlet plenum was seen to be more complex than could be represented with a simple plume model. Further, even if a plume model could be adequately adjusted to represent the mixing behavior in the one-seventh scale facility, its extrapolation to the full-scale plant would be questionable due to the geometric differences in inlet plenum designs. Instead, an alternate approach was developed for predicting the maximum temperature of steam entering the SG tubes which takes advantage of the one-seventh scale test data. With this approach, the test data is used to characterize a normalized temperature ratio, relating the difference between the hottest SG tube temperature and the cold SG tube temperature to the difference between the HL and cold SG tube temperatures (subsequent Westinghouse four-loop plant modeling includes a hottest tube simulation based on this approach, which is described in Section 3.4). The results were extended to more prototypical inlet plenum designs using computational fluid dynamics simulations.

A coordination meeting was held in Rockville, Maryland, March 19-20, 2003 among project participants in the areas of thermal-hydraulics, probabilistic risk assessment and stress analysis. The meeting resulted in a consensus regarding the event sequence and modeling assumptions to be used for the project. The SCDAP/RELAP5 code and Westinghouse four-loop plant model were revised accordingly and a SBO base case calculation was performed and documented in Reference 2.14 to serve as a common reference case for all involved in the project. The code and plant model revisions included in the revised base case calculation are summarized as follows:

RCP shaft seal leakage at 1.32 L/s [21 gpm] per pump was added to the model; previously the base case model assumed no shaft seal leakage.

The SG tube plugging assumption was revised from 15% to 10%.

The axial nodalization of the SG tube region was expanded slightly, such that the first and last cells of the tube models represent only the fluid inside the tubesheet.

The nodalizations for heat structures particularly important for the analysis were revised to increase the number of nodes employed across the thicknesses of the structures.

The thermal material properties for structures in the model were revised for consistency with those used by the project stress analysts. (However, the hot leg and nozzle region continued to be modeled as stainless steel)

RCS heat loss to containment was added to the model. A total of 4 MW heat loss was assumed to be uniformly distributed over the outer surfaces of the primary and secondary coolant system vessels and pipes.

The SCDAP/RELAP5 code was modified to permit the modeling of steam-to-wall radiation heat transfer. The plant model was revised to include the effects of

steam-to-wall radiation on the inside surfaces of all primary coolant system heat structures and the effects of wall-to-wall radiation heat transfer between the piping walls of the upper and lower HL sections.

The plant model was revised to include a representation for the hottest tube in the pressurizer-loop SG as discussed above.

The target SG inlet plenum mixing and flow parameters of the SCDAP/RELAP5 plant model (as defined in Section 3.4) were revised for consistency with the results of initial CFD evaluations (Reference 2.15) of the Westinghouse one-seventh scale experiments and the scale-up of the experimental results to the Westinghouse four-loop plant configuration. Through this process the SCDAP/RELAP5 model is enhanced to reflect the physical behavior of the system observed with the CFD model. The assumed split of the SG tubes into hot and cold regions was revised from 53%/47% to 50%/50%. The target hot and cold mixing fractions were revised from 0.87 to 0.81 and the target recirculation ratio was revised from 1.9 to 2.75. The 30.24% target SG power fraction (the fraction of the total core power deposited into the SGs) was not revised. Note that, to make the modeling of HL circulating flow more physically-based, the target SG power fraction has since been replaced with a target hot leg discharge coefficient, see Section 3.4). The normalized temperature ratio for the hottest tube model was revised from 0.4737 to 0.625.

The results of the SCDAP/RELAP5 SBO base case calculation using the revised Westinghouse four-loop plant model indicated a significant improvement in the SG tube failure margin. A stress multiplier of about 4.5 was now found to be required for the average SG tube to fail prior to the pressurizer surge line (in the previous base calculation that multiplier was about 2.0). The margin improvement was found to result primarily from the significant increase in the target recirculation ratio. In order to attain the higher recirculation ratio and at the same time keep the SG power fraction from increasing above its target value, a general slowing of the steam flows in the two circulating loops (i.e., the upper and lower HL sections and the hot and cold SG-tube sections) was required. The slowing of the transport of heat from the core to the SGs both delayed the heat-up of the SG tubes and (because of the increased demand for pressurizer relief valve operation) accelerated the heat-up of the pressurizer surge line, thereby improving the SG tube failure margin. For the hottest SG tube, a stress multiplier of about 1.5 was found to be required for it to fail prior to the pressurizer surge line.

2.4 Sensitivity Analyses, 2004

Extensive sensitivity studies were performed to evaluate the effects of various changes in the SCDAP/RELAP5 Westinghouse four-loop plant modeling options, event sequence assumptions and plant configuration. These sensitivity studies were documented in Reference 2.16. The base case accident sequence and plant model used for the sensitivity analyses were the same as described in Section 2.3. The sensitivity evaluations performed and the analysis results are summarized here and are more fully described in Appendix A. See Section 3.4 for definitions of the hot and cold mixing fractions and the recirculation ratio.

The target hot and cold mixing fractions were increased to from 0.81 to 0.87 and, separately, the target recirculation ratio was decreased to from 2.75 to 2.0. Both sensitivity runs showed reductions in the SG tube failure margin from the base case.

A variety of assumptions regarding the RCP shaft seal leakage were investigated. The base case event sequence assumed a leak flow area based on an initial 1.32 L/s [21 gpm] leakage rate per pump. In the sensitivity cases, the leakage flow area was increased at different times during the event sequence to as high as 18.9 L/s [300 gpm] per pump. The results of the sensitivity runs indicated that the SG tube failure margins are sensitive to the assumed RCP shaft seal leakage, with small increases in the leakage rate leading to slightly lower the margins, and large increases in the leakage rate leading to significantly improved margins.

Sensitivity evaluations were performed for 0% and 20% SG tube plugging assumptions (10% was assumed in the base case). The SG tube failure margin results were seen to be only slightly affected by the tube plugging assumption.

The sensitivity to variations in the heat transfer processes on the outer surface of the SG tubes was evaluated using multipliers of 0.1, 5.0 and 10.0 on the SCDAP/RELAP5-calculated heat transfer coefficient. The results indicated that the SG tube failure margin is sensitive to this parameter. Enhanced heat transfer leads to a tighter coupling of the SG tube wall with the cooler steam in the SG boiler region and increased SG tube failure margins.

The sensitivity to variations in the modeling of thermal radiation heat transfer processes was evaluated using SCDAP/RELAP5 runs in which multipliers of 0.5 and 2.0 were placed on the steam-to-wall and wall-to-wall radiation heat fluxes on the surfaces of the RCS structures. The results indicated that increased radiation heat flux leads to slightly-improved SG tube failure margins.

Several SCDAP/RELAP5 sensitivity runs were performed to investigate the modeling of countercurrent flow limiting (CCFL) behavior related to pressurizer draining. None of these runs indicated a significant affect on SG tube failure margins.

SCDAP/RELAP5 calculates buoyancy-driven circulations within the RV which affect the temperature of steam transported into the coolant loops. A SCDAP/RELAP5 sensitivity run was performed in which the flow losses within the vessel model were increased so as to reduce the flow rates of the RV internal circulations by an arbitrary 50%. The reduced RV circulation rates were seen to accelerate the core damage process and result in improved SG tube failure margins.

The base case SCDAP/RELAP5 plant system model represents a typical 4 MW of uniformly-distributed heat loss from the outer surfaces of the primary and secondary reactor coolant systems to the containment. Sensitivity runs were made with this assumption changed to 2 MW and 8 MW and the results showed that SG tube failure margin results are moderately affected by the heat loss assumption, with the higher heat loss leading to reduced margins.

A sensitivity run was also performed to evaluate the plant response to mitigative operator intervention. The operators were assumed to depressurize the RCS by opening the pressurizer PORVs following the onset of the core heat-up. The results of the sensitivity run demonstrated the success of this intervention strategy for mitigating containment bypass during the base case SBO severe accident. SG tube failures were prevented by the operator action. The core melted and relocated to the RV lower head; a subsequent failure of the RV lower head would result in a full depressurization of the RCS and a release into the containment.

A limited investigation was performed into the effects of SG tube leakage (from primary-to-secondary, none is assumed in the base case calculation). The results indicated that

the tube leakage assumption affects the SG tube failure margin, with higher leakage rates leading to reduced margins.

A SCDAP/RELAP5 sensitivity run was performed with the assumed core bypass flow due to leakage around the slip fit between the core barrel and RV at the HL nozzle penetrations (1% of total coolant loop flow rate) arbitrarily reduced by 50%. This modeling change was seen to have virtually no effect on the SG tube failure margins.

The SCDAP/RELAP5 Westinghouse four-loop base case calculation indicated that the failure of structural components (HL and pressurizer surge line piping and SG tubes) occurs relatively early during the core damage and relocation processes of the SBO severe accident sequence. The fuel rod cladding oxidation is seen to dramatically increase the core heat load, which in turn leads to a rapid heat-up of components throughout the RCS. The structural failures are encountered shortly after the time when the oxidation power peaks. Heating of the control rods leads to control rod cladding failure and relocation of molten control rod absorber material to the RV lower head shortly after the time of the structural failures. Melting and relocation of the core fuel to the RV lower head are seen to occur long after the time of the structural failures. Three SCDAP/RELAP5 sensitivity runs were performed to evaluate the effects of the core damage progression by varying the modeling of the fuel rod oxidation, control rod melting and fuel rod melting processes. Results from these evaluations are summarized as follows.

At its peak, the fuel rod cladding oxidation power exceeds the fission product decay power by an order of magnitude. A sensitivity run was performed in which the peak oxidation power was limited to 43% of the peak experienced in the base case run. The results showed that limiting the peak oxidation power in this manner tended to slow the RCS system heat-up rate, leading to small reductions in the SG tube failure margins.

A sensitivity run was performed to evaluate the effect of varying the control rod melting behavior. The conclusion was that the effects of uncertainties related to modeling severe accident control rod-related behavior (cladding failure, and melting and relocation of the absorber, cladding and guide tube materials) on SG tube failure margins are small.

A sensitivity run was performed with a significant variation in a parameter that affects the melting and relocation of the core fuel (the fraction of the phase-change heat that must be absorbed by the fuel for it to be considered in the molten state). The sensitivity evaluation concluded that the SG tube failure margins are insensitive to variations in the fuel damage progression behavior (including fuel melting, flow blockage, re-freezing and relocation) primarily because these occur after the time when the HL surge line and SG tube structural failures are experienced.

2.5 ACRS Review Meeting, 2004

A joint meeting of the ACRS Materials and Metallurgy and Thermal-Hydraulic Subcommittees (Reference 2.17) was held on February 3-4, 2004 to review the progress of the SGAP research. Presentations related to thermal-hydraulics covered both the CFD analysis and the SCDAP/RELAP5 systems analysis of plant response during SBO severe accident event sequences. The presentations on the SCDAP/RELAP5 analysis described the Westinghouse four-loop plant modeling and SBO base case calculation in Section 2.3 along with the results of the sensitivity analyses summarized in Section 2.4.

One ACRS concern with the SCDAP/RELAP5 modeling regarded the "SG power fraction" approach for adjusting the model to match a target value based on behavior indicated in Westinghouse one-seventh scale experiments (Reference 2.6) and in the CFD analyses. In the SCDAP/RELAP5 plant model at that time, flow loss coefficients in SG plenum regions were adjusted to attain a target value for the SG power fraction (in addition to target values for mixing fractions and the recirculation ratio, as defined in Section 3.4). The ACRS concern was that the SG power fraction should be an output variable produced by the systems analysis code and not a target parameter (experimentally derived or otherwise) that the input for the system analysis code is adjusted to attain. Because the heat deposited in the SG necessarily results from the transfer of energy from the RV to the SG through the HL, a SG power fraction modeling approach is similar to one in which the HL flow rate is adjusted in order to attain a specified SG power. In response to this ACRS comment, the SCDAP/RELAP5 plant model was subsequently revised such that the HL flows are determined using a target hot leg discharge coefficient that is based on CFD models for horizontal, countercurrent flow between the upper plenum and the steam generator inlet plenum. The approach using a target SG power fraction was therefore replaced by an approach in which the HL flow is determined using a more physically-based hot leg discharge coefficient. This revised modeling approach, which is described in Section 3.4, was employed for the analyses described in Section 2.8 and in all subsequent analyses described in this report.

A second ACRS concern with the SCDAP/RELAP5 analysis regarded the calculated loop seal behavior. Since clearing of water from a loop seal can lead to a flow of hot steam through the SGs in the direction of the normal loop flow and early failure of SG tubes, assurance is needed that the loop seal status is well represented by the system code. This issue is addressed through the SCDAP/RELAP5 code assessments provided in Section 3.2.1.

A third ACRS concern with the SCDAP/RELAP5 analysis regarded the calculation of the fluid circulation rates internal to the RV. This issue is addressed by sensitivity studies evaluating the effects of RV internal circulation rate variations as summarized in Sections 2.4 and 2.9.

Finally, the ACRS suggested that a means be provided to enhance understanding of the flows of heat from the reactor core, through the RV and into the coolant loops and SGs. An analysis of the flow of energy within and out of primary RCS is described in Section 2.8.

2.6 Analyses to Support PRA, 2004-2005

The SCDAP/RELAP5 Westinghouse four-loop plant model used for the analyses described in Sections 2.3 and 2.4 was upgraded and used to support a series of 43 SGAP PRA analyses that were performed in two sets of 20 and 23 runs each. The model upgrades are summarized as follows:

The SCDAP/RELAP5 plant model for the first 20 analyses was revised to improve the representation of the flow behavior in the region of the HL-to-pressurizer surge line connection. This side mounted surge line had been modeled in a manner such that steam flow only from the upper HL section entered the surge line during periods when the pressurizer relief valves were closed. CFD analyses indicated that during those periods flow is drawn equally from the upper and lower HL sections into a side mounted surge line and the SCDAP/RELAP5 connection modeling was modified to reflect that behavior. For the final 23 analyses the pressurizer surge line connection additionally was moved from the top to the side

of the HL (in some Westinghouse four-loop plants this connection is made on the top of the HL while in others it is made on the side of the HL).

Additional considerations of entrance effects were considered for the convective heat transfer coefficient in the hot leg. An average enhancement of the convective heat transfer is applied to the hot leg pipe to account for the fact that the flow is not fully developed. For the final 23 analyses, the SCDAP/RELAP5 plant model was revised to enhance the fully developed heat transfer coefficient calculated on the inside surfaces of the HL piping sections by approximately 50% to account for the average thermal entrance effects along the pipe. A single average multiplier is used for the entire hot leg due to limitations in the SCDAP/RELAP5 input model. It is noted that the entrance effects at the anticipated hot leg failure point are higher and a multiplier near 2.0 on the convective heat transfer coefficient is suggested in this region for use in multi-dimensional analysis of the hot leg.

For all 43 analyses the SCDAP/RELAP5 plant model was modified to independently represent the two pressurizer PORVs. Previously the two valves were lumped together in the model as there was no need to simulate independent operation. The change was made to support the PRA accident sequence simulations, some of which included the opening of only one valve.

Based on prior PRA analyses, the SBO base case accident scenario description was revised as follows:

Leakage from the SG secondary system based on a 3.2-cm² [0.5-in²] flow area per SG was added to the scenario description and the assumption that the PORV on the secondary system of the pressurizer-loop SG sticks open when first challenged was removed from the scenario description. Subsequent to this change, SCDAP/RELAP5 calculations show that all four SGs have completely depressurized by the time when the HL and pressurizer surge line structures fail.

An assumption of a typical lower-limit four-hour station battery life was added; previous analyses had assumed infinite battery life. The effect of this change is to consider both automatic and operator control functions over the pressurizer and SG secondary PORVs to be inoperable after four hours.

The 43 SCDAP/RELAP5 PRA support calculations were performed with the upgraded model to evaluate various combinations of assumptions regarding RCP shaft seal leakage, TDAFW operation, battery depletion time, SG secondary steam leakage and operator intervention. The PRA support analyses performed and the results are summarized in Appendix B. The key findings from these evaluations are summarized as follows.

For the first set of 20 runs the base case SG tube failure margins were found to be reduced as a result of the HL-to-surge line connection modeling revisions. During periods when the pressurizer relief valves are closed, the fluid entering the surge line in the new base case represented a mixture of hot steam drawn from the upper HL section and cool steam drawn from the lower HL section. The temperature of the steam entering the surge line in the revised base case calculation was therefore lower than in the prior base case calculation, where the flow was drawn only from the upper HL section. This difference delayed the surge line failure, but had very little effect on the HL and SG tube failure times. With this modeling change the HL failure was seen for the first time to precede the surge line failure, resulting in reduced SG tube

failure margins. For the second set of 23 runs, moving the pressurizer surge line connection from the top to the side of the HL resulted in still-lower temperatures for the steam entering the pressurizer surge line and even lower SG tube failure margins.

Operator actions to mitigate the SBO accident were generally seen to be effective. Opening one or both pressurizer PORVs either at the time when the core exit temperature reaches 922 K [1,200°F] or 12 minutes afterward were shown to accelerate failure of the HL, pressurizer surge line or RV lower head, thereby preventing containment bypass.

Event sequence assumptions leading to significant depressurizations of the RCS were seen to reduce the SG tube differential pressures, thereby preventing containment bypass. These assumptions included stuck-open pressurizer PORVs and RCP seal leak rates which increased from 1.32 L/s [21 gpm] to 11.3 L/s [180 gpm] and 30.2 L/s [480 gpm] per pump at 13 minutes.

The additional energy which is passed out of the RCS by assuming the RCP shaft seal leakage rate increases to 11.36 L/s [180 gpm] per pump at 13 minutes is seen to generally improve the SG tube failure margins over those where the leakage rate is assumed to remain at 1.32 L/s [21 gpm] per pump.

The assumption of SG secondary side steam leakage is seen to significantly reduce the SG tube failure margins compared with cases where no leakage is assumed. SG steam leakage into the turbine system leads to much lower SG secondary pressures and much less thermal coupling between the outside of the SG tube and the secondary-side steam. Both of these effects increase the potential for SG tube failure. No average or hottest SG tube failures are indicated (even for tube stress multipliers as high as 7.5) in the cases which assume zero SG steam leakage.

2.7 NRC and Consultant PIRT Evaluation and Peer Review, 2005

A Phenomena Identification and Ranking Table (PIRT) exercise was conducted in Rockville, Maryland on September 28-29, 2005 to discuss the thermal-hydraulic behavior associated with the analysis of PWR containment bypass (Reference 2.18). Participants in the PIRT included:

USNRC-RES – David Bessette

USNRC-NRR – Steve Long, Len Ward and Walt Jensen

USNRC Consultants – Marino DiMarzo and Peter Griffith

ISL, Inc. – Don Fletcher, Bill Arcieri, Robert Beaton and Vesselin Palazov

The PIRT exercise served to provide: (1) an independent technical review of the SCDAP/RELAP5 modeling and analysis approaches and (2) expert guidance regarding the dependent variables (figures of merit) and independent variables (important phenomena, processes and behavior) appropriate for an evaluation of the calculation uncertainties. The major technical review issues discussed at the meeting and identification of the parameters which the PIRT participants recommended for the uncertainty evaluation dependent and independent variables are summarized as follows.

2.7.1 Independent Technical Review Issues

The PIRT discussions uncovered modeling questions and uncertainties that were subsequently investigated, leading to SCDAP/RELAP5 plant model upgrades in several areas. These upgrades included: (1) adding a representation of the pressurizer spray system, (2) expanding

the core region axial nodalization from 10 to 40 nodes, (3) employing finer axial nodalizations for the fluid cells and heat structures in the vicinity of the SG tubesheet and (4) replacing the target SG power fraction used in the SG inlet plenum flow-loss adjustment method with a target hot leg discharge coefficient (as described in Section 3.4). The latter of these modeling changes also addressed the earlier comment by the ACRS regarding the unsuitability of using a target SG power fraction for that purpose (see Section 2.5).

2.7.2 Identification of Dependent Variables for the Uncertainty Evaluation

The dependent variables for the uncertainty evaluation are those for which it is desired to determine the uncertainties in the SCDAP/RELAP5-calculated results.

The PIRT participants recommended the dependent variables include the calculated output parameters that the project stress analysts investigating HL, pressurizer surge line and SG tube structural failures use as boundary conditions for their detailed analyses. These parameters are: (1) HL steam temperature, (2) HL piping wall inside-surface heat transfer coefficient, (3) pressurizer surge line steam temperature, (4) pressurizer surge line piping wall inside-surface heat transfer coefficient, and (5) SG tube metal temperatures.

The PIRT participants also acknowledged the importance for the regulatory decision-making process of the timing difference between the HL/surge line and SG tube structural failures and recommended that the SG tube failure margins also be included as dependent variables.

2.7.3 Identification of Independent Variables for the Uncertainty Evaluation

The independent variables for the uncertainty evaluation are those judged to have the most influential impact on the dependent variables.

The PIRT participants discussed a variety of issues related to the thermal-hydraulic response of the Westinghouse four-loop plant during SBO severe accidents and to the containment bypass issue. During the discussions, a list of recommended independent variables for the uncertainty evaluation, and their relative rankings, was developed by consensus view of the PIRT participants.

Regarding the rankings, a prime consideration of the participants was that items seen to similarly affect structural failure times in all three locations (i.e., the HL, surge line and SG tubes) should be considered of lower rank than those items seen to differently affect the three failure times. The latter set of items can logically be seen to have a greater effect on the SG tube failure margin because it has the greatest potential for influencing the *relative* failure times among the structures.

The group also decided to separate out those items that represent basic thermal-hydraulic processes from those items that instead represent event sequence assumptions or variations in the plant configuration.

Table 2.1 summarizes consensus opinions of the PIRT participants on the thermal-hydraulic phenomena, behavior, event sequence assumptions and plant configuration items that are expected to most significantly affect the dependent variables (temperatures, heat transfer coefficients and SG tube failure margins) for the uncertainty evaluation.

The table is separated into three sections. Section A, which includes items that differently affect the behavior at the three locations, represents the high-ranked items. Section B, which includes items that similarly affect the behavior at the three locations, represents the medium-ranked items. Section C includes low-ranked items that relate strictly to the event sequence assumptions or the plant configuration. Within each table section, the relative ranking of the items is indicated by the assigned number (for example, within Section A Item A1 is considered the highest ranked item while Item A5 is considered the lowest ranked item).

Table 2.1 Ranking Table of Items Important for the Containment Bypass Issue During SBO Severe Accident Scenarios in a Westinghouse Four-Loop PWR

Rank	Phenomenon	Location(s) Affected			Reasons for Ranking, Other Pertinent Notes and Comments
		HL	SL	SG Tube	
A1	Full loop circulation (loop seal clearing and reactor vessel lower plenum clearing)			X	Top-level accident sequence assumption is that all cold leg loop seals remained water-filled. Cleared loop seals induce steam circulation throughout the loops, increasing potential for tube failure. Binary parameter, all loop seals are either water-filled or not.
A2	Pressurizer Behavior (phase separation, PORV flow, CCFL & draining, spray nozzle venting)		X		Water draining from the pressurizer preferentially cools the hot steam in the surge line (SL) and a small amount of water helps to delay the SL failure. Timing of pressurizer draining relative to core heat up affects SL failure time and core degradation process. Pressurizer phase separation and relief valve flow inherently affects RCS pressure and RCS energy loss. Spray nozzle venting may affect pressurizer draining process.
A3	Mixing, SG inlet plenum			X	Critical to tube failure prediction, more important in CE plants than Westinghouse plants. May be able to use scatter in the Westinghouse 1/7-scale test data to estimate uncertainty in this parameter. Need to address effects on both hot tubes and average tubes.
A4	SG tube outer wall heat transfer (SG secondary side heat transfer)			X	Strongest potential to change timing of SG tube failure relative to the HL failure. Provides mitigating effect for SG tubes by removing the tube heat to the SG secondary fluid. Include tube sheet modeling effects in a sensitivity study. P. Griffith suggested +30% as a best guess regarding the SG tube outer wall heat transfer coefficient.

Table 2.1 Ranking Table of Items Important for the Containment Bypass Issue During SBO Severe Accident Scenarios in a Westinghouse Four-Loop PWR

Rank	Phenomenon	Location(s) Affected			Reasons for Ranking, Other Pertinent Notes and Comments
		HL	SL	SG Tube	
A5	Buoyancy-driven flows in SG tubes (ratio of SG tube flow to hot leg flow)			X	The SG tube flow directly affects the tube temperatures but only indirectly affects the HL and SL temperatures. The tube flow determines the energy entering the tube. The recirculation ratio using the three-cell inlet plenum model is adjusted to agree with the CFD analysis; its uncertainty is likely small. The hot leg flow model is being improved and will be more physically based.
B1	Core power, especially fuel rod cladding oxidation power	X	X	X	The hot gas generation due to oxidation drives the heat up process. In a sensitivity calculation, a large variation in the oxidation model was not seen to significantly affect the SG tube failure margin results. The hydrogen generation from oxidation affects vessel mixing, buoyancy, and feeds back into the oxidation rate. The hydrogen generation also affects transport of energy away from the core and the wall heat transfer. Hydrogen also affects SG inlet plenum mixing and CFD results may show mixing may help mitigate tube heat up. P. Griffith experiments indicate that hydrogen rapidly mixes with steam. Existing SCDAP/RELAP5 assessment cases may provide data regarding the expected uncertainties in the oxidation process.
B2	Buoyancy-driven flow in vessel (includes effects of vessel internal flow resistances)	X	X	X	The vessel internal flows directly affect the temperatures at the core exit and at the vessel-to-hot leg connections. These flows also affect the oxidation rate and are considered to be of medium importance. The prediction capability for the vessel internal flows was judged to probably be within a factor of two, suggesting that a range between 0.5 and 2.0 be investigated in the uncertainty study.
B3	Buoyancy-driven flow in hot legs	X	X	X	The elevation change within the hot leg provides a buoyancy effect. However, buoyancy in the SG tubes, where the elevation change is much larger, is judged to be the driver for the flow circulation processes.
B4	RCS heat loss to containment	X	X	X	The prior sensitivity study indicated that the SG tube failure margin is affected by the assumed heat loss. Affects the heat transfer processes for all three locations, but to different extents.

Table 2.1 Ranking Table of Items Important for the Containment Bypass Issue During SBO Severe Accident Scenarios in a Westinghouse Four-Loop PWR

Rank	Phenomenon	Location(s) Affected			Reasons for Ranking, Other Pertinent Notes and Comments
		HL	SL	SG Tube	
B5	Mixing at the vessel-to-hot leg connection	X	X	X	Not much mixing occurs at this location. Test data (W 1/7-scale experiments) shows that hot leg and upper plenum temperatures are about the same, indicating that the hot-steam regions are well-mixed. The cooler steam returning through the lower hot leg sections falls into the periphery of the core as it enters the vessel, so there is little interaction with the hot steam exiting the vessel into the upper hot leg sections.
C1	Operator intervention (event sequence definition item)		X		Operator intervention includes depressurization of SGs and opening of the pressurizer PORVs. Prior sensitivity study indicated the success of this mitigation strategy if it is performed in a timely manner. Effect of the operator intervention on the SG tube failure margins was significant.
C2	RC pump seal leakage (event sequence definition item)	X	X	X	This phenomenon affects the primary system pressure and RCS energy balance. Prior sensitivity study indicated that the influence on the SG tube failure margin increases as the assumed leakage rate increases.
C3	SG tube leakage (event sequence definition item)			X	This phenomenon draws additional steam into the SG tubes, decreasing their failure margin. Prior sensitivity study indicated a moderate influence of the tube leakage on the tube failure margin.
C4	Surge line orientation (plant configuration item)		X		The surge line-to-hot leg connection configuration varies from plant to plant. In the current Westinghouse plant model the connection is made on the side of the hot leg pipe, but in some plants the connection is instead made on the top of the hot leg pipe. Prior sensitivity calculations indicate a significantly earlier surge line failure when the surge line is connected on the top of the hot leg because much hotter steam is drawn into the surge line.

Table 2.1 Ranking Table of Items Important for the Containment Bypass Issue During SBO Severe Accident Scenarios in a Westinghouse Four-Loop PWR

Rank	Phenomenon	Location(s) Affected			Reasons for Ranking, Other Pertinent Notes and Comments
		HL	SL	SG Tube	
C5	Distribution of metal mass in the plant (plant configuration item)	X	X	X	The distribution of the metal structures (vessel walls, vessel internals and piping walls) within the plant directly affects the spread of hot steam from the core into the RCS. Large structures near the core, where the steam is the hottest, tend to absorb much heat, reducing the steam temperatures and heat deposited into heat structures that are more distant from the core. The recent energy balance analysis for the Westinghouse plant demonstrates this effect.

2.8 Revised Base Case Calculation and Evaluation of Primary Coolant System Energy Flow, 2006

A revised SCDAP/RELAP5 Westinghouse four-loop plant SBO base case calculation was performed to take advantage of modeling improvements and revisions to the accident scenario description resulting from the project activities through 2005. The revised base case calculation is documented in Reference 2.19. The revised model included all of the modeling upgrades described through Section 2.7. This base case calculation served to support the following important project activities by providing:

A reference case providing boundary conditions for detailed stress analyses related to the HL, pressurizer surge line and SG tube structures.

A reference case for an analysis performed to enhance understanding of the flows of heat from the reactor core, through the RV and into the coolant loops and SGs as requested by the ACRS in 2004 (see Section 2.5). The energy flow analysis performed for that purpose is documented in Appendix C.

A reference case for evaluating uncertainties in the SCDAP/RELAP5 containment bypass simulations, as described in Section 2.9.

A set of reference case results published for the purpose of a public review of the SCDAP/RELAP5 containment bypass analysis, in particular soliciting comments from the Electric Power Research Institute (EPRI). That public review is described in Section 2.10

The target SG inlet plenum mixing and flow parameters for the revised base case calculation were a hot leg discharge coefficient of 0.12, a recirculation ratio of 2.0, an inlet plenum mixing fraction of 0.85, a 41%/59% split of the SG tubes into hot/cold regions and a hottest tube with an inlet temperature based on a conservative NTR of 0.625.

The results of the revised SCDAP/RELAP5 Westinghouse four-loop plant SBO base case calculation indicated that a stress multiplier of 2.10 is required for the average SG tube to fail coincident with the HL failure. The calculation also indicated that the hottest SG tube fails 155 s prior to the HL, even when a stress multiplier of 1.0 is used, representing an undegraded tube strength condition. This average SG tube failure margin was smaller than seen in the prior base case analyses. Failure of the undegraded hottest tube prior to the HL also differed from the prior base case analyses which predicted it to fail after the HL. These reduced margins resulted from the combined effects of multiple modeling changes. In this respect the most important modeling changes implemented were judged to be (in decreasing order of importance):

Expansion of axial noding in the SG regions (especially the significant shortening of the first active tube axial node above the top of the tubesheet), which led to hotter SG tube metal temperatures and an earlier SG tube failure,

Revising from a SG power fraction target to a more physically-based hot leg discharge coefficient target in the model-adjustment procedure, which increased the HL flow rate and the SG heating rate, leading to an earlier SG tube failure, and

Moving the pressurizer surge line connection from the top to the side of the HL leg pipe, which lowered the temperature of steam entering the surge line and delayed the surge line failure, such that the HL failed prior to the surge line.

2.9 Evaluation of Uncertainties in SCDAP/RELAP5 Simulations, 2006

Analyses were performed to estimate the uncertainties in the SCDAP/RELAP5-calculated output for key parameters of importance for the containment bypass application. The key parameters (temperatures, heat transfer coefficients and SG tube failure margins), which represent the dependent variables for the uncertainty evaluation, were defined through the PIRT process and are listed in Section 2.7.2. The independent variables for the uncertainty study were also defined via the PIRT process and are discussed in Section 2.7.3 and summarized in Table 2.1. The SCDAP/RELAP5 Westinghouse four-loop plant SBO base case calculation described in Section 2.8 was used as the base case run for the uncertainty analysis.

Experimental data pertinent for evaluating the uncertainties in the SCDAP/RELAP5 results are generally unavailable due to the high-temperature nature of the containment bypass application. Instead, standard deviations representing the estimated uncertainties in the dependent variables were developed using a sensitivity-study method employing 19 sensitivity runs in addition to the base case run. The standard deviations were calculated through four different approaches, using equal-weighting and biased-weighting of the independent-variable contributions to uncertainty, and with and without consideration of the uncertainties in the means. The base-case values for the dependent variables, the evaluation times from the base case run and the standard deviations for the dependent variables are listed in Table 2.2.

Because many of the sensitivity studies performed for the uncertainty evaluation have additional uses and insights for the containment bypass project, the uncertainty evaluation is summarized in some detail in Appendix D. The uncertainty evaluation is fully documented in Reference 2.20.

Table 2.2 Base Case Values and Standard Deviations for the Dependent Variables

Dependent Variable	Evaluation Time for Base Case Value(s)	Base Case Value	Standard Deviation
Hottest SG Tube Failure Margin [1.0 Stress Multiplier Hottest Tube Failure Time – First Primary Piping Failure Time], s	Not Applicable	-155	54.89
Average SG Tube Failure Margin [Stress Multiplier for Tube Failure Coincident with First Primary Piping Failure], dimensionless	Not Applicable	2.10	0.234
Average SG Tube Wall Temperature, K	13,630	1021.7	20.93
Hottest SG Tube Wall Temperature, K	13,630	1239.6	34.50
Hot Leg Steam Temperature, K	13,517	1776.0	61.48

Table 2.2 Base Case Values and Standard Deviations for the Dependent Variables

Dependent Variable	Evaluation Time for Base Case Value(s)	Base Case Value	Standard Deviation
Hot Leg Wall Inside-Surface Heat Transfer Coefficient, W/m ² ·K	13,517	423.1	29.78
Pressurizer Surge Line Steam Temperature, K	13,517	1373.0	59.94
Pressurizer Surge Line Wall Inside-Surface Heat Transfer Coefficient, W/m ² ·K	13,517	490.9	66.15

2.10 Public Peer Review Meeting, 2007

A Category 2 NRC/EPRI public meeting (Reference 2.21) was held in Washington, DC on May 15, 2007 for the purpose of exchanging technical information on SG tube rupture during PWR severe accidents. A portion of the meeting was devoted to review of the 2006 SCDAP/RELAP5 Westinghouse four-loop PWR base case analysis described in Section 2.8 and the uncertainty evaluation described in Section 2.9. The discussions at the meeting related to the SCDAP/RELAP5 SBO analysis, subsequent evaluations and modeling considerations are summarized as follows.

EPRI indicated that in their analysis using the MAAP computer code (Reference 2.22) the steam-to-wall radiation heat transfer rate greatly exceeds the steam-to-wall convection heat transfer rate to the HL wall at the time when HL failure is predicted. This view differed from the SCDAP/RELAP5 SBO base case analysis described in Section 2.8, which indicated that the heat fluxes from those two processes are roughly the same at the time of HL failure.

Subsequent to the public meeting, the NRC and ISL evaluated the SCDAP/RELAP5 steam-to-wall radiation heat transfer modeling. These evaluations indicated that the emissivity calculated with the model deviated significantly from values for water vapor total emissivity under similar conditions that are reported in the published literature. For example, the model was found to significantly underpredict the emissivity results from Ferriso, Reference 2.23, for the high-pressure high-temperature fluid conditions in the large-diameter HL at the time of its predicted failure. One source of the discrepancy was found to relate to use of a model appropriate at small optical depth (the product of steam partial pressure and path length) at the large optical depth of the SBO HL application. However, the evaluation also uncovered other issues regarding the SCDAP/RELAP5 steam-to-wall thermal radiation modeling which suggested that the code was underpredicting the steam emissivity and steam-to-HL wall heat transfer rate for other reasons as well. Because of these discrepancies, the SCDAP/RELAP5 code was modified by implementing a new steam-to-wall thermal radiation heat transfer model as described in Section 3.1. The modified code version was used for the final SCDAP/RELAP5 SBO simulations that are presented Sections 4 and 5.

EPRI also questioned the validity for the target SG inlet plenum fluid mixing and flow parameters used in the SCDAP/RELAP5 analysis. Subsequent to the meeting, the NRC

re-evaluated its recommendations for the target values made on the basis of CFD calculations. This re-evaluation indicated that no significant changes are needed in the target values for the inlet plenum mixing fraction (0.85), recirculation ratio (2.0) and hot/cold SG tube split (41%/59%). However, the re-evaluation indicated that a reduction in the Normalized Temperature Ratio (NTR) from 0.625 to 0.5 would be more appropriate for a best-estimate model. (Definitions for these parameters are given in Section 3.4). This target NTR revision was implemented in the SCDAP/RELAP5 simulations presented in Sections 4 and 5.

EPRI indicated that the weakest point in the HL for creep rupture failure is at the safe end of the RV outlet nozzle, to which the stainless steel HL is welded. The nozzle safe end is constructed of carbon steel base metal, is clad with stainless steel, and is of approximately the same inner diameter and wall thickness as the HL. The SCDAP/RELAP5 Westinghouse four-loop plant model represents the HL piping using stainless steel structures. SCDAP/RELAP5 lacks the heat structure modeling capability (in particular, axial conduction) and creep rupture simulation capability that would be needed to fully analyze creep rupture within the complex RV nozzle configuration. A SCDAP/RELAP5 sensitivity calculation was performed in which the HLs are assumed to be fabricated entirely from carbon steel for the purpose of estimating the effect on the calculated SG tube failure margins resulting from considering a carbon steel RV nozzle material. This sensitivity evaluation, which is described in Appendix E, indicated that the average-tube and hottest-tube failure margins were significantly increased when a carbon steel HL material is used as compared to when a stainless steel HL material is used. Therefore, the SCDAP/RELAP5-calculated SG tube failure margins, based on solid stainless steel HLs, are expected to be conservative compared with the outcomes that are likely to be obtained from more detailed HL creep rupture failure analyses of the RV outlet nozzle configuration. (Unpublished preliminary detailed stress analyses of the prototype HL nozzle configuration by others in the project confirm the finding that the SCDAP/RELAP5-calculated failure margins based on the solid stainless steel HL structures are conservative.)

At the meeting, ISL's presentation (Reference 2.24) indicated that the expansion of axial nodalization for fluid regions and heat structures within, and just above, the tubesheet was a key factor leading to the reduced SG tube failure margins seen in the 2006 revised Westinghouse four-loop SBO base case calculation (see discussions in Sections 2.7.1 and 2.8). With the expanded axial nodalization the SG tube fluid cells and heat structures immediately above the top of the tubesheet have a length of 0.3048-m [1.0-ft]. Given the potential importance of axial modeling effects, the NRC requested that an estimate be made of the significance of heat conduction along the axis of the SG tube toward the tubesheet, which cannot be simulated with SCDAP/RELAP5. At issue is whether axial conduction might cool the tube structure for a considerable distance above the tubesheet and thereby provide for increased SG tube failure margins. The distance "x" above the tubesheet was calculated where the conduction heat transfer rate down the tube toward the tubesheet equals the radial conduction heat transfer rate through the tube over the height "x." Large values of "x" (relative to the 0.3048-m [1.0-ft] axial node height) therefore indicate that tube axial conduction effects are important while small values of "x" indicate that tube axial conduction effects are unimportant. SG tube temperature and heat flux data from the SBO base case SCDAP/RELAP5 run in Section 2.8 were used to calculate the value of "x." The results over the heat-up period from 9,000 s to 15,000 s indicate that the mean value of "x" is only 0.000823 m [0.00270 ft]. The effects of tube axial conduction are therefore significant over only the lower 0.27% of the first tube fluid cell and heat structure above the tubesheet, indicating that consideration of axial conduction would not significantly affect the SCDAP/RELAP5-calculated SG tube failure margins.

The background of thermal-hydraulic research into the containment bypass issue described in Sections 2.1 through 2.10 led to a best-estimate SCDAP/RELAP5 base case calculation for an extended SBO event sequence using a greatly-improved computer code and greatly-improved model of a Westinghouse four-loop plant. This best-estimate base case calculation (which is described in Section 4) indicates that SG tubes with undegraded strength properties and carrying both average-temperature and hottest-temperature steam fail subsequent to the HL (by 1,285 s and 360 s, respectively). The average-tube and hottest-tube failure margins (stress multipliers required for tube failure coincident with the HL failure) are 2.74 and 1.68, respectively. A final set of sensitivity evaluations was also performed using the improved code and model to categorize event sequence behavior relative to the occurrence of containment bypass. These sensitivity evaluations are described in Section 5.

The SCDAP/RELAP5 predictions described herein provide a conservative estimate of the relative induced failure times between the hot leg, surge line, and steam generator tubes. These calculations are intended to guide and support an analysis of the risk for severe accident induced steam generator tube failures. In addition to indicating the potential for tube failure, the predictions demonstrate the effectiveness of specific operator actions or safety systems in preventing induced tube failures. These predictions can also be used as boundary conditions for more detailed analyses of induced tube failures that would provide more realistic relative failure times. For instance, the SCDAP/RELAP5 model only considers tube failure within the first 12 inches of tubing above the tube sheet where the tube temperatures are highest. A consideration of tube flaws above this region in the tube bundle would delay the tube failures due to the reduction in temperature along the tube length. In addition, a more accurate treatment of entrance effects on the hot leg convective heat transfer and a multi-dimensional structural analysis of the hot leg that includes the carbon and stainless steel sections are both expected to lead to an earlier prediction of hot leg failure. These issues are beyond the scope of the current SCDAP/RELAP5 modeling effort. The SCDAP/RELAP5 predictions provide a conservative estimate of induced failure times and demonstrate the effectiveness of specific operator actions or safety systems in preventing induced tube failures.

3. DESCRIPTION OF ANALYSIS METHODS

A brief description of the SCDAP/RELAP5 severe accident thermal-hydraulics system code is provided in Section 3.1. Assessments of SCDAP/RELAP5 capabilities pertinent for the containment bypass application are provided in Section 3.2 for RELAP5 standard thermal-hydraulic models and in Section 3.3 for SCDAP severe accident models. Section 3.4 describes the SCDAP/RELAP5 model for the Westinghouse four-loop PWR for the containment bypass application, including a discussion of modeling aspects which have benefitted from updated CFD analyses.

3.1 SCDAP/RELAP5 Code Description

The calculations presented in this report were performed with SCDAP/RELAP5 Version 3.3de, which contains the SCDAP source taken from SCDAP/RELAP5/MOD3.3, Version 3.3ld.

The SCDAP/RELAP5 computer code (Reference 3.1) calculates the overall RCS thermal-hydraulic response for severe accident situations that include core damage progression and RV heat-up and damage. The computer code is the result of a merging of the RELAP5 and SCDAP computer codes.

RELAP5 models calculate the overall RCS thermal-hydraulics, control system interactions, reactor kinetics and the transport of non-condensable gases. The RELAP5 code is based on a two-fluid (liquid water and steam/noncondensable vapor mixture) model allowing for unequal temperatures and velocities of the fluids and for the flow of fluid through porous debris and around blockages caused by reactor core damage.

SCDAP models calculate the progression of damage in the reactor core, including the heat-up, oxidation and meltdown of fuel rods and control rods, ballooning and rupture of fuel rod cladding, release of fission products from fuel rods and the disintegration of fuel rods into porous debris and molten materials. A SCDAP model calculates the heat-up and structural damage of the RV lower head which results from the slumping of molten reactor core material with internal heat generation.

SCDAP models also calculate the creep rupture failure of structural components. Specifically important for this project is the calculation of creep failure for stainless steel, carbon steel and Inconel based on the creep rupture theory of Larson and Miller (Reference 3.2 and Reference 3.1, Volume 2, Section 12.0). The model allows one to specify a stress multiplier, whereby a multiplier of 1.0 provides a creep failure prediction for a structure with no material strength degradation, and multipliers greater than 1.0 may be used to represent conditions of degraded structural strength. For example, a stress multiplier of 2.0 may be used to represent a structure with degraded material strength such that creep rupture failure occurs when the applied stress is 50% of the stress required to fail the non-degraded structure. The structures, locations and stress multipliers used for creep rupture failure calculations in the SCDAP/RELAP5 Westinghouse four-loop plant model are described in Section 3.4.

It is noted that the SCDAP/RELAP5-calculated structural failure predictions are intended to be a screening tool for the occurrence of severe accident induced tube failures. Ultimately, best estimate failure timing predictions, especially for the RCS components, should be obtained from more accurate failure models that incorporate multi-dimensional effects such as multi-

dimensional heat conduction within structures and between connected structures, multi-dimensional boundary conditions, complex structural configurations (such as reactor vessel hot leg nozzles), and the influence of cladding on creep rupture failure of a base-metal structure.

For this application, the SCDAP/RELAP5 code was modified to represent thermal radiation heat transfer between the RCS fluid and the walls of the vessels, piping and SG tubes (see discussion in Section 2.10). The code calculates an effective heat transfer coefficient for fluid-to-wall radiation heat transfer and adds it to the existing convection heat transfer coefficient to calculate a single heat transfer coefficient representing a combination of the steam-to-wall thermal radiation and convection heat transfer processes.

The emissivity of steam is calculated using the method described in Section 6.4 of Reference 3.3. A table of steam emissivity at selected temperatures and optical depths is constructed using the following equation and the steam absorption coefficients, $k(\omega)$, given in Table A2-35 of Reference 3.3:

$$e(\Lambda, T) = \frac{1}{\sigma T^4} \int_0^{\infty} \frac{C_1 \omega^3}{e^{\frac{C_2 \omega}{T}} - 1} \left(1 - e^{-k(\omega) \frac{273}{T} \Lambda} \right) d\omega, \quad (1)$$

where,

T = temperature, K,

$C_1 = 3.747 \times 10^{-5}$ (erg-cm²) / s,

$C_2 = 1.4394$ cm-K,

$\sigma = 5.670 \times 10^{-5}$ erg / (s-cm²-K⁴),

$\Lambda = p \ell$, optical depth (steam partial pressure times beam length), atm-cm

$k(\omega)$ = steam absorption coefficient,

ω = wave number.

Figure 3.1 illustrates the steam emissivity obtained using this modeling approach.

In addition to steam-to-wall thermal radiation, the SCDAP/RELAP5 Westinghouse four-loop plant model described in Section 3.4 also contains wall-to-wall radiation network models consisting of the inner surfaces of the HL piping walls. The network models simulate radiation heat transfer from the hot piping walls in the upper HL sections to the cooler piping walls in the lower HL sections. The SCDAP/RELAP5 code was modified so that the network model accounts for the absorption of radiation by the intervening steam in the HL regions.

3.2 RELAP5 Assessments Pertinent for the Containment Bypass Application

Assessments of the RELAP code pertinent for the SCDAP/RELAP5 PWR containment bypass modeling application are described as follows.

3.2.1 Loop Seal Behavior

The status of the loop seals is a key behavior for the containment bypass application because it affects whether hot steam from the core exit is returned to the core inlet via continuous flow through the SGs, RCPs, cold legs and RV downcomer or returned to the RV upper plenum via the SG and hot-leg recirculation paths. Loop seal status refers to whether or not the cold leg loop seal flow paths and the flow path at the bottom of the RV downcomer core barrel, the "downcomer skirt," are predicted to remain water-plugged.

A wealth of assessments for RELAP5-based codes has been performed to address clearing of the cold leg loop seals, especially for small break loss-of-coolant accidents (SBLOCAs). A sampling of those assessments is provided below in this section. The physical processes associated with clearing of the downcomer skirt loop seal are the same as for the cold leg loop seals. A preferential pressurization of the region on the upstream side of the seal depresses the fluid level until it reaches the bottom elevation of the seal flow path, at which time steam flow through the seal begins. If the steam flow is sufficiently high, water may be cleared from the seal, in which case unimpeded steam flow through the path is allowed. It is noted that prediction of loop seal clearing for SBLOCAs using thermal-hydraulic systems codes such as SCDAP/RELAP5 involve uncertainties, especially regarding which loop seal (in a system composed of identical coolant loops) first experiences clearing and the number of loop seals which eventually clear.

Additional loop seal clearing uncertainties are also expected to result from the differences between the SBLOCA application and containment bypass application, for which pertinent loop seal clearing experiments suitable for code assessment are not available. For SBLOCAs, cold leg loop seal clearing results because the production of saturated steam in the reactor core preferentially pressurizes the upstream side of the loop seal until flow through the seals relieves the upstream overpressurization by allowing steam to reach the pipe break in the reactor coolant pump discharge cold leg. For the containment bypass severe accident application, the preferential upstream overpressurization is created not from steam production but instead by the extreme heating of the vapor residing in the reactor coolant system. The vapor heating results from the loss of the SGs as an adequate sink for the combined fission product decay and oxidation heats produced in the core. This heating produces dramatic reductions in the vapor densities and the pressurization is caused by the corresponding increases in vapor specific volumes.

From its inception in the early 1980's, the RELAP5 code was developed to represent the behavior of PWRs during SBLOCAs, for which loop seal clearing is also an important behavior. For cold leg SBLOCAs, the clearing of loop seals allows steam produced in the core to flow through the SGs and reach the break location. Therefore, assessments of RCS pressure and break flow behavior can be used to judge loop seal clearing behavior. RELAP5 loop-seal clearing capability was the subject of much early code assessment using experimental data from the Semiscale, LOFT, and other experimental facilities. Those early assessments resulted in improved simulation of loop seal clearing behavior through code improvements and development of user modeling guidelines for nodalization and code option selection. The RELAP5 code has been developed over the 25 years since those early assessments. In order to gain an updated picture of RELAP5 capabilities, the literature was searched for more recent assessments of its capabilities for predicting loop seal clearing. The following selected code assessments against experiments characterize those capabilities and indicate that SCDAP/RELAP5 can well simulate PWR SBLOCA loop seal clearing behavior.

ROSA-IV Test SB-CL-18

The ROSA-IV experimental facility (Reference 3.4) is a 1/48 volume-scaled, full-pressure, full-height representation of a 3423-MWt Westinghouse-type PWR. The four PWR coolant loops are represented with two equal-volume loops in the test facility. Components included in the loops of the test facility are the HL, SG, RCP, cold leg, pressurizer and emergency core coolant (ECC) systems. ROSA-IV Test SB-CL-18 represents a 5% 15.24-cm [6-in] equivalent diameter scaled break on the side of a cold leg with the reactor in full-power operation. The

high pressure injection (HPI) and AFW systems are assumed to fail. A loss of off-site power, resulting in tripping of all RCPs, is assumed to occur at the time of reactor scram.

A recent assessment for ROSA-IV Test SB-CL-18, performed for the NRC pressurized thermal shock evaluation using RELAP5/MOD3.2.2Gamma, is documented in Reference 3.5. Figure 3.2 compares the measured and calculated break mass flow responses from that assessment. When the loop seal clears, steam reaches the break location, greatly reducing the break mass flow rate. In the test the loop seal cleared at 140 s and this is closely matched by the 148-s RELAP5 calculated loop seal clearing time. The assessment indicates that the RELAP5 prediction of the loop seal clearing behavior in the experiment is excellent.

PMK-2 CAMP-CLB Experiment

The PMK-2 experimental facility (Reference 3.6) is a 1/2070 volume-scaled full-pressure representation of a VVER-440/213 six-loop PWR. Loop seals are employed in both the cold leg and HL. The six loops of the PWR are represented using a single loop in the test facility. PMK-2 Experiment CAMP-CLB represents a 2% cold leg SBLOCA with the reactor in full-power operation. The failure of the HPI system was assumed and a plant recovery operation involving depressurization of the SG secondary systems was simulated. A main objective of the test was to evaluate the effect of the HL loop seal behavior on the RCS flow, SG heat transfer and accumulator injection.

A recent assessment for the PMK-2 CAMP-CLB experiment using RELAP5/MOD3.2.2Gamma, is documented in Reference 3.7. Figures 3.3 and 3.4 compare the measured and calculated levels in the RV-side and SG-side of the hot-leg and cold-leg loop seals. The assessment judged that the RELAP5 prediction of the initial opening of the steam path through the HL loop seal due to partial clearing is very good. However, this event was not seen to lead to loop flow stagnation in the calculation as it did in the test and, as a result, the cold leg loop seal opened about 120 s earlier in the calculation than in the test. The assessment judged that simulating the behavior in this experiment is challenging for the code because of the partial clearing experienced in both the HL and cold leg loop seals. It was noted that flow and pressure oscillations caused by partial cold leg loop seal clearing had the effect of causing repeated core heat-up and quenching cycles in both the test and calculation. The assessment concluded that code prediction of the system parameters and (with the exceptions noted above) the loop seal behavior was in good agreement with the test data.

BETHSY SBLOCA Experiments

The BETHSY experimental facility is a full-pressure, full-height, 1/100 volume-scaled model of a 2,775 MWt Framatome PWR. The test rig includes three coolant loops, each of which contains a loop seal between the SG and RCP.

As reported in the summary of RELAP5/MOD3 independent code assessments (Reference 3.8), INEL evaluated the capabilities of RELAP5/MOD3 Version 7 for predicting two BETHSY small break LOCA experiments. Test 9.1b represented a 5.08-cm [2-in] cold leg break with HPI unavailable and Test 6.2TC represented a 15.2-cm [6-in] cold leg break with both high and low pressure injection systems unavailable. INEL concluded that the RELAP5/MOD3 simulations for these two tests showed reasonable agreement with the loop seal clearing behavior observed in the experiments.

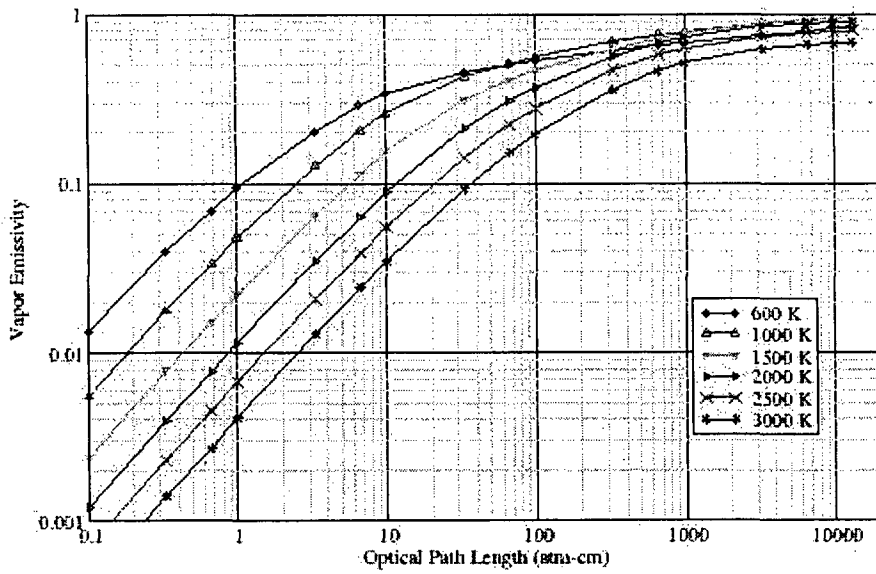


Figure 3.1 Steam Emissivity as a Function of Temperature and Optical Depth

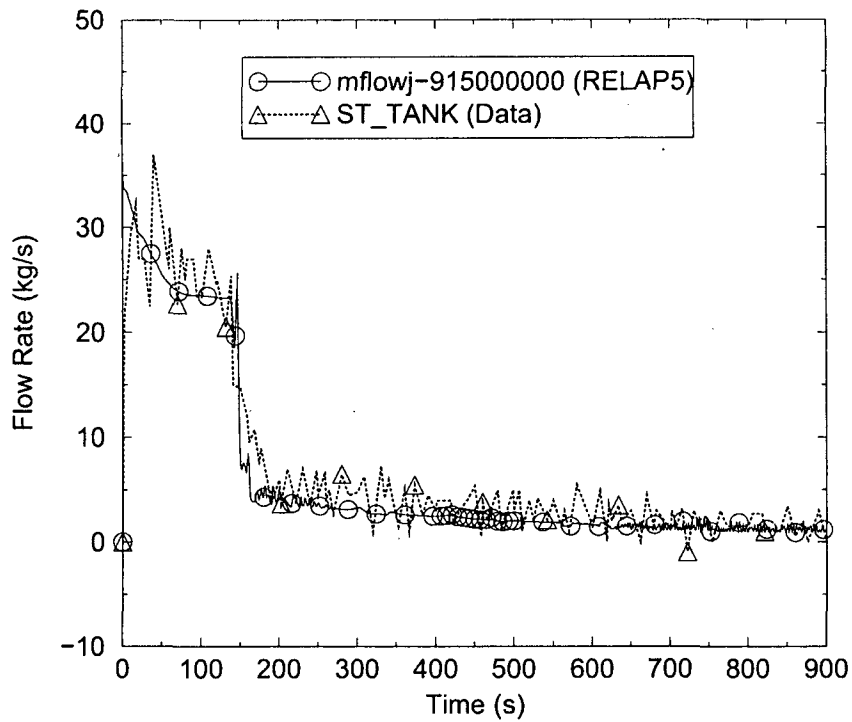


Figure 3.2 Break Flow for ROSA-IV Test SB-CL-18

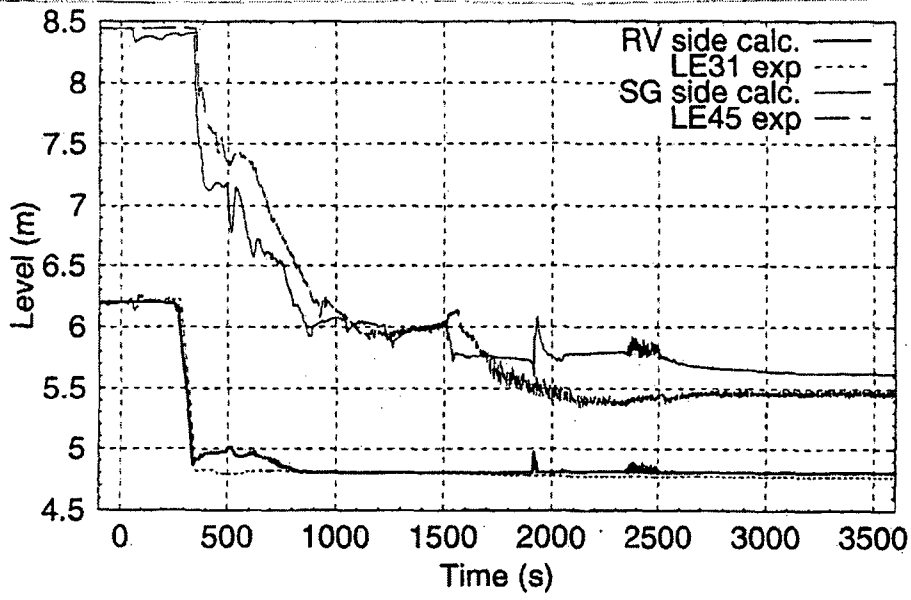


Figure 3.3 Hot Leg Loop Seal Collapsed Levels for the PMK CAMP-CLB Experiment

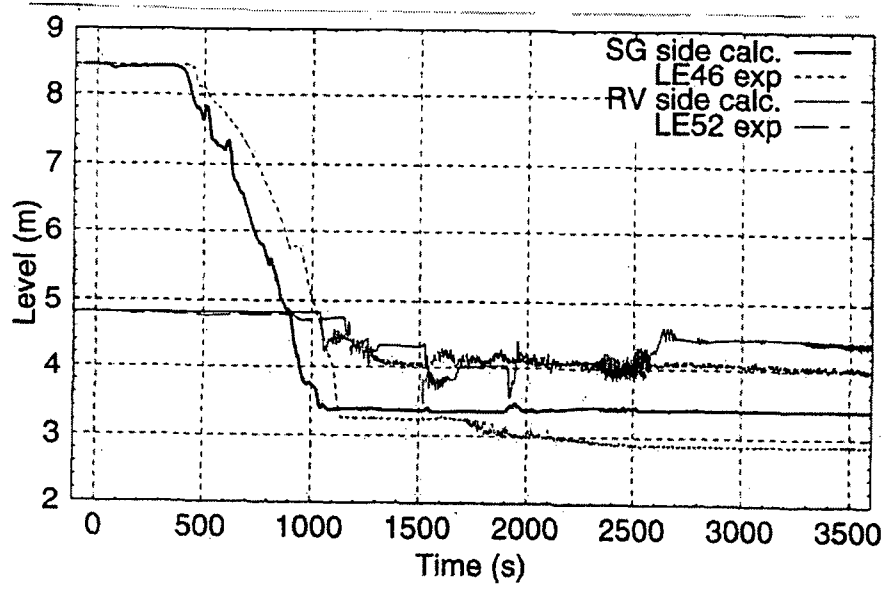


Figure 3.4 Cold Leg Loop Seal Collapsed Levels for the PMK CAMP-CLB Experiment

3.2.2 Pressurizer Filling, Draining and Relief Valve Behavior

Pressurizer behavior is key for the containment bypass application because it affects the distribution of water and steam within the RCS and the flow of mass and energy out of the RCS. Little change is seen in the pressurizer water inventory during the early portion of the SBO accident sequence, when heat is removed through the SGs. After the dry-out of the SGs, the water in the RCS is heated, increasing the RCS pressure and swelling up the water level in the pressurizer. The RCS pressure is relieved through the pressurizer PORVs and SRVs which are located on piping connected to the top of the pressurizer. The flow of energy through the relief valves is a major contributor to the RCS energy balance and the fluid mass exiting through the valves is afterward lost to the RCS. The pressurizer liquid inventory declines as a result of the fluid lost through the relief valves and as a result of draining of water through the surge line into the HL.

From its inception in the early 1980's, the RELAP5 code was developed to represent the behavior of PWRs during SBLOCAs, for which pressurizer draining, pressurizer filling and relief valve flow are important behavior. RELAP5 pressurizer behavior was therefore the subject of much early code assessment using experimental data from the Semiscale, LOFT, and other experimental facilities. Those early assessments resulted in improved simulation of pressurizer behavior through code improvements and development of user modeling guidelines for nodalization and code option selection. The RELAP5 code has been developed over the 25 years since those early assessments. In order to gain an updated picture of RELAP5 capabilities, the literature was searched for more recent assessments of its capabilities for predicting pressurizer behavior. The following code assessments against experiments characterize those capabilities and indicate that SCDAP/RELAP5 can well simulate PWR pressurizer behavior.

MIT Pressurizer Test ST4

Tests simulating a PWR pressurizer under inflow and outflow conditions were performed at the Massachusetts Institute of Technology (MIT), Reference 3.9. The MIT pressurizer was a small-scale, low-pressure representation of a PWR pressurizer. The vessel representing the pressurizer was 1.14-m [3.74-ft] tall with an inner diameter of 0.203 m [0.667 ft]. For Test ST4 the tank was initialized with a low level of saturated water at 0.493 MPa [71.5 psia] under quiescent conditions. Subcooled water was injected into the tank, increasing the water level at approximately 1 cm/s [0.394 in/s]. The steam in the upper part of the vessel was compressed. As the saturation temperature rose, the vessel walls became subcooled and film condensation occurred.

An assessment of RELAP5/MOD3.2.2Gamma against the ST4 test data, recently documented in Reference 3.5, concluded that the code well predicts the tank pressure, level, and vapor temperature seen in the experiment. Figure 3.5 shows good agreement between the measured and code-calculated tank pressures from that assessment, which indicates the code can well simulate the RCS pressurization experienced during the SBO event sequence following the loss of the SG heat sink.

APEX-CE-13

APEX-CE is a one-quarter height scale low-pressure integral systems experimental facility configured to model the thermal-hydraulic phenomena in PWRs of CE design. Test

APEX-CE-13 (Reference 3.10) simulates a stuck-open pressurizer SRV event that occurs with the reactor in full power operation. The valve was opened at the start of the test and the HPI system was subsequently activated. The valve was kept open for an hour and was then closed. The test was terminated about 20 minutes later, after the RCS had refilled.

An assessment of RELAP5/MOD3.2.2Gamma against the APEX-CE-13 test data, documented in Reference 3.5, indicated that the code well predicts the pressurizer pressure and level seen in the experiment. Figures 3.6 and 3.7, respectively, compare the measured and code-calculated RCS pressures and pressurizer levels from that assessment. The pressure comparison indicates that the energy flow out of the pressurizer relief valve is well simulated.

MIST Test 360499

MIST (Multi-loop Integral System Test) is a scaled, full-pressure experimental facility that represents a Babcock and Wilcox lowered-loop PWR with two HLs and four cold legs. The plant-to-test facility power scaling factor is 817 and the plant-to-test facility volume scaling factor is 620. Major components in MIST include two once-through steam generators with full-length tubes, two HL piping segments, four cold leg piping segments, four RCPs, a RV with an external downcomer, a pressurizer with spray and PORV connections and one core flood tank. Boundary systems provide simulation of the high and low pressure injection and emergency feedwater systems, and various types of failures such as SG tube ruptures and LOCAs. The configuration of the MIST facility is described in Reference 3.11.

Mist Test 360499, represents a HPI/pressurizer PORV feed-and-bleed cooling operation. At the beginning of the test, the MIST facility was operating at 110% scaled reactor coolant flow, 10% scaled power and an RCS pressure of 14.82 MPa [2,150 psia]. The feed-and-bleed operation was initiated by interrupting all feedwater flow and isolating the steam flow paths on both steam generators.

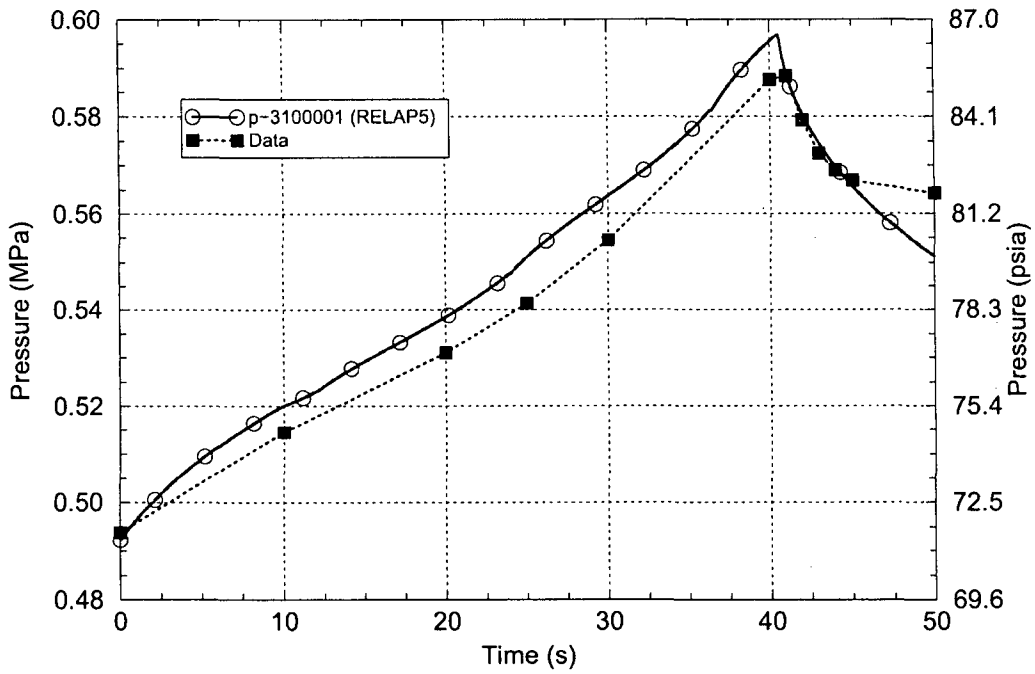


Figure 3.5 Pressurizer Level for MIT ST4 Pressurizer Insurge Experiment

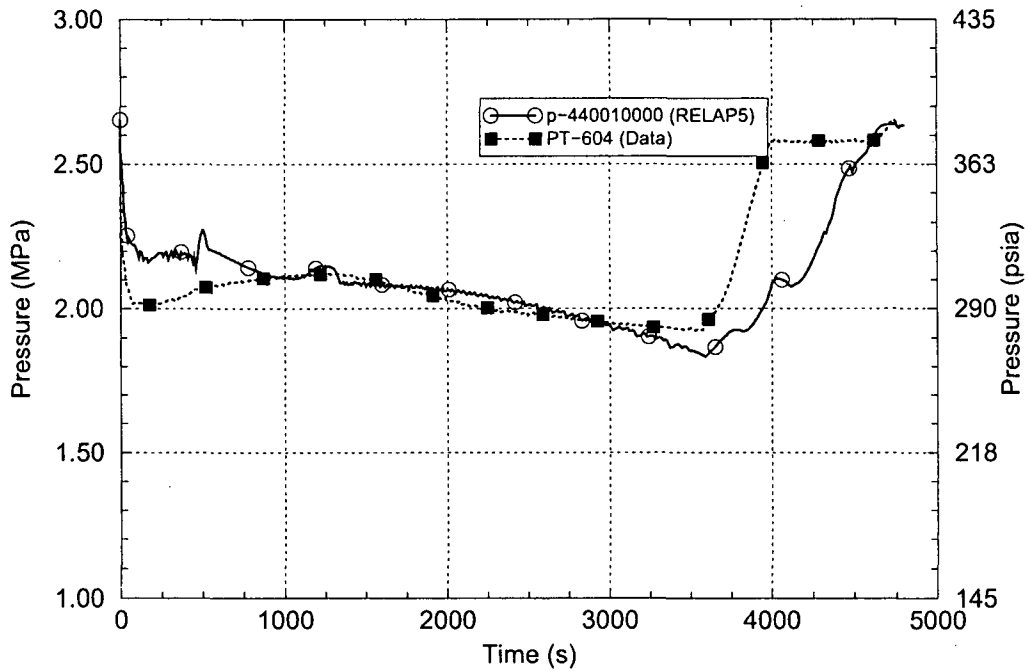


Figure 3.6 RCS Pressure for APEX-CE-13 Stuck-Open Pressurizer SRV Experiment

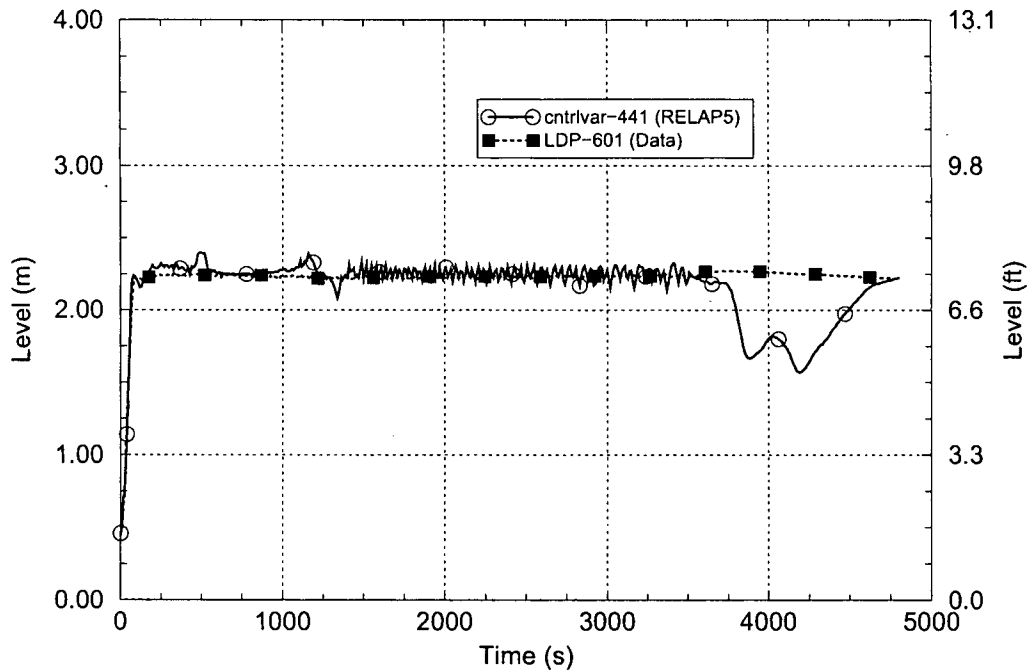


Figure 3.7 Pressurizer Level for APEX-CE-13 Stuck-Open Pressurizer SRV Experiment

An assessment of RELAP5/MOD3.2.2Gamma against the MIST 360499 test data, documented in Reference 3.5, indicated that the code well predicts the PORV flow and RCS pressure seen in the experiment. Figures 3.8 and 3.9, respectively, compare the measured and code-calculated PORV flows and RCS pressures from that assessment. The PORV flow comparison indicates that code simulation of the fluid drawn into the pressurizer and the phase separation within the tank are well simulated. The pressure comparison indicates that the energy flow out of the pressurizer relief valve is well simulated.

LOBI Test BT-56

The LOBI-MOD2 experimental facility is a high-pressure, 1/712-scale, two-loop representation of a 1,300-MWe, four-loop KWU PWR. Each loop in the test facility includes a HL, SG, crossover leg, RCP and cold leg. The pressurizer is connected to one of the loops.

LOBI Test BT-56 (Reference 3.12) was intended to represent a loss-of-feedwater event, but multiple unintended and inadvertent failures during the conduct of the experiment caused the test to represent a more challenging accident. In addition to a loss of feedwater, the test simulated a loss of pumped coolant loop flow, a delay in the reactor trip function and, as a result of the overpressurization, a loss of primary inventory due to the rupture of a pressure safety disk. As performed, Test BT-56 simulates many of the processes and behaviors expected during a PWR SBO severe accident, including the loss of all feedwater, loss of SG inventory, tripping of the RCPs, RCS overpressurization and RCS inventory depletion.

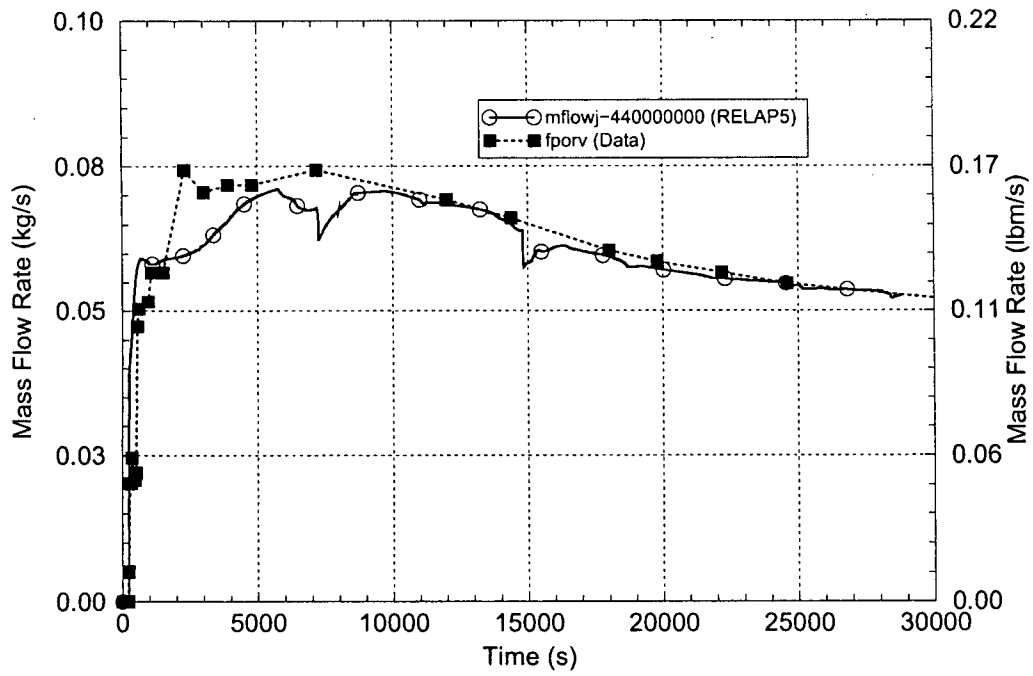


Figure 3.8 Pressurizer PORV Flow for MIST 360499 Feed-and-Bleed Cooling Experiment

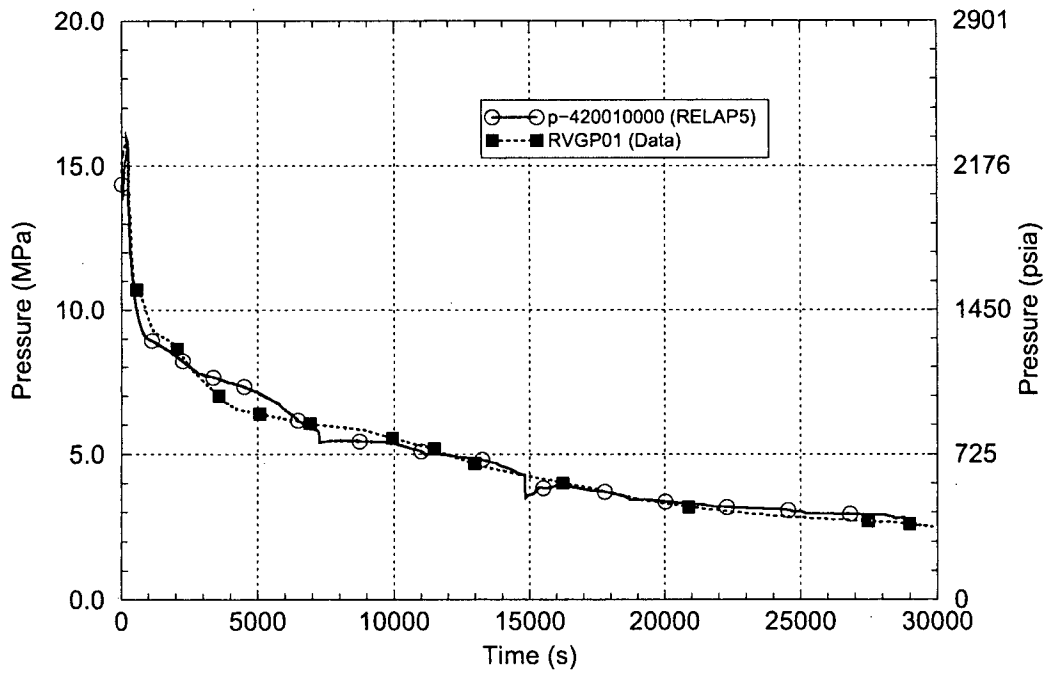


Figure 3.9 RCS Pressure for MIST 360499 Feed-and-Bleed Cooling Experiment

An assessment of RELAP5/MOD3.2 against the LOBI BT-56 test data, documented in Reference 3.13, indicated that the code well predicts the RCS pressure, pressurizer surge line flow and RCS inventory responses seen in the experiment. Figures 3.10, 3.11 and 3.12, respectively, compare the measured and code-calculated RCS pressures, pressurizer surge line volumetric flow rates and intact-loop cold leg fluid densities from that assessment. In these figures the test begins at 500 s, the pressure disk ruptures at ~518 s, the reactor trip occurs at ~524 s and the pressurizer empties at ~540 s. The assessment report indicated that the code well predicted the times for the pressure disk rupture and the emptying of the pressurizer.

The RCS pressure comparison indicates an excellent code simulation during both the pressurization and depressurization portions of the test sequence. The surge line flow comparison indicates good simulations of the flow rates into the pressurizer during the pressurization period and out of the pressurizer during the depressurization period. (Note that the instrument upon which the measured flow is based measures the rate but not the direction of the flow and that the RELAP5-calculated data is presented in the figure on the same basis). The cold leg density comparison indicates good agreement between the measured and calculated RCS inventories following the opening of the rupture disk and the draining of the pressurizer.

3.3 SCDAP Assessments Pertinent for the Containment Bypass Application

For the containment bypass base case event sequence application, the failure of the plant structures (HLs, pressurizer surge line and SG tubes) occurs relatively early in the core damage process. The RCS fluid temperatures rise rapidly and lead to the structural failures shortly after the time when the fuel rod cladding oxidation process peaks. For this reason, early-phase severe accident behavior (core boil-off and uncover, fuel rod heat-up, hydrogen production due to fuel rod cladding oxidation and fuel rod cladding ballooning and rupture) are the most pertinent for the containment bypass application. Late-phase severe accident behavior (fuel rod melting, the formation and re-freezing of porous debris, slumping and relocation of molten fuel and molten fuel-coolant interaction in the lower head of the RV) occurs subsequent to the critical time period (i.e., when the HL and pressurizer surge line structures are predicted to fail) in the base case accident sequence as well as in most of the other event sequences analyzed in this report.

A comprehensive assessment of SCDAP/MOD3.3 code capabilities for simulating PWR severe accident behavior is documented by INEL in Volume 5 of the code manual, Reference 3.1. The INEL SCDAP assessments related to the early-phase severe accident behavior are summarized as follows.

3.3.1 Models for PWR Fuel Assembly Heat-Up Behavior

Assessments of the SCDAP models for fuel rod heat-up were performed for situations of gradual core uncover using test data from the FLHT-5, PBF SFD ST and PBF SFD 1-1 experiments and for situations of complete core uncover using test data from the PBF SFD 1-4, CORA-5, CORA-7, CORA-13, PHEBUS-9+, and PHEBUS FPT0 experiments.

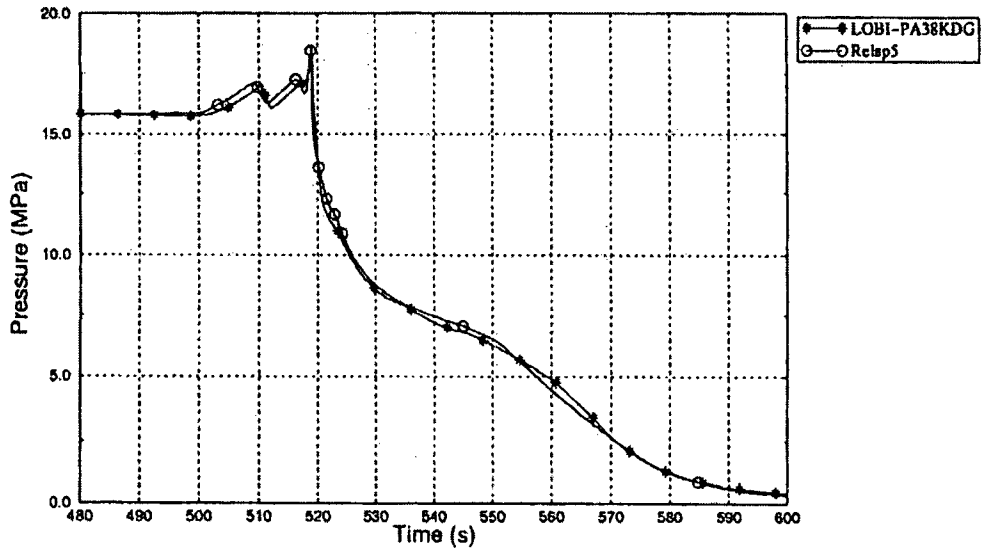


Figure 3.10 RCS Pressure for LOBI BT-56 Loss-of-Feedwater Experiment

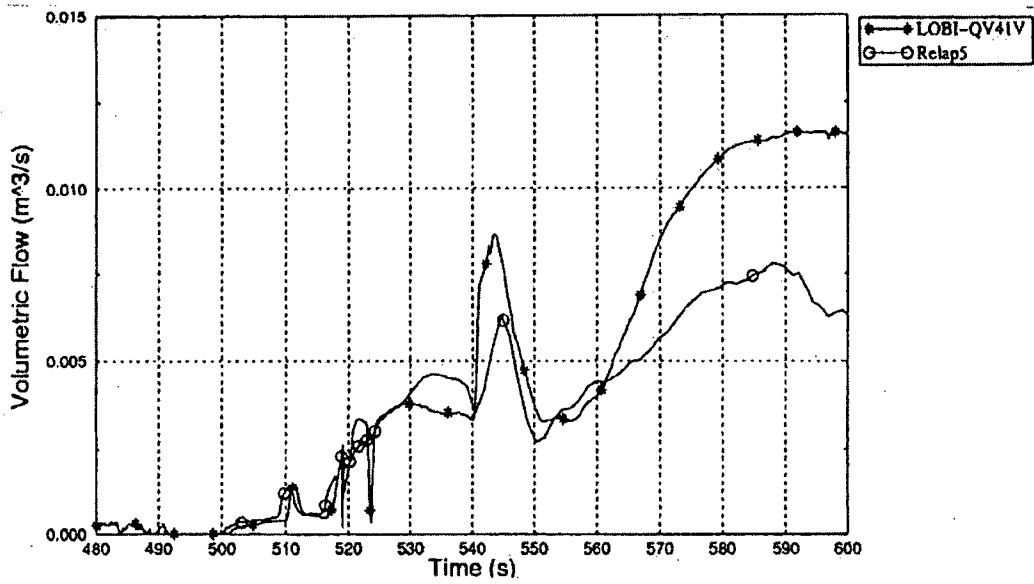


Figure 3.11 Pressurizer Surge Line Flow for LOBI BT-56 Loss-of-Feedwater Experiment

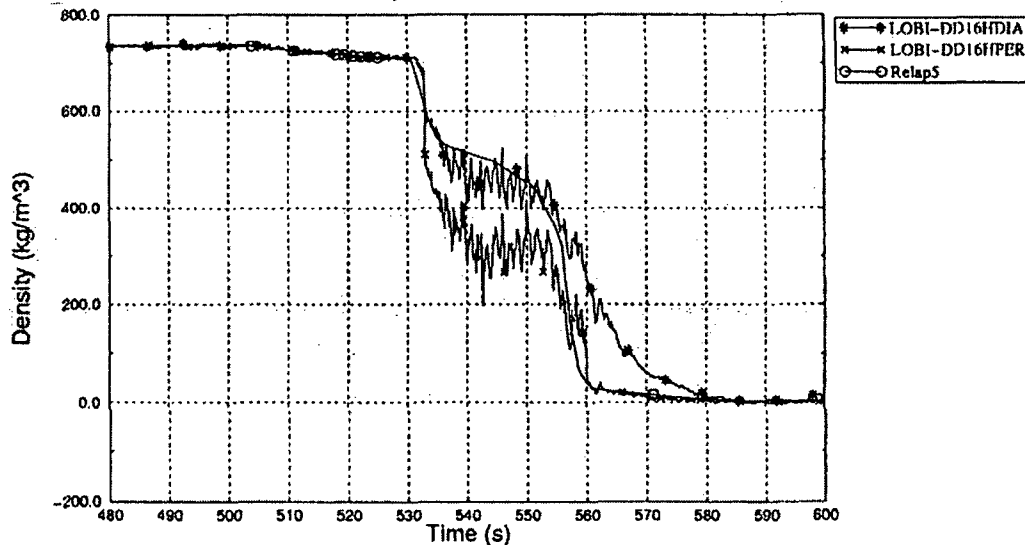


Figure 3.12 Intact Loop Cold Leg Density for LOBI BT-56 Loss-of-Feedwater Experiment

The assessment performed using data from the CORA-7 experiment is described as follows; assessment results for this test are representative of code capabilities for predicting the fuel rod heat-up behavior. The CORA test facility in Karlsruhe, Germany was designed to investigate core damage progression under severe accident conditions. The tests used bundles of electrically-heated and unheated 2-m [6.56-ft] fuel rods to simulate decay heating in a reactor core. CORA-7 was a 56-rod experiment with 32 electrically-heated rods, 19 fresh PWR-type fuel rods and five typical PWR silver-indium-cadmium control rods. The test was performed by powering the electrically-heated rods with argon flowing through the bundle. Superheated steam was added to the bundle, the power to the electrically-heated rods was increased and the test rig temperatures, pressures, flow rates and hydrogen generation rates were measured. Figure 3.13 compares the CORA-7 measured and SCDAP calculated fuel rod temperatures. The assessment concluded that the SCDAP-calculated behavior of the test fuel assembly is in good agreement with the measured behavior.

3.3.2 Models for Fuel Rod Cladding Oxidation

SCDAP capabilities for predicting hydrogen production due to oxidation of fuel rod cladding during severe accidents were assessed using data from nine severe accident experiments in five experimental facilities. Table 3.1 compares the measured and calculated total hydrogen production for the nine experiments. The calculated hydrogen production was less than the measured production for four tests, greater than the measured production for two tests and within the uncertainty in the measured hydrogen production for the other tests. The calculated hydrogen production among the assessment cases ranged from 50% too large to 15% too small. The assessment concluded that the calculated hydrogen production was generally in good agreement with measured test behavior.

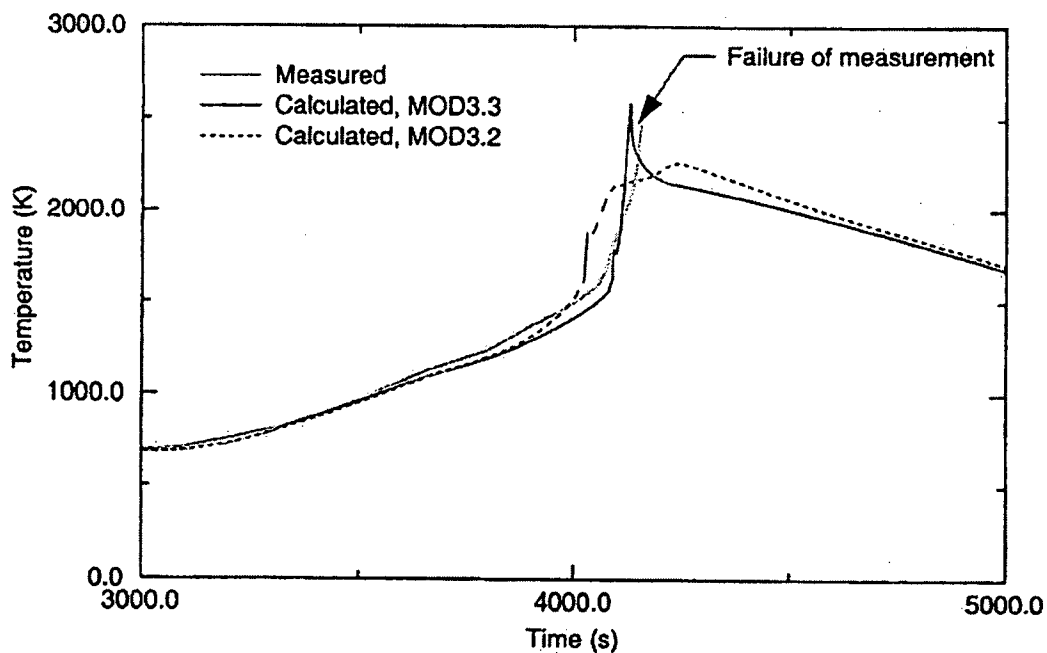


Figure 3.13 Fuel Rod Temperature at the 0.75-m Elevation for CORA-7 Test

Table 3.1 Summary of Measured and SCDAP-Calculated Hydrogen Production During Severe Accident Experiments

Experiment	Measured Total Hydrogen Production (g)	SCDAP/MOD3.3-Calculated Total Hydrogen Production (g)
FLHT-5	300 ±30	231
PBF SFD ST	150 ±35	125
PBF SFD 1-1	64 ±7	105
PBF SFD 1-4	86 ±12	82
CORA-7	114	91
CORA-13	161	158
PHEBUS B9+	39	46
PHEBUS FPT0	90	77
ACRR DF-4	40	29

3.3.3 Models for Fuel Rod Ballooning and Rupture

SCDAP capabilities for predicting fuel rod ballooning and rupture during severe accidents were assessed using data from five severe accident experiments in three experimental facilities. Table 3.2 compares the measured and calculated fuel rod rupture temperatures and rupture times for the five experiments. The calculated and measured rupture temperatures and times were in good agreement for three of the experiments. For the other two tests, PBF SFD 1-1 and PBF SFD 1-4, the calculated rupture times were significantly later or earlier than observed in the tests. The assessment concluded that there is potential for improving the SCDAP fuel rod ballooning and rupture code models.

Table 3.2 Summary of Measured and SCDAP-Calculated Fuel Rod Rupture Behavior During Severe Accident Experiments

Experiment	Measured Rupture Temperature (K)	Calculated Rupture Temperature (K)	Measured Rupture Time (s)	Calculated Rupture Time (s)
FLHT-5	1950	1900	1010	1230
PBF SFD ST	1150-1200	1050	5850-6260	6015-6385
PBF SFD 1-1	1538-1632	1785-1798	1150-1280	1785-1795
PBF SFD 1-4	1720-1900	1360-1530	1300-1600	1100-1150
PHEBUS FPT0	973	1060-1070	N/A	7350-7410

3.4 Description of SCDAP/RELAP5 Westinghouse Four-Loop Plant Model, Including Features Benefitting from Supporting CFD Analyses

The SCDAP/RELAP5 Westinghouse four-loop plant model represents the fluid volumes and structures in the core, RV and primary and secondary coolant system regions in the plant. The model also includes a simple representation of the containment. The final SCDAP/RELAP5 model is the culmination of model development and improvement activities spanning the period from 1998 through 2007. Those activities, and analysis results obtained with interim models that remain pertinent today, are summarized in Section 2. The SCDAP/RELAP5 modeling benefitted from ongoing CFD analyses carried out by the NRC staff. Reference 3.14 documents the updated NRC CFD evaluations. The SCDAP/RELAP5 predictions did not include all of the final recommendations from the CFD evaluations since the predictions were completed prior to the conclusion of the CFD work. However, the SCDAP/RELAP5 model is consistent with the most significant aspects of the CFD evaluations.

The nodalization diagrams for the final SCDAP/RELAP5 Westinghouse four-loop plant model are provided in Figures 3.14 through 3.17. In these diagrams, open areas typically represent fluid regions, arrows represent flow paths and shaded regions represent the structures of the model (such as fuel rods, vessel internals and piping walls). The reader is cautioned that for practical reasons the sub-structure of some components in the model cannot be accurately shown in these diagrams.

SCDAP/RELAP5 SBO accident calculations are performed in four sequential steps, which are described as follows.

In **Step 1** (steady state) the plant model using the RV nodalization in Figure 3.14 and the coolant loop nodalization for normal-operation water flow in Figure 3.15 is used to establish full-power steady-state conditions from which the SBO transient accident sequence is initiated. Figure 3.15 shows the nodalization for only one of the coolant loops; identical models are used for all four coolant loops (with the exception of the pressurizer and surge line, which are connected only on Loop 1).

In **Step 2** (time reset), the same model is used to perform a brief restart calculation for the purpose of resetting the problem time to zero at the start of the transient SBO accident sequence.

In **Step 3** (event initiation), the model continues using the nodalization schemes shown in Figures 3.14 and 3.15, but model features and changes are implemented to initiate the SBO accident sequence. These include: tripping of the reactor, turbine, main feedwater and RCPs and opening of the SG steam leakage and RCP shaft seal leakage paths. This model is run from the time of the SBO event initiation until the time when the core uncovers and superheated steam begins to enter the coolant loops.

In **Step 4** (post core uncover), significant modeling changes are made to permit the simulation of the two different coolant loop natural circulation modes shown in Figure 1.2. The mode shown on the right side of Figure 1.2 represents a countercurrent flow situation: hot steam is passed through the upper halves of the HLs to the SG inlet plenum where mixing occurs (resulting in a counter flow of hot and cool steam through the SG tubes) and cool steam is returned to the RV via counter flow through the lower halves of the HLs. The mode shown on the left side of Figure 1.2 represents a flow of steam from the RV upper plenum, through the HLs and completely around the coolant loop to the RV downcomer. The model selects the coolant loop circulation mode based upon whether or not the loop seal piping (between the SGs and the RCPs, see Component 116 in Figures 3.15 and 3.16) and the region at the bottom of the downcomer skirt in the RV (Cell 504-6, see Figure 3.14) remain filled with water, blocking the path for steam to flow from the SG outlet plenum through the RCPs, cold legs and the RV downcomer to the core inlet. The selection is made independently for each of the four coolant loops in the model. The model therefore is capable of representing both of the coolant loop flow behaviors shown in Figure 1.2.

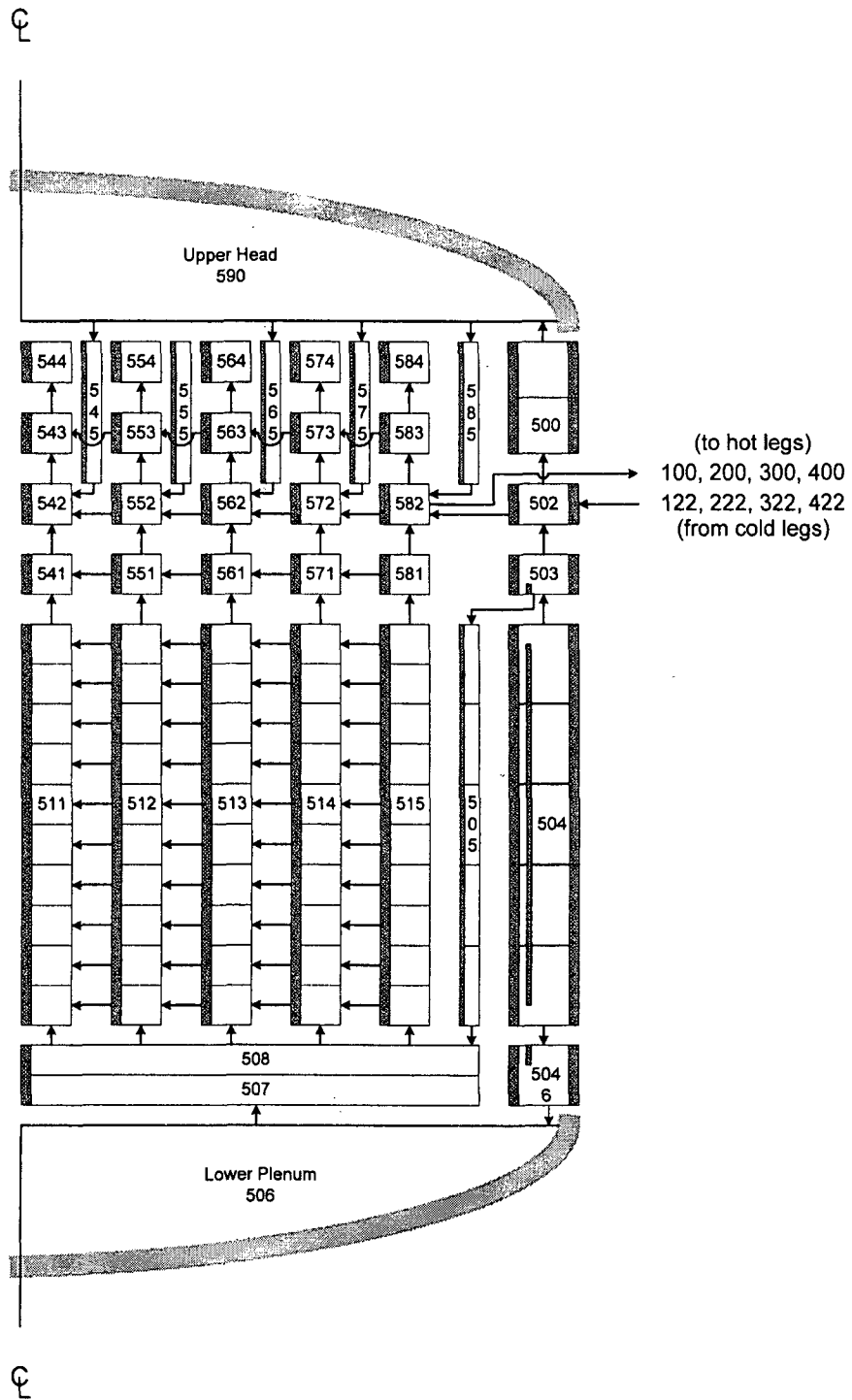


Figure 3.14 Reactor Vessel Nodalization

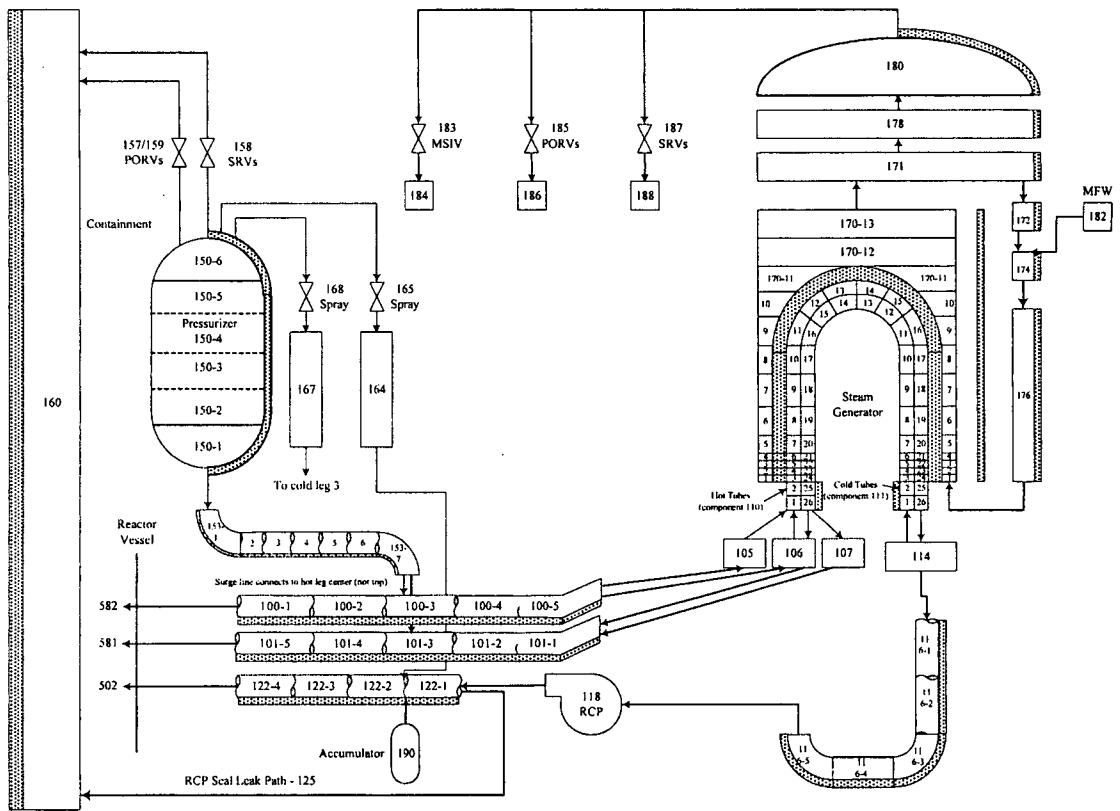


Figure 3.16 Coolant Loop Nodalization With Provisions for Countercurrent Natural Circulation

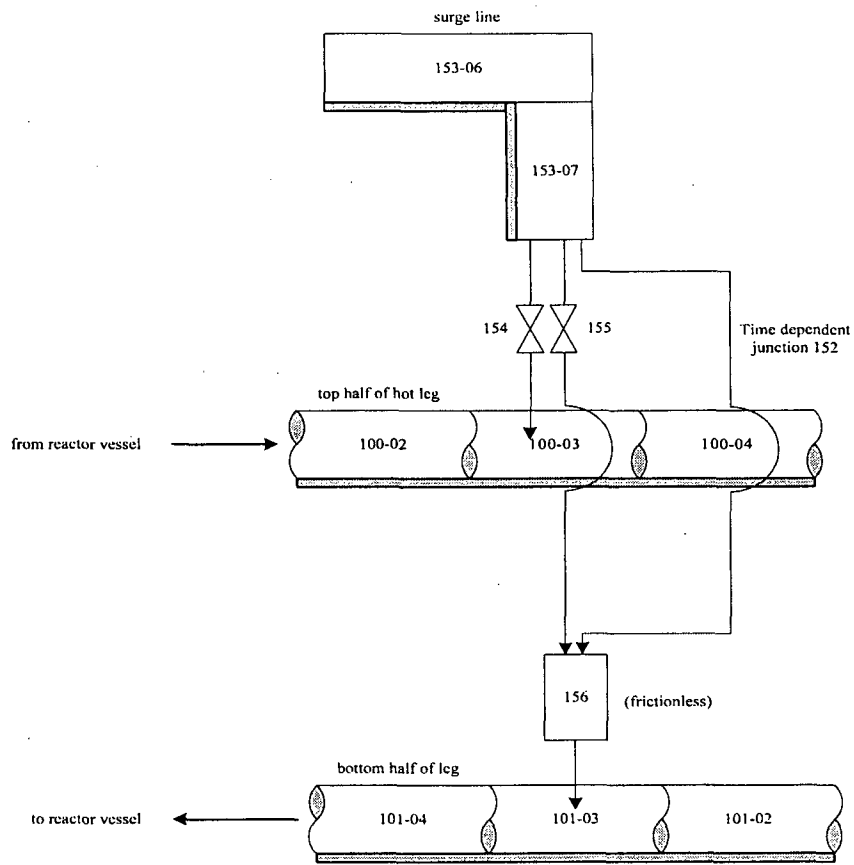


Figure 3.17 Surge Line Connections to the Split Hot Leg During Countercurrent Natural Circulation

The major features of the SCDAP/RELAP5 Westinghouse four-loop plant model are summarized as follows:

The RV is nodalized using five cross-connected, vertical flow channels as shown in Figure 3.14. The five reactor core region channels (511 through 515) represent a center-peaked radial power profile. Each channel is modeled using 40 axial cells. The RV upper plenum region is correspondingly modeled with five channels, four axial cells, and guide tube flow paths to the RV upper head region. Simpler nodalization schemes are used to model the lower plenum, upper head, core bypass and downcomer regions of the RV.

For calculation Steps 1 through 3 (i.e., up to the time when the core uncovers) the HLs are modeled using a single flow path with five axial cells as shown in Figure 3.15. The pressurizer surge line connects to the middle HL cell in Coolant Loop 1. The loop seals are modeled with five axial cells and the pump discharge cold legs are modeled with four axial cells. Connections are made to the coolant loop model representing the accumulator injection lines and the RCP shaft seal leakage. The pressurizer is represented with six axial cells and the pressurizer surge line is represented with seven axial cells. The spray lines and control valves are represented in the model, along with the pressurizer PORV and SRV pressure relief functions. RCS coolant flows lost through the RCP shaft seal leaks and through the pressurizer PORVs and SRVs are discharged into the containment, which is represented using a single hydrodynamic cell.

In the SGs, single cells represent the inlet plenum and outlet plenum. The active portion of the SG tubes is modeled using a single flow path with 22 axial cells. Each pass through the tubesheet is represented with two axial cells. Fine axial nodalization is used for the tube regions within the tubesheet and just above the upper surface of the tubesheet. The axial nodalization used in the SG secondary boiler region is consistent with that used for the SG tube primary-side flow path. Less complex nodalization is used to represent the SG separator, dryer, steam dome and downcomer regions. Connections to the SG secondary system are made to represent MFW flow, the main steam flow to the turbine, the SG PORV and SRV pressure relief functions, and the steam leakage. Heat losses to containment from the external walls of the primary and secondary reactor coolant systems are included in the model. For this purpose, the model uses a heat transfer coefficient on the external surfaces which provides a total heat loss to containment of 4 MW during normal full-power operation; this heat transfer coefficient is held constant throughout the steady state and transient accident calculations.

For calculation Step 4 (i.e., after the time when the core uncovers), the coolant loop models are switched to the nodalization shown in Figure 3.16. In this configuration the model uses two flow paths to represent the upper and lower HL sections, three cells (105, 106 and 107) to represent hot, mixing and cold SG inlet plenum regions and two flow paths to represent forward-flowing and reverse-flowing groups of SG tubes. Model discretization in the axial direction is not changed between calculation Steps 3 and 4. The HLs are split into two equal-area flow paths and the lower sections of the four HLs connect to RV upper plenum Cell 581, see Figure 3.14.

The pressurizer surge line connects on the side of the HL (in some plants, this connection is instead made on the top of the HL). Figure 3.17 shows the HL-to-surge line connection scheme employed for joining the surge line to the upper and lower HL sections. The NRC performed CFD evaluations (Reference 3.14) of the behavior at this connection following the time when the water has been drained out of the pressurizer. The evaluations indicated that the flow into a side mounted surge line is drawn equally from the upper and lower HL regions during periods when the pressurizer PORVs are closed. The valve and flow boundary conditions employed at

this connection allow the SCDAP/RELAP5 model to match the behavior seen in the CFD calculations.

To represent thermal radiation heat transfer from the superheated steam encountered during calculation Step 4, the steam-to-wall radiation heat transfer model described in Section 3.1 was generally activated for surfaces representing the interior boundaries of the primary and secondary coolant systems in the plant model. The model was activated at the interior surfaces of heat structures representing the RV, HLs, pressurizer, pressurizer surge line, cold legs, SG inlet plenum, SG outlet plenum, tubesheet and SG shell. The model was also activated on the inner surfaces but not on the outer surfaces of the SG tubes. For the outer SG tube surfaces, it was judged that thermal radiation heat transfer within the tight tube bundle configuration could not be well represented, given the limitations imposed by the coarse SCDAP/RELAP5 SG tube and secondary-side model nodalizations.

Because the temperatures of steam carried by the upper and lower HL sections are very different, radiation enclosure (network) models were also included to represent wall-to-wall thermal radiation processes involving the HL piping walls connected to the upper and lower HL sections.

The SCDAP/RELAP5 code does not have models capable of calculating from first principles the fluid mixing behavior in the SG inlet plenum region and the resulting circulating flows in the split HL and split SG tube flow paths during calculation Step 4. Instead, the SCDAP/RELAP5 system model analyses are performed by incorporating flow resistance adjustments in the SG inlet plenum region for the purpose of matching target values for the HL flow and SG inlet plenum fluid mixing parameters.

Reference 3.15 describes experiments conducted for the purpose of evaluating buoyancy-driven flows through horizontal ducts connecting two tanks containing fluids of different densities. The experiments correlate the volumetric flow rate (Q) in the horizontal duct, the average fluid density (ρ) and the difference between the two tank fluid densities ($\Delta\rho$) using a discharge coefficient (C_D):

$$Q = C_D [g (\Delta\rho / \rho) D^5]^{1/2}$$

where g is the acceleration due to gravity.

The HL in the Westinghouse plant is analogous to the horizontal duct in the experiments, the RV and SG inlet plenum in the plant are analogous to the two tanks in the experiments, and the discharge coefficient characterizes the HL flow in the plant. CFD analyses (Reference 3.14) using the geometry of interest for the plant were performed to define a target C_D for this specific SCDAP/RELAP5 plant model.

SG inlet plenum fluid mixing parameters were defined based on the flow paths observed in a set of Westinghouse one-seventh scale experiments (Reference 3.16). The hot mixing fraction is defined as the fraction of the upper HL section flow that is directed to the mixing region of the SG inlet plenum (i.e., from Cell 100-5 to Cell 106 in Figure 3.16). Similarly, the cold mixing fraction is defined as the fraction of the cold return SG tube flow that is directed to the mixing region of the SG inlet plenum (i.e., from Cell 111-26 to Cell 106 in Figure 3.16). The recirculation ratio is defined as the ratio of the flows circulating through the hot and cold SG tubes to the flows circulating in the upper and lower HL sections.

CFD analyses were performed to extend the experimental results to full scale conditions in the HL, SG inlet plenum and SG tube regions of a Westinghouse plant during a SBO event. This initial CFD analyses resulted in the following recommendations for the target mixing parameters for use in the SCDAP/RELAP5 system analyses:

SG Tubes in Hot / Cold Regions: 41% / 59%
Hot Leg $C_D = 0.12$
Hot Mixing Fraction = 0.85
Cold Mixing Fraction = 0.85
Recirculation Ratio = 2.0

During calculation Step 4, the hydrodynamic cells and heat structures in the SG model are reconfigured to represent the desired 41%/59% split of the unplugged SG tubes into hot average (forward-flowing) and cold average (reverse-flowing) regions. Ten percent of the tubes in each SG are assumed to be plugged. The SCDAP/RELAP5 flow coefficients in the inlet plenum regions of the four SGs are adjusted to achieve the above target values for hot leg C_D , hot and cold mixing fractions and recirculation ratio. Once the flow coefficients needed to attain the desired target mixing parameter values have been determined, they are held constant throughout calculation Step 4. An identical set of flow coefficients is used in each of the four SGs in the model.

In addition to the hot average and cold average SG tube regions, during calculation Step 4 a representation for a hottest tube is added to the SG model in the pressurizer loop. (Due to the pressurizer relief valve flows, hot steam is drawn into the pressurizer loop HL at a higher rate than in the other loops and this places the most challenging tube conditions in the pressurizer-loop SG). The hottest tube model uses a normalized temperature ratio (NTR) to characterize the temperature of the fluid entering the hottest tube. The NTR relates the difference between the hottest SG tube inlet fluid temperature and the cold average (reverse-flowing) SG tube outlet fluid temperature to the maximum expected temperature difference (between the upper HL section outlet and cold average SG tube outlet fluid temperatures):

$$NTR = (T_{\text{hottest tube}} - T_{\text{cold tube}}) / (T_{\text{hot leg}} - T_{\text{cold tube}})$$

Experimental data from the Westinghouse one-seventh scale experiments (Reference 3.16) and CFD evaluations are used to select the NTR. The SCDAP/RELAP5 Westinghouse four-loop plant SBO base case calculation in Section 4 assumes a NTR of 0.5 as recommended in Reference 3.14. (Other values for NTR have also been investigated, see Sections 2.3 and 2.8.) The hottest tube model represents a single tube from the bottom of the tubesheet to the top of the tube U-bend and uses axial nodalization consistent with that used in the average tube model. The hydraulics for the primary side of the hottest tube model are based on an inlet fluid temperature calculated via the NTR, inlet fluid conditions and inlet velocity that are otherwise consistent with the hot average tube model, and an outlet pressure consistent with the pressure at the top of the U-bend of the hot average tube model. On the secondary side, the heat structure representing the hot average tube is connected to the same SG boiler-region fluid cells as the hot average tube model.

In the Westinghouse four-loop plant model, creep rupture failure calculations are performed for the hot average SG tubes (at the inlet, just above the tubesheet), for the upper HL piping sections (at the RV end) in all four coolant loops, for the pressurizer surge line (at the HL end) and for the hottest tube in the pressurizer-loop SG (at the inlet, just above the tubesheet). A stress multiplier of 1.0 is used for the HL and surge line structure calculations while stress

multipliers from 1.0 to 7.5 in increments of 0.5 are used for the SG tube calculations. The range of stress multipliers evaluated for the SG tubes allows comparison of failure times for tubes with varying degrees of strength degradation. See Section 3.1 for a description of the creep rupture model and the definition of the stress multiplier. The principal outcomes from the SCDAP/RELAP5 analysis are the HL, pressurizer surge line and SG tube structure failure times and the SG tube failure margins for the hot average tube and hottest tube. These margins are expressed as the tube stress multiplier (i.e., the extent of strength degradation) required for tube failure to occur concurrently with the earlier of HL or pressurizer surge line failure.

4. WESTINGHOUSE FOUR-LOOP PLANT STATION BLACKOUT BASE CASE ANALYSIS

The SCDAP/RELAP5 simulation for the base case extended SBO event sequence in a Westinghouse four-loop PWR is presented in this section. The base case SBO accident event sequence assumptions are described in Section 1.2 and a summary of the expected overall plant behavior during the event sequence is given in Section 1.3. Definitions for the SG tube failure margins and criteria for judging the containment bypass outcome are given in Section 1.4. The SCDAP/RELAP5 computer code is described in Section 3.1 and assessments of the code pertinent for the containment bypass application are described in Sections 3.2 and 3.3. The SCDAP/RELAP5 Westinghouse four-loop plant model used for this base case calculation is described in Section 3.4. The SCDAP/RELAP5 simulation results for steady full-power plant operation, from which the transient SBO event sequence begins, are given in Section 4.1 and the SCDAP/RELAP5 simulation results for the transient base case SBO event sequence are given in Section 4.2.

4.1 Full-Power Steady State Calculation

The SCDAP/RELAP5 plant model was run to a steady solution. For reference, the file name of the input model for the steady-state run is "wnewbases1.i". The file name of a short SCDAP/RELAP5 restart calculation from the end point of the steady-state run (to reset the problem time to zero) is "wnewbases2.i". These are Steps 1 and 2 of the sequential four-step modeling process described in Section 3.4.

Table 4.1 compares the SCDAP/RELAP5-calculated steady state conditions with target values for a typical Westinghouse four-loop plant in normal full-power operation. The comparisons show that the code-calculated parameters are in excellent agreement with the target values. The calculated steady state solution therefore represents an acceptable set of initial conditions from which to start the SCDAP/RELAP5 transient SBO base case accident simulation.

Table 4.1 SCDAP/RELAP5 Full-Power Steady State Results

Parameter	Target Value ^a	SCDAP/RELAP5 Calculated Value
Reactor power (MW _t)	3,250	3,250
Pressurizer pressure (MPa)	15.51	15.509
Pressurizer water/steam volume (%)	60/40	61.2/38.8
Total RCS coolant loop flow rate (kg/s)	17,010	17,010
Cold leg temperature (K)	549.9	549.90
Hot leg temperature (K)	585.5	585.45
SG secondary pressure (MPa)	4.964	4.892
Feedwater temperature (K)	493.5	493.48
Steam flow rate per SG (kg/s)	440.9	439.9
Liquid volume per SG (m ³)	52.05	52.66

a. Target values are based on information for a typical Westinghouse four-loop PWR with 10% SG tube plugging.

4.2 Transient Station Blackout Calculation

The SBO base case event sequence was simulated with SCDAP/RELAP5, starting from time zero when the loss of off-site power occurs. The transient simulation is performed as Steps 3 and 4 of the four-step modeling process described in Section 3.4. For reference, the file name of the Step 3 input model, which is used up to the time of core uncovering, is "wnewbases3.i". The file name of the Step 4 input model, which implements the split HL and SG tube modeling features used after the time of core uncovering, is "wnewbases4.i".

Table 4.2 shows the SCDAP/RELAP5 calculated sequence of events for the base case SBO simulation. The calculated time-history results for key parameters are shown in Figures 4.1 through 4.22 and are summarized as follows.

The RCS pressure response is shown in Figure 4.1. After a short period when the RCS pressure initially falls and rises slightly due to the effects of the reactor and turbine trips, the RCS pressure declines in response to the cooling provided by heat removed to the SGs, the flow of coolant out of the RCS through the RCP shaft seal leaks and the RCS heat loss to containment. Figure 4.2 shows the SG secondary pressure responses and Figure 4.3 shows the RCP shaft seal leak flow responses. The RCS depressurization continues until the SG secondary liquid inventories, shown in Figure 4.4, have been boiled and discharged to the atmosphere through the SG PORVs. After the SG heat sink is lost, the cooling afforded by system heat loss to containment and RCP shaft seal leak flow is insufficient to remove the RCS heat load, causing the RCS pressure to increase as shown in Figure 4.1 to the opening setpoint pressures of the pressurizer PORVs and SRVs.

Figures 4.5 and 4.6, respectively, show the pressurizer PORV and pressurizer SRV flows. After SG dry-out, the RCS pressure increase is limited by multiple cycling of the PORVs and by two cycles of the SRVs during the period with the most-challenging RCS pressurization conditions. This challenge is presented when the increasing temperatures cause the RCS fluid to swell, completely filling the pressurizer with water. The pressurizer level response is shown in Figure 4.7.

The RCS fluid mass lost through the pressurizer PORVs and SRVs and through the RCP shaft seal leakage paths depletes the RCS inventory, the core uncovers and superheated steam flows out from the RV into the coolant loops starting at 9,226 s. Water remains trapped in the cold leg RCP-suction loop seal piping of the RCS, thus blocking the paths for the steam to flow all the way around the coolant loops to the RV inlet nozzles. This blockage is a necessary condition for setting up of the countercurrent flows through the HLs and SG tubes. Figure 4.8 shows the void fractions calculated in the bottom cells of the loop seal piping. The piping at the bottom of the loop seals in all four coolant loops remains virtually water filled, with only minor bubbling of steam through the loop seals seen during the period of the maximum RCS pressurization.

Following core uncover, countercurrent flow of superheated steam is calculated through two circulation flow paths within each of the four coolant loops. In one circulation path, hot steam flows upward from the SG inlet plenum through a portion (41%) of the unplugged SG tubes and cool steam returns from the SG outlet plenum through the remaining portion (59%) of the unplugged SG tubes, flowing downward as it reaches the SG inlet plenum. In the other circulation path, hot steam flows through the RV outlet nozzle and upper half of the HL to the SG inlet plenum and cooler steam is returned from the SG inlet plenum to the RV outlet nozzle through the lower half of the HL. Mixing between these two circulation flow paths occurs in the

Table 4.2 Sequence of Events from the SCDAP/RELAP5 SBO Base Case Calculation

Event Description	Event Time (s)
SBO event initiation (loss of AC power, reactor trip, turbine trip, MFW flow stops, RCPs trip, RCP shaft seal leaks begin, SG steam leaks begin).	0
RCP rotors coast to a stop, coolant loop natural circulation begins.	106
SG dry-out (99% void fraction in bottom secondary cell), SG1 / SG2 / SG3 / SG4.	5,905 / 6,020 / 6,020 / 6,020
Pressurizer PORV cycling begins.	6,698
First pressurizer SRV cycle, open/close.	8,606 / 8,714
Loop natural circulation flow interrupted by steam collecting at the tops of the SG tube U-bends, SG1 / SG2 / SG3 / SG4.	8,682 / 8,570 / 8,600 / 8,577
Second pressurizer SRV cycle, open / close.	9,032 / 9,086
Collapsed liquid level in the RV falls below the top of the core heated length (6.323 m above the bottom of RV lower head).	9,157
Steam at the core exit begins to superheat, HL and SG tube flow circulations begin, end of SCDAP/RELAP5 modeling Step 3 and start of modeling Step 4.	9,226
Collapsed liquid level in the RV falls below the bottom of the core heated length (2.666 m above the bottom of the RV lower head).	10,077
Pressurizer empties.	10,704
Onset of fuel rod oxidation.	10,747
First control rod cladding failure.	12,234
First fuel rod cladding rupture.	13,002
Peak fuel rod oxidation rate reached.	13,566
Hot Leg 1 fails by creep rupture.	13,625
Hot Legs 2, 3 and 4 fail by creep rupture.	13,660
Hottest SG tube creep rupture failure (SG 1, non-degraded tube, 1.0 stress multiplier).	13,985
Pressurizer surge line fails by creep rupture.	14,140
Molten fuel pool begins forming near center of the hottest core channel, partial blocking of the core flow begins.	14,241
Station batteries assumed to be depleted, pressurizer PORVs and SG PORVs fail closed and are no longer operable.	14,400
Average SG tube creep rupture failure (SG 1, non-degraded tube, 1.0 stress multiplier).	14,910
First relocation of control rod absorber material to RV lower head.	15,532
End of calculation. Molten fuel pool near center of hottest core channel continues to grow. Partially liquefied fuel debris is found in the other four core channels. Molten fuel has not yet relocated to the RV lower head.	18,000

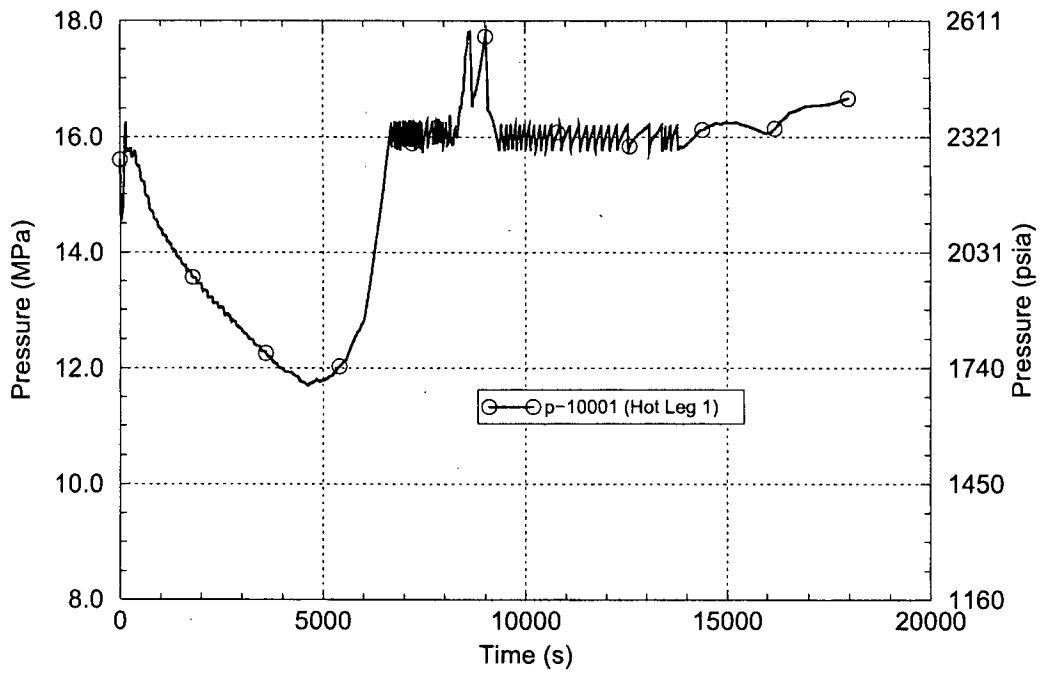


Figure 4.1 Reactor Coolant System Pressure

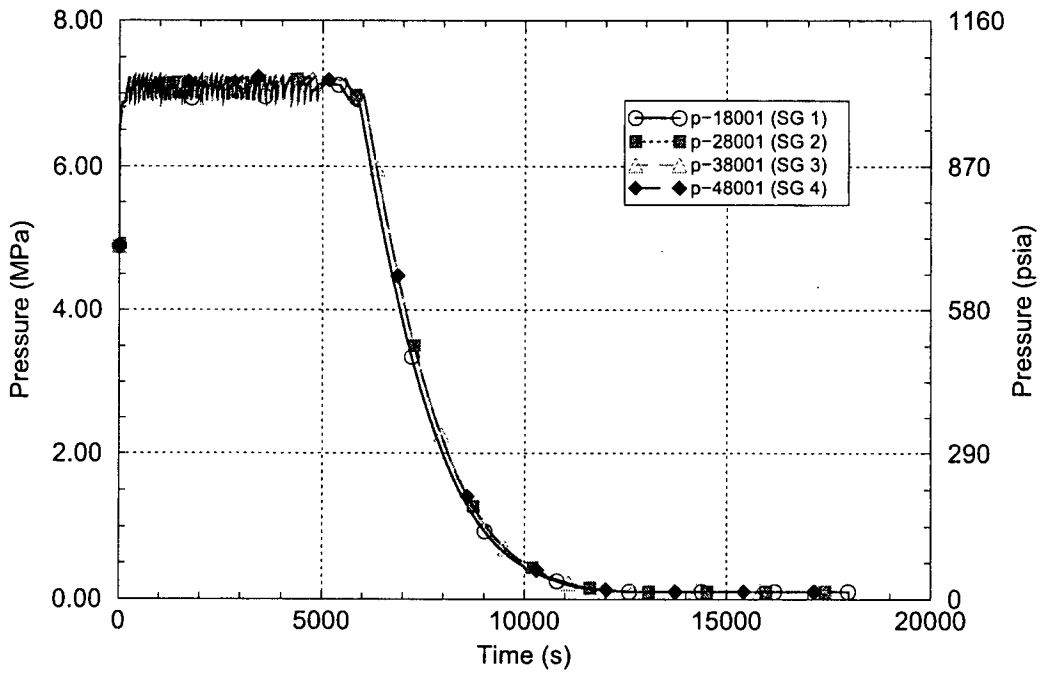


Figure 4.2 Steam Generator Secondary Pressures

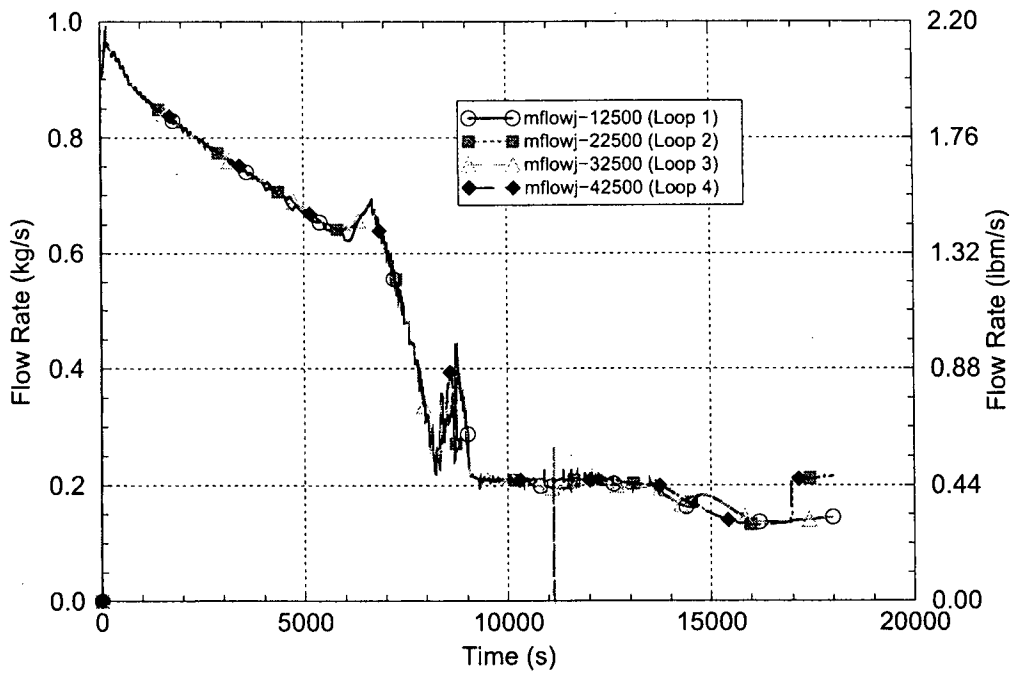


Figure 4.3 Reactor Coolant Pump Shaft Seal Leakage Flows

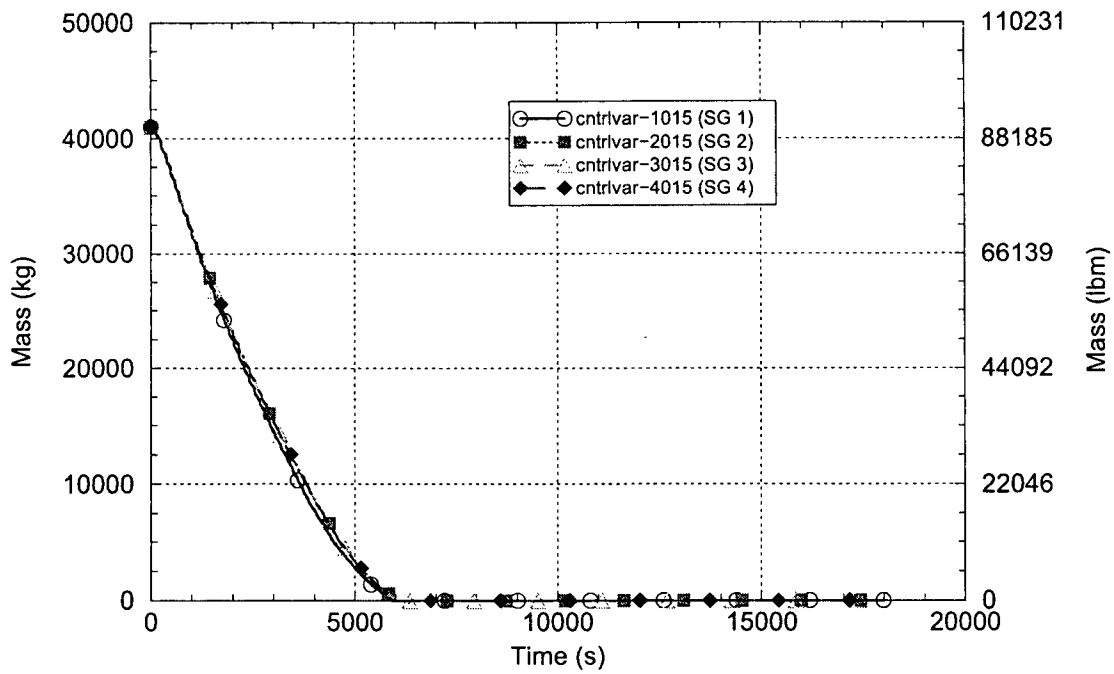


Figure 4.4 Steam Generator Secondary Liquid Masses

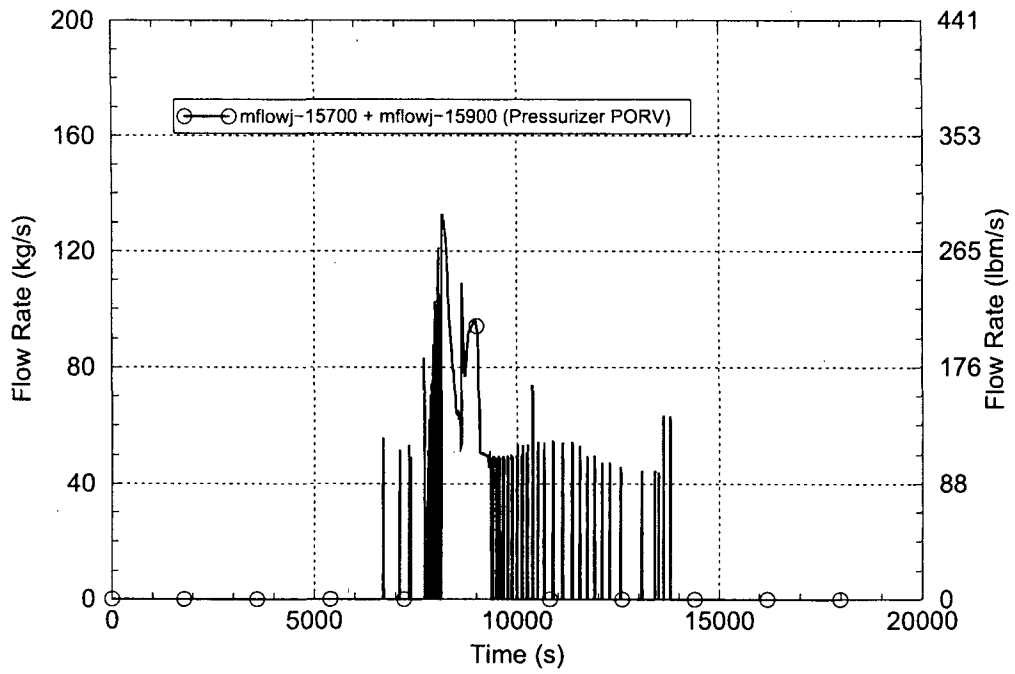


Figure 4.5 Total Pressurizer PORV Flow

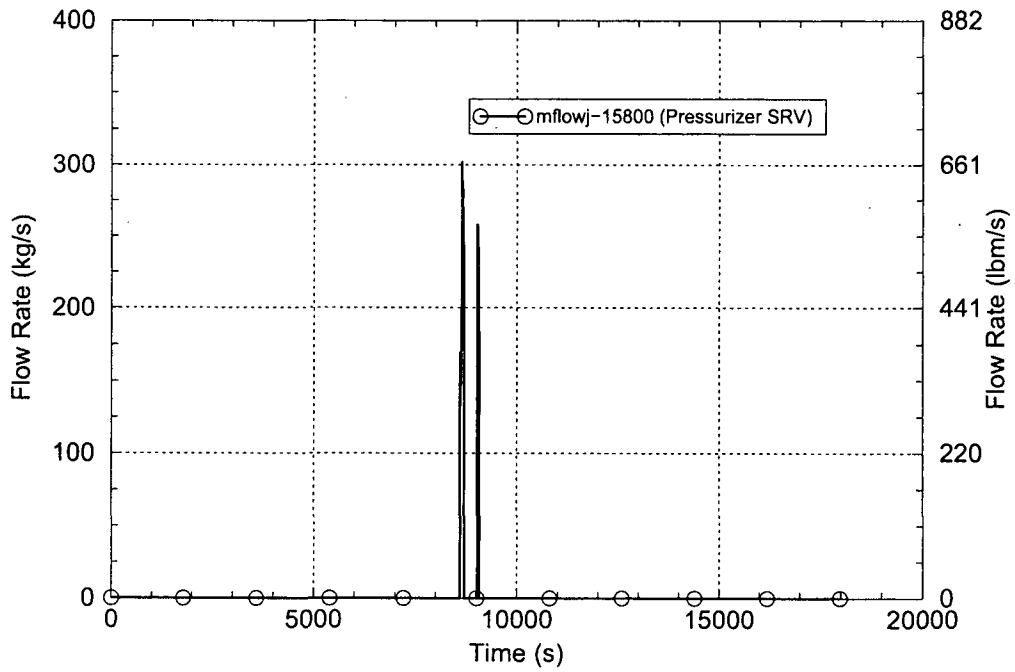


Figure 4.6 Pressurizer SRV Flow

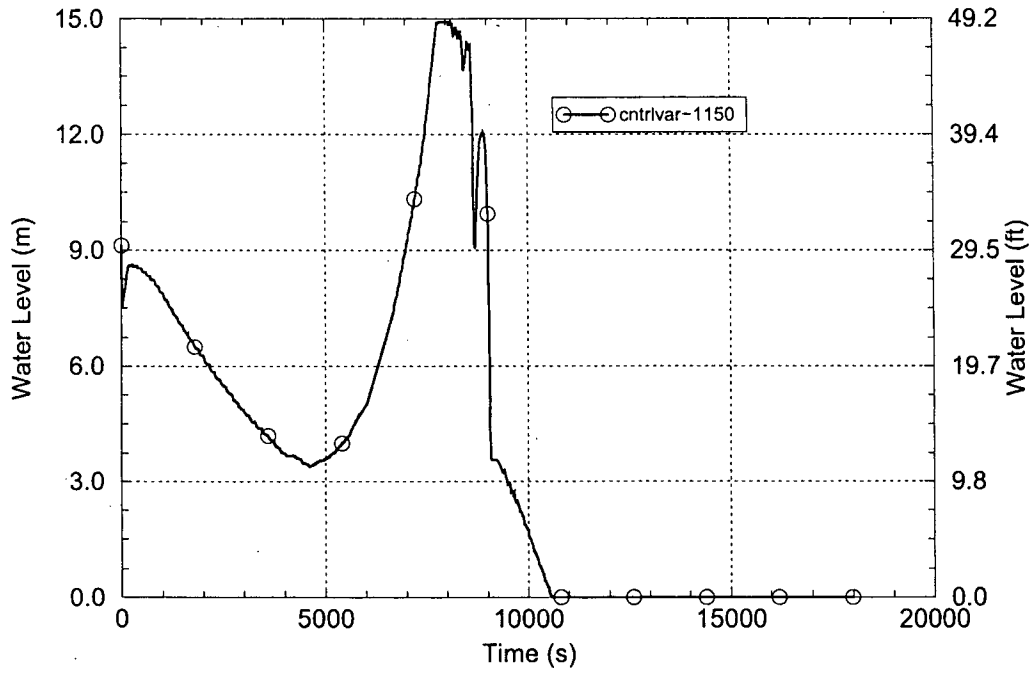


Figure 4.7 Pressurizer Level

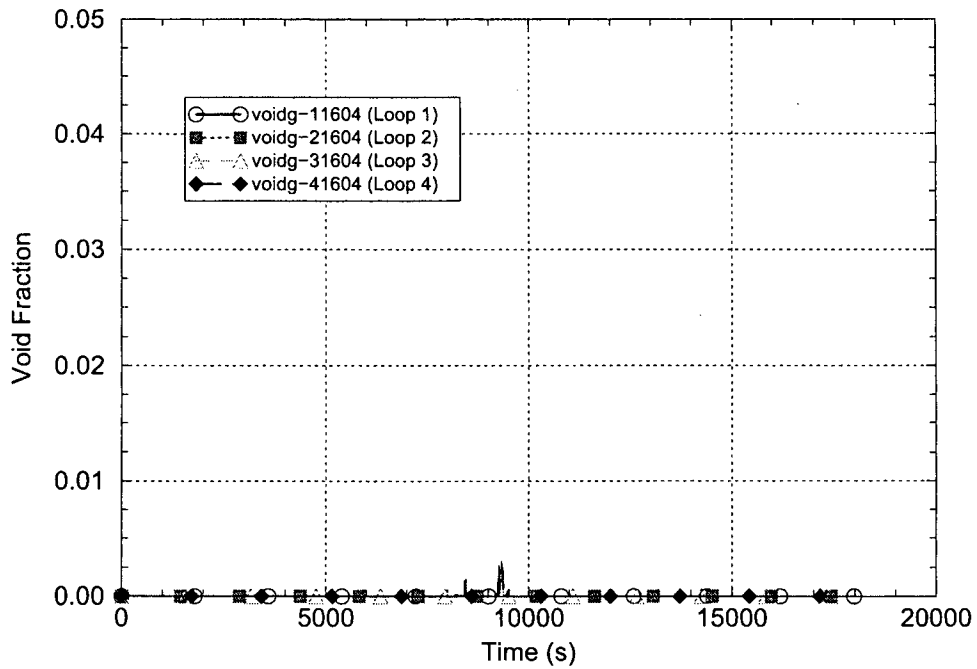


Figure 4.8 Reactor Coolant Pump Loop Seal Void Fractions

SG inlet plenum. In Coolant Loop 1, which contains the pressurizer, steam may be diverted from the HL into the pressurizer surge line. The time-history behavior of the plant parameters is generally affected by the cyclic opening and closing of the pressurizer PORVs and pressurizer SRVs.

The flow rates in the SG 1 hot (forward-flowing) and cold (reverse-flowing) average tube sections are shown in Figure 4.9. The flow around this circulation path is driven by the net positive buoyancy driving head created by the differences in steam densities (resulting from temperature differences) in the hot and cold tube sections. Referring to Figure 3.16, the hot tube section is represented by Component 110 and the cold tube section is represented by Component 111. The declining trend in the SG tube circulation rate in Figure 4.9 results from two effects. First, because the initial rise in the temperature of the steam entering the SG is rapid and the SGs initially are cold, the initial steam temperature difference is large. However over the course of the event sequence, the steam temperature difference declines as a result of transfer of heat into to the SG. Second, because the entire RCS is experiencing a transient heat-up, steam densities are generally declining and this results in correspondingly declining steam mass flow rates. To place the SG tube mass flow rates shown in Figure 4.9 into perspective, the 8.0-kg/s [17.6-lbm/s] mass flow rate seen at 13,000 s corresponds to an average SG tube steam flow velocity of 0.52 m/s [1.72 ft/s]

The flow rates in the Loop 1 upper and lower HL sections are shown in Figure 4.10. Unlike the SG tube circulation path where the flow rates in the hot and cold sections are the same, in the Loop 1 HL circulation path the flow through the upper HL section is greater than that in the lower HL section during periods when the pressurizer PORVs are open (the PORV flow response is shown in Figure 4.5). The flow around the HL circulation path is driven by the buoyancy head created by the steam temperature and density differences between the two sections over the vertical portion of the HL and within the SG inlet plenum. The HL bends upward from its horizontal run to the SG inlet plenum, with an elevation rise of 0.924 m [3.03 ft] and the elevation rise within the SG inlet plenum adds another 1.206 m [3.958 ft]. The declining trend in the HL circulation rate results for the same reasons described above for the SG tube circulation path. To place the HL mass flow rates shown in Figure 4.10 into perspective, the 4.76-kg/s [10.5-lbm/s] upper HL section mass flow rate seen at 13,000 s corresponds to a steam flow velocity of 0.700 m/s [2.30 ft/s].

In addition to the SG tube and HL flow circulations, there are also flow circulations within the RV. Referring to Figures 3.14 and 3.16, flow of hot steam into the upper HL sections leaves the RV from Component 582 and the cooler steam flowing through the lower HL sections returns to the RV at Component 581. The difference in densities between the hot and cool steam sets up circulation paths within the RV. The cooler steam returning from the lower HL sections tends to flow downward through the peripheral core regions and then upward through the central core regions. Another circulation path also sets up in the RV upper plenum region, with hotter steam flowing from the core channel exits across the upper region (through Components 542, 552, 562, 572 and 582) to reach the entrances to the upper HL sections and with cooler steam flowing from the exits of the lower HL sections across the lower region (through Components 581, 571, 561, 551 and 541) toward the RV centerline. The RV circulation is characterized in Figure 4.11, which shows the mass flow rates near the tops of one of the upward-flowing central core regions and one of the downward-flowing peripheral core regions (Core Channels 512 and 514, as shown in Figure 3.14). To place the core mass flow rates shown in Figure 4.11 into perspective, the 13.0-kg/s [28.7-lbm/s] central core channel flow seen at 13,000 s corresponds to a steam velocity of 0.49 m/s [1.6 ft/s].

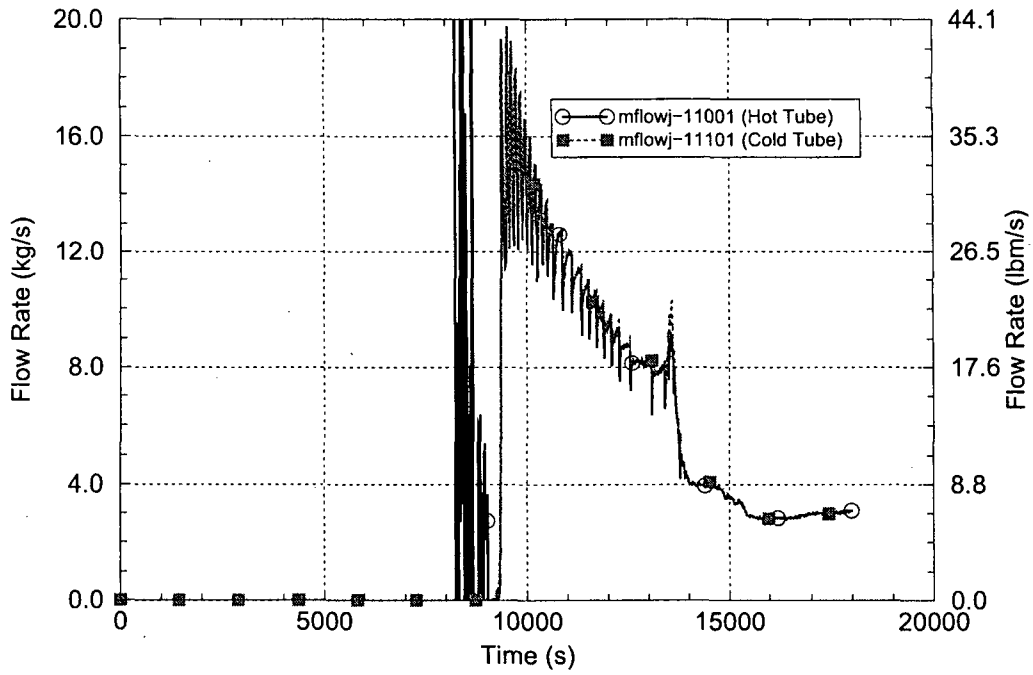


Figure 4.9 SG 1 Hot and Cold Average Tube Flows

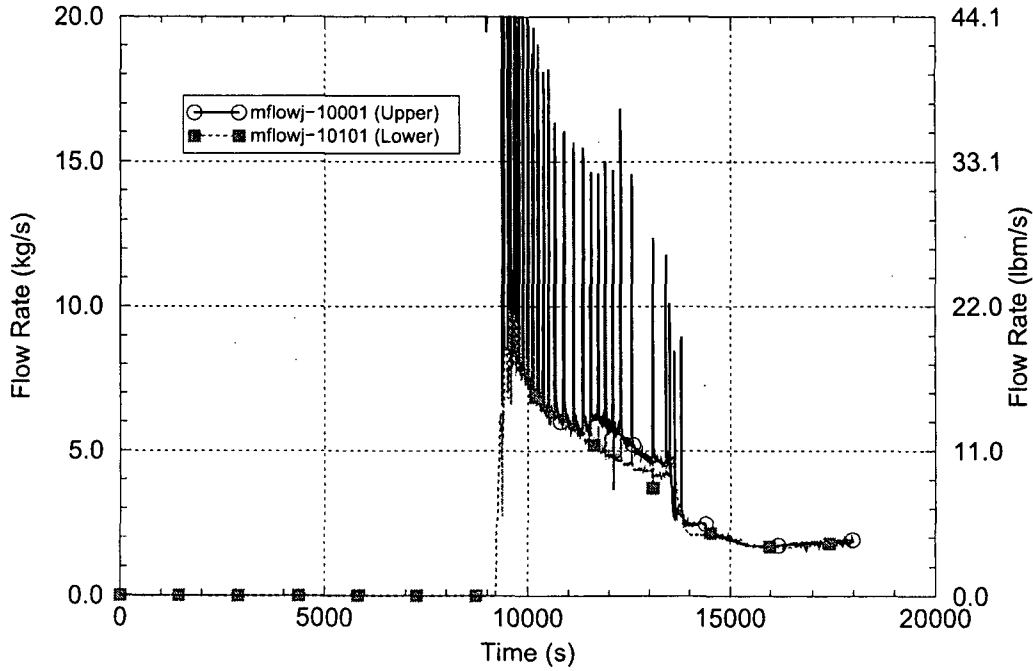


Figure 4.10 Hot Leg 1 Upper and Lower Section Flows

The flow resistances of the SCDAP/RELAP5 plant model in the regions of the SG inlet plenum are preset so as to match the behavior of the hot leg discharge coefficient, recirculation ratio, hot mixing fraction and cold mixing fraction observed during Westinghouse 1/7th-scale experiments and CFD analyses simulating plant behavior during SBOs. (See discussions in Section 3.4). Figures 4.12 through 4.15 show the SCDAP/RELAP5-calculated responses for these inlet plenum fluid mixing and flow parameters. Table 4.3 compares the smoothed SCDAP/RELAP5-calculated values for these parameters (averaged over the four coolant loops) with their nominal target values at 13,000 s. Smoothing is necessary because the parameter values vary significantly with the cyclic opening and closing of the pressurizer PORVs and the rate of PORV cycling increases as the system heat-up rate becomes larger. 13,000 s was chosen for the comparison time because parameter values at that time remain relatively stable and yet are close to the values experienced at the time when the critical structural failures are predicted to occur. Table 4.3 shows excellent agreement of the smoothed SCDAP/RELAP5-calculated and target values for hot leg discharge coefficient, hot and cold mixing fractions and recirculation ratio.

The responses of the hot leg discharge coefficients for the four coolant loops are shown in Figure 4.12. This parameter characterizes the countercurrent flow in a horizontal pipe between two tanks containing fluids of different densities (see Section 3.4). The average SCDAP/RELAP5 calculated value for the hot leg discharge coefficient in the four coolant loops is within 0.6% of the 0.12 target value.

The recirculation ratio, hot mixing fraction and cold mixing fraction responses are shown in Figures 4.13, 4.14 and 4.15, respectively. The recirculation ratio is defined as the ratio of the SG tube mass flow rate to the HL mass flow rate. The mixing fractions are defined as the portions of the flow entering the SG inlet plenum which are directed to the "mixing" plenum (Cell 106, see Figure 3.16). The hot mixing fraction is thus the portion of the upper HL flow which is directed to the mixing plenum while the cold mixing fraction is the portion of the "cold" tube return flow which is directed to the mixing plenum (see Section 3.4). As listed in Table 4.3, the target value for the recirculation ratio is 2.0 and the target value for the hot and cold mixing fractions is 0.85. The average SCDAP/RELAP5 calculated values for the hot and cold mixing fractions are within 0.5% of the target value. The average SCDAP/RELAP5 calculated value for the recirculation ratio is within 1.5% of the target value.

The responses of the SG power fractions are shown in Figure 4.16. This parameter is defined as the ratio of the heat removed to each SG (to the tubes, tubesheet, inlet plenum wall and outlet plenum wall) to the total core heat (fission product decay and fuel rod oxidation heat). The SG power fractions are calculated on an integrated basis, starting at the time of core uncovering. The power fractions increase after the core uncovers as the hot steam flows outward through the HLs and into the SGs. A first peak in the SG power fractions occurs during the period when the fuel rod oxidation process is peaking. The oxidation heat is immediately absorbed by the fuel rods, thereby reducing for a time the fraction of the core heat that is absorbed by the SGs. After the oxidation process subsides, the excess heat that was absorbed in the fuel rods is dissipated into the steam and transported outward into the coolant loops and SGs, causing the SG power fractions to again rise. Note that no target value for SG power fraction is listed in Table 4.3 (target values for SG power fraction were used in some of the earlier analyses, see Sections 2.1 through 2.6). For this final analysis, the previously-used target SG power fraction for the modeling process has been replaced with the target hot leg discharge coefficient described above. The calculated SG power fraction responses described here are provided only for purposes of comparison with the prior analyses.

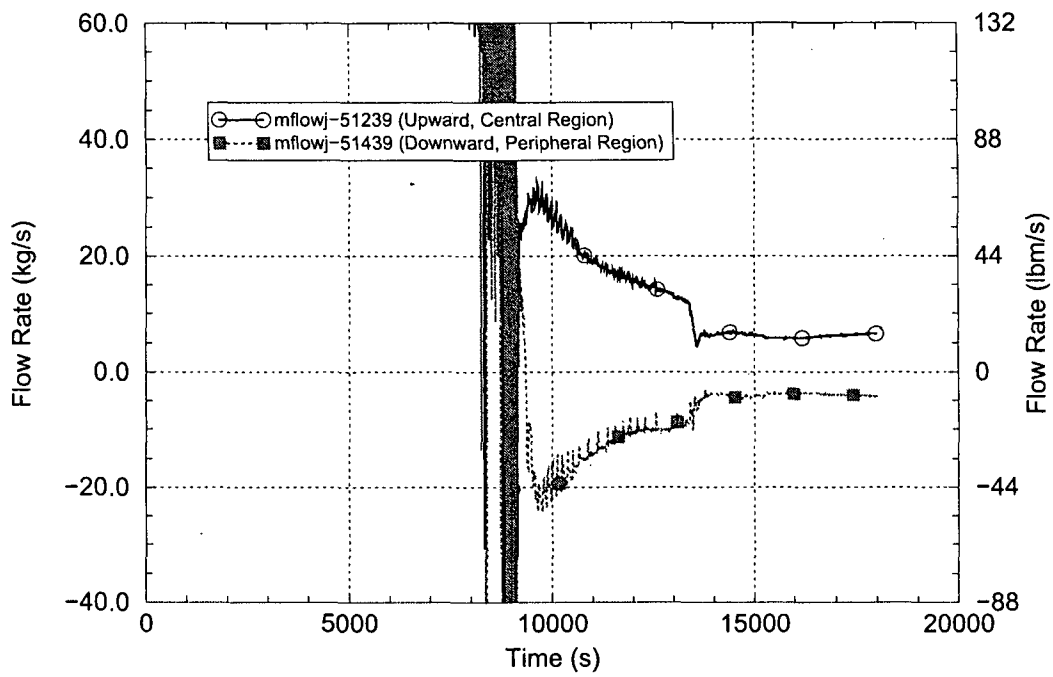


Figure 4.11 Vessel Circulation Flows

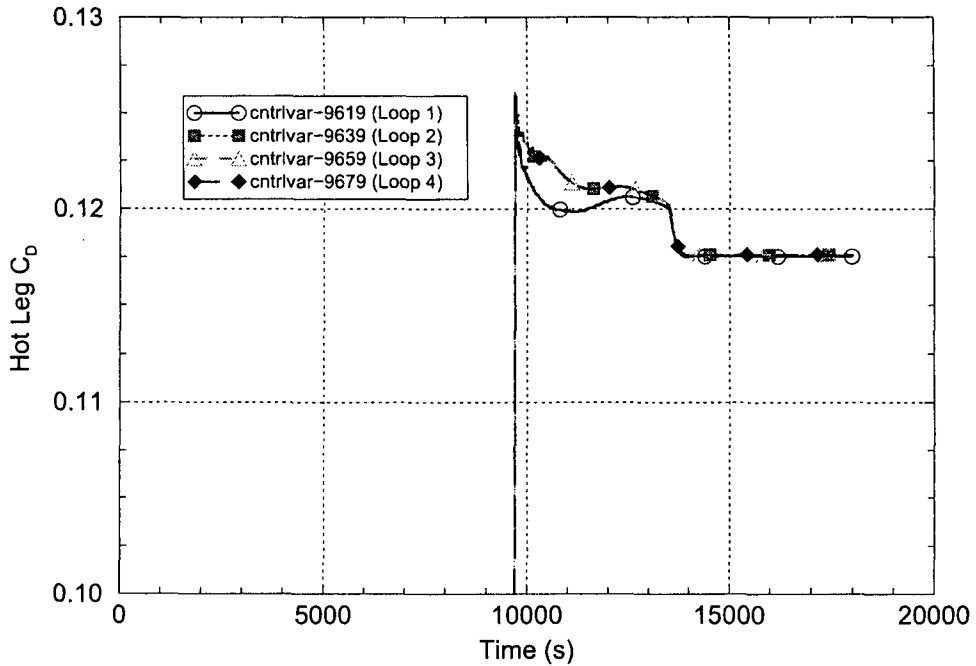


Figure 4.12 Hot Leg Discharge Coefficients

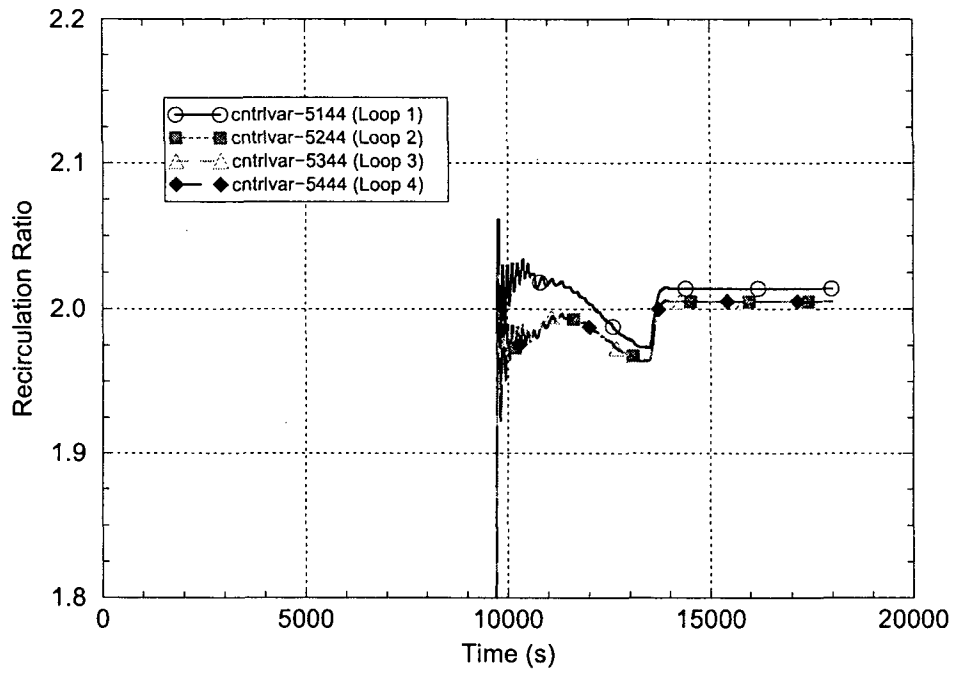


Figure 4.13 Recirculation Ratios

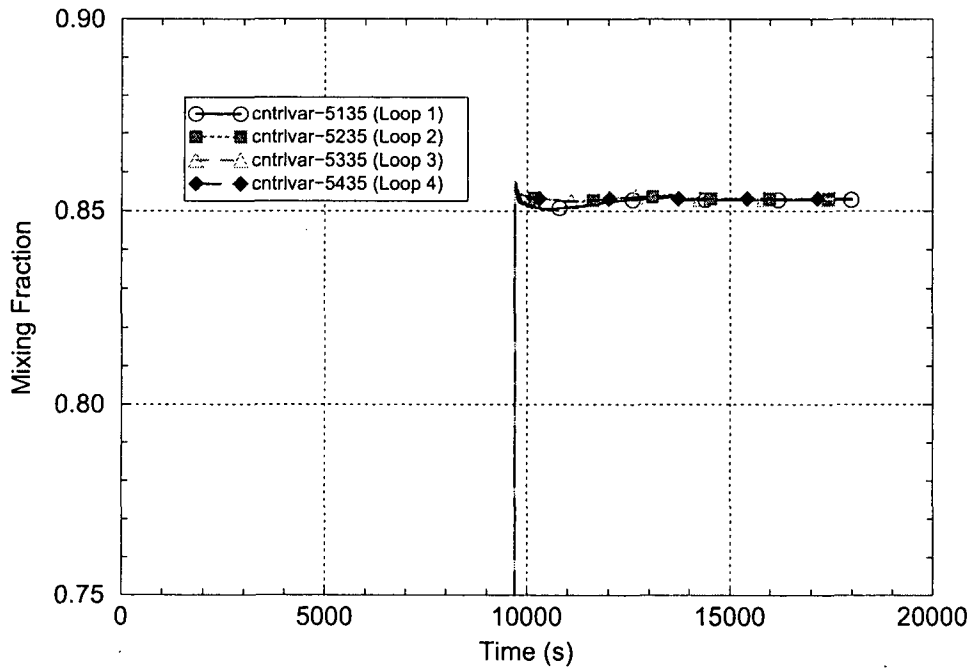


Figure 4.14 Hot Mixing Fractions

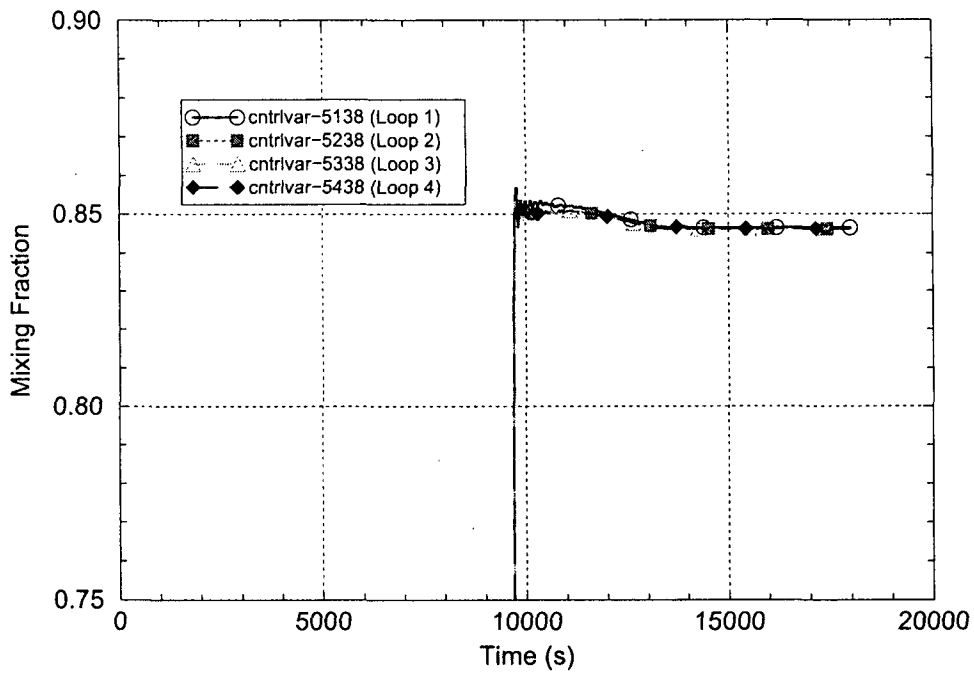


Figure 4.15 Cold Mixing Fractions

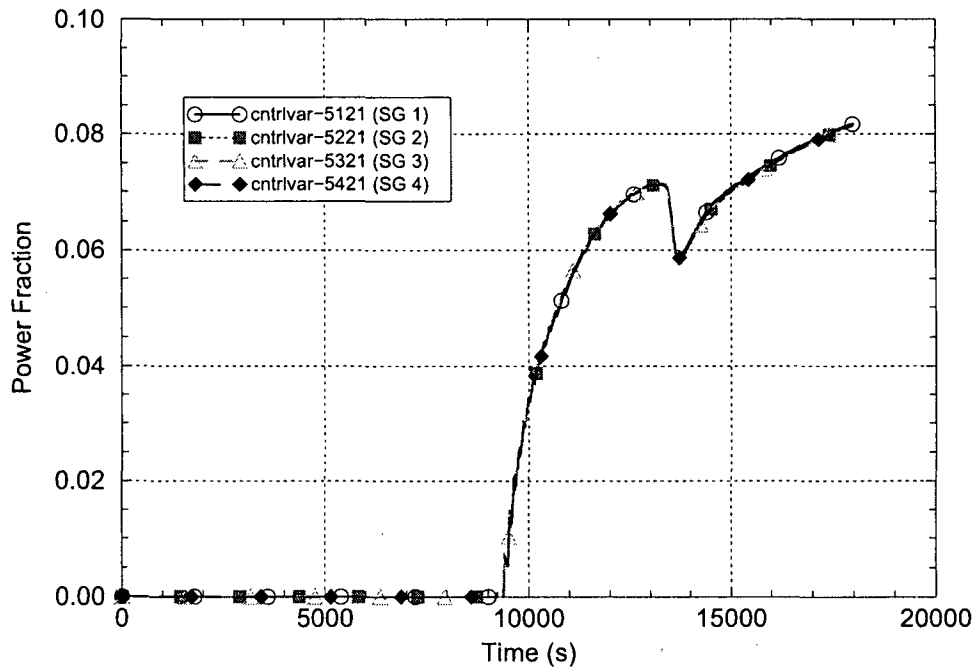


Figure 4.16 SG Power Fractions

Table 4.3 Comparison of Target and SCDAP/RELAP5-Calculated SG Inlet Plenum Fluid Mixing and Flow Parameters

Parameter	Target Value	SCDAP/RELAP5 Calculated Value
Assumed Split of SG Tubes into Hot/Cold Regions	41%/59%	41%/59%
Hottest Tube Normalized Temperature Ratio	0.5	0.5
Average Hot Leg Discharge Coefficient	0.12	0.1207
Average Hot Mixing Fraction	0.85	0.854
Average Cold Mixing Fraction	0.85	0.847
Average Recirculation Ratio	2.0	1.971
Portion of the Integrated Total Core Heat Addition which is Absorbed in the Four SGs	Not Applicable	28.4%

The rate of hydrogen generation resulting from fuel rod cladding oxidation is shown in Figure 4.17. The oxidation process resulting from metal-water reaction on the exterior surfaces of the fuel rod cladding begins gradually, starting in the high-power core regions. The oxidation rate increases rapidly as fuel temperatures climb, with the process spreading into lower-power regions of the core. Fuel rod oxidation begins at 10,747 s and the peak oxidation rate is reached at 13,566 s. The major peak in the oxidation rate seen in Figure 4.17 occurs because the process accelerates as a result of fuel rod cladding rupture and the involvement of the inner cladding surfaces in addition to the outer surfaces. The peak core oxidation power is 300.2 MW and during the period of its peak the oxidation power is the dominant contributor to the system heat-up. To place the significance of the oxidation power into perspective, at the time of its peak the oxidation power is 10.1 times the fission product decay power and 9.2% of the plant normal-operation full rated thermal power.

Figure 4.18 compares the thermal responses for the key structures in Coolant Loop 1. The data shown represent the average temperatures across the structure thickness at the hottest axial locations. The pressurizer surge line temperature presented is at the end of the line adjacent to the HL. The HL temperature presented is for the upper half of the HL adjacent to the RV. The average and hottest SG tube temperatures presented are for the upward-flowing tube sections just above the top of the tubesheet.

As the HL steam temperatures rise, the rates at which the structure temperatures increase vary, depending on the local steam temperature, the fluid-to-wall heat transfer, and on the material and thickness of the structure. Generally, the temperatures of the thin-wall SG tubes respond quickly to an increasing steam temperature, while the temperature of the thicker pressurizer surge line responds more slowly and the still-thicker HL structure temperature responds even more slowly. Because the hottest steam is modeled at its inlet, the temperature of the hottest SG tube structure increases more rapidly than the temperature of the average SG tube structure. The start of the pressurizer surge line heat-up is delayed until the pressurizer empties at 10,704 s. Before that time, liquid intermittently drains out of the pressurizer into the surge line during periods when the pressurizer PORVs are closed. The draining cools both the steam

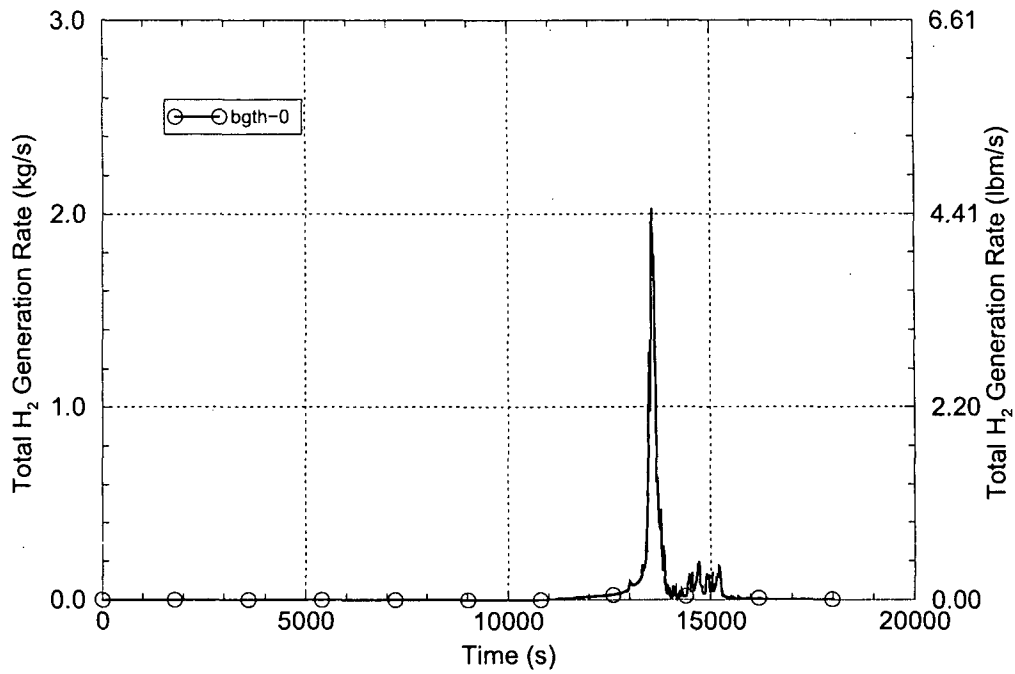


Figure 4.17 Hydrogen Generation Rate

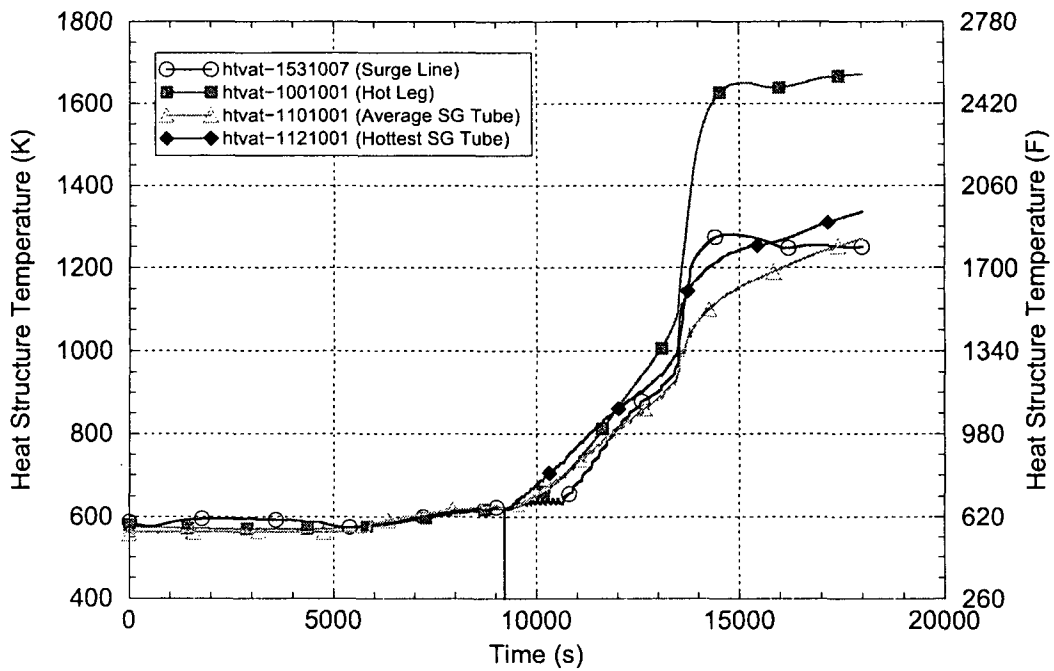


Figure 4.18 Loop 1 Structure Temperatures

inside the surge line and the surge line wall. This behavior directly affects the response of the surge line heat structure but not the HL or SG tube heat structures. After the pressurizer empties, the pressurizer PORVs continue to cycle and hot steam is drawn upward through the surge line without the cooling benefit afforded by liquid draining downward, causing the surge line temperatures to rapidly rise.

Pressurizer PORV cycling ceases at 14,400 s (four hours after event initiation) when the station batteries are assumed to be depleted. Afterward, the RCS pressure increases, but not sufficiently to open the pressurizer SRVs, see Figures 4.1 and 4.6. The turnover in the surge line structure temperature in Figure 4.18 reflects the cessation of surge line steam flow at that time. With neither the pressurizer PORVs nor SRVs opening, the flow of increasingly-hotter steam through the surge line stops and the heat loss from the outside of the surge line to the containment cools the surge line wall. Figure 4.19 shows a detailed view of the structure temperature responses from Figure 4.18 overlaid with the SCDAP/RELAP5-calculated failure times for the structures.

Figures 4.20 through 4.22 compare the Larson-Miller creep rupture damage indexes for the surge line, HL and SG tube structures. The damage index indicates the accumulation of creep damage as a fraction of the creep damage needed to cause failure; the structural failure is predicted to occur at the time when the index value reaches 1.0. The creep rupture model allows use of a stress multiplier that represents the effect on the creep calculation corresponding to a specific degree of degradation in the strength of a structure due to other factors, such as cracks that were present before the accident event sequence started. For the pressurizer surge line and HL structures only a stress multiplier of 1.0 is used. A set of stress multipliers from 1.0 to 7.5, in increments of 0.5, is used for the SG tube structures as a means to introduce tube material strength degradation as an analysis variable.

Figure 4.20 compares the damage indexes for the pressurizer surge line and the four HLs. The failure of Hot Leg 1 occurs first, followed by failures of Hot Legs 2, 3 and 4 and then by the failure of the surge line (the calculated creep rupture failure times for all structures in the model are listed in Table 4.4). The failure of Hot Leg 1 precedes the failures of the other HLs (by 35 s) because of effects related to the connection of the pressurizer to Hot Leg 1. The opening of the pressurizer PORVs and SRVs causes steam flow to be drawn through Hot Leg 1 at a higher rate than for Hot Legs 2, 3 and 4, resulting in slightly greater heating and the earlier creep rupture failure prediction. The prediction of the surge line failure is delayed, relative to the HLs, because flow into the surge line is drawn equally from the hot steam in the upper section and cool steam in the lower section of Hot Leg 1.

Figure 4.21 compares the damage indexes for Hot Leg 1 and the average tubes in SG 1. The figure and table show that an average tube with a stress multiplier of 2.74 is predicted to fail at the same time that Hot Leg 1 fails. In other words, tubes that are subjected to the average steam conditions on the inside are not expected to fail before the HL fails as long as degradation of the tube strength has not progressed past the point where a tube will fail when subjected to a stress of only $(1.0 / 2.74 =)$ 36.5% of the stress that would fail a non-degraded SG tube.

Figure 4.22 compares the damage indexes for Hot Leg 1 and the hottest tube in SG 1 (see Section 3.4 for a description of hottest tube modeling). This figure and the event times in Table 4.4 indicate that the hottest tube with a stress multiplier of 1.68 is predicted to fail at the same time that Hot Leg 1 fails. In other words, tubes that are subjected to the hottest steam on the inside are not expected to fail before the HL as long as degradation of the tube strength has

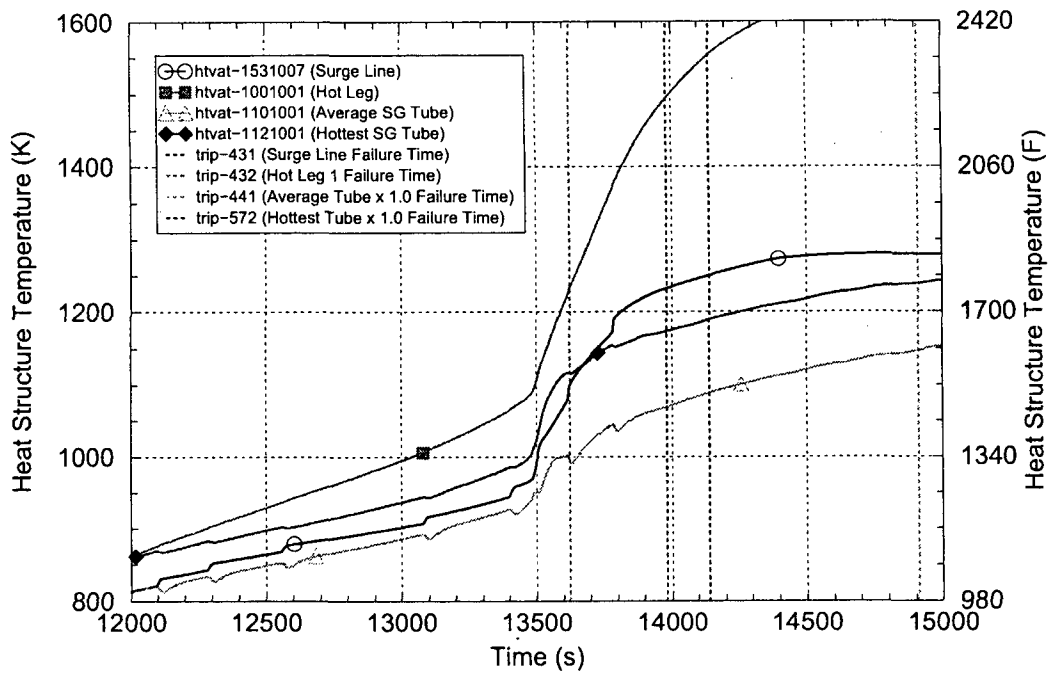


Figure 4.19 Correspondence Between Loop 1 Structure Temperatures and Failure Times

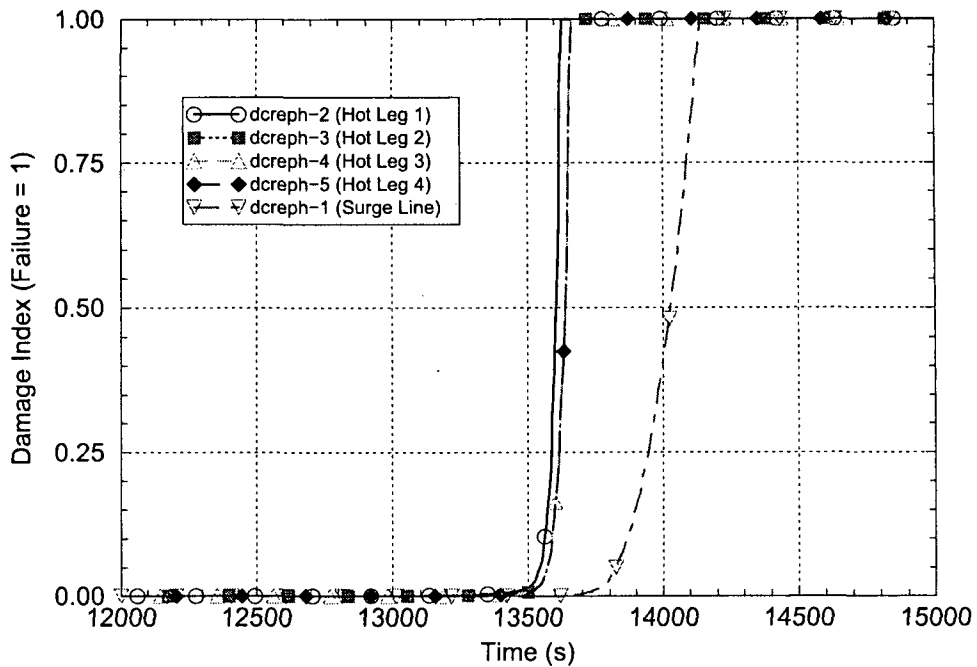


Figure 4.20 Hot Leg and Pressurizer Surge Line Creep Rupture Damage Indexes

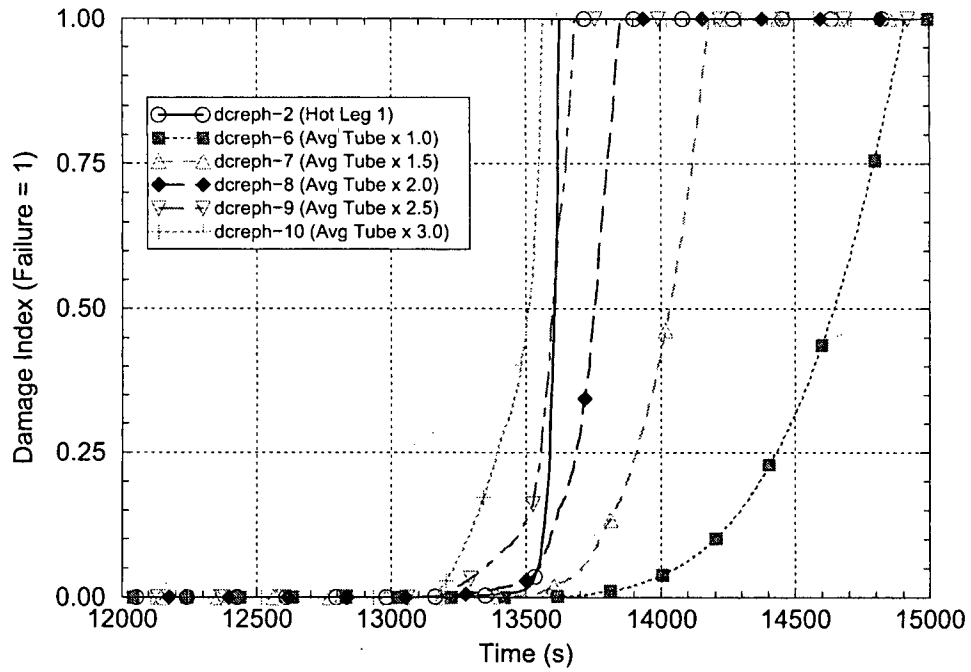


Figure 4.21 SG 1 Average Tube and Hot Leg 1 Creep Rupture Damage Indexes

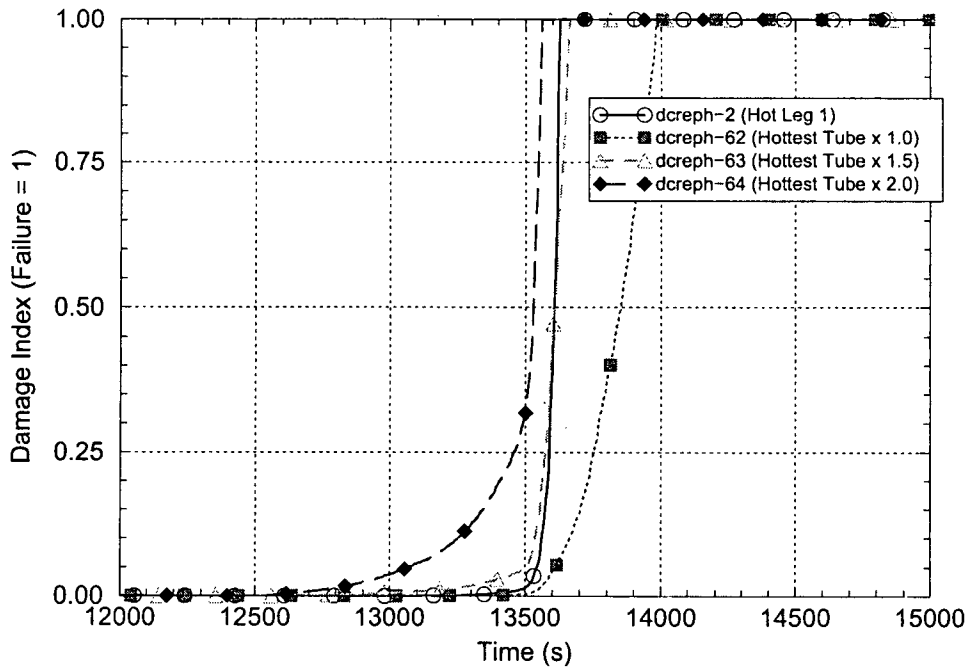


Figure 4.22 SG 1 Hottest Tube and Hot Leg 1 Creep Rupture Damage Indexes

Table 4.4 Summary of Calculated Creep Rupture Failure Times from the Base Case Calculation

Structure		Calculated Failure Time (s)
Pressurizer surge line		14,140
Hot Leg 1 / Hot Leg 2 / Hot Leg 3 / Hot Leg 4		13,625 / 13,660 / 13,660 / 13,660
SG 1 / SG 2 / SG 3 / SG 4		
Average SG Tube, Stress Multiplier:	1.0	14,910 / 14,975 / 14,975 / 14,975
	1.5	14,180 / 14,220 / 14,220 / 14,220
	2.0	13,850 / 13,880 / 13,880 / 13,880
	2.5	13,680 / 13,700 / 13,700 / 13,700
	3.0	13,565 / 13,575 / 13,575 / 13,575
	3.5	13,460 / 13,475 / 13,475 / 13,475
	4.0	13,315 / 13,330 / 13,330 / 13,330
	4.5	13,240 / 13,255 / 13,255 / 13,255
	5.0	13,205 / 13,220 / 13,220 / 13,220
	5.5	13,185 / 13,200 / 13,200 / 13,200
	6.0	13,175 / 13,190 / 13,190 / 13,190
	6.5	13,170 / 13,185 / 13,185 / 13,185
	7.0	13,165 / 13,180 / 13,180 / 13,180
	7.5	13,165 / 13,180 / 13,180 / 13,180
SG 1		
Hottest SG Tube, Stress Multiplier:	1.0	13,985
	1.5	13,660
	2.0	13,560
	2.5	13,440
	3.0	13,140
	3.5	12,880
	4.0	12,715
	4.5	12,620
	5.0	12,570
	5.5	12,550
	6.0	12,540
	6.5	12,535
	7.0	12,530
	7.5	12,530

not progressed past the point where a tube will fail when subjected to a stress of only ($1.0 / 1.68 =$) 59.5% of the stress that would fail a non-degraded SG tube.

The formation of a molten fuel pool is predicted near the center of the hottest core channel (Component 511 in Figure 3.14) starting at 14,241 s, blocking the flow in that channel. Partially liquefied fuel debris is also predicted to form, but not to block flow, at various locations in the other four core channels later during the simulation. Relocation of molten control rod absorber to the RV lower head is predicted, starting at 15,532 s.

The SCDAP/RELAP5 calculation was continued beyond the predicted times of the HL, pressurizer surge line and SG tube structural failures until 18,000 s. Note that the calculation does not simulate the actual thermal-hydraulic behavior associated with opening of breaks from the RCS into the containment and SG secondary systems. Structural failures are predicted but the effects of the failures are not implemented into the thermal-hydraulic model. So the calculated thermal-hydraulic behavior subsequent to the time of the first structural failure does not reflect the impacts of that failure. Those impacts are addressed in Section 5.5.

In summary, the final SCDAP/RELAP5 simulation of the base case SBO accident sequence in a Westinghouse four-loop PWR indicates positive failure margins for SG tubes carrying average-temperature steam and for SG tubes carrying the hottest-temperature steam. The tube failure margins are expressed as the stress multiplier (representing degraded structural strength) required for SG tube failure to occur coincident with the earliest other RCS pressure boundary structural failure (predicted to be Hot Leg 1, at 13,625 s). The average-tube predicted failure margin is 2.74 and the hottest-tube predicted failure margin is 1.68. From the perspective of structural failure timing, a non-degraded SG tube carrying average-temperature steam is predicted to fail 1,285 s after the HL fails and a non-degraded SG tube carrying the hottest-temperature steam is predicted to fail 360 s after the HL fails.

5. KEY SENSITIVITIES

As discussed in Section 1, the objective of this report is to coalesce the findings from current and prior containment bypass thermal-hydraulic evaluations into a view of the SBO severe accident event sequences that (1) result in containment bypass, (2) provide a potential for containment bypass, and (3) do not result in containment bypass. As discussed in Section 1.4, the criteria for judging into which category an event sequence falls are based on the SCDAP/RELAP5-predicted hottest SG tube failure margin. Sequences for which the hottest SG tube with no degradation in structural strength is predicted to fail coincident with or prior to another RCS component (a HL, the pressurizer surge line or the RV) are considered to fall into Category (1). Sequences for which the hottest SG tube has a predicted failure margin (i.e., stress multiplier) of between 1.0 and 3.0 are considered to fall into Category (2). Sequences for which the hottest SG tube has a failure margin of 3.0 or greater are considered to fall into Category (3).

Prior containment bypass thermal-hydraulic analyses were reviewed and a final set of SCDAP/RELAP5 sensitivity analyses was developed in order to provide a comprehensive database permitting the categorization of all extended SBO severe accident event sequences. These reviews covered PRA evaluations (as documented in Reference 5.1), updated CFD evaluations regarding fluid mixing behavior, event-sequence definition evaluations regarding consistency with another ongoing containment bypass research project, and SCDAP/RELAP5 modeling related evaluations regarding confirmation of important prior findings using the latest computer code and plant model. The final set of sensitivity analyses are documented in this section.

Sensitivity analyses related to the expected RCP shaft seal leakage behavior are described in Section 5.1. Sensitivity analyses related to variations in TDAFW operation and steam leakage from the SG secondary systems are described in Section 5.2. Sensitivity analyses of opportunities for mitigative operator intervention are described in Section 5.3. An analysis of the sensitivity of results to variations in the subdivision of SG tubes into hot and cold tube sections is described in Section 5.4. Sensitivity analyses related to directly modeling the opening of SG tube and HL piping rupture flow paths are described in Section 5.5.

5.1 RCP Shaft Seal Leakage Behavior

During normal plant operation, the charging system injects a cooling flow into the RCS through the RCP shaft seals. During SBO events, the seal injection flow is lost and the RCP shaft seals become a path for leakage flow from the RCS into the containment. The postulated minimum shaft seal leakage rate is 1.325 L/s [21 gpm] in each RCP. Additionally, failures of various shaft seal components may lead to larger leakage rates. Certain seal failures are expected to occur at about 13 minutes following the initiation of the SBO and certain other seal failures are expected to occur when, due to heating, the fluid in the RCP changes from liquid to steam. In the SBO base case accident sequence this transition from liquid to steam occurs at about 2 hours into the event sequence, when the fluid in the RCPs reaches the saturation temperature. The maximum expected shaft seal leakage rate in each RCP is 30.2 L/s [480 gpm], assuming a worst-case combination of shaft seal failures.

RCP shaft seal leakage behavior is important for the containment bypass issue from many perspectives. Larger leakage rates lead to lower RCS pressures, thereby reducing stresses on

the SG tubes. Larger leak rates accelerate the loss of RCS fluid, thereby affecting event sequence timing, core inventory and core damage behavior. The lower RCS pressures associated with larger leak rates also increase the potential for the water in loop seals to clear, which is of key importance for containment bypass. The analyses presented here address the sensitivity of results to RCP shaft seal leakage. Section 5.1.1 discusses increases in the leakage rate at 13 minutes. Section 5.1.2 discusses increases in the leakage rate at the time when saturated fluid conditions are reached in the RCPs.

5.1.1 Leakage Rate Increases Due to Seal Failures at 13 Minutes

A series of SCDAP/RELAP5 sensitivity calculations were performed to evaluate the effects of the RCP shaft seal leak rate increasing above 1.325 L/s [21 gpm] per pump after 13 minutes. The sensitivity calculation assumptions are the same as for the base case calculation presented in Section 4, except for the increased shaft seal leak rates. The results from the base case and sensitivity calculations are listed in Table 5.1 and are summarized as follows.

Increased leak rates result in additional cooling of the RCS, leading to less demand for SG heat removal, cooler SG tubes and higher SG tube failure margins. The additional RCS cooling also keeps the water in the loop seals cooler, which inhibits flashing and prevents the loop seals from clearing, even during rapid RCS depressurizations which are experienced at large assumed leak rates.

The cases with leak rates of 9.464 L/s [150 gpm] and lower indicate minimum SG tube failure margins of less than 3.0. For these cases, whether or not containment bypass occurs depends upon the SG tube strength degradations and on the distribution of the inlets to the lowest-strength tubes relative to the location of the hot plume on the bottom surface of the tubesheet.

The cases with leak rates of 11.36 L/s/pump [180 gpm] through 27.76 L/s [440 gpm] indicate minimum tube failure margins of greater than 3.0. These cases do not result in containment bypass.

For the case with a leak rate of 30.2 L/s [480 gpm], the core is predicted to be significantly damaged prior to the failure of the HL or any SG tubes. This case therefore also does not result in containment bypass.

A sensitivity evaluation into SCDAP/RELAP5 modeling of the RCP leaks was also performed. Relocating the RCP seal leak location in the model from the cold leg centerline to 0.9906 m [39"] below the cold leg centerline (the elevation span over which RCP seal leaks may effectively be located) was not seen to significantly affect the overall outcome or the SG tube failure margins.

Table 5.1 Sensitivity of Results to Increased RCP Shaft Seal Leakage After 13 Minutes

Assumed Per-RCP Shaft Seal Leak Rate After 13 Minutes	Average Tube Failure Margin	Hottest Tube Failure Margin	Loop Seals Cleared?	Early Core Failure?	Containment Bypass Condition Indicated?
21 gpm (Base Case) No Leak Rate Increase	2.7	1.7	No	No	Depends on Tube Strength Degradations and Locations (Minimum Margin < 3.0)
60 gpm Case A-60	2.8	1.8	No	No	Depends on Tube Strength Degradations and Locations (Minimum Margin < 3.0)
100 gpm Case A-100	3.2	2.0	No	No	Depends on Tube Strength Degradations and Locations (Minimum Margin < 3.0)
150 gpm Case A-150	4.1	3.5	No	No	Depends on Tube Strength Degradations and Locations (Minimum Margin < 3.0, Judgment Includes Effects of a Hottest Tube Modeling Uncertainty Specific to this Case)
180 gpm Case A-180	4.7	4.4	No	No	No (Minimum Margin >3.0)
200 gpm Case A-200	5.0	4.6	No	No	No (Minimum Margin >3.0)
250 gpm Case A-250	>7.5	6.9	No	No	No (Minimum Margin >3.0)
300 gpm Case A-300	>7.5	>7.5	No	No	No (Minimum Margin >3.0)
350 gpm Case A-350	>7.5	>7.5	No	No	No (Minimum Margin >3.0)
400 gpm Case A-400	>7.5	>7.5	No	No	No (Minimum Margin >3.0)
440 gpm Case A-440	>7.5	>7.5	No	No	No (Minimum Margin >3.0)
480 gpm Case A-480 (Maximum Leak Rate)	>7.5	>7.5	No	Yes	No (Core Fails Prior to HL and Tubes)

5.1.2 Leakage Rate Increases Due to Seal Failures When RCPs Experience Saturated Fluid Conditions

A series of SCDAP/RELAP5 sensitivity calculations were performed to evaluate the effects of the RCP shaft seal leak rate increasing above 1,325 L/s [21 gpm] per pump for a first time at 13 minutes and then for a second time when the fluid conditions in the RCPs transition from liquid to steam at about 2 hours into the event sequence. The sensitivity calculation assumptions are the same as for the base case calculation presented in Section 4, except for the increased shaft seal leak rates. The results from the base case and sensitivity calculations are listed in Table 5.2 and are summarized as follows.

The relatively minor RCS cooling resulting from a 3.786-L/s [60-gpm] leak rate after 13 minutes leads to a warming of the water in the loop seals (as compared with the sensitivity cases described in Section 5.1.1, for which much-higher RCP leak rates are assumed to start at 13 minutes). When the fluid conditions in the RCPs reach saturation, the shaft seal leak rate increases for the second time and the warm loop seal water tends to flash and clear the loop seals.

The results of the sensitivity calculations show that for leak rates after the time of RCP saturation from 11.36 L/s [180 gpm] to 25.23 L/s [400 gpm] fluid flashing in the loop seals is not sufficient to clear them and a containment bypass condition does not result. For leak rates after the time of RCP saturation of greater than 25.23 L/s [400 gpm], however, the loop seals clear leading to a containment bypass condition. The judgments shown in Table 5.2 for the leakage range between 22.08 L/s [350 gpm] and 28.39 L/s [450 gpm] are based on the core damage and loop seal clearing trends seen at the lower and higher leak rates.

The results for a case where the leak rate between 13 minutes and the time of RCP fluid saturation is 11.48 L/s [182 gpm] are similar to those for the case where the leak rate during that period is 3.786 L/s [60 gpm].

5.2 Effect of Variations in Turbine-Driven Auxiliary Feedwater Operation and SG Steam Leakage

The results from six SCDAP/RELAP5 sensitivity calculations for more-realistic event sequence assumptions than used in the SBO base case accident sequence are discussed here. These "Group E" runs were performed for three purposes:

Evaluate the effects of TDAFW system operation on the results for key SBO accident event sequences.

Reconfirm the sensitivity of SG tube failure margin results to the assumed SG steam leakage flow area using the final upgraded code and plant models. (Earlier analyses found that smaller assumed SG steam leakage flow areas resulted in significantly improved SG tube failure margins.)

Evaluate the possibilities for interactions between the TDAFW operation and SG steam leakage flow area assumptions.

Table 5.2 Sensitivity of Results to Increased Shaft Seal Leakage After Transition of RCP Fluid from Liquid to Steam

Assumed Per-RCP Shaft Seal Leak Rate (gpm) (0 – 13 min) – (13 min – RCP Sat) – (After RCP Sat)	Average Tube Failure Margin	Hottest Tube Failure Margin	Loop Seals Cleared?	Early Core Failure?	Containment Bypass Condition Indicated?
21 – 21 – 21, (Base Case, No Increases)	2.7	1.7	No	No	Depends on Tube Strength Degradations and Locations (Minimum Margin < 3.0)
Case C-21-60-180	>7.0	>5.0	No	No	No (Minimum Margin >3.0)
Case C-21-60-300	>6.5	>5.0	No	No	No (Minimum Margin >3.0)
Case C-21-60-350	>7.0	>7.0	No	No	No (Minimum Margin >3.0)
From 21 – 60 – 350 to 21 – 60 – 400	>7.0	>7.0	No	Yes	No (Core Fails Prior to HL and Tubes)
From 21 – 60 – 400 to 21 – 60 – 450	N/A	N/A	Yes	No	Yes Loop Seal Clears Prior to HL Failure or Core Damage
Case 21-60-450	N/A	N/A	Yes	No	Yes Loop Seal Clears Prior to HL Failure or Core Damage
Case 21-60-480	N/A	N/A	Yes	No	Yes Loop Seal Clears Prior to HL Failure or Core Damage
Case 21–182-300	>7.5	>5.5	No	No	No (Minimum Margin >3.0) Results for 21-182-300 are similar to those for 21-60-300

The assumptions used for the Group E calculations, as well as other calculations against which they are compared, and the key results are listed in Table 5.3. The results from the individual sensitivity evaluations are summarized below. For the cases involving TDAFW system operation, note is made of the delay in the time of HL failure relative to the corresponding comparative cases where the TDAFW system was assumed not to operate. From the perspective of containment bypass risk, the additional time delays represent a period when opportunities for restoration of AC power may prove successful.

Case E1-A (RCP Shaft Seal Leak Rate Increases to 480 gpm at 13 Minutes and TDAFW Operates Until Battery Depletion at 4 Hours)

The Case E1-A assumptions are the same as for the base case except that the RCP shaft seal leak rate increases to 30.2 L/s [480 gpm] per pump at 13 minutes and TDAFW operates for the first four hours of the event sequence. The shaft seal leak rate assumptions for Case E1-A are the same as for Case A-480, which is described in Section 5.1.1. TDAFW is assumed to operate for four hours in Case E1-A whereas Case A-480 assumes no TDAFW operation.

The key findings from Case A-480 are that: (1) the loop seals do not clear even when the maximum 30.2-L/s [480-gpm] leak rate starts at 13 minutes and (2) the very high leak rate results in early core damage and a relocation of the core to the RV lower head prior to the time when the HL fails. Loop seal clearing is avoided for this case because the RCS depressurization occurs before the water in the loop seals can be significantly warmed by the steam in the RCS. Early core damage and relocation occurs for this case because the core is quickly voided of liquid as a result of the RCS mass lost through the large RCP shaft seal leaks.

Case E1-A was run to confirm that the key findings from Case A-480 remain valid even when TDAFW operation is considered. The Case E1-A results confirm those findings. Since a complete failure of the TDAFW system is unlikely, Case E1-A perhaps represents a more-realistic accident scenario than does Case A-480.

Case E2-A (RCP Shaft Seal Leak Rate Increases to 60 gpm at 13 Minutes and Again to 350 gpm When the RCP Fluid Temperature Reaches Saturation, TDAFW Operates Until Battery Depletion at 4 Hours)

The Case E2-A assumptions are the same as for Case C-21-60-350 (which is described in Section 5.1.2) except that TDAFW is assumed to operate until battery depletion at 4 hours. The HL failure time in Case E2-A is 33,020 s whereas in Case C-21-60-350 without TDAFW operation the HL failure time is 13,445 s.

The findings from Case C-21-60-350 are: (1) increasing the RCP shaft seal leak rate to 22.08 L/s [350 gpm] when the RCP fluid saturates does not result in loop seal clearing and (2) the SG tube failure margins are very large.

Case E2-A was run to confirm that the key findings from Case C-21-60-350 remain valid even when TDAFW operation is considered. The Case E2-A results confirm those findings. Since a complete failure of the TDAFW system is unlikely, Case E2-A perhaps represents a more-realistic accident scenario than does Case C-21-60-350.

Case E2-B (RCP Shaft Seal Leak Rate Increases to 60 gpm at 13 Minutes and again to 450 gpm When the RCP Fluid Temperature Reaches Saturation, TDAFW Operates Until Battery Depletion at 4 Hours)

The Case E2-B assumptions are the same as for Case C-21-60-450 (which is described in Section 5.1.2) except that TDAFW is assumed to operate until battery depletion at 4 hours. The HL failure time in Case E2-B is 28,265 s whereas in Case C-21-60-340 without TDAFW operation the HL failure time is 12,995 s.

The key finding from Case C-21-60-450 is that increasing the RCP shaft seal leak rate to 28.39 L/s [450 gpm] when the RCP fluid saturates results in clearing of one of the loop seals

Table 5.3 Results of Sensitivity Calculations Evaluating Variations in TDAFW System Operation and SG Secondary System Steam Leakage

Case Number	RCP Shaft Seal Leakage (gpm) Assumed per Pump	Steam Leak Flow Area per SG (in ²)	TDAFW Operation	SG Tube Failure Margins, Average/ Hot Tubes	Notes and Comments
Case E1-A	480 after 13 min	0.5	4 hours	N/A	No loop seal clearing. Core relocates to lower head prior to failure of HL, SL and SG tubes. Compare to Case A-480.
Case E2-A	21, 60 after 13 min and 350 after time of cold leg saturation	0.5	4 hours	N/A	No loop seal clearing. HL fails at 33,020 s. No failures of average or hottest SG tubes predicted. Core relocates to lower head at 34,889 s. Compare to Case C-21-60-350.
Case E2-B	21, 60 after 13 min and 450 after time of cold leg saturation	0.5	4 hours	N/A	No loop seal clearing. HL fails at 28,265 s. No failures of average or hottest SG tubes predicted. Core relocates to lower head at 28,692 s. Compare to Case C-21-60-450.
Case E3-A	21	0.2	None	3.41/2.09	Compare to Base Case.
Case E3-B	21	0.5	8 hours	2.04/1.52	Compare to Base Case.
Case E3-C	21	0.2	8 hours	2.08/1.53	Compare to Case E3-B and to Case E3-A.
Base Case	21	0.5	None	2.74/1.68	HL fails at 13,625 s.

Table 5.3 Results of Sensitivity Calculations Evaluating Variations in TDAFW System Operation and SG Secondary System Steam Leakage

Case Number	RCP Shaft Seal Leakage (gpm) Assumed per Pump	Steam Leak Flow Area per SG (in ²)	TDAFW Operation	SG Tube Failure Margins, Average/ Hot Tubes	Notes and Comments
Case A-480	480 after 13 min	0.5	None	N/A	No loop seal clearing. Core relocates to lower head prior to failure of HL, SL and SG tubes.
Case C-21-60-350	21, 60 after 13 min and 350 after time of cold leg saturation	0.5	None	N/A	No loop seal clearing. HL fails at 13,445 s. No failures of average SG tubes predicted. Core relocates to lower head at 14,991 s.
Case C-21-60-450	21, 60 after 13 min and 450 after time of cold leg saturation	0.5	None	Loop Seal Clearing Results in Tube Failure Prior to HL Failure or Core Relocation	One loop seal clears at 12,251 s. HL fails at 12,995 s. Core relocates to lower head at 14,187 s.

prior to HL failure or core relocation. Therefore SG tube failure resulting in containment bypass is indicated under those event sequence assumptions. The heating of water in the loop seals occurring prior to the time when the RCP fluid saturates promotes fluid flashing and clearing of water from the loop seals when the leak rate increases to 28.39 L/s [450 gpm].

Case E2-B was run to evaluate the effect that TDAFW operation would have on the key finding from Case C-21-60-450. The Case E2-B results indicate that if TDAFW operates the loop seal clearing does not occur, the SG tube failure margins are very large and the containment bypass condition is avoided. TDAFW operation in Case E2-B is found to keep the water in the loop seals cooler (relative to Case C-21-60-450) such that flashing of the loop seal water is inhibited and the loop seals do not clear when the RCP shaft seal leak rate increases to 28.39 L/s [450 gpm] per pump. Additionally, operation of the TDAFW system is seen to move forward the time when core damage and relocation occur, although HL failure still precedes the core relocation. Since a complete failure of the TDAFW system is unlikely, Case E2-B perhaps represents a more-realistic accident scenario than does Case C-21-60-450.

Case E3-A (0.2 in² per SG Steam Leakage Flow Area)

The Case E3-A assumptions are the same as the base case except that the assumed flow area for steam leakage from the SGs is reduced. The purpose of the Case E3-A calculation is to reconfirm the findings from an evaluation described in Section 2.6 that SG tube failure margins are significantly improved if reduced SG steam leakage flow areas are assumed. A comparison of the results for the base case calculation from Section 4 and the Case E3-A calculation using

the upgraded SCDAP/RELAP5 code and plant model confirm the previous finding. The comparison shows that reducing the steam leakage path flow area from 3.23 cm² [0.5 in²] to 1.29 cm² [0.2 in²] greatly increases the SG tube failure margins.

Case E3-B (TDAFW Operates Until Battery Depletion at 8 Hours)

The purpose of the Case E3-B calculation is to evaluate the effects of the TDAFW system operating temporarily for 8 hours on the SG tube failure margins under event-sequence assumptions that are otherwise the same as for the base case. The HL failure time in Case E3-B is 33,020 s whereas in the base case calculation without TDAFW operation the HL failure time is 13,625 s.

The results from the base case and Case E3-B calculations indicate that temporary TDAFW operation reduces the SG tube failure margins.

The heat-up of the RCS system occurs much later in the event sequence when TDAFW operates for eight hours than when it does not. The core decay power during the heat-up period is therefore much lower and the RCS heat-up rate is correspondingly slower. A slower heat-up rate reduces SG tube failure margins because the time constants involved with transporting heat from the RV into the SGs are less effective at delaying the SG tube heat-up (relative to the HL heat-up) than is the case at a faster heat-up rate. In other words, at a slow heat-up rate the inherent delays in transporting the heat into the SGs do not buffer the SG tubes from the effects of the increasing temperatures as well as they do when the heat-up rate is fast.

Case E3-C (0.2 in² per SG Steam Leakage Flow Area, TDAFW Operates Until Battery Depletion at 8 Hours)

The Case E3-C assumptions are the same as for the base case except that the flow area for SG steam leakage is reduced and TDAFW is assumed to operate until the time of battery depletion at 8 hours. The purpose of Case E3-C is to evaluate together the effects of reduced SG steam leakage and temporary TDAFW operation.

Comparing the failure margin results in Table 5.3 for Cases E3-C and E3-B, it is observed that when TDAFW operates only a small benefit results from the reduced SG steam leakage flow area. This result contrasts with the much-larger tube failure margin benefit seen for the same reduction in SG steam leakage flow when the TDAFW system does not operate (see margins for the base case and Case E3-A).

Comparing the results in Table 5.3 for Case E3-C and Case E3-A (1.29 cm² [0.2 in²] SG steam leakage in both cases) it is seen that the margin reduction resulting from temporary TDAFW operation is similar to that seen between the base case and Case E3-B (1.29 cm² [0.5 in²] SG steam leakage in both cases). The HL failure time in Case E2-C is 54,540 s whereas in Case E3-A without TDAFW operation the HL failure time is 13,950 s.

Comparisons among the results for the base case, Case E3-A, Case E3-B and Case E3-C in Table 5.3 indicate that the SG steam leakage assumption has considerable influence on the SG tube failure margins for sequences with no TDAFW operation and very little influence on the SG tube failure margins for sequences with temporary TDAFW operation. The conclusion is therefore that event-sequence assumptions related to temporary TDAFW operation (which directly affect the differential heat-up behavior between the SG and HL) have more influence on the analysis outcome than do the assumptions related to SG steam leakage.

5.3 Mitigative Operator Intervention

The effectiveness of two operator intervention strategies for mitigating the consequences of extended SBO accident events effects were evaluated.

In the first strategy, the operators implement SG feed-and-bleed cooling by using the turbine-driven auxiliary feedwater (TDAFW) system and opening the SG PORVs to depressurize the SGs at 30 minutes into the event sequence. An evaluation of this pre-core damage strategy is presented in Section 5.3.1.

In the second strategy, the operators depressurize the RCS by opening the pressurizer PORVs after plant instrumentation has indicated that the core damage process is underway. An evaluation of this post-core damage strategy is presented in Section 5.3.2.

Both operator intervention strategies require that action be taken prior to the time when the station batteries have been depleted. Afterward, operator control over PORVs on the secondary and primary coolant systems is lost and ability to deliver or control TDAFW may also be lost.

5.3.1 Pre-Core Damage Operator Action

Five SCDAP/RELAP5 sensitivity calculations were performed to evaluate the effectiveness of pre-core damage mitigative operator intervention. This intervention strategy assumes that the TDAFW system is operable. (This assumption is not included in the base case event sequence, but consideration that the TDAFW system operates, at least initially, may represent a more-realistic assumption.) The pre-core damage intervention strategy is based on SG secondary feed-and-bleed cooling in which cold TDAFW enters the SGs and the operators open the SG PORVs to depressurize and bleed steam from the SG secondary system at 30 minutes into the SBO event sequence. Issues affecting the timing of the operator intervention include the life of the station batteries and the available water inventory in the condensate storage tank (CST). Operator control over the SG PORVs and pressurizer PORVs is lost when the battery power is depleted, and the ability to deliver or control TDAFW may also be affected. The initial CST inventory is immediately available as a water source for TDAFW system, but after it is depleted another source of water would need to be available for the TDAFW system to continue operating.

The five calculations performed and the results obtained are listed in Table 5.4 along with the corresponding information for the base case calculation from Section 4, which assumes neither TDAFW operation nor operator intervention. Of particular note in the table is that TDAFW operation results in slight reductions in the SG tube failure margins but also significant delays in the time of HL failure relative to the base case event sequence. From the perspective of containment bypass risk, the additional time delays represent a period when opportunities for restoration of AC power may prove successful. Results for the individual sensitivity cases are summarized here, followed by conclusions regarding the effectiveness of pre-core damage operator intervention.

Case 153 (SG Depressurization at 30 Minutes, 4-Hour Battery Life, and TDAFW Stops When Batteries are Depleted)

Case 153 investigates the effects of the operators: (1) depressurizing the SGs at 30 minutes into the SBO event sequence and (2) controlling the delivery of TDAFW to the SGs until four hours, when the station batteries are assumed to be depleted. The Case 153 event sequence assumptions related to the SG depressurization and TDAFW operation are based on the Zion plant procedures, which are described as follows:

The operators are assumed to open the SG PORVs on all four SGs at 30 minutes (with additional requirements that in order to do so the SGs must have narrow range levels above 5% and the RCS average temperature must be above 138°C [280°F]). The operators are assumed to close the SG PORVs when the SG pressures have fallen to 1.86 MPa [270 psia], and afterward are assumed to control the SG PORVs to maintain the SG pressures between 1.93 and 2.0 MPa [280 and 290 psia]. The SG PORVs are assumed to become inoperative and fail closed at four hours, when the batteries are depleted.

A single TDAFW pump, with a total capacity of 56.8 L/s [900 gpm], is assumed to be operating and the flow available for delivery to each of the four SGs is 14.2 L/s [225 gpm]. It is assumed that the operators throttle the TDAFW flows to maintain normal SG levels. The TDAFW is assumed to be drawn from a 567,812 L [150,000 gallon] CST. The TDAFW system is assumed to fail when the entire CST inventory has been injected into the SGs or when the batteries are assumed to fail at four hours, whichever occurs first.

The results of the SCDAP/RELAP5 simulation for Case 153 are described as follows. The SG pressure responses are shown in Figure 5.1. The operators open the SG PORVs at 30 minutes. The SG pressures quickly fall to 1.86 MPa [270 psia] and the throttling of the SG PORVs to control the SG pressures between 1.93 and 2.0 MPa [280 and 290 psia] begins. With the SG PORVs fully open, it takes only ~1,000 s for the SG pressures to reach 1.86 MPa [270 psia]; the effective RCS cooldown rate associated with this process is ~265°C/hr [~477°F/hr].

Figure 5.2 shows that the SG depressurization causes a significant loss of secondary-side mass inventory and that the delivery of TDAFW replenishes the lost inventory. When the TDAFW flow stops, a boil-off of the SG inventory begins and by ~35,000 s the SGs have boiled dry. In Case 153 a total of 281,468 L [74,356 gal] of AFW, less than 50% of the CST inventory, is delivered to the SGs before the TDAFW system stops operating at four hours.

Figure 5.3 shows the RCS pressure response; the RCS depressurization is deeper than seen for the base case in Figure 4.1 because of the additional RCS cooling caused by the SG depressurization. The RCS pressure falls below the initial accumulator pressure (4.24 MPa [615 psia]) at 7,550 s and the accumulators inject water into the RCS until 14,688 s. About 17% of the initial accumulator water inventory is expelled into the RCS over this period. No accumulator injection is indicated in the base case run.

When the TDAFW flow stops the fluids in the SGs and RCS begin heating up and this causes the SG and RCS pressures to start rising. After the SGs have boiled dry, there is no longer liquid in the SGs to convert to steam and the flows through the steam valve leakage paths cause the SG pressures to decline. On the primary side however, the continuing heat-up

Table 5.4 Results of Sensitivity Calculations Evaluating Pre-Core Damage Mitigative Operator Intervention

Case No.	Case Description	HL Failure Time (s)	Stress Multiplier for Average SG Tube Failure Coincident with HL Failure	Stress Multiplier for Hottest SG Tube Failure Coincident with HL Failure
69	Base case	13,625	2.74	1.68
153	SGs depressurized at 30 min using Zion procedures, TDAFW runs to 4 hr	47,565	2.05	1.47
153A	SGs depressurized at 30 min using Surry procedures, TDAFW runs to 4 hr	53,645	2.00	1.44
161	SGs depressurized at 30 min using Zion procedures, TDAFW runs to 8 hr	67,120	1.89	1.31
161m	SGs depressurized at 30 min using Zion procedures, station batteries depleted at 8 hr, TDAFW runs until condensate storage tank depletion	93,085	1.96	1.53
165m	RCP leakage increases to 3.79 L/s [60 gpm] per pump at 13 min, SGs depressurized at 30 min using Zion procedures, station batteries depleted at 8 hr, TDAFW runs until condensate storage tank depletion	93,180	2.56	2.23

causes the RCS pressure to increase to the pressurizer SRV opening setpoint pressure. Afterward, the cycling of the pressurizer SRVs prevents further increases in the RCS pressure. The pressurizer PORVs (which have a lower opening setpoint pressure than the pressurizer SRVs) are assumed to not be operable after battery depletion at four hours.

The RCS and SG behavior seen for Case 153 are very similar to that seen for the base case event sequence, except that the event timing has been significantly extended as a result of the SG depressurization and TDAFW system operation. For Case 153, the first predicted creep rupture failure is Hot Leg 1 at 47,565 s, which is 33,940 s [9.4 hr] later than seen for the base case.

For Case 153 the tube failure margins are 2.05 for the average tube (compared with 2.74 in the base case) and 1.47 for the hottest tube (compared with 1.68 in the base case). It is therefore concluded that SG depressurization at 30 minutes and TDAFW operation for the first four hours (followed by TDAFW failure) results in lower SG tube failure margins than if the SGs are not depressurized and TDAFW never operates. The primary cause for the reduced SG tube failure margins is related to the core decay power at the time when the RCS experiences the heat-up. In Case 153, the heat-up is encountered 9.4 hours later than in the base case and as a result

the core decay power is much lower and the RCS heat-up is much slower than in the base case. As the heat-up rate declines the tube failure margins also decline because the time lag for heat to be passed from the reactor vessel into the SGs becomes less effective at slowing the rate of tube temperature increase relative to the rate of HL temperature increase. This time lag is related to the HL and SG tube circulation rates, which are determined by the target hot leg discharge coefficient and target SG recirculation ratio and which are the same, regardless of the RCS heat-up rate.

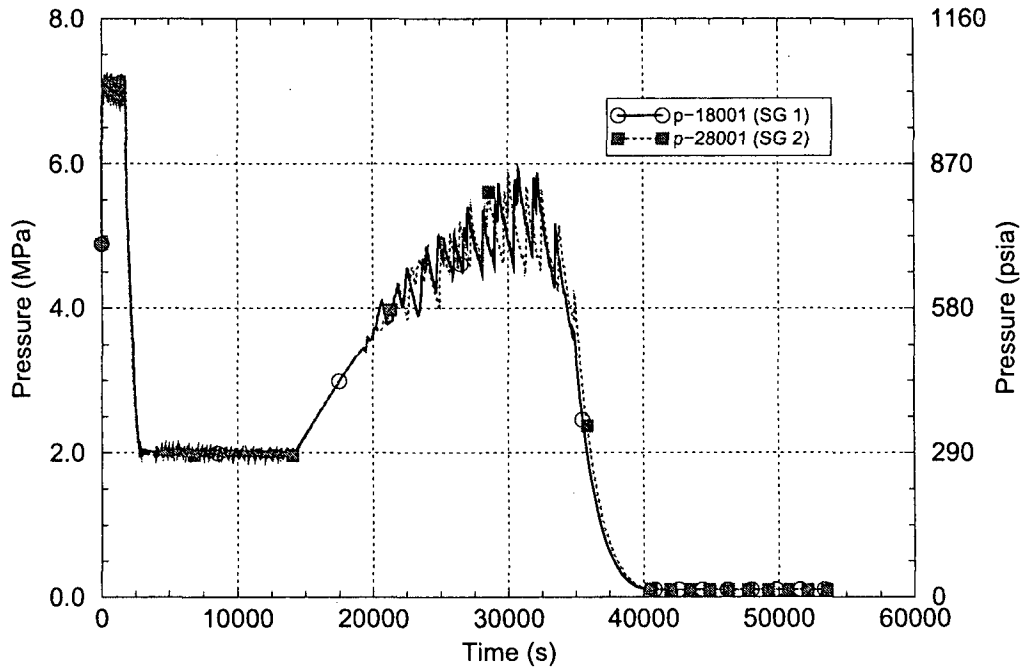


Figure 5.1 Case 153 SG Secondary Pressures

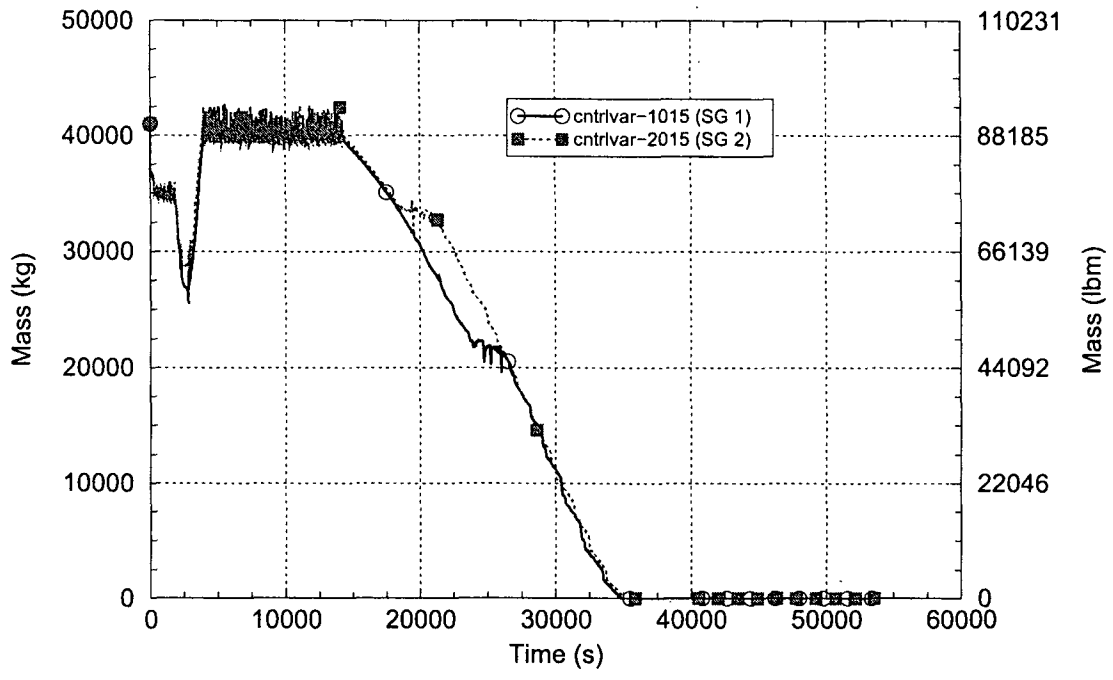


Figure 5.2 Case 153 SG Water Masses

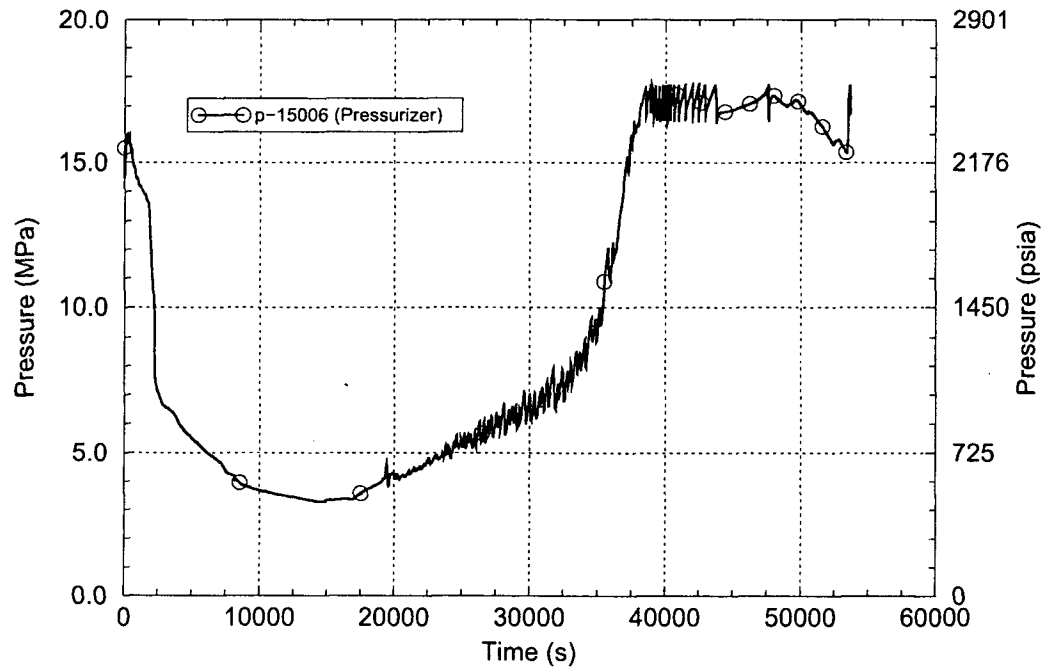


Figure 5.3 Case 153 RCS Pressure

Case 153A (Evaluation of Plant-Specific Assumptions for the SG Depressurization)

Case 153, described above, assumes that the operators depressurize the SGs by opening the SG PORVs at 30 minutes, leave them open until the SG pressures decline to 1.86 MPa [270 psia], and afterward control the SG PORVs to maintain the SG pressures between 1.93 and 2.0 MPa [280 and 290 psia]. These Zion plant procedures result in an effective RCS cooldown rate of $\sim 265^{\circ}\text{C/hr}$ [$\sim 477^{\circ}\text{F/hr}$].

Case 153A evaluates the effects of changing the operator action procedure for the SG depressurization to those for the Surry plant as provided in Reference 5.2. For Surry, the operators are assumed to manually control the SG PORVs to maintain a 55.6°C/hr [100°F/hr] cooldown rate and to stop the depressurization when the SG pressures reach 0.827 MPa [120 psia]. The Case 153A event sequence is therefore the same as Case 153, except that the SG depressurization implemented by the operators is much slower.

Figures 5.4, 5.5 and 5.6 show the Case 153A SG pressures, SG masses and RCS pressure responses. The responses for Case 153A are seen to be very similar to those for Case 153, except because of the slower depressurization the event sequence timing for Case 153A is extended by $\sim 5,000$ s [~ 1.4 hr]. This much additional time is needed in Case 153A to deplete the SG secondary inventory, fully depressurize the SGs and heat up the RCS. The HL failure is experienced at 53,645 s in Case 153A, compared with 47,565 s in Case 153. Even though the SG and RCS cooldown rates are lower, the depressurization of the SGs to the lower pressure in Case 153A results in a greater depressurization of the RCS and more accumulator injection.

For Case 153A the tube failure margins are 2.00 for the average tube (compared with 2.05 for Case 153) and 1.44 for the hottest tube (compared with 1.47 for Case 153). The small margin reductions seen from Case 153 to Case 153A, in which the sequence timing is delayed by $\sim 5,000$ s [~ 1.4 hr], are consistent with the finding that extending the event sequence timing reduces the margins. However no significant differences are noted between the results from the two cases and therefore it is concluded that the impact of using the Surry procedures rather than the Zion procedures for the SG depressurization is small. On that basis, the remaining analyses in this section are completed using only the Zion SG depressurization procedures.

Case 161 (SG Depressurization at 30 Minutes, 8-Hour Battery Life and TDAFW Stops When Batteries are Depleted)

Case 161 evaluates the effects of operator actions: (1) depressurizing the SGs 30 minutes into the SBO event sequence and (2) controlling the delivery of TDAFW to the SGs until eight hours, when the station batteries are assumed to be depleted. This case is identical to Case 153 except that the battery life is increased from four hours to eight hours.

When the TDAFW flow stops, a boil-off of the SG inventory begins and by $\sim 51,500$ s the SGs have boiled dry. In Case 161 a total of 408,052 L [107,796 gal] of AFW, about 72% of the CST inventory, is delivered to the SGs before the TDAFW system stopped operating.

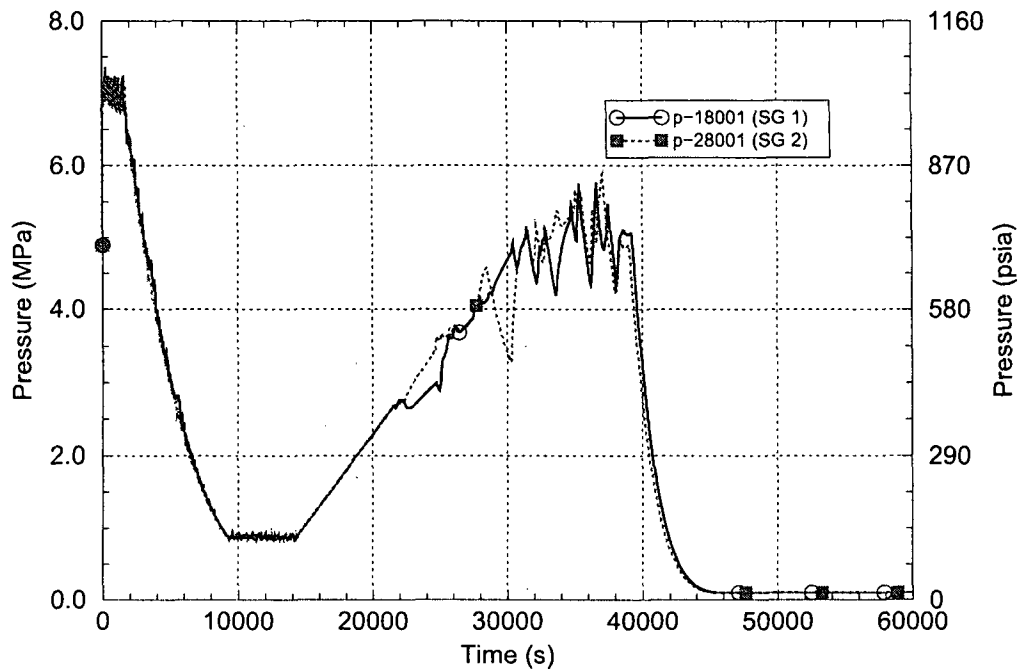


Figure 5.4 Case 153A SG Pressures

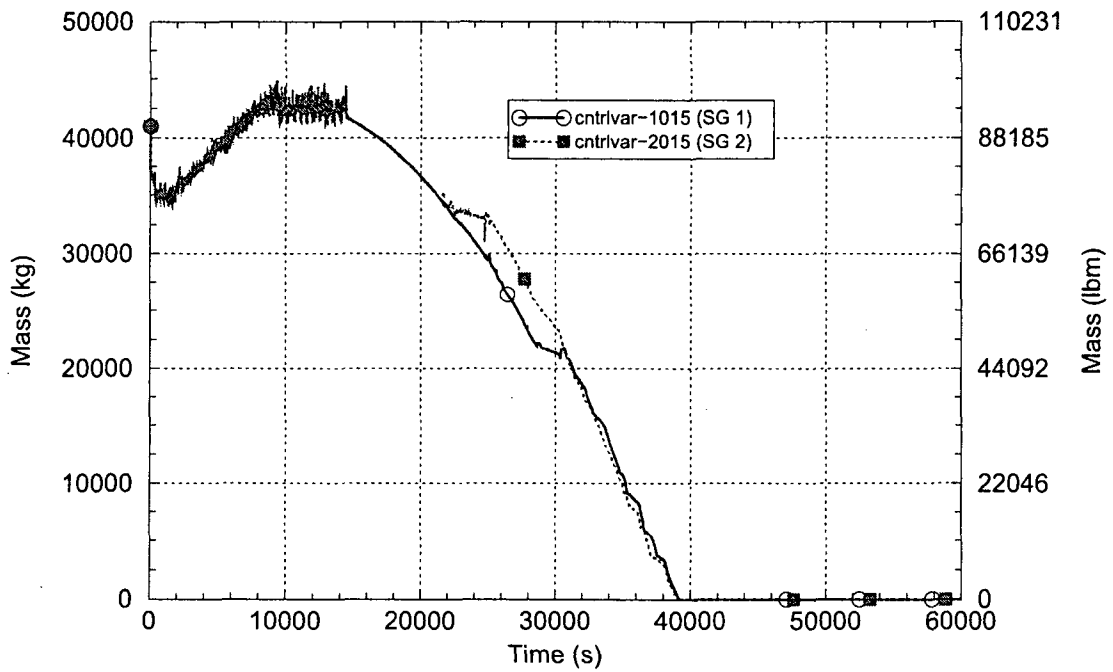


Figure 5.5 Case 153A SG Water Masses

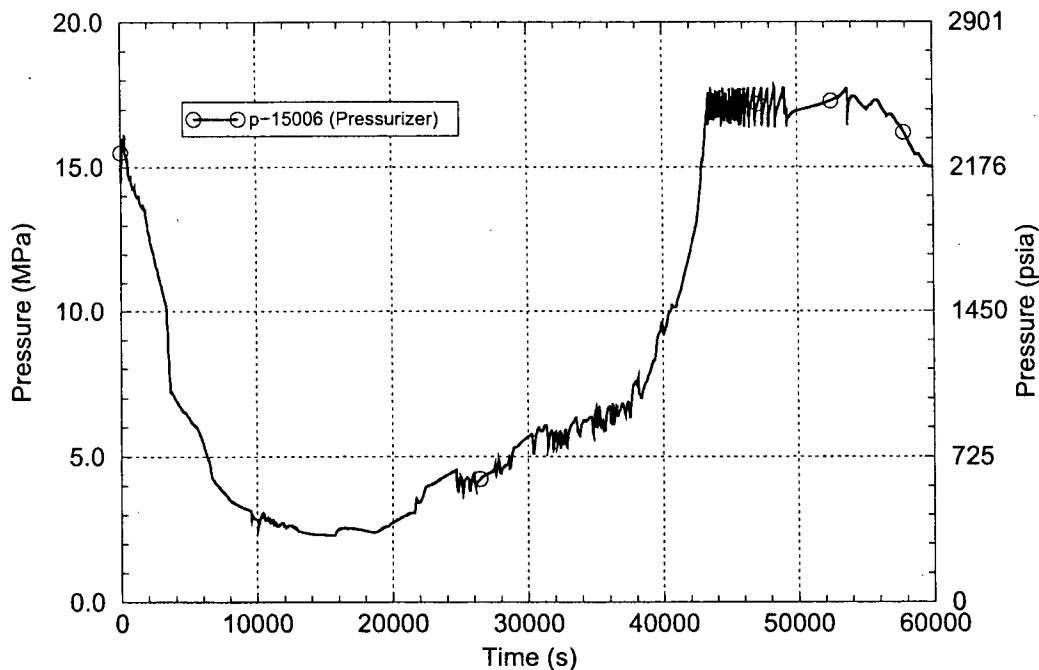


Figure 5.6 Case 153A RCS Pressure

Figure 5.7 shows the RCS pressure response for Case 161. The minimum RCS pressure is somewhat lower for Case 161 than for Case 153 because of the additional RCS cooling resulting from the longer TDAFW system operation and the longer period over which the SGs are maintained at low pressure. In Case 161, the RCS pressure falls below the initial accumulator pressure (4.24 MPa [615 psia]) at 7,555 s and the accumulators inject water into the RCS until 28,560 s. About 59% of the initial accumulator water inventory is expelled into the RCS over this period.

When the TDAFW flow stops the fluids in the SGs and RCS begin heating up, and this causes the SG and RCS pressures to begin rising. After the SGs boil dry, there is no longer liquid in the SGs to convert to steam and the flows through the steam valve leakage paths cause the SG pressures to decline, as shown in Figure 5.8. On the primary side however, the continuing heat-up causes the RCS pressure to increase to the pressurizer SRV opening setpoint pressure. Afterward, the cycling of the pressurizer SRVs prevents further increases in the RCS pressure. The pressurizer PORVs (which have a lower opening setpoint pressure than the pressurizer SRVs) are assumed to not be operable after battery depletion at eight hours.

For Case 161, the first predicted creep rupture failure is Hot Leg 1 at 67,120 s, which is 19,555 s [5.4 hours] later than seen for Case 153. The Case 161 SG tube failure margins are 1.89 for the average tube (compared with 2.05 in Case 153) and 1.31 for the hottest tube (compared with 1.47 in Case 153).

The primary cause for the lower SG tube failure margins in Case 161 is related to the lower core decay power at the time when the RCS encounters the heat-up. In Case 161, the heat-up is experienced 5.4 hours later than in Case 153 and as a result the core decay power is lower and the RCS heat-up is slower than in Case 153.

It is concluded that SG depressurization at 30 minutes and TDAFW operation for the first eight hours (followed by TDAFW failure) results in lower SG tube failure margins than if the TDAFW had instead operated only for four hours.

Case 161m (SG Depressurization at 30 Minutes, 8-Hour Battery Life and TDAFW Continues Running Until Condensate Storage Tank Depletion)

Case 161m is used to evaluate the effects of operator actions: (1) depressurizing the SGs 30 minutes following the start of the SBO event sequence and (2) controlling the delivery of TDAFW to the SGs until the CST has been depleted of water. The sequence assumes an eight-hour battery life; afterward the pressurizer PORVs and SG PORVs are inoperable. This case is identical to Case 161 except that TDAFW runs past the time when the station batteries are depleted until the CST empties, which occurs at 54,890 s [15.3 hours]. After the TDAFW flow stops the SG inventories are boiled off, followed by heat-up and pressurization of the RCS and SG systems. The continuation of the TDAFW operation from eight hours to 15.3 hours in Case 161m retards the SG pressurization and delays the heat-up relative to Case 161. The Case 161m HL failure occurs at 93,085 s [25.9 hours]; for Case 161 the HL failed 25,965 s [7.21-hours] earlier than that.

For Case 161m the tube failure margins are 1.96 for the average tube (compared with 1.89 in Case 161) and 1.53 for the hottest tube (compared with 1.31 in Case 161). The tube failure margin comparisons between the two cases are the opposite of what was expected given the trends seen in the other comparisons among the other cases. Those trends suggest that continuing the TDAFW system operation longer prior to its failure results in reduced failure margins. Yet, the margins calculated for Case 161m (for which the TDAFW system runs 7.3 hours longer than in Case 161) are increased, not reduced, relative to Case 161.

The cause for this difference was found to be related to the operation of SG PORVs, which are assumed to fail closed at eight hours in both cases. A separate run, Case 161mA, was made in which Case 161m was repeated except that the SG PORVs were allowed to continue operating along with the TDAFW system after eight hours and up to the time of CST depletion. The Case 161mA run indicated that the HL failure occurs 460 s later than in Case 161m and also showed the expected tube failure margin reduction (in comparison with the Case 161).

Figure 5.9 compares the HL temperatures between Case 161m and Case 161mA. After eight hours, the HL temperatures are lower for Case 161mA where the SG PORVs continue operating, than for Case 161m where they do not. This result is expected because of the better cooling of the RCS provided by continued operation of the SG PORVs in Case 161mA. However, the lower HL temperatures in Case 161mA should result in an increased, not reduced SG, tube failure margin.

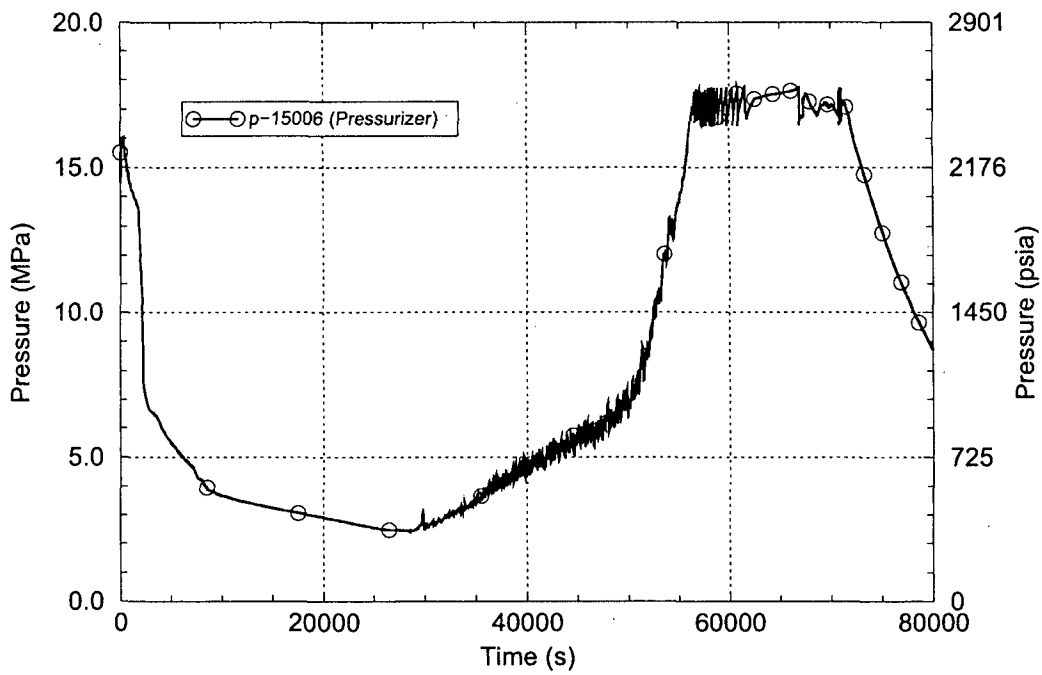


Figure 5.7 Case 161 RCS Pressure

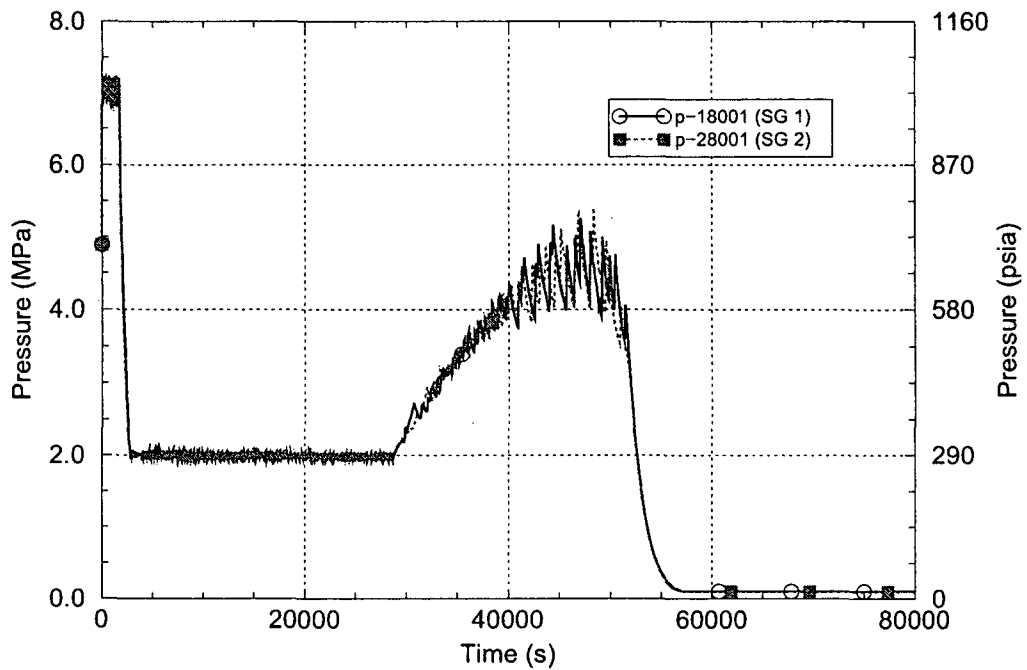


Figure 5.8 Case 161 SG Secondary Pressures

Figure 5.10 compares the RCS pressures between Case 161m and Case 161mA. This figure shows that at eight hours the RCS pressure in Case 161m immediately begins increasing but in Case 161mA the RCS pressure continues declining until the SG PORV operation is finally stopped when the CST empties at 54,890 s [15.3 hours]. The continuation of the RCS depressurization in Case 161mA is caused by heat removal to the SGs resulting from operation of the SG PORVs. Since at eight hours the RCS pressure is below the accumulator pressure, the continuing RCS pressure decline in Case 161mA results in additional accumulator injection into the RCS in comparison to Case 161m. When the RCS heat-up is eventually encountered, the additional RCS inventory in Case 161mA leads to higher RCS pressures, which persist into the period, at ~93,300 s [~25.9 hours], when the HL failures are encountered in both cases. The reduced failure margin seen in Case 161mA (in comparison with Case 161m) is therefore caused by the higher RCS pressures that result from continuing the operation of the SG PORVs past the time of station battery depletion.

The conclusion drawn from the analysis of Case 161m is that continuing the TDAFW system operation past the time of battery depletion (when the pressurizer PORVs and SG PORVs cease operating) improves the SG tube failure margins.

Case 165m (RCP Shaft Seal Leakage Increased to 60 gpm/pump at 13 Minutes, SG Depressurization at 30 Minutes, 8-Hour Battery Life and TDAFW Continues Running Until Condensate Storage Tank Depletion)

Case 165m assumes that the RCP shaft seal leakage rate increases from 1.32 L/s [21 gpm] to 3.77 L/s [60 gpm] per pump at 13 minutes and is used to evaluate the effects of operator actions: (1) depressurizing the SGs 30 minutes into the SBO event sequence and (2) controlling the delivery of TDAFW to the SGs until the CST has been depleted of water. The sequence assumes an eight-hour battery life; afterward the pressurizer PORVs and SG PORVs are inoperable. This case is identical to Case 161m except for the increased RCP shaft seal leakage rate.

The results of the SCDAP/RELAP5 run for Case 165m are described as follows. Figure 5.11 compares the RCS pressure responses for Cases 165m and 161m. The RCS depressurization seen during the SG depressurization period is deeper for Case 165m because of the additional RCS cooling afforded the RCS by the higher RCP shaft seal leakage rate. The RCS pressure falls below the initial accumulator pressure (4.24 MPa [615 psia]) at 3,161 s [0.88 hr] in Case 165m and the accumulators inject water into the RCS until 28,659 s [7.96 hr]. About 60% of the initial accumulator water inventory is expelled into the RCS over this period (this value compares with about 41% for Case 161m).

The TDAFW system continues to operate until the CST empties, which occurs at 55,550 s [15.4 hours]. This time is 660 s later for Case 165m than for Case 161m. The additional RCS cooling afforded by the greater RCP shaft seal leakage in Case 165m reduces the demand for AFW, moderately extending the CST depletion time.

The Case 165m HL failure occurs at 93,180 s [25.88 hours]. This is only 95 s different from the time when the HL fails in Case 161m. For Case 165m the tube failure margins are 2.56 for the average tube (compared with 1.96 for Case 161m) and 2.23 for the hottest tube (compared with 1.53 for Case 161m). As the RCS and SG systems heat up and the conditions leading to HL failure are approached, the lower RCS pressure resulting from the higher RCP shaft seal leakage rate in Case 165m reduces the stresses on the SG tubes compared with Case 161m, where the RCS remains at a high pressure. At the times of the respective HL failures, the RCS

pressure is 3.88 MPa [563 psi] lower in Case 165m than in Case 161m. However by the times of the HL failures the SGs in both cases have been completely depressurized, as shown in Figure 5.12, and the SG pressures for the two cases differ by only 68 Pa [0.01 psi]. As a result of the lower RCS pressure, the SG tube failure margins for Case 165m are higher than for Case 161m.

The conclusion drawn from the comparative analysis of Case 165m and Case 161m is that the modest 2.46 L/s [39 gpm] per pump increase in the RCP seal leakage rate significantly improves the SG tube failure margins. The margin gained from the higher RCP seal leakage rate is seen to be much larger than the margin lost as a result of continuing TDAFW system operation past the time of the station battery depletion.

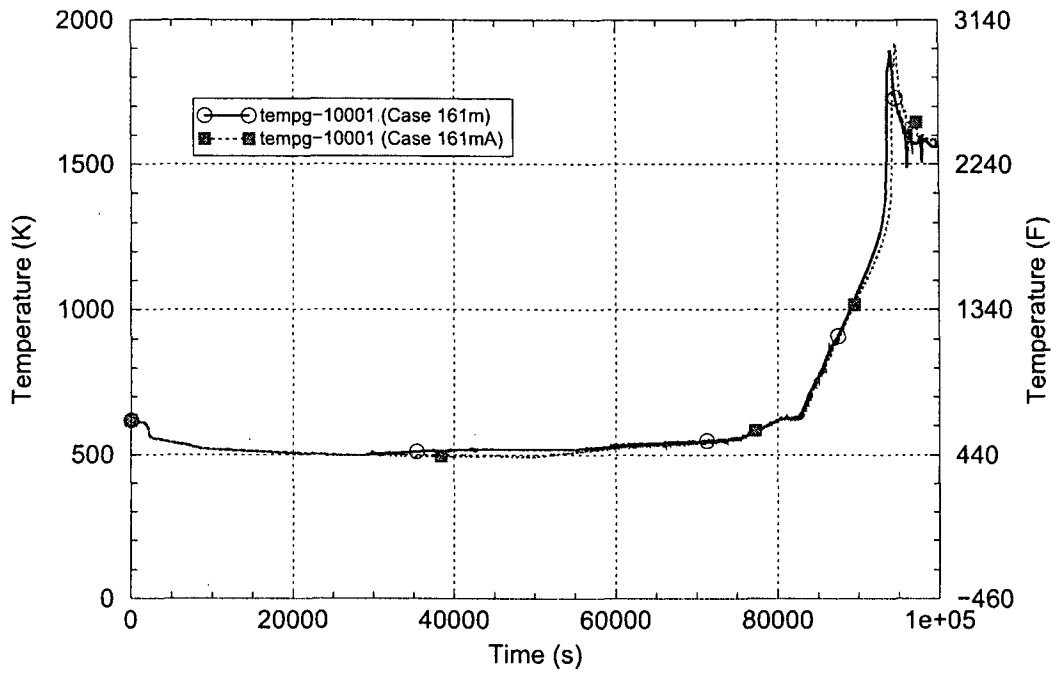


Figure 5.9 Case 161m and Case 161mA HL Vapor Temperatures

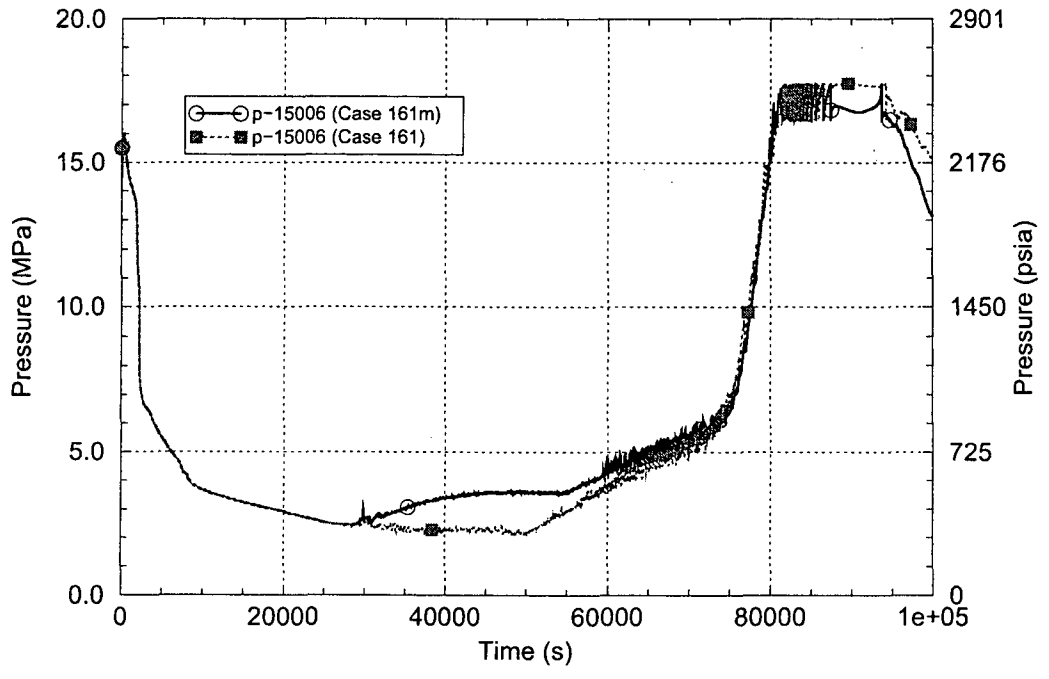


Figure 5.10 Case 161m and Case 161mA RCS Pressures

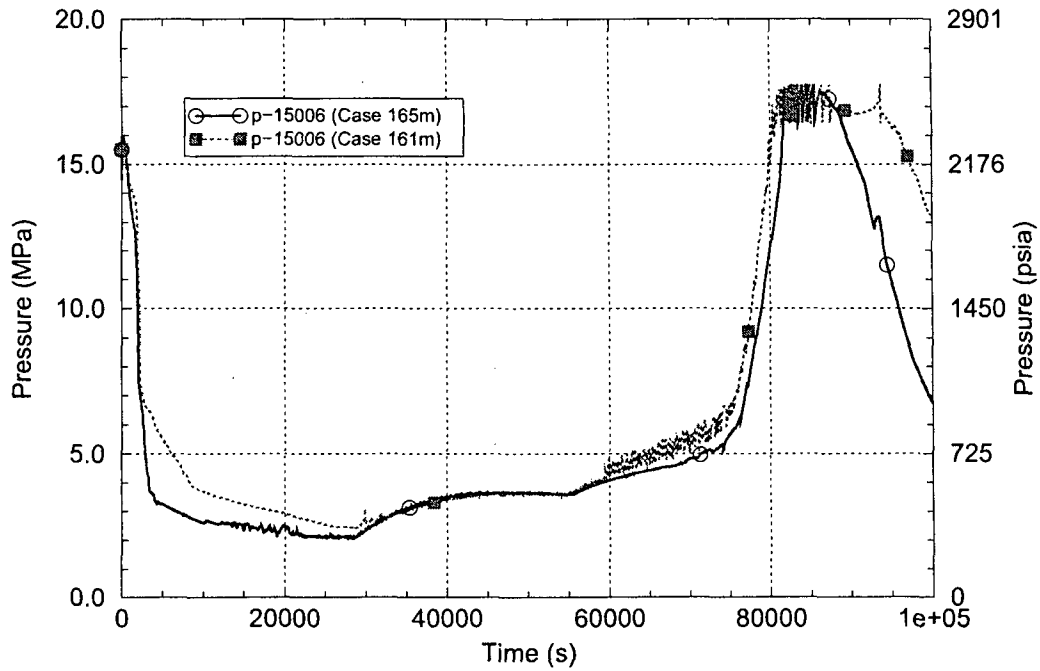


Figure 5.11 Case 165m and Case 161m RCS Pressures

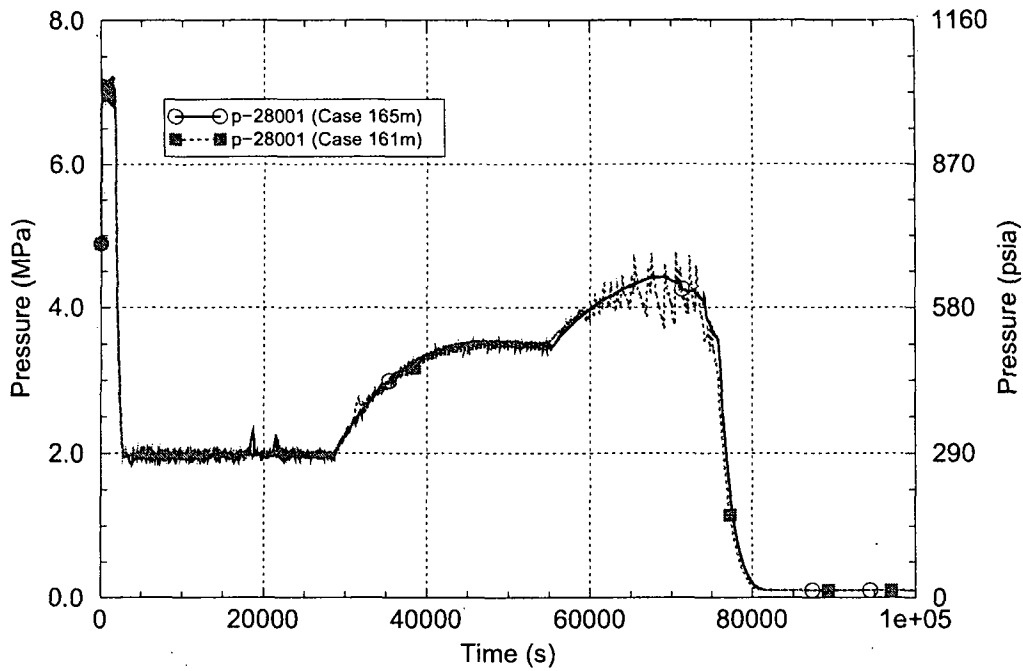


Figure 5.12 Case 165m and Case 161m SG 2 Pressures

Summary of the Effectiveness of Pre-Core Damage Mitigative Operator Intervention

The pre-core damage operator intervention strategy (feeding the SGs with TDAFW and bleeding steam from the SGs through the SG PORVs at 30 minutes into the SBO event sequence) is seen to be effective in the short term for removing core decay heat and preventing an RCS heat-up that could lead to containment bypass. At a minimum, this strategy significantly delays the onset of an RCS heat-up, thereby providing time for other plant recovery opportunities to be considered and implemented.

In the long term, the SG PORVs fail closed and the ability to deliver or control TDAFW may be lost after the station battery power has been depleted. Additionally, a means of replenishing the CST water inventory or aligning a separate water source for the TDAFW system is needed. To be successful in the long term, the pre-core damage operator intervention strategy requires that a TDAFW water source remain available and that some capability to deliver the water into the SGs continues.

For the event sequences analyzed with assumptions that lead to an RCS heat-up in the long term, no large changes in SG tube failure margins (relative to the corresponding no-operator intervention cases) were seen to result from implementing the pre-core damage operator intervention strategies. Depending upon the operator intervention procedure, the assumed life of the station batteries and assumptions regarding operation of the TDAFW system, both minor increases and minor decreases in SG tube failure margins may be experienced relative to the no-operator intervention cases. For the purpose aiding future evaluations of pre-core damage operator intervention, the following minor parametric sensitivities are identified:

The combination of the operators depressurizing the SGs at 30 minutes and TDAFW system operation until the time of battery depletion at four hours is seen to result in reductions in the SG tube failure margins compared with the base case (which assumed neither SG depressurization nor TDAFW operation). The primary cause for the margin reduction is related to the time when the RCS heat-up is experienced. A later heat-up is slower as a result of reduced core decay power. As the heat-up rate declines the SG tube failure margins also decline because the time lag for heat to be passed from the RV into the SGs becomes less effective at slowing the rate of tube temperature increase relative to the rate of HL temperature increase.

For the same reason, SG tube failure margin reductions are seen for cases where the heat-up is experienced later because the TDAFW system is assumed to operate longer.

An evaluation of the effect of varying the SG depressurization rate allowed during the operator intervention indicated no significant sensitivity of results to that parameter.

Continuing the TDAFW system operation past the time of battery depletion (when the pressurizer PORVs and SG PORVs cease operating) and until the time when the CST water inventory is depleted moderately improves the SG tube failure margins.

A modest 2.46 L/s [39 gpm] per pump increase in the RCP seal leakage rate improves the SG tube failure margins. The improvement so gained is seen to be larger than the SG tube failure margin lost as a result of continuing the TDAFW system operation past the time of the station battery depletion.

5.3.2 Post-Core Damage Operator Action

Four SCDAP/RELAP5 sensitivity calculations were performed to evaluate the effectiveness of mitigative operator intervention to depressurize the RCS by opening pressurizer PORVs once the plant instrumentation has provided an indication that core damage is in progress. The calculations performed and the results obtained are listed in Table 5.5 along with the corresponding information for the base case calculation from Section 4, which assumed no operator intervention.

The sensitivity-case assumptions are the same as for the base case except that the operators take action by opening one or two pressurizer PORVs. In the model, two PORVs are represented, each with a saturated steam flow capacity of 26.5 kg/s [210,000 lbm/hr] at 16.2 MPa [2,350 psia]. (A survey of Westinghouse plants indicates that this valve flow capacity is typical, with some plants employing two PORVs and others employing three PORVs. Another potential plant-to-plant variation regards the period that PORVs remain operable, depending on whether they are air-operated or electric-operated.) The operators are assumed to take action either at the time when the core exit temperature reaches 922 K [1,200°F], or 12 minutes after that time. A high core-exit temperature is an indicator that the core has been uncovered, causing superheated steam to flow from the top of the core, and that core damage is in process. The 12-minute delay reflects an estimate of the additional time required for the Technical Support Center to analyze the plant data and to agree that PORVs should be opened. The base case and all four of the sensitivity case event sequences assume a four-hour station battery depletion time. After that time the pressurizer PORVs and SG PORVs are assumed to fail closed, their automatic functions are assumed to be inoperative and operator control over the valves is assumed to be lost. The results of the post-core damage operator intervention calculations are summarized as follows.

For the one-PORV cases the HL fails before battery depletion. The RCS cooling afforded by opening only one pressurizer PORV is limited. The core fails early, with damaged fuel starting to block the core flow at about the time that the HL is predicted to fail. The core heat therefore goes into melting the core and not into the SGs, resulting in very large SG tube failure margins. No containment bypass is indicated for the one-PORV cases.

For the two-PORV cases the HL fails after battery depletion. The greater RCS cooling afforded by opening two pressurizer PORVs rapidly depressurizes the RCS and also prevents early core damage. The low RCS pressure reduces the stresses on the HL and SG tube structures, significantly delaying their failures. When the pressurizer PORVs fail closed after battery depletion, the RCS begins re-pressurizing and re-heating and this subsequently leads to HL and SG tube failures. The SG tube failure margins are seen to improve relative to the base case as a result of the pressurizer PORVs having been open. During the period when PORVs are open, the primary flow of hot steam from the core and out of the RCS through the pressurizer PORVs passes through the pressurizer-loop HL, keeping its structure temperature elevated. However, during this period, flows through the SGs stagnate, allowing the SG tubes to significantly cool

Table 5.5 Results of Sensitivity Calculations Evaluating Post-Core Damage Mitigative Operator Intervention

Assumed Operator Actions	Average Tube Failure Margin	Hottest Tube Failure Margin	Loop Seals Cleared?	Early Core Failure?	Containment Bypass Condition Indicated?
None (Base Case)	2.7	1.7	No	No	Depends on Tube Strength Degradations and Locations (Minimum Margin < 3.0)
1 Pressurizer PORV Opened When Core Exit Temperature Reaches 1,200°F	>7.5	>7.5	No	Yes	No (Core Fails at About Same Time as the Hot Leg)
1 Pressurizer PORV Opened 12 Minutes After Core Exit Temperature Reaches 1,200°F	>7.5	>7.5	No	Yes	No (Core Fails at About Same Time as the Hot Leg)
2 Pressurizer PORVs Opened When Core Exit Temperature Reaches 1,200°F	4.6	4.1	No	No	No (Minimum Margin >3.0)
2 Pressurizer PORVs Opened 12 Minutes After Core Exit Temperature Reaches 1,200°F	3.2	2.9	No	No	Marginally No (Minimum Margin ~3.0)

down. After the PORVs fail close and the RCS begins to heat-up again, the difference in the HL and tube temperatures at the start of the re-heat process causes the HL failure conditions to be reached earlier (with respect to the SG tube failure conditions) than is seen in the base case run, which assumed no operator intervention. Because the minimum SG tube failure margins are ~3 or higher, no containment bypass is indicated for the two-PORV cases. As shown Table 5.5, this judgment is marginal for the two-PORV case with the 12-minute delay.

The finding that opening only one pressurizer PORV looks to be more effective at preventing containment bypass than opening two pressurizer PORVs is counter-intuitive. Opening only one PORV is not sufficient to prevent the rapid progression of core damage, fuel melting and core flow blockage. Containment bypass is therefore avoided when opening one PORV because of early core damage and core flow blockage. Opening two PORVs prevents the rapid core-damage progression, but as a result the challenges to the integrity of the HL and SG tube structures persist. Compared with opening only one PORV, opening two PORVs provides an advantage in that additional time becomes available during which recovery of plant systems (for

example, restoration of AC power or arrangement of some source of auxiliary feedwater) could prove effective in preventing failure of the core, the HLs and the SG tubes.

In summary, all four of the post-core damage operator interventions evaluated are shown to be effective at preventing containment bypass.

5.4 Sensitivity of Results to Assumed Split of SG Tubes into Hot and Cold Sections

The SBO base case calculation in Section 4 assumes that 10% of the tubes in each SG are blocked and that the SG tubes are split into hot and cold tube sections representing 41% and 59%, respectively, of the remaining unblocked SG tubes.

The most recent CFD evaluations (Reference 3.14) indicate that a 30%/70% tube split is within the range of possibilities for some periods of the transient. Employing fewer tubes in the hot tube section results in the same mass flow of hot steam passing through a smaller number of tubes, thereby increasing the SG tube heating rate and reducing tube failure margins.

To evaluate the effects of this worst-case tube split assumption, a SCDAP/RELAP5 sensitivity calculation using the 30%/70% assumption was performed. Results for the sensitivity case are very similar to those for the base case. The first primary system failure in the sensitivity case is Hot Leg 1 at 13,565 s (it occurred at 13,625 s in the base case). The average tube multiplier for failure coincident with the HL is 2.57 (in the base case it was 2.74). The hottest tube multiplier for failure coincident with the hot leg is 1.48 (in the base case it was 1.67). The SG tube failure margin reductions resulting from changing the tube split from 41%/59% to 30%/70% are judged to be moderate. Therefore, uncertainties related to this issue for the findings in this report regarding containment bypass in general are also judged to be moderate.

5.5 Effects Related to Opening SG Tube and HL Rupture Flow Paths

Independent thermal-hydraulic analyses related to the containment bypass issue are underway as a part of a separate project, the State-of-the-Art Reactor Consequences Analyses (SOARCA) Project. Unlike, the SCDAP/RELAP5 analyses presented in this report, in the SOARCA analyses, the opening of rupture flow paths (from the primary to secondary coolant system through ruptured SG tubes and from the primary coolant system into the containment through ruptured HLs) are directly modeled. The SOARCA analysis results therefore include system pressure responses and tube and pipe rupture flows not seen in the SCDAP/RELAP5 analyses. The tube and piping rupture flow responses are primarily of interest for considering the radiological release aspects of containment bypass.

To provide a basis for comparing results between the SCDAP/RELAP5 and SOARCA analysis methods, four SCDAP/RELAP5 sensitivity calculations were performed in which SG tube rupture and HL rupture flow paths were directly modeled. The SCDAP/RELAP5 sensitivity calculations performed are listed in Table 5.6 and are summarized as follows.

Table 5.6 Results of Sensitivity Calculations Evaluating the Effects of Opening SG Tube Rupture and HL Rupture Flow Paths

Case Number	Size of SG Tube Rupture Modeled	Time of SG Tube Rupture	Hot Leg Break Modeled
F1	Equivalent to the double-ended rupture of one tube	Time in the base case run when the hottest tube with a stress multiplier of 2.0 is predicted to fail (13,560 s)	No
F2	Equivalent to the double-ended rupture of one tube	Time in the base case run when the hottest tube with a stress multiplier of 2.0 is predicted to fail (13,560 s)	Yes. The HL is predicted to fail at 13,630 s and the break is opened at that time.
F3	Equivalent to the double-ended rupture of one tube	Time in the base case run when the hottest tube with a stress multiplier of 3.0 is predicted to fail (13,140 s)	No
F4	Equivalent to the double-ended rupture of four tubes	Time in the base case run when the hottest tube with a stress multiplier of 2.0 is predicted to fail (13,560 s)	No

Cases F1 through F4 use the same set of assumptions as in the base calculation in Section 4 except that simulation of SG tube ruptures in the pressurizer-loop steam generator are directly modeled. The SG tube inner diameter is 1.97 cm [0.775 in]. The size of the assumed tube break between the SG primary and secondary systems varies from case to case, along with the time when the tube break is assumed to open. The tube breaks are assumed to be double-ended, with a total flow area per ruptured tube of twice the tube flow area: 6.08 cm² [0.943 in²]. The SG tube ruptures are modeled in the first active tube cell above the top of the tubesheet in the hot tube section (Component 110, Cell 3, see Figure 3.16). Additionally, rupture of the HL in Loop 1 with a break size equivalent to the flow area of the pressurizer surge line is modeled in one of the cases.

For reference, pertinent data from the base case calculation in Section 4 are as follows:

HL failure time: 13,625 s

SG-1 average tube multiplier for failure coincident with HL: 2.74

SG-1 hottest tube multiplier for failure coincident with HL: 1.68

At end of calculation (18,000 s) the core is partially molten but not yet relocated

Case F1 (Rupture of a Single Tube at Time When the 2.0 Stress Multiplier Hottest Tube Fails)

The SG tube rupture is modeled to occur at 13,560 s, which is 65 s prior to the time of HL failure in the base case. The SG tube ruptures when the 2.0 stress multiplier SG-1 hottest tube is predicted to fail in the base case. In Case F1 the HL fails 5 s later than in the base case (at 13,630 s) and the SG-1 average tube multiplier for failure coincident with the HL declines to 2.49. For this case the HL is predicted to fail 70 s after the time the SG tube rupture opens. The flow through the SG tube break peaks (at ~13 kg/s) at the time of the rupture and continues at a reduced rate throughout the remainder of the run (averaging ~3 kg/s). The pressurization of SG 1 by the tube break causes the SG-1 PORV to cycle open and closed several times between 13,884 s and the time of battery depletion at 4 hours. The SG PORVs fail closed and are inoperative after the batteries are depleted. The SG-1 SRVs did not open. The total integrated mass lost to the environment through the SG-1 PORV is 600 kg. Note that in this run an actual rupture of the HL is not modeled and that the first time the SG-1 PORV opens is 254 s after the time when the HL is predicted to fail. Had the RCS depressurization effects of opening the HL break been modeled, none of the 600 kg release to the environment would have been predicted to occur. The effects of opening the HL break, including the prevention of the environmental release are included in the modeling for Case F2. In Case F1, a significant portion of the core relocates to the RV lower head at 16,304 s.

Case F2 (Rupture of a Single Tube at Time When the 2.0 Stress Multiplier Hottest Tube Fails and Subsequent Rupture of the Hot Leg)

The SG tube rupture is modeled to occur at 13,560 s, which is 65 s prior to the time of HL failure in the base case. In Case F2 the HL failure is predicted to occur at 13,630 s (which is 5 s later than in the base case) and the HL break path is opened at that time. The HL break is simulated as a flow path from HL 1 to the containment with a flow area equivalent to that of the 0.284-m [11.2-in] I.D. pressurizer surge line. For this case the HL is predicted to fail 70 s after the time the SG tube rupture opens. The flow through the SG tube break peaks (at ~13 kg/s) at the time of the tube rupture, but quickly turns negative as a result of the rapid RCS depressurization caused by opening the HL break. The pressurization of SG 1 by the tube break is not sufficient to open the SG-1 PORV prior to the time when the HL break opens. Therefore, in Case F2 no

SG-1 PORV or SG-1 SRV flow to the environment is experienced. The Case F2 run failed at 13,723 s, which is 93 s after the HL break opens. We attempted to advance the run further but were unsuccessful in doing so. At the end of the Case F2 calculation the core has been significantly damaged but has not yet relocated to the RV lower head. Melted and refrozen fuel blocks the two hottest fuel channels and molten porous debris resides in major portions of other three core channels. It is concluded that opening the HL break rapidly blows down the RCS into containment, thus removing further challenges to the integrity of the SG tubes, accelerating the core damage process and preventing a release to the environment.

Case F3 (Rupture of a Single Tube at Time When the 3.0 Stress Multiplier Hottest Tube Fails)

The SG tube rupture is modeled to occur at 13,140 s, which is 485 s prior to the time of HL failure in the base case. The SG tube ruptures when the 3.0 stress multiplier SG-1 hottest tube failed in the base case. In case F3 the HL fails 45 s later than in the base case (at 13,670 s) and the SG-1 average tube multiplier for failure coincident with the HL increases to 4.39. For this case the HL is predicted to fail 530 s after the time the SG tube rupture opens. The flow through the SG tube break peaks (at ~16 kg/s) at the time of the rupture and continues at a reduced rate throughout the remainder of the run (averaging ~4 kg/s). The pressurization of SG 1 by the tube break causes the SG-1 PORV to cycle open and closed many times between 13,516 s and the time of battery depletion at 4 hours. The SG PORVs fail closed and are inoperative after the batteries are depleted. The total integrated mass lost to the environment through the SG-1 PORV is 2,068 kg. Following battery depletion, the SG-1 SRVs open for the first time at 15,666 s and cycle open and closed many times between then and the end of the calculation at 18,000 s. During that period, the total integrated mass lost to the environment through the SG-1 SRVs is 2,438 kg. Note that in this run an actual rupture of the HL is not modeled and that only a portion of the time period when the SG-1 PORV opens and none of the time period when the SG-1 SRVs open is prior to the time when the HL is predicted to fail. Had the RCS depressurization effects of opening the HL break been modeled, only 864 kg of the release through the SG-1 PORV and none of the release through the SG-1 SRVs would have been predicted to occur. In Case F3, a significant portion of the core relocates to the RV lower head at 15,064 s, which is shortly before the SG-1 SRVs open for the first time.

Case F4 (Rupture of Four Tubes at Time When the 2.0 Stress Multiplier Hottest Tube Fails)

The SG tube rupture is modeled to occur at 13,560 s, which is 65 s prior to the time of HL failure in the base case. The SG tube ruptures when the 2.0 stress multiplier SG-1 hottest tube failed in the base case. In case F4 the HL fails 15 s later than in the base case (at 13,640 s) and the SG-1 average tube multiplier for failure coincident with the HL declines to less than 1.5. For this case the HL is predicted to fail 80 s after the time the SG tube rupture opens. The flow through the SG tube break peaks (at ~45 kg/s) at the time of the rupture and continues at a reduced rate throughout the remainder of the run (averaging ~3 kg/s). The pressurization of SG 1 by the tube break causes the SG-1 PORV to continuously cycle open and closed between 13,615 s and the time of battery depletion at 4 hours. The SG PORVs fail closed and are inoperative after the batteries are depleted. The total integrated mass lost to the environment through the SG-1 PORV is 5,241 kg. Following battery depletion, the SG-1 SRVs open for the first time at 17,436 s and cycle open and closed continuously between then and the end of the calculation at 18,000 s. During that period, the total integrated mass lost to the environment through the SG-1 SRVs is 8,014 kg. Note that in this run an actual rupture of the HL is not modeled and that only a portion of the time period when the SG-1 PORV opens and none of the time period when the

SG-1 SRVs open is prior to the time when the HL is predicted to fail. Had the RCS depressurization effects of opening the HL break been modeled, only 344 kg of the release through the SG-1 PORV and none of the release through the SG-1 SRVs would have been predicted to occur. In Case F4, a significant portion of the core relocates to the RV lower head at 17,237 s.

Conclusions from the SOARCA-Counterpart SCDAP/RELAP5 Calculations

Ruptures of the equivalent of one and four SG tubes were modeled at the times when the 2.0 and 3.0 stress multiplier hottest tubes were predicted to fail in the base case run. These assumed SG rupture times are 65 s and 485 s, respectively, prior to the time when the HL fails in the base case calculation in Section 4. These predictions indicate that opening the SG tube break flow paths does not significantly affect the timing of the subsequent HL failure. Modeling the tube break does delay the HL failure and this is as expected since the tube breaks begin to depressurize the RCS. However, the predicted HL failure time delays are very small: only 5 s (one tube) and 15 s (four tube) for breaks that open 65 s prior to the base case HL failure and 45 s for a one-tube break that opens 485 s prior to the base case HL failure.

The peak flows through the tube breaks are found to be ~15 kg/s per double-ended tube rupture. A single ruptured tube removes fluid from the RCS at a rate which is on the same order as the circulating flows in the HLs (~5 kg/s) and in the SG tubes (~10 kg/s) near the time when the HL is predicted to fail. CFD predictions (NUREG-1922) indicate that leakage rates of this magnitude completely break down the overall natural circulation flow patterns and tubes near the leaking tube are subjected to temperatures approaching the hot leg flow temperatures. These results suggest that a potential exists for propagation of tube failures, with the first tube to fail drawing additional hot steam into that SG potentially leading to additional tube failures.

As expected, the fluid released to the environment through the PORV and SRVs of the SG containing ruptured tubes is seen to be proportional to the number of tubes assumed to rupture and to the time period during which flow from the RCS passes into the SG.

Directly modeling the tube ruptures is seen to result in an acceleration of the core degradation process. In comparison with the base case run, which did not model tube breaks, the effects of modeling tube ruptures are seen to result in earlier melting of fuel, blockage of core flow channels and relocation of molten core materials to the RV lower head.

Finally, it is concluded that opening a HL break rapidly blows down the RCS into containment, thus removing further challenges to the integrity of the SG tubes, additionally accelerating the core damage process and significantly reducing or eliminating the environmental release.

6. GROUPING OF EXTENDED SBO EVENT SEQUENCES INTO CONTAINMENT BYPASS, POTENTIAL FOR CONTAINMENT BYPASS, AND NO CONTAINMENT BYPASS CATEGORIES

The Westinghouse four-loop plant thermodynamic conditions experienced *during a typical non-LOCA accident event sequence with normal operation of the safety systems* are characterized in Table 6.1. With the safety systems available, both the primary and secondary cooling systems remain pressurized and water-filled. The core heat passes from the fuel rods into the RCS cooling water, and from there through the SG tubes into the SG water inventory. Steam produced in the SGs is released to the environment through the SG PORVs and the SG inventory lost is replenished by the AFW system. The plant conditions with safety systems available reflect a continuation of these safe and stable fluid conditions.

The plant thermodynamic conditions experienced *during the hypothetical extended SBO severe accident event sequences evaluated in this report* are characterized in Table 6.2. The loss of AC-powered plant safety systems is assumed to prevent replenishment of the water inventories, resulting in dry conditions in both the primary and SG secondary systems. Because of the dry SGs, the heat sink available for the core fission product decay power is insufficient and as a result the RCS remains pressurized and experiences a transient heat-up. The assumed dry conditions in the secondary system make it susceptible to depressurization due to leakage through valves in the main steam system and as a result the secondary system pressure falls. The high differential pressure across the SG tubes and the weakened structural strength caused by the increasing temperatures significantly increase the likelihood of SG tube failures. The containment bypass risk is therefore created during for extended SBO events because of the increased potential for SG tube failure during the system heat-up. Of note is that the SGs remain a heat sink for the RCS (albeit a poor one), and this induces hot steam to be drawn from the reactor core into the SGs. Also of note is that, because the total heat sink for the reactor core heat is insufficient, both the RCS and SG systems experience transient heat-ups and it is the *differences between the heat-up behaviors (especially the heat-up timing and rates) experienced in various portions of the plant*, in particular between the HLs and the SG tubes, which are of most importance for the containment bypass issue.

The objective of this report is to coalesce the findings from prior and current evaluations (using the failure margin definitions and selection criteria described in Section 1.4) into a view of the extended SBO severe accident event sequences that fall into the following three categories:

- Sequences **resulting in containment bypass** (undegraded, 1.0-stress multiplier, hottest SG tube is predicted to fail prior to the HL)
- Sequences with a **potential for resulting in containment bypass** (hottest SG tube failure margin is between 1.0 and 3.0)
- Sequences **not resulting in containment bypass** (hottest SG tube failure margin is 3.0 or higher).

This categorization of event sequences provides information that (when combined with results from pertinent SG tube structural analyses, probabilistic risk assessments and environmental release evaluations) permits an evaluation of risks due to containment bypass.

Table 6.1 Characterization of Plant Fluid Conditions During Typical Non-LOCA Accident Sequences with Normal Operation of Safety Systems

RCS Pressure	RCS Water Inventory	SG Water Inventory	SG Pressure
High	Wet	Wet	High
~15.5 MPa [~2,250 psia]	RCS water-filled, with a liquid/steam interface within the pressurizer	SG downcomer and boiler regions water-filled, with a liquid/steam interface in the separator region	~6.9 MPa [~1,000 psia]
RCS pressure maintained by operation of pressurizer heater and spray systems, pressurizer PORVs and SRVs prevent overpressure condition	Water inventory replenished by HPI and charging systems, pressurizer level controlled within normal range by operation of charging system	SG water level controlled within normal range by operation of AFW system	Heat transfer from RCS to SGs pressurizes the secondary coolant system, SG PORVs and SRVs prevent overpressure condition

Table 6.2 Characterization of Plant Fluid Conditions During an Extended Station Blackout Accident Sequence

RCS Pressure	RCS Water Inventory	SG Water Inventory	SG Pressure
High	Dry	Dry	Low
~16 MPa [~2,320 psia]	RCS becomes mostly steam-filled	SG secondary system becomes steam-filled	~0.1 MPa [~15 psia]
Insufficient heat sink for the reactor core causes the RCS fluid to heat up	Heat-up causes RCS water inventory to be expelled through the pressurizer PORVs and SRVs	Core heat is first removed to the SG water inventory, which is boiled to steam	The boiling process causes SG pressure to remain elevated until the water inventory has been lost
Fluid expansion effects increase and maintain RCS pressure near the pressurizer PORV/SRV opening setpoint pressures	Water remains in the cold leg loop seal regions and in the region below the core in the RV, core heat causes RCS temperatures to significantly increase	Steam is expelled from the secondary system through the SG PORVs and SRVs	After SG dry-out the steam-filled secondary system is susceptible to depressurization due to leakage through main steam outlet valves
High RCS pressure maintains stress on the SG tubes	High RCS temperatures weaken the SG tube material strength	Steam in the SGs is cooler than the steam in the RCS, causing the SGs to remain an inefficient heat sink for the reactor core heat	Low SG pressure greatly increases stress on SG tubes

The categorization of event sequences is performed by using the evaluations and considerations described in this report to select the parameters which have been found to have major influences on the four fluid conditions required for occurrence of containment bypass (high-pressure RCS, dry RCS, dry SG and low-pressure SG as listed in the columns of Table 6.2). From among this set of parameters, those which are identified as being the most influential are selected as the key event-sequence parameters regarding the containment bypass outcome. The quantitative results from the evaluations summarized in this report are then used to map the containment bypass outcome as a function of the key event sequence parameters.

It is cautioned that the event sequence categorizations presented here are estimates which may be affected by many factors, some of which are summarized as follows. The 3.0 hottest-tube failure margin criterion is arbitrary. Prototype SGs may or may not contain SG tubes with material-strength properties that have been degraded to that extent. The criterion assumes that the hottest steam entering any of the SG tubes enters a tube with that reduced material strength. The event sequence categorization is made based on limited number of SCDAP/RELAP5 simulations; the borders between the regions for the three categories are necessarily assigned using judgments about the behavior to be expected between data points directly supported by the simulations. The total uncertainty in the SCDAP/RELAP5-predicted hottest-tube failure margin is judged to be about 0.4. The methodical PIRT-based uncertainty evaluation summarized in Section 2.9 found that the standard deviation in the hottest tube failure time was 54.89 s which, when used with the base-case hottest-tube failure time data from Table 4.4, gives a two-sigma uncertainty around the 3.0 hottest tube failure margin of about 0.20. However, additional uncertainties affecting the hottest-tube failure margin prediction likely also apply (such as the +0.58 attributed to the assumed HL nozzle material, see Section 2.10, and the -0.19 attributed to modeling a worst-case split of the SG tubes into hot and cold sections, see Section 5.4).

Despite the limitations of the event sequence categorization process described in the preceding paragraph, the results are useful for defining the set of event sequences which clearly pose a risk for containment bypass and the set of event sequences which clearly do not. For those event sequences providing only a potential for containment bypass, the results are also useful for focusing upon the parameters for which additional analyses may be productively employed to further clarify event-sequence outcomes.

Event sequences which do not involve operator intervention are categorized in Section 6.1 and event sequences involving operator intervention are categorized in Section 6.2.

6.1 Categorization of Event Sequences Without Operator Intervention

At the highest level, the containment bypass outcomes for certain event sequences are seen to be determined by loop seal clearing behavior or by the timing of core damage and relocation behavior:

The analyses in this report demonstrate that event sequences resulting in the clearing of one or more loop seals lead to containment bypass. With a loop seal cleared of water, hot steam flows around the coolant loop (from the RV outlet nozzle, through the HL, SG, RCP and CL to the RV inlet nozzle) in direction of normal flow during powered operation. In this situation the SG tubes rapidly fail because they are continually exposed to the hottest steam given off by the core; see the discussion in Section 1.3.

The analyses in this report also demonstrate that certain event sequence assumptions promote acceleration of the core damage process such that containment bypass is avoided. If core damage progresses rapidly enough, then the core geometry may be significantly altered and the core may be relocated to the lower head of the RV prior to the time when coolant loop piping or SG tube structural failures occur. In this situation the core decay heat primarily goes into altering the structure of the core, which generally results in blockage of the flow paths through the core, reduction of the effective area for transfer of heat from the core material to the core fluid, and relocation of significant portions of the core to the lower head of the RV. With the core reconfigured in such a manner and the flow of heat to the SGs correspondingly reduced, the challenge to the structural integrity of the SG tubes is removed and containment bypass does not occur.

Beyond these top level considerations, the evaluations presented in this report were reviewed for the purpose of identifying other considerations related to event sequence assumptions, plant configuration, and SCDAP/RELAP5 modeling important for determining the containment bypass outcome. The results of this review (and references to pertinent evaluations in this report) for event sequences without operator intervention are listed in Table 6.3.

The items listed in the "Modeling Considerations" table column reflect SCDAP/RELAP5 modeling uncertainties affecting the calculated SG tube failure margins but which were generally not found to be sufficiently influential to alter the containment bypass outcome.

The items listed in the "Plant Configuration Considerations" table column reflect plant-specific assumptions related to piping configuration, component materials and plant operating condition. These items also were found to affect the calculated SG tube failure margins but generally not sufficiently to alter the containment bypass outcome.

The items listed in the "Event Sequence Consideration" table column reflect assumptions defining the event sequences themselves and evaluations related to these items were found to most-directly affect the containment bypass outcomes. Of the seven items listed in this column, the top four items, shown in bold, were judged to be the most significant regarding containment bypass outcome. The assumptions related to the size and timing of RCP shaft seal leakage affect the depressurization of the RCS, which reduces the stresses on SG tubes. However, if the RCS depressurization is sufficiently rapid, loop seal clearing or early core damage and relocation may result. The assumption as to the operability of the TDAFW system directly affects removal of core heat from the RCS and prevents heat-up of the SG tubes. While most of the analyses presented in this report assumed the TDAFW system inoperable, an assumption that TDAFW operates, at least initially, likely represents a more-realistic condition. Leakage of steam from the SGs through closed main steam line valves results in depressurization of the SG secondary systems, which increases the stresses on the SG tubes. The analyses demonstrate that after SG dry-out relatively small steam leakage paths are sufficient to fully depressurize the SGs by the time when piping and SG tube structures are predicted to fail.

These four items (RCP shaft seal leakage rate, RCP shaft seal leakage timing, TDAFW system operation and leakage of steam from the SG secondary system) are judged to be the key parameters affecting the containment bypass outcome for event-sequences without operator intervention. The quantified evaluations for these key parameters in this report are used to

Table 6.3 Major Considerations and Influences on the Containment Bypass Outcome for Event Sequences Without Operator Intervention

Event Sequence Considerations	Plant Configuration Considerations	Modeling Considerations
RCP shaft seal leakage rate (See Sections 2.3, 2.4, 5.1, 5.2 and Appendices A and D)	SG tube plugging (See Sections 2.3, 2.4 and Appendix A)	Heat loss from RCS and SGs to containment (See Sections 2.3, 2.4 and Appendixes A and D)
RCP shaft seal leakage timing (See Sections 2.3, 2.4, 5.1, 5.2 and Appendix D)	Configuration of the connection of the surge line to the HL (See Appendix D)	Prediction of the transient fuel rod cladding oxidation rate (See Sections 2.4, 3.3.2 and Appendix D)
TDAFW system operation (See Sections 2.6, 5.2 and Appendix B)	RV outlet nozzle materials (See Section 2.10 and Appendix E)	HL discharge coefficient (See Sections 2.5, 2.8, 3.4 and Appendix D)
Leakage of steam from SG secondary system (See Sections 2.6, 5.2 and Appendixes B and D)		Hot and cold mixing fractions (See Sections 2.3, 2.4, 2.8, 2.10, 3.5 and Appendixes A and D)
Stuck-open SG secondary system relief valves (See Section 2.3 and Appendix D)		Recirculation ratio (See Sections 2.3, 2.8, 2.10, 3.5 and Appendixes A and D)
Station battery life (See Sections 2.6, 5.2 and Appendix B)		Split of SG tubes into hot and cold sections (See Sections 2.3, 2.8, 2.10, 3.5 and Appendix D)
Pre-existing SG tube leakage (See Section 2.4 and Appendix D)		Tube-to-tube inlet steam temperature variations, NTR (See Sections 2.3, 2.8, 2.10 and 3.5)
		Heat transfer coefficient on outside of SG tubes (See Section 2.4 and Appendixes A and D)
		Circulating flows internal to the RV (See Sections 2.4, 2.5 and Appendixes A and D)
		Core damage and relocation modeling (See Sections 2.4, 3.3 and Appendix A)

construct the maps of containment bypass outcome shown in Figures 6.1 through 6.5. The findings shown in these maps are discussed as follows.

Variations in SG Steam Leakage and RCP Shaft Seal Leakage Which Increases After 13 Minutes

Figure 6.1 illustrates the estimated containment bypass outcome as a function of the assumed SG steam leakage flow area and the assumed RCP shaft seal leakage rate after 13 minutes.

Very small assumed SG steam leakage flow areas (up to $0.64 \text{ cm}^2/\text{SG}$ [$0.1 \text{ in}^2/\text{SG}$]) were found to keep the SG secondary pressures elevated and sufficiently reduce the stresses on the SG tubes to prevent their failure. For larger assumed SG steam leakage flow areas the SGs are significantly depressurized prior to the time of the RCS heat-up, providing a potential for containment bypass.

Following the loss of RCP seal injection at the beginning of the event sequence, a shaft seal leakage rate of 1.325 L/s [21 gpm] per pump represents postulated minimum leakage from the RCS into the containment through the shaft seals. In addition, certain seal failures may occur at around 13 minutes into the SBO event, possibly resulting in shaft seal leakage rates as high as 30.2 L/s [480 gpm] per pump. The evaluations show that potential for containment bypass exists for increased RCP shaft seal leakage rates below 11.36 L/s [180 gpm] per pump. At that rate and higher, the shaft seal leakage flow depressurizes the RCS sufficiently to reduce the stresses on the SG tubes and prevent their failure. The evaluations show that the RCS depressurizations experienced from increases in RCP shaft seal leakage up to the maximum 30.2 L/s [480 gpm] per pump at 13 minutes do not result in loop seal clearing. An important factor influencing this finding is that at 13 minutes the SGs have not yet dried out and the temperature of the water in the loop seals is far below the RCS saturation temperature. The flashing of the cool water in the loop seals caused by the increased RCP shaft seal leak rates after 13 minutes is not sufficient to clear the water from the loop seals.

Variations in SG Steam Leakage and RCP Shaft Seal Leakage Which Increases When the RCP Fluid Reaches the Saturation Temperature

Figure 6.2 illustrates the estimated containment bypass outcome as a function of the assumed SG steam leakage flow area and the assumed RCP shaft seal leakage rate after the time when the fluid in the RCPs reaches the saturation temperature.

As in the discussion in the preceding section, very small assumed SG steam leakage flow areas (up to $0.64 \text{ cm}^2/\text{SG}$ [$0.1 \text{ in}^2/\text{SG}$]) were found to keep the SG secondary pressures elevated and sufficiently reduce the stresses on the SG tubes to prevent their failure. For larger assumed SG steam leakage flow areas the SGs are significantly depressurized prior to the time of the RCS heat-up, providing a potential for containment bypass.

Following the loss of RCP seal injection at the beginning of the event sequence, a SG shaft seal leakage of 1.325 L/s [21 gpm] per pump represents the postulated minimum leakage flow from the RCS into the containment through the shaft seals. In addition, certain seal failures may occur at around 13 minutes into the SBO event and certain other seal failures may occur when the fluid in the RCPs changes from liquid to steam. The presence of steam in the RCPs is indicated by the liquid temperature reaching the saturation temperature, which occurs at about 2 hours into the base case event sequence.

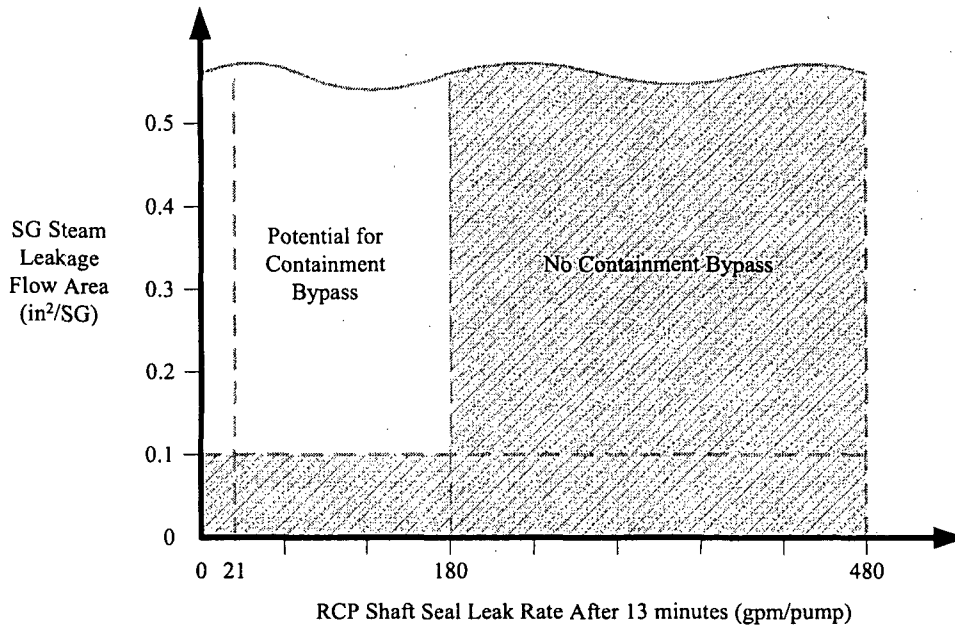


Figure 6.1 Map of Containment Bypass Outcome for No Operator Intervention and Variations in SG Steam Leakage and RCP Shaft Seal Leakage Which Increases at 13 Minutes

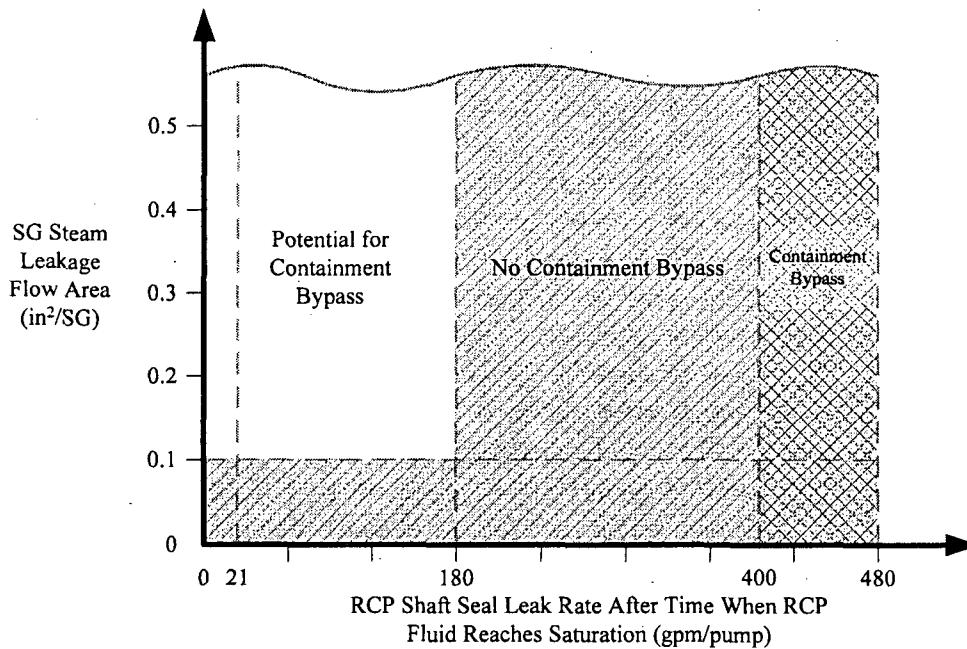


Figure 6.2 Map of Containment Bypass Outcome for No Operator Intervention and Variations in SG Steam Leakage and RCP Shaft Seal Leakage Which Increases When the RCP Fluid Reaches the Saturation Temperature

The investigations in this report evaluated the effects of a shaft seal leakage increase to 3.786 L/s [60 gpm] per pump at 13 minutes followed by a second increase to a higher rate when the RCP fluid temperature reaches saturation. The evaluations show a potential for containment bypass for increased RCP shaft seal leakage rates of less than 11.36 L/s [180 gpm] per pump. At that rate and up to 25.23 L/s [400 gpm] per pump, the shaft seal leakage depressurizes the RCS sufficiently to reduce the stresses on the SG tubes, preventing their failure and avoiding containment bypass. However, (unlike the sequences for which the increase to a high leakage rate occurs at 13 minutes) above a 25.23 L/s [400 gpm] per pump leak rate the RCS depressurization is sufficient to clear the loop seals, resulting in containment bypass. The heating of the water in the loop seals that occurs between 13 minutes and 2 hours (which is after SG dry-out and during the RCS heat-up period) results in increased flashing of the loop seal water and the clearing of the loop seals when the leakage rate increases for the second time.

Variations in Temporary TDAFW System Operation and RCP Shaft Seal Leakage Which Increases After 13 Minutes

Figure 6.3 illustrates the estimated containment bypass outcome as a function of temporary TDAFW system operation and RCP shaft seal leakage which increases at 13 minutes.

Event sequences in which the TDAFW system operates and continues operating do not lead to containment bypass. In this situation, heat passes from the RCS into the water-filled SGs. The outer surfaces of the SG tubes remain cool and the low tube temperatures prevent their rupture, regardless of the pressure stresses caused by high RCS pressure and low SG pressure. RCP shaft seal leakage does result in a loss of the RCS inventory, however heat removal to the SGs continues even after the upper regions of the RCS become steam filled. The continued loss of the RCS inventory may eventually lead to a condition where the core is uncovered or otherwise not adequately cooled. In this event core failure may occur but, because TDAFW operation would continue cooling the SG tubes, containment bypass would not occur.

Challenges to continued TDAFW operation result from: (1) depletion of the station batteries, which may result in valve failures preventing delivery or control of the TDAFW flow, (2) the need to arrange for an alternate source of water for the TDAFW system following depletion of the CST inventory and (3) a loss of SG pressure sufficient to affect operation of the TDAFW turbine, which powers the pump. Station battery depletion is estimated to occur between 4 and 8 hours and CST water inventory depletion is estimated to occur at about 15 hours. Extrapolations of the behavior seen in SCDAP/RELAP5 simulations in which TDAFW operates and maintains SG levels until 8 hours suggest that sufficient SG pressure will remain available for driving the TDAFW turbine until 15 hours, and perhaps beyond that.

For event sequences in which the TDAFW system is assumed to initially operate and then later fail, results are similar to those seen when the TDAFW does not operate at all. For RCP shaft seal leak rates after 13 minutes from 11.36 L/s [180 gpm] per pump up to the maximum 30.2 L/s [480 gpm] per pump, loop seal clearing does not occur and the tube stresses are sufficiently reduced by the RCS depressurization to prevent SG tube failure and containment bypass. A potential for containment bypass is seen for RCP shaft seal leak rates below 11.36 L/s [180 gpm] per pump.

Variations in Temporary TDAFW System Operation and RCP Shaft Seal Leakage Which Increases When the RCP Fluid Reaches the Saturation Temperature

Figure 6.4 illustrates the estimated containment bypass outcome as a function of temporary TDAFW system operation and the assumed RCP shaft seal leakage rate after the time when the fluid in the RCPs reaches the saturation temperature.

For event sequences in which the TDAFW system is assumed to initially operate and later fail, results are similar to those seen when the TDAFW does not operate at all. A potential for containment bypass is seen for sequences in which the RCP shaft seal leak rate after the time when the RCP fluid saturates is less than 11.36 L/s [180 gpm] per /pump. Above a 11.36 L/s [180 gpm] per pump leak rate and up to a 25.3 L/s [400 gpm] per pump leak rate, no loop seal clearing is seen and the RCS depressurization is sufficient to either reduce SG tube stresses and prevent their failure or to result in early core failure. In either case containment bypass is avoided.

Note that the results for TDAFW operation and leak rates above 25.23 L/s [400 gpm] per pump are different than seen for when the TDAFW does not operate at all (compare Figures 6.4 and 6.2). With no TDAFW operation, leak rates above 25.23 L/s [400 gpm] per pump are seen to result in loop seal clearing and containment bypass. The analyses indicate that a 4-hour period of TDAFW operation sufficiently cools the water in the loop seals such that when the leak rate increases to the maximum 30.2 L/s [480 gpm] per pump, loop seal clearing and containment bypass do not occur. Figure 6.4 portrays this effect as persisting down to a TDAFW operation period of 3 hours, however the actual minimum TDAFW operation period which produces this beneficial effect is not known.

Variations in Temporary TDAFW System Operation and SG Steam Leakage

Figure 6.5 illustrates the estimated containment bypass outcome as a function the temporary TDAFW system operation and the assumed SG steam leakage flow area.

The data shown in the figure are based on a limited number of SCDAP/RELAP5 cases. Evaluations were made using an RCP shaft seal leakage rate of 1.325 L/s [21 gpm] per pump, TDAFW operation times of 0 hours and 8 hours and SG steam leakage flow areas of 1.29 cm²/SG [0.2 in²/SG] and 3.23 cm²/SG [0.5 in²/SG].

The results of these evaluations show that for event sequences with no TDAFW operation and very small SG steam leakage flow areas (less than 0.64 cm²/SG [0.1 in²/SG]) the SG pressures remain elevated sufficiently to reduce SG tube stresses, prevent tube failure and avoid containment bypass.

The evaluations also show that for sequences in which the TDAFW system initially operates and later fails the SG tube failure margins are reduced, in comparison with sequences in which the TDAFW system never operates. A temporary period of TDAFW operation causes the system heat-up to occur later, and the system heat-up rates are slower due to reduced core decay power. A slower system heat-up reduces SG tube failure margins because the time constants associated with transporting heat from the RV to the SG become less effective at delaying the SG tube heat-up relative to the HL piping heat-up.

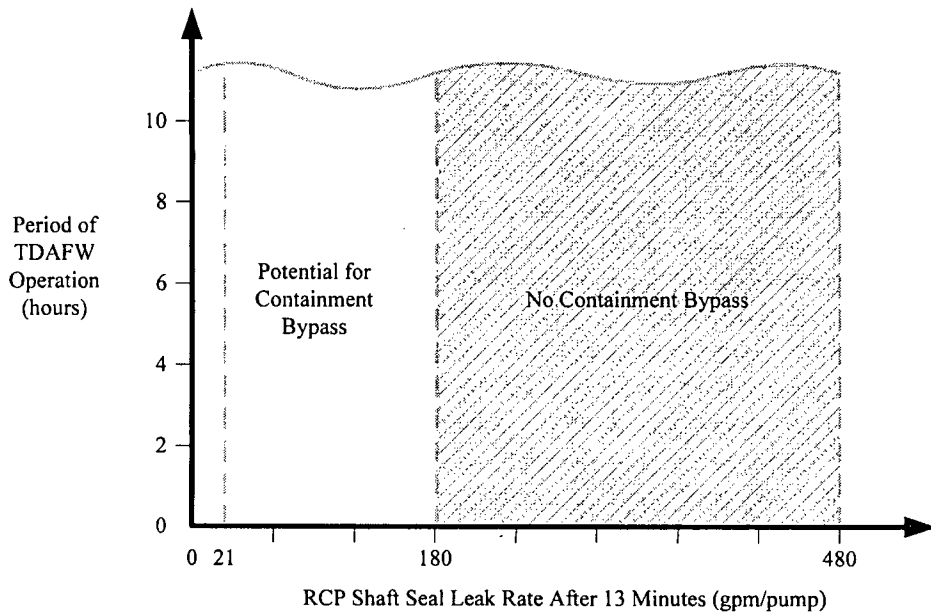


Figure 6.3 Map of Containment Bypass Outcome for No Operator Intervention and Variations in Temporary TDAFW System Operation and RCP Shaft Seal Leakage Which Increases at 13 Minutes

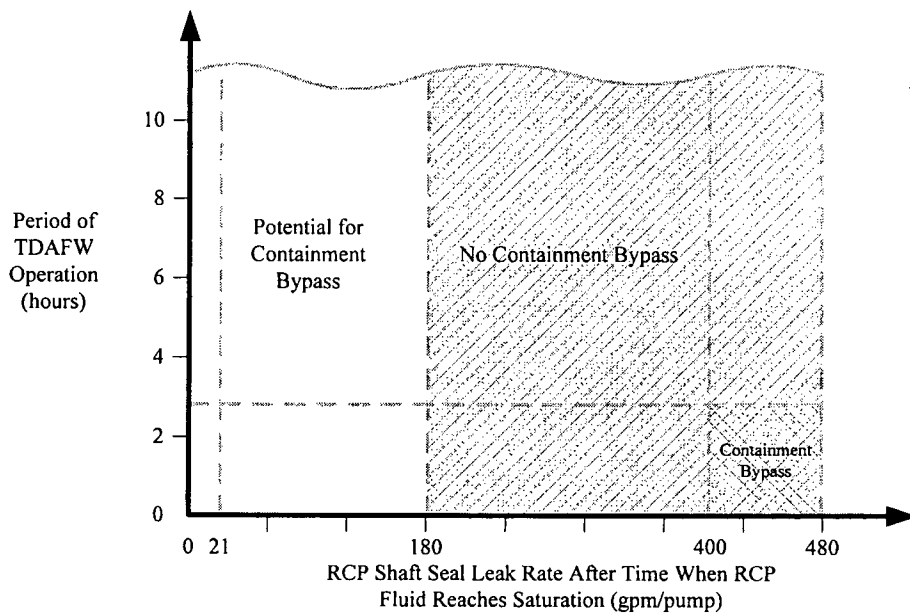


Figure 6.4 Map of Containment Bypass Outcome for No Operator Intervention and Variations in Temporary TDAFW System Operation and RCP Shaft Seal Leakage Which Increases When the RCP Fluid Reaches the Saturation Temperature

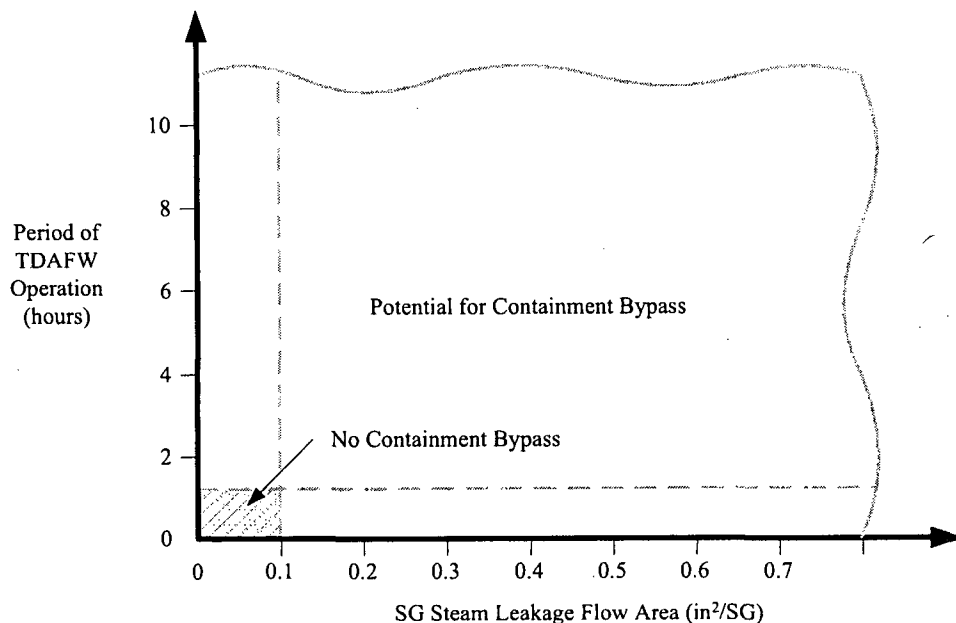


Figure 6.5 Map of Containment Bypass Outcome for No Operator Intervention and Variations in Temporary TDAFW System Operation and SG Steam Leakage

The margin lost from temporary TDAFW operation is seen to exceed the margin gained from assuming a very small SG steam leak flow area. As a result, sequences that include a period temporary TDAFW operation generally provide a potential for containment bypass, even when very low SG steam leakage flow areas are assumed.

On the other hand, the margin reductions caused by eight hours of TDAFW operation were not seen to be large, regardless of the assumed SG steam leakage flow area. It is therefore concluded that event sequences in which the TDAFW system operates for a very long period before failing continue to provide only a potential for containment bypass and not a certainty of containment bypass.

6.2 Categorization of Event Sequences with Operator Intervention

The effectiveness of two operator intervention strategies (pre-core damage and post-core damage) were evaluated. Both operator intervention strategies require that action be taken prior to the time when the station batteries have been depleted. Afterward, operator control over PORVs on the secondary and primary coolant systems is lost and ability to deliver or control TDAFW may also be lost. The core damage outcomes for the two strategies are summarized separately below.

Pre-Core Damage Operator Intervention

In the pre-core damage intervention strategy (which is evaluated in Section 5.3.1) the operators implement SG feed-and-bleed cooling at 30 minutes into the event sequence, using the TDAFW system and opening the SG PORVs to depressurize the SGs. Table 6.4 characterizes the four fluid conditions required for occurrence of containment bypass (high-pressure RCS, dry RCS,

dry SG and low-pressure SG) for event sequences without intervention (from Table 6.2) and for event sequences with pre-core damage intervention. Figure 6.6 illustrates the estimated containment bypass outcomes as a function the TDAFW system operation and the assumed RCP shaft seal leakage flow area.

The evaluation indicates that the intervention strategy is effective in the short term for removing core decay heat and preventing an RCS heat-up that could lead to containment bypass. At a minimum, this strategy significantly delays the onset of an RCS heat-up, thereby providing time for other plant recovery opportunities to be considered and implemented. In the long term, the SG PORVs fail closed when the batteries are depleted and continued success of the intervention strategy requires that a TDAFW water source remain available and that some capability to deliver the water into the SGs continues.

For sequences in which the TDAFW system initially operates but later fails, no large changes in SG tube failure margins (relative to the no-operator intervention base case event sequence) were seen to result from implementing the pre-core damage operator intervention strategy. The evaluation also showed that increasing the assumed RCP shaft seal leak rate from 1.325 L/s [21 gpm] per pump to 3.786 L/s [60 gpm] per pump at 13 minutes significantly improved the SG tube failure margin, although not sufficiently to indicate that containment bypass cannot occur. Based on an extrapolation of this margin improvement, Figure 6.6 reflects that containment bypass is avoided at RCP shaft seal leak rates of 7.572 L/s [120 gpm] per pump and higher.

Post-Core Damage Operator Intervention

In the post-core damage strategy (which is evaluated in Section 5.3.2) the operators depressurize the RCS by opening the pressurizer PORVs after plant instrumentation has indicated that the core damage process is underway. Table 6.5 characterizes the four fluid conditions required for occurrence of containment bypass (high-pressure RCS, dry RCS, dry SG and low-pressure SG) for event sequences without intervention (from Table 6.2) and for event sequences with post-core damage intervention. Figure 6.7 illustrates the estimated containment bypass outcomes as a function the number of pressurizer PORVs the operators open and the time in the event sequence when the operator action is assumed to begin.

The evaluations show that opening only one PORV limits the cooling afforded to the RCS, the core fails early (prior to battery depletion) and containment bypass is avoided for both of the operator intervention times evaluated.

The evaluations show that the RCS cooling afforded by opening two PORVs prevents early core damage and also prevents early failure of the HL and SG tube structures. When the PORVs fail closed after battery depletion, the RCS begins re-pressurizing and re-heating and this subsequently leads to HL and SG tube failures. The SG tube failure margins seen for the operator intervention cases are significantly improved (compared to the no-intervention case) and containment bypass is seen to be avoided for both of the operator intervention times evaluated.

The evaluations indicate that the post-core damage mitigative operator intervention strategy is effective for preventing containment bypass, regardless of whether the intervention begins at the time when the core exit temperature reaches 922 K [1,200°F] or 12 minutes later, and regardless of whether one or two pressurizer PORVs are opened.

Table 6.4 Pre-Core Damage Mitigative Operator Intervention Strategy

RCS Pressure	RCS Water Inventory	SG Water Inventory	SG Pressure
Without Intervention: High	Without Intervention: Dry	Without Intervention: Dry	Without Intervention: Low
Following Intervention: Low	Following Intervention: Wet	Following Intervention: Wet	Following Intervention: Medium
The heat removal to depressurized SGs greatly reduces RCS pressure	The RCS depressurization is sufficient to produce a period of accumulator injection (accumulators do not completely empty)	TDAFW operation keeps the SG water inventory up as long as it operates	Open PORVs depressurize SGs
If TDAFW later stops operating, a long period is required to heat up and repressurize the RCS due to reduced core decay power	If TDAFW later stops operating, a long period is required to expel the RCS water due to reduced core decay power	If TDAFW later stops operating, a long inventory boil-off period results from reduced core decay power	The SGs repressurize after the PORVs fail closed following battery depletion

Table 6.5 Post-Core Damage Mitigative Operator Intervention Strategy

RCS Pressure	RCS Water Inventory	SG Water Inventory	SG Pressure
Without Intervention: High	Without Intervention: Dry	Without Intervention: Dry	Without Intervention: Low
With Intervention: Low	With Intervention: Mostly Dry	With Intervention: Dry	With Intervention: Low
Opening only one PORV limits RCS cooling and core fails early, prior to the battery depletion	The RCS depressurization is sufficient to produce a period of accumulator injection (accumulators do not completely empty)		
Opening two PORVs affords sufficient RCS cooling to avoid early core failure. PORVs fail closed after battery depletion and RCS heat-up and pressurization lead to HL and SG tube failures.	Boiling of the injected accumulator water and release of steam through the PORVs enhances RCS cooling, but the upper half of the core remains dry.		

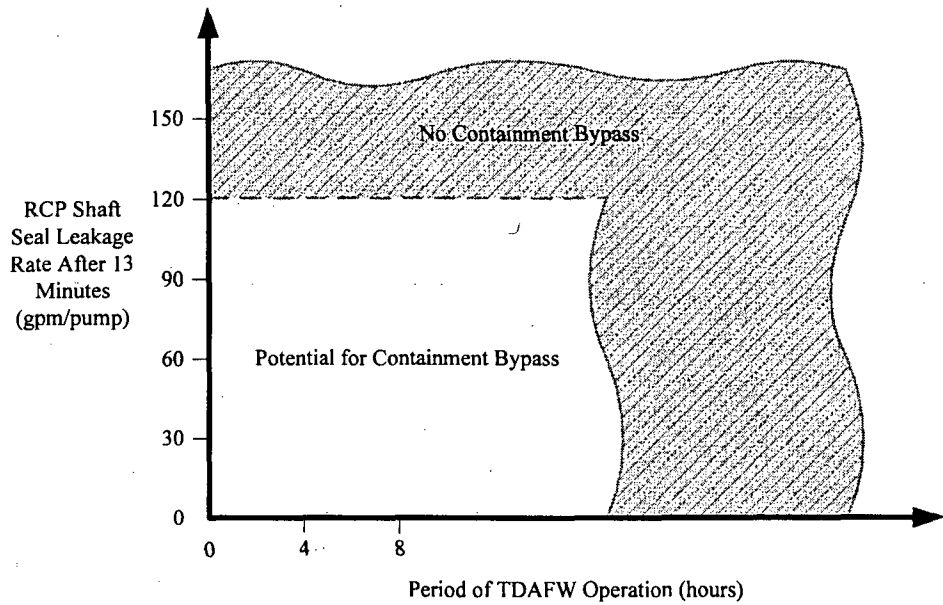


Figure 6.6 Map of Containment Bypass Outcome for Pre-Core Damage Operator Intervention

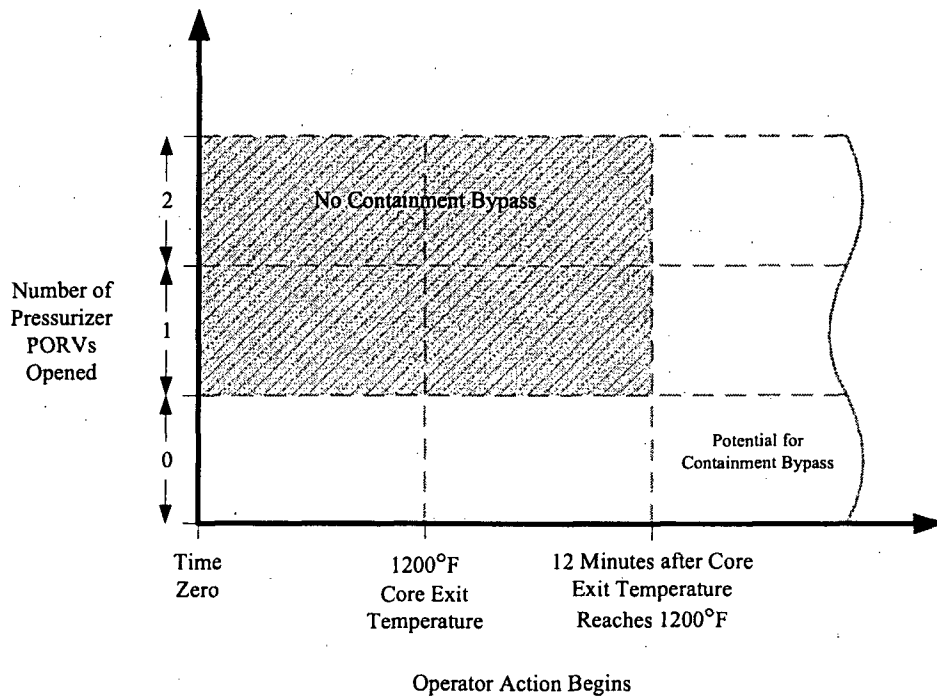


Figure 6.7 Map of Containment Bypass Outcome for Post-Core Damage Operator Intervention

7. CONCLUSIONS

Over the past 12 years, the NRC has sponsored extensive evaluations into the containment bypass issue for extended SBO accident events in Westinghouse four-loop plants. This report coalesces the findings from those former evaluations, along with selected additional evaluations, into a view of the extended SBO event sequences that fall into each of the following three categories:

- Sequences resulting in containment bypass.
- Sequences with a potential to result in containment bypass, for which an outcome may be determined by comparing the degradation of tube strengths in a prototype SG against the SCDAP/RELAP5-predicted tube failure margins.
- Sequences not resulting in containment bypass.

This categorization of event sequences provides information that (when combined with results from pertinent SG tube structural analyses, probabilistic risk assessments and environmental release evaluations) permits an evaluation of risks due to containment bypass for Westinghouse four-loop plants.

The event sequence categorization is described in Section 6 for situations where no operator actions are assumed and for situations where the operators are assumed to implement mitigative actions. Cautions related to uncertainties in the criteria used to categorize the event sequences and related to limitations of the supporting analyses are discussed there. The maps of containment bypass outcomes provided in Section 6 are considered to be the main product of the detailed research summarized in this report. The major findings are summarized below:

For situations where the operators are assumed to take no action the key results are summarized as follows.

Event sequences which assume very small leakage paths for steam to escape the SG secondary system ($0.64 \text{ cm}^2/\text{SG}$ [$0.1 \text{ in}^2/\text{SG}$] and smaller) generally do not result in containment bypass. The reduced SG tube stresses resulting from the SG secondary pressures remaining elevated prevent SG tubes from failing prior to the reactor core or a HL piping structure.

Event sequences which assume RCP shaft seal leakage rates lower than 11.36 L/s [180 gpm] per pump generally provide a potential for containment bypass. Event sequences which assume RCP shaft seal leakage rates of 11.36 L/s [180 gpm] per pump and higher generally do not result in containment bypass. A high leak rate leads to lower RCS pressures, and the reduced SG tube stresses prevent SG tubes from failing prior to the reactor core or a HL piping structure. However, there are exceptions related to the time when RCP shaft seal failures are assumed to occur. For RCP shaft seal failures that occur late in the event sequences, loop seal clearing and therefore containment bypass occur for leakage rates above 25.23 L/s [400 gpm] per pump.

Event sequences in which the TDAFW system operates and continues operating generally do not result in containment bypass. The outer surfaces of the SG

tubes remain wet and cool and the RCS heat removal provided prevents system heat-up.

For event sequences in which the TDAFW system is assumed to initially operate and later fail, results are very similar to those seen when the TDAFW does not operate at all. Challenges to continued TDAFW operation result from depletion of the station batteries, the need to arrange for an alternate source of water for the TDAFW system following depletion of the CST inventory and a loss of SG pressure sufficient to affect operation of the TDAFW turbine.

For situations where the operators take mitigative action the key results are summarized as follows.

An evaluation was performed for a pre-core damage mitigative strategy in which operators implement SG feed-and-bleed cooling at 30 minutes into the event sequence, using the TDAFW system and opening the SG PORVs. The evaluation shows that this strategy is effective in the short term for preventing containment bypass. At a minimum, this strategy significantly delays the onset of an RCS heat-up, thereby providing time for other plant recovery opportunities to be considered and implemented. In the long term, the SG PORVs fail closed when the batteries are depleted and continued success of this intervention strategy requires that a TDAFW water source remain available and that some capability for delivering the water into the SGs continues. For sequences in which the TDAFW system initially operates but later fails, no large changes in SG tube failure margins (relative to the no-operator intervention base case event sequence) were seen to result from implementing the pre-core damage operator intervention strategy. Event sequences in which the TDAFW system operates and continues operating generally do not result in containment bypass. The outer surfaces of the SG tubes remain wet and cool and the RCS heat removal provided prevents system heat-up.

An evaluation was also performed for a post-core damage mitigative strategy in which the operators depressurize the RCS by opening one or two pressurizer PORVs after plant instrumentation indicates that core damage is in progress. PORVs are opened at the time when the core exit temperature reaches 922 K [1,200°F] or 12 minutes later. The evaluation shows that opening only one PORV limits the cooling afforded to the RCS, the core fails early (prior to battery depletion) and containment bypass is avoided for both operator action times. The evaluations also show that the greater RCS cooling afforded by opening two PORVs prevents early core damage and also prevents early failure of the HL and SG tube structures. When the PORVs fail closed after battery depletion, the RCS begins re-pressurizing and re-heating and this subsequently leads to HL and SG tube failures. The SG tube failure margins seen for the operator intervention cases are significantly improved (compared to the no-intervention case) and containment bypass is seen to be avoided for both post-core damage operator action times.

In addition to the analyses that led to the above event sequence categorization, limited SCDAP/RELAP5 analyses were performed to evaluate the effects of opening SG tube rupture and HL rupture flow paths. The findings of these analyses, which were performed to provide a basis for comparison with SOARCA Project calculation results, are summarized as follows.

Opening SG tube break flow paths into the SG secondary system does not significantly affect the timing of the subsequent HL failure but does significantly reduce the RCS pressure, which has a generally beneficial effect on the subsequent stresses in all of the RCS pressure boundary components (including the other HLs and the SG tubes which remain intact). However, for the remaining tube structures in the SG containing ruptured tubes the beneficial effect of the RCS depressurization is exceeded by the detrimental effect of drawing additional steam into that SG. This suggests that a potential exists for a propagation of tube failures, with the first tube to fail drawing additional hot steam into that SG, leading to additional tube failures. The fluid released to the environment through the PORV and SRVs of the SG containing ruptured tubes is proportional to the number of tubes assumed to rupture and to the time period during which flow passes through the ruptured tubes. Opening a HL break rapidly blows down the RCS into containment, thus removing further challenges to the integrity of the SG tubes.

This detailed thermal-hydraulic evaluation of station blackout event sequences provides information that (when combined with results from pertinent SG tube structural analyses, probabilistic risk assessments and environmental release evaluations) permits an evaluation of risks due to containment bypass for Westinghouse four-loop plants. The integration of this work is currently underway within the Office of Nuclear Regulatory Research, Division of Risk Analysis and this work supports the closure of the agency's Steam Generator Action Plan.

8. REFERENCES

- 2.1 SGTR Severe Accident Working Group, *Risk Assessment of Severe Accident-Induced Steam Generator Tube Rupture*, U. S. Nuclear Regulatory Commission, NUREG-1570, March 1998.
- 2.2 K. Almenas, et al., *Natural Circulation Induced Heating of Primary System Components: Final Report*, University of Maryland at College Park, June 1994.
- 2.3 E. W. Coryell, et al., *SCDAP/RELAP5/MOD3.1 Code Manual*, Idaho National Engineering Laboratory, NUREG/CR-6150, June 1995.
- 2.4 *Voltage-Based Repair Criteria for Westinghouse Steam Generator Tubes Affected by Outside Diameter Stress Corrosion Cracking*, U. S. Nuclear Regulatory Commission, Generic Letter 95-05, August 3, 1995.
- 2.5 *Voltage-Based Alternative Repair Criteria, A Report to the Advisory Committee on Reactor Safeguards by the Ad Hoc Subcommittee on a Differing Professional Opinion*, U. S. Nuclear Regulatory Commission, NUREG-1740, March 2001.
- 2.6 W. A. Stewart, et al., *Natural Circulation Experiments for PWR High Pressure Accidents*, EPRI Project No. RP2177-5, Westinghouse Electric Corp., December 1992.
- 2.7 S. J. Collins (NRR) memorandum to A. C. Thadani (RES), *User Need Request Related to Steam Generator Severe Accident Response and Testing of Steam Generator tubes During Severe Accident Conditions*, U. S. Nuclear Regulatory Commission, February 8, 2000.
- 2.8 A. C. Thadani (RES) memorandum to S. J. Collins (NRR), *NRR Users Need Request Related to Steam Generator Severe Accident Response and Testing of Steam Generator tubes During Severe Accident Conditions*, U. S. Nuclear Regulatory Commission, September 7, 2000.
- 2.9 S. J. Collins (NRR) and A. C. Thadani (RES) memorandum to W. D. Travers (OPS), *Steam Generator Action Plan Revision to Address Differing Professional Opinion on Steam Generator Tube Integrity (WITS Item 200100026)*, U. S. Nuclear Regulatory Commission, May 11, 2001.
- 2.10 D. L. Knudson (INEEL) letter to S. A. Arndt (NRC), *Transmittal of Zion Plant Design Differences Letter Report under Task 32 of JCN W6095*, Idaho National Engineering and Environmental Laboratory, November 20, 2000.
- 2.11 L. W. Ward and V. V. Palazov, *Sequence Variations, Task 3.2: Accident Sequence Variations*, Information Systems Laboratories, Inc., ISL-NSAD-NRC-01-004, September 2001.
- 2.12 L. W. Ward and V. V. Palazov, *Sequence Variations, Task 3.3: Potential Conservatism*, Information Systems Laboratories, Inc., ISL-NSAD-NRC-01-004 (Draft), March 2002.

- 2.13 L. W. Ward, *Tube-to-Tube Temperature Variations During the Station Blackout Event, Task 3.5: Tube-to-Tube Temperature Variations*, Information Systems Laboratories, Inc., ISL-NSAD-TR-02-03, (Draft), August 2002.
- 2.14 C. D. Fletcher, R. W. Shumway and D. A. Barber, *Revised SCDAP/RELAP5 Base Case Calculation for Zion TMLB' Station Blackout Event*, Information Systems Laboratories, Inc., ISL-NSAD-TR-03-18, October 2003.
- 2.15 C. F. Boyd, D. M. Helton and K. Hardesty, *CFD Analysis of Full-Scale Steam Generator Inlet Plenum Mixing During a PWR Severe Accident*, U. S. Nuclear Regulatory Commission, NUREG-1788, May 2004.
- 2.16 C. D. Fletcher, R. M. Beaton and W. C. Arcieri, *SCDAP/RELAP5 Sensitivity Evaluations for a Zion TMLB' Station Blackout Event*, Information Systems Laboratories, Inc., ISL-NSAD-TR-04-05, March 2004.
- 2.17 Minutes, Advisory Committee on Reactor Safeguards, Joint Materials and Metallurgy and Thermal-Hydraulic Subcommittees Meeting, "Steam Generator Action Plan," February 3-4, 2004, Rockville, MD.
- 2.18 "Minutes of PIRT Meeting on Containment Bypass Issue," C. D. Fletcher, Information Systems Laboratories, Inc., email to PIRT meeting participants, October 13, 2005.
- 2.19 C. D. Fletcher and R. M. Beaton, "SCDAP/RELAP5 Base Case Calculation for the Station Blackout Uncertainty Study," Information Systems Laboratories, Inc., August 2006.
- 2.20 C. D. Fletcher and R. M. Beaton, "Evaluation of Uncertainties in SCDAP/RELAP5 Station Blackout Simulations," Information Systems Laboratories, Inc., August 2006.
- 2.21 "EPRI/NRC Technical Meeting on Steam Generator Tube Rupture During a PWR Severe Accident (Public Meeting)," Electric Power Research Institute Washington Office, Washington DC, May 15, 2007.
- 2.22 Fauske and Associates, Inc. "MAAP4 – Modular Accident Analysis Program for LWR Power Plants Volume 2, Part1: Code Structure and Theory," prepared for Electric Power Research Institute, May 1994.
- 2.23 C. C. Ferriso, et al., "Total Emissivity of Hot Water Vapor: 1. The High-Pressure Limit," General Dynamics Space Science Laboratory Technical Report GDA-DBE64-055, September 1964.
- 2.24 D. Fletcher, "Responses to EPRI Comments on SCDAP/RELAP5 Containment Bypass Analysis," presentation at Joint EPRI/NRC Public Meeting, Washington DC, May 15, 2007.
- 3.1 L. J. Siefken et al., *SCDAP/RELAP5/MOD3.3 Code Manual*, NUREG/CR-6150, INEL-96/0422, Revision 2, Idaho National Engineering and Environmental Laboratory, January 2001.

- 3.2 F. R. Larson and J. Miller, "A Time Temperature Relationship for Rupture and Creep Stress," *Transactions of the ASME*, July 1952, pp. 765-775.
- 3.3 C. B. Ludwig, et al.: "Handbook of Infrared Radiation From Combustion Gases," NASA SP-3080, 1973.
- 3.4 ROSA-IV Large Scale Test Facility (LSTF) System Description, Japan Atomic Energy Research Institute, JAERI-84-237, January 1985.
- 3.5 C. D. Fletcher, D. A. Prelewicz and W. C. Arcieri, *RELAP5/MOD3.2.2 Gamma Assessment for Pressurized Thermal Shock Applications*, Information Systems Laboratories, Inc., NUREG/CR-6857, October 2004.
- 3.6 L. Szabados, et al., *PMK-2 HANDBOOK, Technical Specification of the Hungarian Integral Test Facility for VVER-440/213 Safety Analysis*, KFKI Atomic Energy Research Institute, Budapest, Hungary, TERSDI/4NT/2459/41, 1996.
- 3.7 L. Perneczky, et al., *Description and RELAP5 Assessment of the PMK-2 CAMP-CLB Experiment*, KFKI Atomic Energy Research Institute, Budapest, Hungary, NUREG/IA-0201, March 2001.
- 3.8 S. M. Sloan, R. R. Schultz and G. E. Wilson, *RELAP5/MOD3 Code Manual, Summaries and Reviews of Independent Code Assessment Reports*, Idaho National Engineering Laboratory, NUREG/CR-5535, EGG-2596, Vol. 7, June 1994, p. 25.
- 3.9 H. R. Saedi and P. Griffith, *The Pressure Response of a PWR Pressurizer During an Insurge Transient*, Transactions of the American Nuclear Society," 1983 Annual meeting, Detroit, Michigan, June 12-16, 1983.
- 3.10 *APEX-CE Stuck Open Pressurizer Safety Relief Valve (SRV) from Full Power with Subsequent Reclosure*, OSU-CE-13, Oregon State University, October 19, 2001.
- 3.11 T. F. Habib, et al., *Multiloop Integral System Test (MIST): MIST Facility Functional Specification*, NUREG/ CR-5670, April 1991.
- 3.12 *Experimental Data Report, LOBI-MOD2 Test BT-56*, Commission of the European Communities, JRC 4352, LEC 93-73, December 1993.
- 3.13 J. Blanco, et al., *Analysis of the LOBI Experiment Test BT-56 Using the RELAP5/MOD3.2 Code*, Union Fenosa Generacion S.A., Central Nuclear Jose Cabrera, Madrid, Spain, NUREG/IA-0183, June 2000.
- 3.14 Boyd, C.F. and Armstrong, K, *Computational Fluid Dynamics Analysis of Natural Circulation Flows in a Pressurized-Water Reactor Loop under Severe Accident Conditions*, NUREG 1922, To be published November 2009
- 3.15 S. J. Leach and H. Thompson, "An Investigation of Some Aspects of Flow into Gas Cooled Reactors Following an Accidental Depressurization," *Journal of British Nuclear Energy Society*, Vol. 14, No. 3, 1975, pp. 243-250.

- 3.16 W. A. Stewart, et al., *Natural Circulation Experiments for PWR High Pressure Accidents*, EPRI Project No. RP2177-5, Westinghouse Electric Corp., December 1992.
- 5.1 J. L. LaChance, "Recommended Thermal-Hydraulic Runs and Sensitivity Calculations for SAI-SGTR Project," Sandia National Laboratories, email to C. D. Fletcher (ISL), October 31, 2007.
- 5.2 K. C. Wagner, Sandia National Laboratories, email, subject "Re: SGAP work on ISL contract," January 3, 2008.

APPENDIX A – RESULTS OF 2004 SENSITIVITY ANALYSES

An extensive set of sensitivity studies were performed to evaluate the effects of various changes in the SCDAP/RELAP5 Westinghouse four-loop plant modeling options, event sequence assumptions and plant configuration. These sensitivity studies are fully documented in Reference 2.16. The base case accident sequence and plant model used for the sensitivity analyses were the same as described in Section 2.3. The sensitivity evaluations performed and the analysis results are summarized as follows:

A.1 Target Values for the SG Inlet Plenum Region Mixing and Flow Parameters

See Section 3.4 for the definitions of the mixing and flow parameters which were varied in these sensitivity runs. The target hot and cold mixing fractions were increased to 0.87 from the base case value of 0.81. The higher target mixing fraction was seen to result in only a slight reduction in the SG tube failure margin. The target recirculation ratio was decreased to 2.0 from the base case value of 2.75. The lower target recirculation ratio was seen to result in a small reduction in the SG tube failure margin.

A.2 Reactor Coolant Pump Shaft Seal Leakage

A variety of assumptions regarding the RCP shaft seal leakage were investigated. The base case event sequence assumes a constant leak flow area over the duration of the transient event sequence. That flow area provides an initial 1.32 L/s [21 gpm] leakage rate per pump. In the sensitivity cases, the leakage flow area was increased at different times during the event sequence to as high as 18.9 L/s [300 gpm] initial leakage rate per pump. The results of the sensitivity runs indicated that the SG tube failure margins are sensitive to the assumed RCP shaft seal leakage. Small increases in the leakage rate above 1.32 L/s [21 gpm] were seen to slightly lower the margin, while the lower RCS pressures caused by much larger increases in the leakage rate reduced the stresses on the SG tubes and significantly increased the SG tube failure margins.

A.3 SG Tube Plugging

Sensitivity evaluations were performed for 0% and 20% SG tube plugging assumptions (10% was assumed in the base case). The SG tube failure margin results were seen to be only slightly affected by the tube plugging assumption.

A.4 SG Tube Outer Wall Heat Transfer Heat Transfer Coefficient

The sensitivity to variations in the heat transfer processes on the outer surface of the SG tubes was evaluated using multipliers of 0.1, 5.0 and 10.0 on the SCDAP/RELAP5-calculated heat transfer coefficient. The results indicated that the SG tube failure margin is sensitive to this parameter. Enhanced heat transfer leads to a tighter coupling of the SG tube wall with the cooler steam in the SG boiler region and increased SG tube failure margins.

A.5 Radiation Heat Transfer Modeling

The sensitivity to variations in the modeling of thermal radiation heat transfer processes was evaluated using SCDAP/RELAP5 runs in which multipliers of 0.5 and 2.0 were placed on the

steam-to-wall and wall-to-wall radiation heat fluxes on the surfaces of the RCS structures. The results indicated that increased radiation heat flux leads to a slightly improved SG tube failure margins.

A.6 Pressurizer Surge Line CCFL

Several SCDAP/RELAP5 sensitivity runs were performed to investigate the modeling of countercurrent flow limiting (CCFL) behavior related to pressurizer draining. Different CCFL models and applicable hydraulic diameters were evaluated. Neither the pressurizer draining behavior nor the SG tube failure margins were seen to be significantly affected by the CCFL modeling approach.

A.7 Reactor Vessel Internal Circulations

SCDAP/RELAP5 calculates buoyancy-driven circulations within the RV which affect the temperature of steam transported into the coolant loops. A SCDAP/RELAP5 sensitivity run was performed in which the flow losses within the vessel model were increased so as to reduce the flow rates of the RV internal circulations by 50%. The reduced RV circulation rates accelerated the core damage process. The SG tube failure margins were seen to be affected by the RV internal circulation rates, with the slower circulations resulting in improved margins.

A.8 Reactor Coolant System Heat Loss

The base case SCDAP/RELAP5 plant system model represents 4 MW of uniformly-distributed heat loss from the outer surfaces of the primary and secondary reactor coolant systems to the containment. Sensitivity runs were made with this assumption changed to 2 MW and 8 MW. SG tube failure margin results were seen to be moderately affected by the heat loss assumption, with higher heat loss leading to reduced margins. An increased heat loss preferentially delays the failure of the HLs and surge line with respect to the failures of the SG tubes because the heat loss boundary condition is applied directly to the HL and surge line structures but not to the SG tube structures.

A.9 Pressurizer PORV Modeling and Operator Intervention

A SCDAP/RELAP5 sensitivity run performed assuming that the pressurizer PORVs are blocked closed indicated very little effect on the SG tube failure margins. In this run the RCS pressure rose to the opening setpoint pressure of the pressurizer SRVs, but otherwise the closed PORVs had little effect on the plant response.

A sensitivity run was also performed to evaluate the plant response to mitigative operator intervention. The operators were assumed to depressurize the RCS by opening the pressurizer PORVs following the onset of the core heat-up. The results of the sensitivity run demonstrated the success of this intervention strategy for mitigating containment bypass during the base case SBO severe accident. SG tube failures were prevented by the operator action. The core melted and relocated to the RV lower head, and the subsequent failure of the RV lower head resulted in a full depressurization of the RCS and a release into the containment.

A.10 SG Tube Leakage Effects

A limited investigation was performed into the effects of SG tube leakage (from primary-to-secondary). Assumed SG tube leakages of 3.15, 6.31 and 12.6 L/s [50, 100 and 200

gpm] were added to the pressurizer-loop SG of the plant model. It is noted that this leakage represents a distributed leakage among all of the tubes in the SG and not the leakage associated with only one or a few tubes. The model also does not include any effects whereby the tube leakage might alter the distribution of hot steam into the hottest tube. The results of the SCDAP/RELAP5 sensitivity runs indicated that the tube leakage assumption affects the SG tube failure margin, with higher leakage rates leading to reduced margins.

A.11 Core Bypass Modeling

A SCDAP/RELAP5 sensitivity run was performed with the assumed core bypass flow due to leakage around the slip fit between the core barrel and RV (at the HL nozzle penetrations) reduced by 50%. This modeling change was seen to have virtually no effect on the SG tube failure margins.

A.12 Progression of Core Damage

The SCDAP/RELAP5 Westinghouse four-loop base case calculation indicated that the failure of structural components (HL and pressurizer surge line piping and SG tubes) occurs relatively early during the core damage and relocation processes of the SBO severe accident sequence. The fuel rod cladding oxidation is seen to dramatically increase the core heat load, which in turn leads to a rapid heat-up of components throughout the RCS. The structural failures are encountered shortly after the time when the oxidation power peaks. Heating of the control rods leads to control rod cladding failure and relocation of molten control rod absorber material to the RV lower head shortly after the time of the structural failures. Melting and relocation of the core fuel to the RV lower head are seen to occur long after the time of the structural failures. Three SCDAP/RELAP5 sensitivity runs were performed to evaluate the effects of the core damage progression by varying the modeling of the fuel rod oxidation, control rod melting and fuel rod melting processes. These sensitivity runs and their results are described as follows.

At its peak, the fuel rod cladding oxidation power exceeds the fission product decay power by an order of magnitude. A sensitivity run was performed in which the peak oxidation power was limited to 43% of the peak experienced in the base case run. The results showed that limiting the peak oxidation power in this manner tended to slow the RCS system heat-up rate, leading to small reductions in the SG tube failure margins.

A sensitivity run was performed with the control rods removed from the model. Because control rod melting behavior occurs after the time of structural failures in the base case run, the sensitivity run was instead compared against another sensitivity run in which the control rod melting process more affected the results. The results indicated that removing the control rods from the model resulted in only slight improvement in the SG tube failure margins. It was concluded that the effects of uncertainties related to modeling severe accident control rod-related behavior (cladding failure, and melting and relocation of the absorber, cladding and guide tube materials) on the key outcome for the containment bypass analyses are small.

A sensitivity run was performed with a significant variation in a parameter that affects the melting and relocation of the core fuel (the fraction of the phase-change heat that must be absorbed by the fuel for it to be considered in the molten state). This sensitivity run was compared against another sensitivity run in which the fuel rod melting and relocation behavior more affected the results than in the base case. The results indicated no change in the SG tube failure margins between the two sensitivity runs. It was concluded that the SG tube failure

margins are insensitive to variations in the fuel damage progression behavior (including fuel melting, flow blockage, re-freezing and relocation).

APPENDIX B – ANALYSES TO SUPPORT PRA

B.1 Introduction and Background

An extensive series of SCDAP/RELAP5 thermal hydraulic analyses was performed in 2004 and 2005 to support the PRA and stress/fracture mechanics activities of the Containment Bypass Project. These analyses were performed using variations on the base case accident scenario. Two sets of PRA support calculations were performed. The first set was performed in 2004 and was called the Task 8 PRA Calculations; results from these calculations are summarized in Section B.2. The second set was performed in 2005 and was called the Phase 3 Calculations; results from these calculations are summarized in Section B.3. References for Appendix B are provided in Section B.4.

B.2 Task 8 PRA Calculation Set, September 2004

The Task 8 series of 20 SCDAP/RELAP5 simulations for Westinghouse four-loop SBO PRA event sequences is documented in Reference B.1. The plant model used for the simulations is described in Section 2.6. The base case model featured a 50%/50% split between the hot and cold SG tube regions and loss coefficients were adjusted to provide hot and cold mixing fractions of 0.81, a recirculation ratio of 2.75 and a total SG power fraction of 30.24%. Prior to this series of calculations, the base case accident scenario was assumed to include a stuck-open SG secondary power operated relief valve (PORV) on the pressurizer-loop SG. However, in this and subsequent calculation sets, this assumption was replaced with the assumption that steam leakage paths, with flow areas of 3.26 cm² [0.5 in²], open in each of the four SGs at the beginning of the event sequence.

The Task 8 PRA event sequence definitions are listed in Table B.1 (the base case event sequence is shown as Case 69). The SG tube failure margin results from the 20 SCDAP/RELAP5 simulations are provided in Table B.2.

The key results from the Task 8 analysis are summarized as follows:

The effectiveness of operator intervention (opening the pressurizer PORVs) for preventing SG tube failure is demonstrated with Cases 21 and 53. Similarly, SG tube failure is seen to be avoided with an assumption of a stuck open pressurizer PORV which fails to reclose, as seen in Case 83.

The results obtained when SG secondary depressurization is caused by a stuck-open PORV on SG 1 are seen to be the same as when 3.23-cm² [0.5-in²] steam leakage paths in all four SGs are assumed. See Case 183 vs. Case 69 and Case 184 vs. Case 72.

Increasing the assumed RCP shaft seal leakage rate from 1.32 L/s [21 gpm] per pump to 3.79 L/s [60 gpm] per pump is shown to result in slightly reduced SG tube failure margins, see Case 70 vs. Case 69 and Case 154 vs. Case 153.

Table B.1 Summary of Assumptions for the Task 8 PRA Event Sequences, September 2004

Case No.	RCP Shaft Seal Leakage or Stuck-Open Pzr PORV ¹	Operator Action, SG Depress. before Core Damage ²	TDAFW Runs Until Battery Depletion ³	Valves Reclose Before Core Damage ⁴	Operator Action, RCS Depress. After Core Damage ⁵	Battery Depletion Time (Valves Reclose) ⁶	Steam Leakage Flow Area (in ² /SG) or Stuck-Open ADV ⁷
21	21 gpm	No	No	N/A	1 PORV, TSC	4 hours	0.5
53	21 gpm	No	No	N/A	2 PORV, TSC	4 hours	0.5
69	21 gpm	No	No	N/A	No	4 hours	0.5
70	60 gpm	No	No	N/A	No	4 hours	0.5
71	180 gpm	No	No	N/A	No	4 hours	0.5
72	480 gpm	No	No	N/A	No	4 hours	0.5
83	1 PORV	No	No	No	No	4 hours	0.5
153	21 gpm	Yes	Yes	N/A	No	4 hours	0.5
154	60 gpm	Yes	Yes	N/A	No	4 hours	0.5
155	180 gpm	Yes	Yes	N/A	No	4 hours	0.5
157	21 gpm	No	Yes	N/A	No	4 hours	0.5
160	480 gpm	No	Yes	N/A	No	4 hours	0.5
161	21 gpm	Yes	Yes	N/A	No	8 hours	0.5
165	21 gpm	No	Yes	N/A	No	8 hours	0.5
177	21 gpm	No	No	N/A	No	4 hours	0.1
178	480 gpm	No	No	N/A	No	4 hours	0.1
179	21 gpm	No	No	N/A	No	4 hours	1.0
180	480 gpm	No	No	N/A	No	4 hours	1.0
183	21 gpm	No	No	N/A	No	4 hours	ADV
184	480 gpm	No	No	N/A	No	4 hours	ADV

Notes for Table B.1:

- 1 - The column headed "RCP Shaft Seal Leakage or Stuck-Open Pzr PORV" indicates the primary system leakage assumption. Shaft seal leakages given in gpm are on a per-pump basis. All cases have an overriding assumption of 21 gpm per pump shaft seal leakage starting at time zero. For cases with "21 gpm" indicated, the leakage flow area does not change during the sequence. For cases where a higher leakage rate is indicated, the leakage flow area is assumed to increase accordingly at 13 min into the event sequence. For cases where a stuck-open PORV is indicated, the PORV is assumed to stick open at the time of the tenth PORV opening.
- 2 - The information shown in the column headed "Operator Action, SG Depress. Before Core Damage" indicates whether or not the operators are assumed to intervene by depressurizing the SG secondary systems at 30 min into the event sequence.
- 3 - The information shown in the column headed "TDAFW Runs Until Battery Depletion" indicates whether or not the turbine-driven auxiliary feedwater system is assumed to operate until control is lost at the time when the station batteries are depleted.

- 4 - The column headed "Valves Reclose Before Core Damage" only has significance for cases involving a stuck-open pressurizer PORV and is listed as not applicable for most of the cases.
- 5 - The column headed "Operator Action, RCS Depress. After Core Damage" indicates if the operators are assumed to intervene by opening one or two pressurizer PORVs after the core uncovers. An entry of "TSC" indicates that the decision to intervene is made by the Technical Support Center, in which case the pressurizer PORVs are assumed to be opened 12 min after the time when the core exit steam temperature reaches 922 K [1,200°F].
- 6 - The column headed "Battery Depletion Time (Valves Reclose)" indicates the time after the initiation of the event sequence when station battery power is lost, resulting in termination of turbine-driven auxiliary feedwater flow (for cases where it is active) and the loss of both automatic and operator control over the pressurizer PORVs and steam generator secondary PORVs. All PORVs are assumed to fail closed following the time of battery depletion.
- 7 - The column headed "Steam Leakage Flow Area or Stuck-Open ADV" indicates the steam leakage flow area assumed per steam generator. For cases where "ADV" is indicated, the assumption is that the PORV on Steam Generator 1 (in the loop containing the pressurizer) fails open at the beginning of the event sequence and that the other steam generators each have the nominal steam leakage flow area of 3.23 cm² [0.5 in²].

Table B.2 Summary of SG Tube Failure Margin Results for the Task 8 PRA Event Sequences

Case No.	Highest Stress Multiplier for which <u>Average</u> SG Tube Failure Occurs After Pressurizer Surge Line or Hot Leg Failure	Highest Stress Multiplier for which <u>Hottest</u> SG Tube Failure Occurs After Pressurizer Surge Line or Hot Leg Failure
21	DNF	DNF
53	DNF	3.5
69	4.0	1.0
70	3.5	1.0
71	DNF	DNF
72	DNF	DNF
83	DNF	DNF
153	3.0	1.0
154	2.5	< 1.0
155	6.0	3.5
157	3.0	1.0
160	DNF	DNF
161	2.5	1.0
165	2.5	1.0
177	4.0	3.5
178	DNF	DNF
179	4.0	1.0
180	DNF	DNF
183	4.0	1.0
184	DNF	DNF

In this table "DNF" indicates that SG tube failure was not calculated until after pressurizer surge line failure, hot leg failure or a change in core configuration (melting/refreezing or relocation) for SG tube stress multipliers of 7.5 and less.

Further increasing the assumed RCP shaft seal leakage rate to 11.36 L/s [180 gpm] and 30.28 L/s [480 gpm] per pump at 13 minutes is seen to generally remove the SG tube failure potential (for example see Cases 71 and 72 vs. Case 69). This finding results because the increased shaft seal leakage rates are high enough to reduce the RCS pressure and lower the stress on the tubes such that SG tube failure is prevented. Early in the runs with the higher shaft seal leak rates, the core is calculated to melt and relocate to the reactor vessel lower head (from which failure of the vessel head would result in a release into the containment). In none of the Task 8 cases with the higher RCP shaft seal leakage rate assumptions did any of the loop seals clear of water.

B.3 Phase 3 PRA Calculation Set, January 2005

The Phase 3 series of 23 SCDAP/RELAP5 simulations for Westinghouse four-loop SBO PRA event sequences is documented in Reference B.2. The plant model used for this series of calculations was the same as that described in the Task 8 simulations in Section B.2 except that: (1) the pressurizer surge line connection was moved from the top to the side of Hot Leg 1 (in some Westinghouse four-loop plants this connection is made on the top of the HL while in others it is made on the side of the HL), and (2) based on an analysis of thermal entrance effects, a 50% enhancement was made to the HL inside surface convective heat transfer coefficient to better represent that heat transfer process.

The Phase 3 PRA event sequence definitions are listed in Table B.3 (the base case event sequence is shown as Case 69). The SG tube failure margin results from the 23 SCDAP/RELAP5 simulations are provided in Table B.4.

The key results from the Phase 3 analysis are summarized as follows:

Moving the pressurizer surge line connection from the top to the side of Hot Leg 1 results in lower temperature steam entering the pressurizer surge line than was previously the case. This model modification therefore generally leads to later surge line failure times. The results shown here for cases not involving locked-open pressurizer PORVs (whether by operator action or by failed-open assumptions) indicate that the HL failure now generally precedes the surge line failure. For cases involving locked-open pressurizer PORVs, the influence of hot steam drawn up the surge line by the opened valves generally results in surge line failure preceding HL failure, although in certain of these cases (Cases 37, 185 and 200) other event-timing considerations result in the HL failure still preceding the surge line failure.

The additional energy which passes out of the RCS by assuming that the RCP shaft seal leakage rate increases to 11.36 L/s [180 gpm] per pump at 13 minutes is seen to generally improve the SG tube failure margins over those where the leakage rate is assumed to remain at 1.32 L/s [21 gpm] per pump. This margin improvement is seen by comparing the results for Case 39 against Case 37, Case 55 against Case 53, and Case 71 against Case 69.

The assumption of SG secondary side steam leakage significantly reduces the SG tube failure margins from those obtained when no leakage is assumed. This is seen, for example, by comparing the results from Case 198 (no leakage) and Case 69 (3.23-cm² [0.5-in²] leakage flow area per SG). SG steam leakage leads

to lower SG secondary pressures and less thermal coupling between the outside of the SG tube and the steam in the secondary side of the SG. Both of these effects increase the potential for SG tube failure. None of the cases where no SG steam leakage was assumed resulted in prediction of average or hot SG tube failure, even for stress multipliers as high as 7.5.

Table B.3 Summary of Assumptions for the Phase 3 PRA Event Sequences, January 2005

Case No.	RCP Shaft Seal Leakage or Stuck-Open Pzr PORV ¹	Operator Action, SG Depress. before Core Damage (at 30 min.) ²	TDAFW Runs Until Battery Depletion ³	PORV Recloses Before Core Damage ⁴	Operator Action, RCS Depress. After Core Damage ⁵	Battery Depletion Time ⁶	Steam Leakage Flow Area (in ²) ⁷
5	21 gpm	No	No	N/A	1 PORV, No TSC	4 hours	0.5
7	180 gpm	No	No	N/A	1 PORV, No TSC	4 hours	0.5
21	21 gpm	No	No	N/A	1 PORV, TSC	4 hours	0.5
23	180 gpm	No	No	N/A	1 PORV, TSC	4 hours	0.5
37	21 gpm	No	No	N/A	2 PORVs, No TSC	4 hours	0.5
39	180 gpm	No	No	N/A	2 PORVs, No TSC	4 hours	0.5
53	21 gpm	No	No	N/A	2 PORVs, TSC	4 hours	0.5
55	180 gpm	No	No	N/A	2 PORVs, TSC	4 hours	0.5
69	21 gpm	No	No	N/A	No	4 hours	0.5
71	180 gpm	No	No	N/A	No	4 hours	0.5
155	180 gpm	Yes	Yes	N/A	No	4 hours	0.5
159	180 gpm	No	Yes	N/A	No	4 hours	0.5
163	180 gpm	Yes	Yes	N/A	No	8 hours	0.5
167	180 gpm	No	Yes	N/A	No	8 hours	0.5
185	PORV	No	No	Yes	No	4 hours	0.5
192	21 gpm	No	No	N/A	1 PORV, TSC	4 hours	None
198	21 gpm	No	No	N/A	No	4 hours	None
199	180 gpm	No	No	N/A	No	4 hours	None
200	PORV	No	No	Yes	No	4 hours	None
205	180 gpm	Yes	Yes	N/A	No	4 hours	None
206	180 gpm	No	Yes	N/A	No	4 hours	None
207	180 gpm	Yes	Yes	N/A	No	8 hours	None
208	180 gpm	No	Yes	N/A	No	8 hours	None

Notes for Table B.3:

- 1 - The column headed "RCP Shaft Seal Leakage or Stuck-Open Pzr PORV" indicates the primary system leakage assumption. The shaft seal leakage rate is on a per-pump basis. All cases have an overriding assumption of 21 gpm per pump shaft seal leakage starting at time zero. For cases with "21 gpm" indicated, the leakage flow area does not change during the sequence. For cases where a higher leakage rate is indicated, the leakage flow area is assumed to increase to the rate shown at 13 min into the event sequence. For cases where a stuck-open PORV is indicated, a single pressurizer PORV is assumed to fail open the tenth time that the valve opens.
- 2 - The information shown in the column headed "Operator Action, SG Depress. Before Core Damage" indicates whether or not the operators are assumed to intervene by depressurizing the SG secondary systems at 30 min into the event sequence.
- 3 - The information shown in the column headed "TDAFW Runs Until Battery Depletion" indicates whether or not the turbine-driven auxiliary feedwater system is assumed to operate until control is lost at the time when the station batteries are depleted.
- 4 - The column headed "PORV Re-Closes Before Core Damage" only has significance for the cases involving a stuck-open pressurizer PORV and a "Yes" entry indicates that the stuck-open PORV is assumed to re-close when the reactor coolant system pressure has declined to 6.89 MPa [1,000 psia].
- 5 - The column headed "Operator Action, RCS Depress. After Core Damage" indicates if the operators are assumed to intervene by opening one or two pressurizer PORVs after the core uncovers. An entry of "No TSC" indicates that the operators are assumed to immediately open the PORVs at the time when the core exit steam temperature reaches 922 K [1,200°F]. An entry of "TSC" indicates that the decision to intervene is made by the Technical Support Center, in which case the pressurizer PORVs are assumed to be opened 12 min after the time when the core exit steam temperature reaches 922 K [1,200°F].
- 6 - The column headed "Battery Depletion Time" indicates the time after the initiation of the event sequence when station battery power is assumed to be lost, resulting in termination of turbine-driven auxiliary feedwater flow (for cases where it is active) and the loss of both automatic and operator control over the pressurizer PORVs and steam generator secondary PORVs. All PORVs are assumed to fail closed following the time of battery depletion.
- 7 - The column headed "Steam Leakage Flow Area" indicates the leakage flow area assumed per steam generator.

Table B.4 Summary of SG Tube Failure Margin Results for the Phase 3 PRA Event Sequences

Case No.	First RCS Component Failure	Highest Stress Multiplier for which <u>Average</u> SG Tube Failure Occurs After Pressurizer Surge Line or Hot Leg Failure	Highest Stress Multiplier for which <u>Hottest</u> SG Tube Failure Occurs After Pressurizer Surge Line or Hot Leg Failure
5	Surge Line	DNF	7.0
7	Surge Line	DNF	DNF
21	Surge Line	DNF	DNF
23	Surge Line	DNF	DNF
37	Hot Leg	1.5	1.0
39	Surge Line	DNF	DNF
53	Surge Line	DNF	4.0
55	Surge Line	DNF	DNF
69	Hot Leg	3.5	1.0
71	Hot Leg	4.5	2.0
155	Hot Leg	DNF	4.5
159	Hot Leg	DNF	3.5
163	Hot Leg	DNF	5.0
167	Hot Leg	DNF	DNF
185	Hot Leg	DNF	3.5
192	Surge Line	DNF	DNF
198	Hot Leg	DNF	DNF
199	Hot Leg	DNF	DNF
200	Hot Leg	DNF	DNF
205	Hot Leg	DNF	DNF
206	Hot Leg	DNF	DNF
207	Hot Leg	DNF	DNF
208	Hot Leg	DNF	DNF

In this table "DNF" indicates that SG tube failure was not calculated until after pressurizer surge line failure or HL failure for SG tube stress multipliers of 7.5 and less.

B.4 References for Appendix B

- B.1 C. D. Fletcher (ISL) Letter to C. F. Boyd (NRC), "SCDAP/RELAP5 Zion PRA Calculation Set 1, Contract GS-23F-0060L," September 14, 2004.
- B.2 C. D. Fletcher (ISL) Letter to C. F. Boyd (NRC), "SCDAP/RELAP5 Zion Station Blackout Phase III PRA Calculation Set, Contract GS-23F-0060L," January 18, 2005.

APPENDIX C – EVALUATION OF PRIMARY COOLANT SYSTEM ENERGY FLOW

An analysis of energy balance data was performed for the purpose of understanding the distribution and flow of energy in the primary RCS during the SCDAP/RELAP5 extended SBO base case calculation described in Section 2.8. The energy balance analysis considers the flow of energy into, within, and out of the primary RCS fluid following the time when the core uncovers and the system heat-up is in progress. In this analysis, the primary RCS is defined to include the fluid in the regions of the RV, HLs, SG inlet and outlet plenums, the interior of the SG tubes, RCPs, cold legs, pressurizer and surge line.

C.1 Energy Balance Model and Analysis Approach

The RCS fluid was subdivided into the control volume scheme shown in Figure C.1. Table C.1 summarizes the specific RCS fluid regions contained within each control volume. The calculated behavior among the three coolant loops not connected to the pressurizer is virtually identical during the calculated event sequence; the RCS fluid in those three loops was lumped together for the purposes of the energy balance analysis.

Because the SCDAP/RELAP5 model nodalization scheme is more detailed than the energy balance control volume scheme, the energy balance information for each control volume represents a summation of data over the SCDAP/RELAP5 hydrodynamic fluid cells that, when combined, make up the control volume regions. Inflows of energy result when fluid flows into a control volume and as heat is transferred from structures to the fluid. Outflows of energy result when fluid flows out of a control volume and as heat is transferred from the fluid to structures. Since the opening and closing of the pressurizer relief valves cause the system fluid flows and wall heat transfer rates to oscillate considerably during the SCDAP/RELAP5 calculation, the energy balance data was smoothed through integration.

As would be expected, the energy flow patterns vary over the course of the transient sequence as fluid distributions, fluid conditions and the phenomena that dominate the RCS system thermal-hydraulic response change. The transient system heat-up period is subdivided into five phases for which the RCS energy flows are separately evaluated. The criteria for selecting the time periods for the phases and the RCS behavior during each phase are summarized as follows:

Phase 1, Pressurizer Draining (9,222 s - 10,637 s) This phase extends from the time when the core uncovers to the time when the pressurizer tank has emptied. During this phase the water remaining in the pressurizer at the time of core uncovering drains out of the pressurizer and downward through the surge line toward the HL. Superheated steam coming up the surge line from the HL tends to vaporize this liquid, which enhances steam production and steam flow. The pressurizer PORVs cycle open and closed to limit the RCS pressurization and much steam and fluid energy is lost from the RCS through the flow out the pressurizer PORVs. This loss of RCS inventory causes the pressurizer level to decline until the tank is empty. Fuel and steam temperatures are generally still low and the core power is generated only as a result of the fission product decay process.

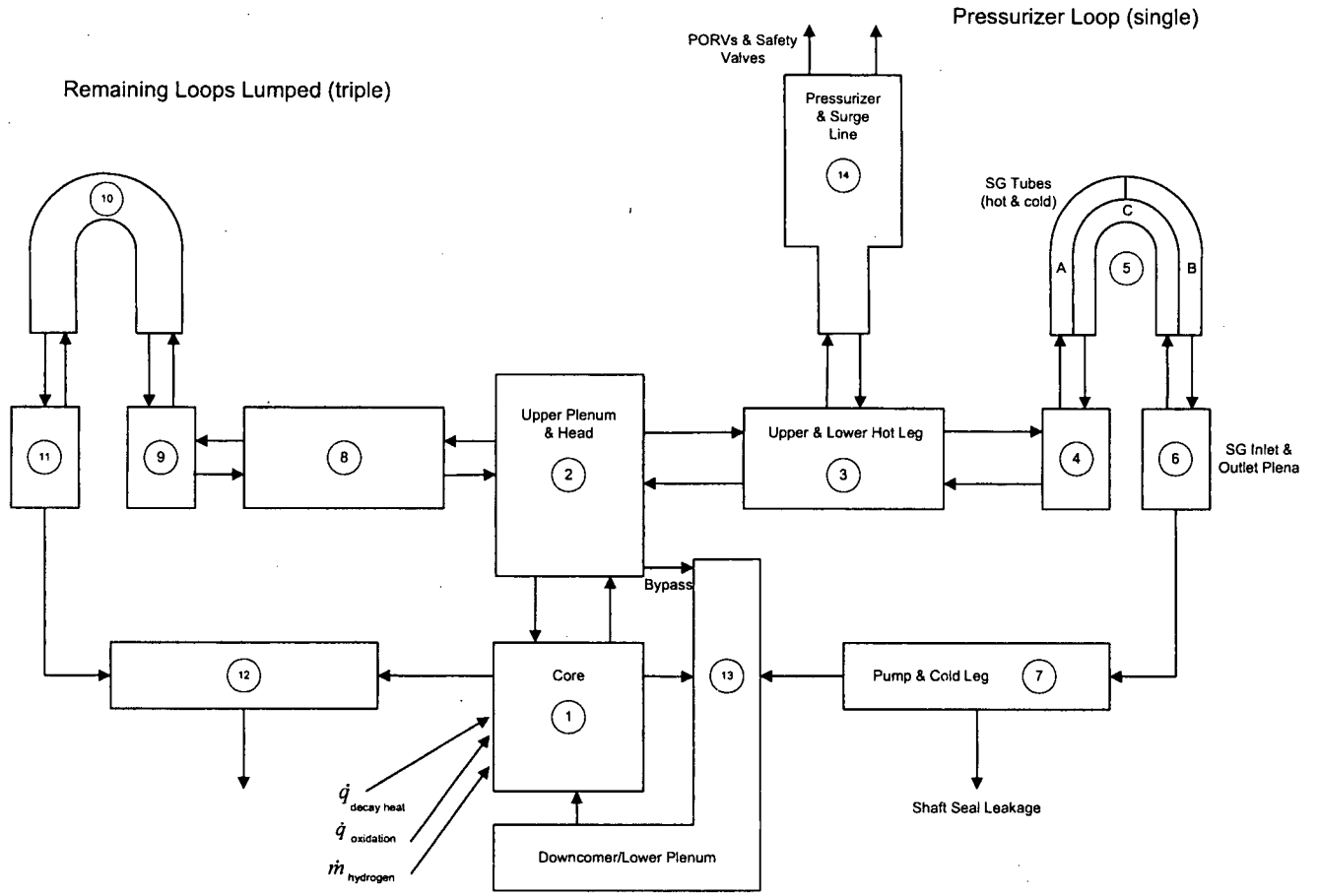


Figure C.1 Control Volume Arrangement for the Energy Balance Analysis

Table C.1 Description of Control Volumes for the Energy Balance Analysis

Control Volume Number	RCS Fluid Region Included in the Control Volume	Notes
1	Reactor core	Includes heat structures for fuel rods. Heat generation considered due to core fission product decay and fuel rod metal-water oxidation.
2	Reactor vessel region above the core and inside the core barrel	Includes heat structures for vessel wall and internals in the upper head and plenum region.
3	Coolant Loop 1 hot leg	Includes heat structures for hot leg wall.
4	SG 1 inlet plenum	Includes heat structures for tube sheet and plenum wall.
5	SG 1 tubes	The portions of the tubes located inside the tubesheet are considered to be part of the inlet and outlet plena. The SG 1 tube control volume was separated into three sub-control volumes: 5A (Hot average tubes, upward-flowing section), 5B (Hot average tubes, downward-flowing section) and 5C (Cold average tubes, upward and downward-flowing section).
6	SG 1 outlet plenum	Includes heat structures for tube sheet and plenum wall
7	Coolant Loop 1 cold leg, reactor coolant pump and pressurizer spray line	Includes heat structures for the cold leg wall. Fluid exits the system via reactor coolant pump shaft seal leak.
8	Coolant Loop 2/3/4 hot leg	Includes heat structures for hot leg wall.
9	SG 2/3/4 inlet plenum	Includes heat structures for tube sheet and plenum wall
10	SG 2/3/4 tubes	The portions of the tubes located inside the tubesheet are considered to be part of the inlet and outlet plena.
11	SG 2/3/4 outlet plenum	Includes heat structures for tube sheet and plenum wall.
12	Coolant Loop 2/3/4 cold legs, reactor coolant pumps and pressurizer spray line.	Includes heat structures for the cold leg walls. Fluid exits the system via reactor coolant pump shaft seal leaks.
13	Reactor vessel downcomer, lower head and lower plenum regions	Includes heat structures for the vessel wall and internals.
14	Pressurizer tank and surge line	Includes heat structures for the tank and surge line walls. Fluid exits the system via flow through the pressurizer PORVs and SRVs.

Phase 2, Empty System Heat-Up (10,637 s - 13,200 s) This phase extends from the time when the pressurizer has emptied until the time when the system heat-up causes the fuel rod oxidation rate to increase to the point where the core power is produced roughly equally by fission product decay and fuel rod oxidation. During this phase the pressurizer has completely drained and the RCS (except for the loop seals and the RV lower plenum and head) is filled with vapor. The pressurizer PORVs continue to cycle open and closed. Fuel temperatures, steam temperatures and the fuel rod oxidation power are all rising.

Phase 3, Peak Fuel Rod Oxidation (13,200 s - 13,475 s) This phase extends from the time when the core power is produced roughly equally by fission product decay and fuel rod oxidation, through the peak in the oxidation rate and up to the time when the first significant structural failure is encountered. The failure time for the hottest SG tube structure with a stress multiplier of 1.0 was selected as the end time for this phase. Except for the loop seals and the RV lower plenum and head, the RCS is filled with a mixture of steam and hydrogen, which is released by the oxidation process. The pressurizer PORVs continue to cycle open and closed. Fuel and steam temperatures are now rising more rapidly. During this phase the core power is dominated by the fuel rod oxidation process, not by the fission product decay. The oxidation power peaks at about 11.2 times the fission decay power and then begins to fall as the cladding is consumed. A key feature of this phase is that the heat produced by the oxidation process tends, at first, to be retained locally in the fuel rods and core regions of the RCS.

Phase 4, Structure Failure (13,475 s – 14,590 s) The time period for this phase includes the failure times for all remaining significant structures: HLs, pressurizer surge line and average SG tubes with stress multipliers lower than 3.0. The failure time for the average SG tube with a stress multiplier of 1.0 was used as the end time for this phase. Except for the loop seals and the RV lower plenum and head, the RCS is filled with a mixture of steam and hydrogen. Before 14,400 s (four hours, the assumed station battery depletion time), the pressurizer PORVs continue to cycle open and closed, but less frequently during this phase than during the earlier phases. The fuel rod oxidation power continues to decline and during this phase the core power is produced roughly equally by the fission product decay and fuel rod oxidation processes. A key feature of this period is that the heat that had built up in excess in the fuel and core regions during the rapid peak of the oxidation process is carried by the flow of the RCS fluid outward into the coolant loops. It is the arrival of this excess heat in the loop components which quickly drives the structure temperatures upward, leading to their failure.

Phase 5, Post-Structure Failure (14,590 s – 15,500 s) This phase extends from the time when the average SG tube with a 1.0 stress multiplier fails up until the time when molten control rod absorber is relocated to the RV lower head. The pressurizer PORVs are no longer functional because the station batteries are assumed to be depleted. The fuel rod oxidation power remains low and is only a very small portion of the total core power. The system fluid and structure temperatures (which had risen in order to remove the excess core power produced during the peak oxidation phase) are roughly at the levels which are needed to remove the now-lower core power. This effect causes the fluid and structure temperatures to generally stop rising and level off during this phase of the accident sequence. The energy analysis is truncated at 15,500 s because afterward the RCS energy balance is controlled by the relocation of large quantities of molten materials (control rod absorber and fuel rods) which cause significant changes in the RCS configuration.

C.2 Results of RCS Energy Flow Analysis

The behavior of the energy flows into, within and out of the RCS are summarized as follows. Figures C.2 through C.10 show the transient behavior of the various energy flow terms. The data points shown with the triangle symbols in these figures are located in the middle of the periods for the five phases and represent the average integrated energy flow during each phase. The data points are joined with solid lines in the figures only for clarity.

Figure C.2 shows the average total core power resulting from fission product decay heat and fuel rod oxidation heat. The data for the first two phases represents the fission product decay power, prior to the onset of significant fuel rod oxidation. The increase seen in the third phase results from the acceleration and peaking of the fuel rod oxidation process. During the fourth and fifth phases the oxidation process is mostly complete and the core power is once again dominated by the fission product decay heat, which declines as a function of time after reactor trip.

Figures C.3 and C.4, respectively, portray the percentages of the integrated total core power that are retained in the fuel and transferred to the core fluid. The figures show that, except during the peak in the oxidation process in Phase 3, about 20% of the core heat is retained in the fuel and about 80% of the core heat is transferred to the fluid in the core. The spike in total core power during the peak oxidation period causes these percentages to significantly change, with about 60% of the core heat retained locally in the fuel (where the oxidation process deposits it) and only about 40% of the core heat transferred to the core fluid. Subsequent to the oxidation peak during Phase 3, the passage of time allows the "excess" oxidation heat which had built up in the fuel to flow into the core fluid and from there to be distributed throughout the RCS.

Figure C.5 shows the integrated changes in the RV fluid energy expressed as a percentage of the integrated total core power (negative values indicate a loss of fluid energy). During Phases 1 and 2, the negative vessel energy inventory change is caused by the loss of liquid mass from the RV as the core fluid is boiled off and the downcomer level declines. The small positive changes seen in Phases 3 through 5 reflect an increase in vessel fluid energy resulting from heating the vessel fluid to very high temperatures and releasing high-energy hydrogen from the fuel rod oxidation process directly into it.

Figure C.6 shows the integrated changes in the pressurizer fluid energy expressed as a percentage of the integrated total core power. The figure reflects the rapid loss of liquid from the pressurizer as it empties due to draining during Phase 1 and the passing of liquid and steam through the PORVs when those valves open to limit the RCS pressurization during Phases 1 through 4. The PORVs fail closed after the station batteries are assumed to be depleted at four hours (14,400 s). During Phase 5 this figure therefore reflects a situation where the PORVs no longer cycle open and closed and the pressurizer region is stagnant and vapor-filled.

Figure C.7 shows the integrated changes in the fluid energy for RCS regions other than the RV and pressurizer expressed as a percentage of the integrated total core power. For Phase 1, the figure reflects the loss of liquid mass from the hot and cold legs as the liquid remaining at the time of core uncovering drains into the RV or is swept out of the RCS through the pressurizer PORVs. During Phases 2 through 4, the HL, SG primary and cold leg regions of the plant are vapor-filled and the small negative energy changes seen in the figure reflect a loss of vapor mass as the fluid temperatures increase. The fluid becomes hotter and its specific energy

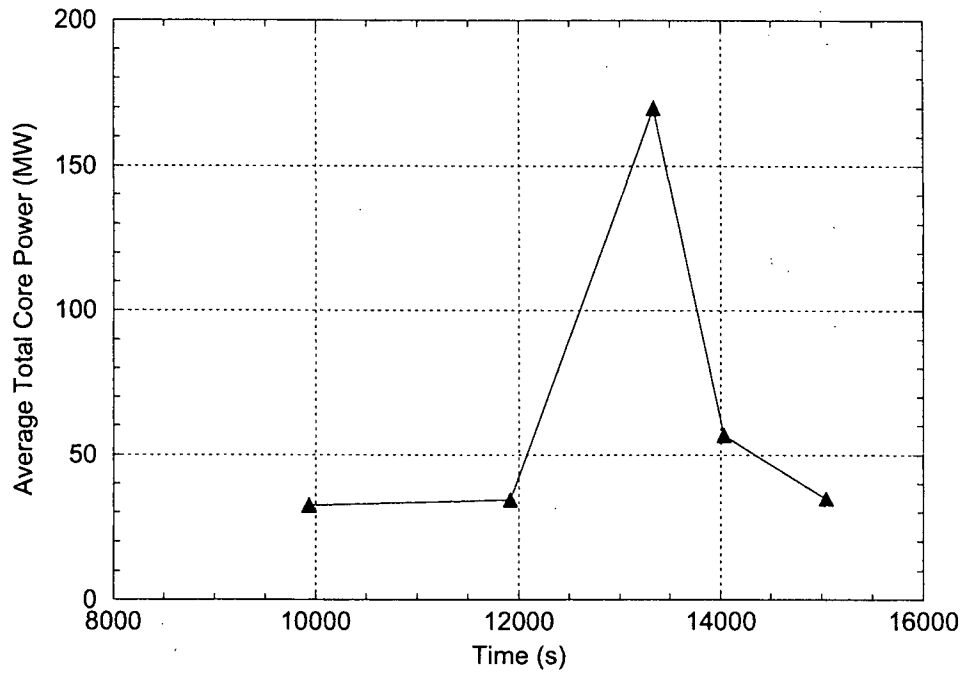


Figure C.2 Average Total Core Power Generated During the Five Phases of the SBO Accident Heat-Up Period

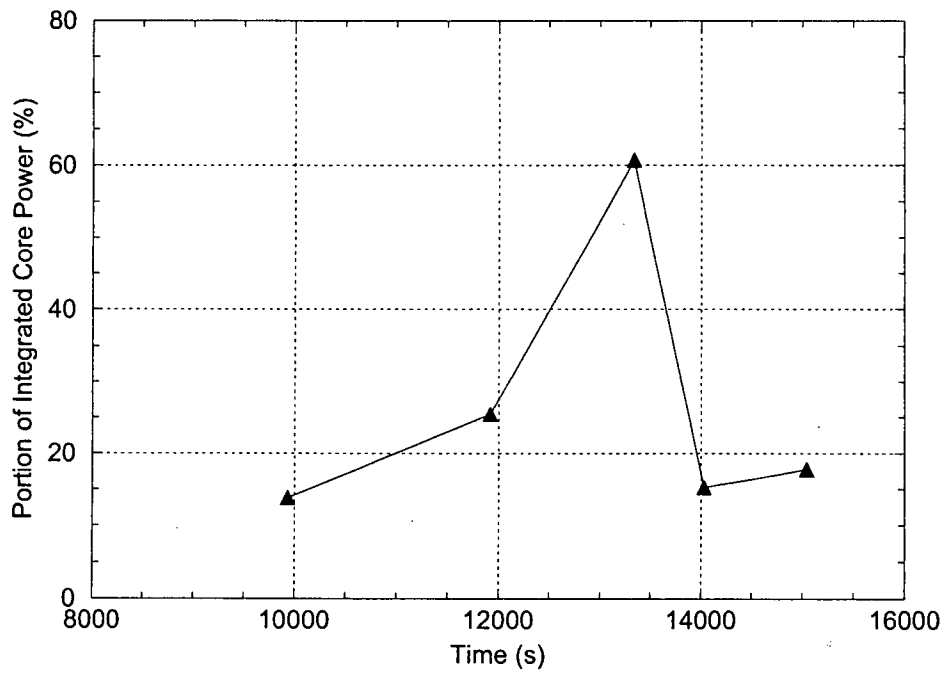


Figure C.3 Portion of the Integrated Core Power Retained in the Fuel During the Five Phases of the SBO Accident Heat-Up Period

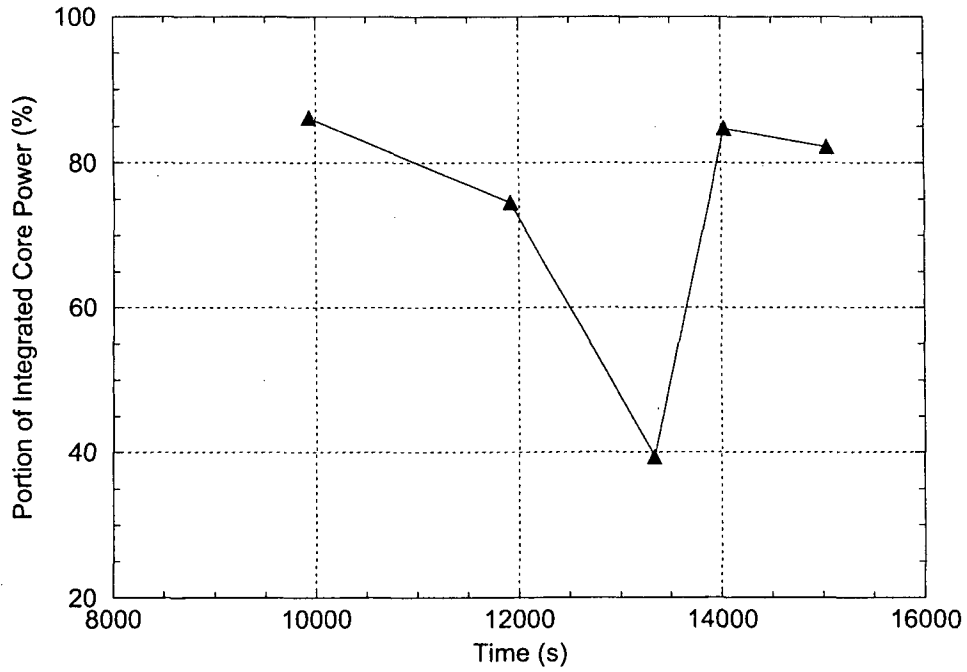


Figure C.4 Portion of the Integrated Core Power Transferred to the Core Fluid During the Five Phases of the SBO Accident Heat-Up Period

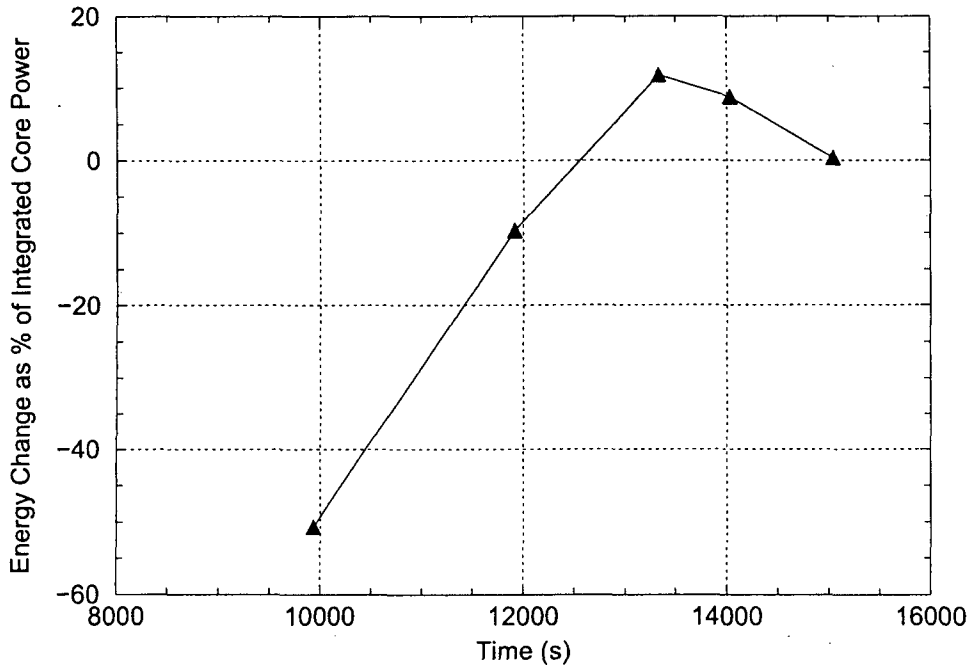


Figure C.5 Change in Reactor Vessel Fluid Energy During the Five Phases of the SBO Accident Heat-Up Period

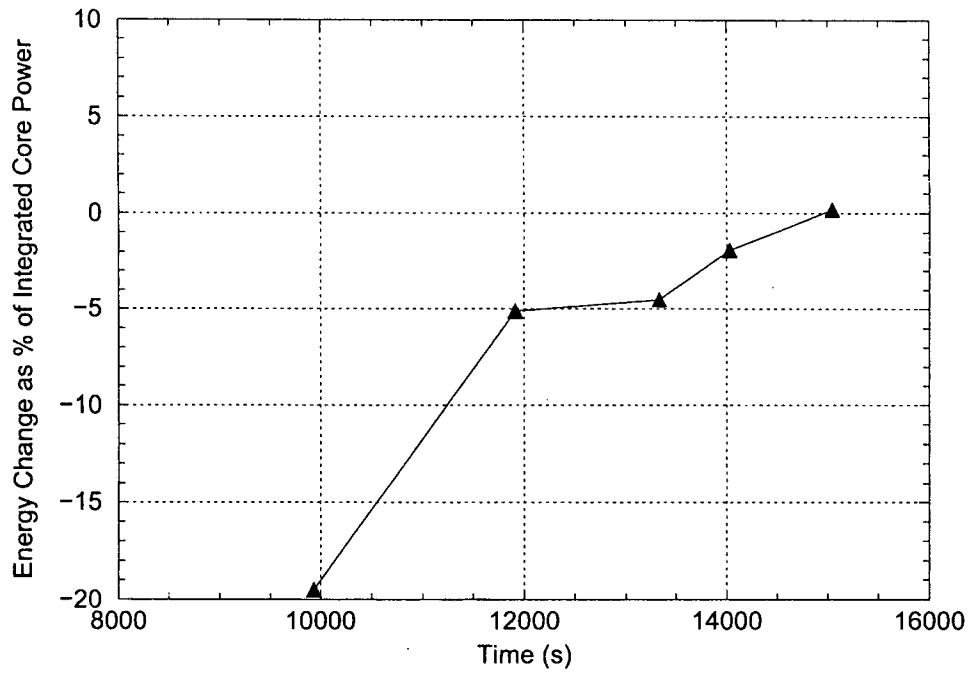


Figure C.6 Change in Pressurizer Fluid Energy During the Five Phases of the SBO Accident Heat-Up Period

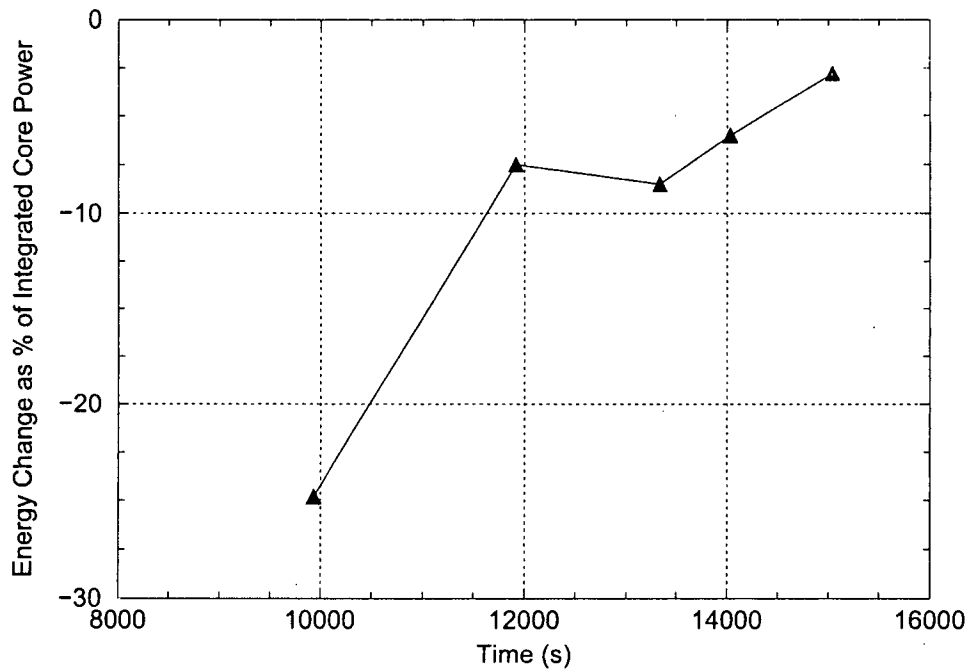


Figure C.7 Change in Fluid Energy in RCS Regions Other Than the Reactor Vessel and Pressurizer During the Five Phases of the SBO Accident Heat-Up Period

becomes higher, but its density becomes lower and the net result is a lower absolute fluid energy.

Figure C.8 shows the integrated flow of energy out of the RCS by way of the pressurizer PORVs and RCP shaft seal leaks expressed as a percentage of the integrated total core power. In this figure, negative values indicate a flow of energy out of the RCS. The figure indicates a high rate of energy flow out of the RCS during Phase 1, followed by successively smaller energy flows during Phases 2 through 5. The high rate of RCS energy loss during Phase 1 reflects a continued high rate of steam production prior to the time when the core completely empties of liquid. Opening of the pressurizer PORVs causes liquid in the core to flash and the steam produced requires the PORVs to cycle frequently and remain open for extended periods in order to control the RCS pressure. After the core dries out near the end of Phase 1, the core steam production rate falls, the PORVs cycle open less frequently and remain open for shorter periods. The reduced rates of RCS energy loss for Phases 2, 3 and 4 reflect this lowered demand on the pressurizer PORVs. The station batteries are depleted prior to the start of Phase 5 and the small negative RCS energy loss seen in the figure results solely from the RCP shaft seal leakage.

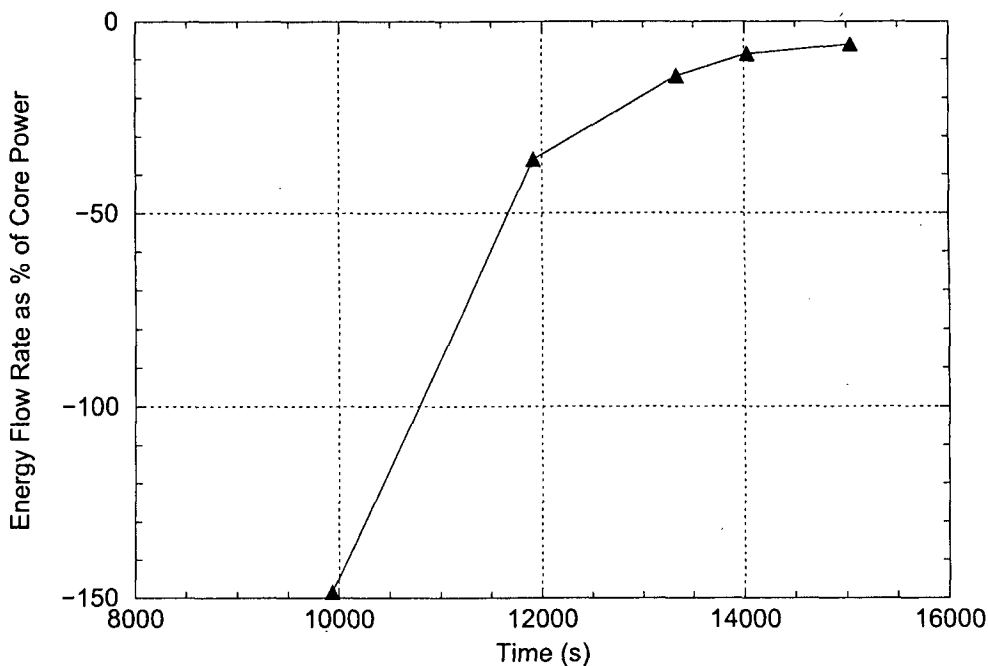


Figure C.8 Integrated Flow of Energy Through the Pressurizer PORVs and Reactor Coolant Pump Shaft Seal Leaks During the Five Phases of the SBO Accident Heat-Up Period

Figure C.9 shows the integrated flow of heat from the tubes of the four SGs to the fluid inside the tubes expressed as a percentage of the integrated total core power. In this figure, negative values represent transfer of heat from the fluid inside the SG tubes to the tube inner wall surface. The figure shows data only for the heat transferred between the tube wall and the fluid; heat transferred between the fluid and other SG structures (the walls of the spherical inlet and outlet plenum walls, the plenum divider plate and the tubesheet) is not included here. The figure shows that, except for the peak oxidation period when much heat initially stays in the fuel, the portion of the total core heat which flows to the SG tubes is relatively stable at between about 13% and 23%.

Figure C.10 shows the integrated flow of heat from all RCS structures other than SG tubes to the fluid inside the RCS expressed as a percentage of the integrated total core power. In this figure, negative values represent transfer of heat from the fluid to the structures. The structures represented by this data include the RV cylindrical wall and spherical upper and lower head walls, RV internals (core barrel, support plates, columns, etc.), HL, cold leg and pressurizer surge line pipe walls, the pressurizer tank wall, steam generator spherical inlet and outlet plenum walls and the SG tubesheets. When compared with the very thin SG tube structures which have a large heat transfer area, these structures are in general very thick, but with much smaller heat transfer areas. The figure shows that prior to the peak fuel rod oxidation period the portion of the total core heat which flows to these structures is between about 20% and 40%. After the peak fuel rod oxidation period, this percentage increases to about 55%. The increase reflects: (1) the close proximity of the thick RV heat structures to the hot vapor in the core and (2) the massive heat sinks provided by these thick-wall heat structures in general.

Regarding the effectiveness of heat sinks provided by the thick-wall structures, a key feature of the SBO transient event sequence is that vapor temperatures are for the most part continuously increasing. Consider first a situation where structures might be subjected to a large step-change increase in fluid temperature, but where the fluid temperature is held constant afterward. In that situation, heat flows from the fluid into the colder wall, but the temperature increase that is induced in the wall near the surface tends to restrict the subsequent flow of heat into the wall. The fluid-wall heat transfer process becomes limited by conduction heat transfer within the wall. Now consider the situation we have here, where the vapor temperatures continuously increase. The heat transfer process still induces a temperature increase in the wall near the surface. But, because the vapor temperatures continue increasing, the fluid-to-wall differential temperature remains high and wall heat sink remains very effective.

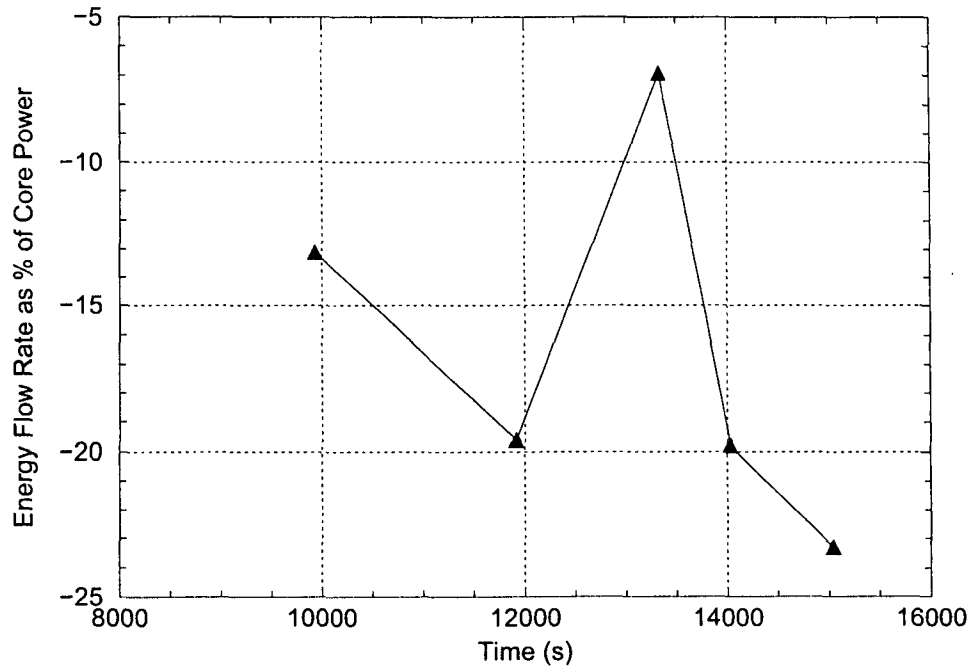


Figure C.9 Integrated Heat Transfer Rate from SG Tubes to Fluid During the Five Phases of the SBO Accident Heat-Up Period

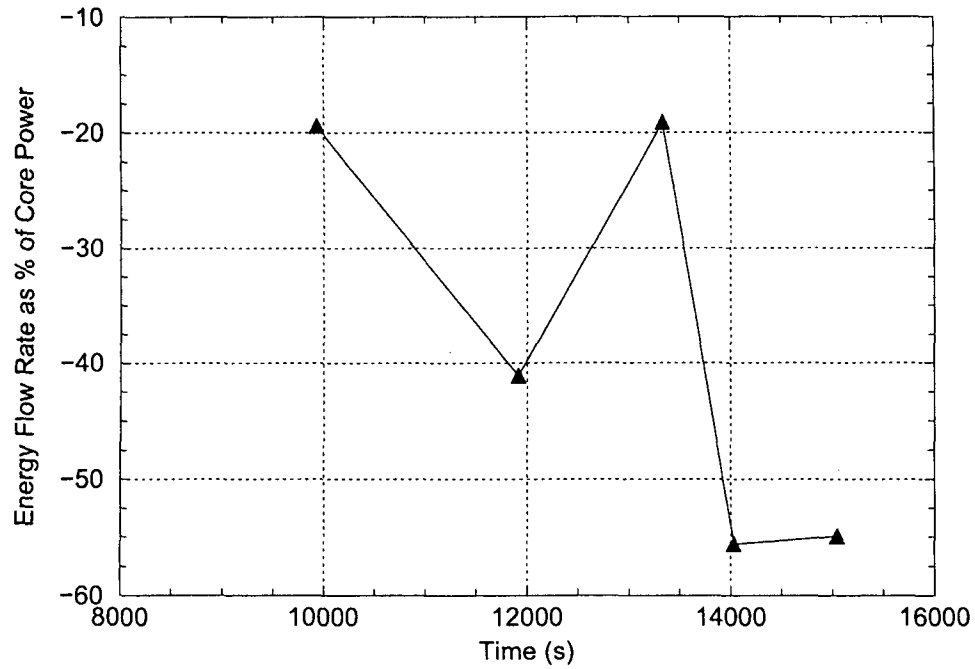


Figure C.10 Integrated Heat Transfer Rate from All Structures (Except SG Tubes) to Fluid During the Five Phases of the SBO Accident Heat-Up Period

APPENDIX D - ESTIMATES OF UNCERTAINTIES IN THE SCDAP/RELAP5 SIMULATIONS

Analyses were performed to estimate the uncertainties in the SCDAP/RELAP5 output parameters of key importance for the containment bypass application. These analyses are summarized here and are fully documented in Reference 2.20. The key output parameters (temperatures, heat transfer coefficients and SG tube failure margins) listed in Section 2.7.2 represent the dependent variables for the uncertainty study. The independent variables for the uncertainty study are discussed in Section 2.7.3 and are summarized in Table 2.1. The SCDAP/RELAP5 Westinghouse four-loop plant SBO base case calculation described in Section 2.8 was used as the base case run for the uncertainty analysis.

Section D.1 identifies the SCDAP/RELAP5 sensitivity cases. Model features representing the independent variables are varied around the nominal conditions that were assumed in the base case calculation. The SCDAP/RELAP5 sensitivity case calculations are then performed and the results of the sensitivity and base case calculations are compared in Section D.2. The deviations in the dependent variables between the base and sensitivity cases are calculated and used to estimate the uncertainties in the dependent variables as described in Section D.3. The uncertainty estimates are summarized in Section D.4. References pertinent to this appendix are provided in Section D.5.

D.1 Selection of Sensitivity Cases

Section D.1.1 describes the specific forms (locations, evaluation times, smoothing processes, etc.) used for each of the dependent variables. Section D.1.2 describes the selection of the sensitivity cases, including descriptions of the SCDAP/RELAP5 modeling feature revisions implemented and justifications for the ranges of the variations investigated.

D.1.1 Specific Forms of the Dependent Variables

The locations selected for evaluation of the dependent variable SCDAP/RELAP5 output are those where the fluid conditions important for structural failure considerations are the most limiting. For the HLs, the most limiting location is in the upper section of Hot Leg 1, adjacent to the RV. For the pressurizer surge line, the most limiting location is at the HL end of the surge line. For the steam generator tubes, the most limiting locations are for the hot average tube and hottest tube, just above the tubesheet in SG 1.

Since the SCDAP/RELAP5-calculated output variables are functions of time, for the purpose of comparing results among many similar runs, it is necessary to: (1) smooth the output in time to remove the oscillatory behavior related to opening and closing of the pressurizer relief valves and (2) use an evaluation-time selection criterion that can adjust for the effects of event sequence timing differences among the runs.

The failures of the HL, surge line and SG tube structures are tightly clustered within a short period (of about 500 s) following the time of the peak in the fuel rod oxidation rate. The lack of adequate cooling for the core fission product decay heat results in a slow system heat-up prior to the onset of fuel rod oxidation. But it is the core power spike resulting from fuel rod oxidation which dramatically increases the system heat-up rate, causing the structural failures to be so tightly clustered.

The structural failures of the HLs, surge line and SG tubes occur subsequent to the oxidation peak because time is required to transport the increasingly-hotter steam from the core through the HLs and out into the surge line and SGs (see the discussion of the RCS energy flow in Section 2.8 and Appendix C). Key aspects of the problem are therefore related to: (1) the core power and core heat-up rate, (2) the rates at which heat is carried away from the core and through the various RCS flow paths, (3) the proximity of the structures with respect to the core and (4) the structure geometries and materials which determine the temperatures at which the structures fail. The essence of the problem is whether the critical effects of the rapidly-increasing steam temperatures are felt in the HL and surge line structures before they are felt in the SG tube structures. Based on this discussion and results of the base case calculation, the specific forms of the dependent variables used for the uncertainty analysis were selected as follows:

Average SG Tube Failure Margin

The average SG tube failure margin is represented by the tube stress multiplier (1.0 or greater) that results in SG tube failure coincident with the earliest RCS piping failure. The failure margin values are calculated by interpolating the failure time data for the HL and SG tube structures.

Hottest SG Tube Failure Margin

The hottest SG tube failure margin is also represented by the tube stress multiplier that results in SG tube failure coincident with the earliest RCS piping failure. However, for cases in which the hottest tube is predicted to fail prior to the HL and pressurizer surge line even when a 1.0 tube stress multiplier is applied, the hottest tube failure margin is instead expressed as the time interval by which hottest tube failure precedes the earlier of the HL or surge line failures. The time interval is expressed in negative seconds, indicating that the non-degraded hottest tube failure margin is negative.

Average and Hottest SG Tube Metal Temperatures

The average and hottest SG tube metal temperatures represent the smoothed (100-s lag) values for the average temperatures (across the tube wall thickness) at the time of the earliest RCS piping failure. The data are taken for the first axial SG tube heat structure above the top of the tubesheet in SG 1, where the tube temperatures are the highest. The time of earliest RCS piping failure was selected for the evaluation time because the SG tube failure margins are most affected by the relative relationships between the SG tube and RCS piping wall temperatures as the failure conditions for both structures are approached.

Hot Leg Steam Temperature and Wall Inside-Surface Heat Transfer Coefficient

The HL steam temperature and wall inside-surface heat transfer coefficient represent smoothed (100-s lag) values for those parameters 100 s after the time of the peak in the fuel rod oxidation rate. The data are taken for the first axial cell (adjacent to the RV) in the upper section of Hot Leg 1, where the HL temperature is the highest. The evaluation time was selected because it is the time when the rate of increase in the smoothed steam temperature is the highest.

For the HL upper section, the wall inside surface heat transfer in the model represents a combination of convection from steam to the wall, radiation from steam to the wall and radiation from the wall to the opposing wall surfaces of the lower HL section. Both the differential temperature and the direction of the heat flow for the wall-to-wall radiation heat transfer process

are different from those for the two steam-to-wall heat transfer processes, and this complicates the calculation of a single, effective HL inside-wall heat transfer coefficient. For the purposes of the uncertainty evaluation, the effective total heat transfer coefficient is calculated by dividing the total wall heat flux (the net from all three of the heat transfer processes) by the differential temperature between the steam and HL upper section wall inside surface.

Pressurizer Surge Line Steam Temperature and Wall Inside-Surface Heat Transfer Coefficient

The pressurizer surge line steam temperature and wall inside-surface heat transfer coefficient represent smoothed (100-s lag) values for those parameters 100 s after the time of the peak in the fuel rod oxidation rate. The data are taken for the axial cell of the surge line adjacent to Hot Leg 1, where the surge line temperature is the highest. The evaluation time was selected because it is the time when the rate of increase in the smoothed steam temperature is the highest.

D.1.2 Selection and Implementation of the Independent Variable Modeling Revisions

Table D.1 identifies the sensitivity cases needed to evaluate variations in the independent variables for the uncertainty study as suggested by the PIRT, and summarizes the model feature revisions that implement those variations into the model. Table D.2 provides a concise list of all sensitivity cases run, including those cases used in the uncertainty study and additional cases which were run to address various other issues. Information regarding the selection of the cases, the exclusion of others, the modeling revisions and the justifications for the ranges of variables evaluated is described as follows.

A1 Full loop circulation (loop seal clearing and reactor vessel lower plenum clearing)

An important underlying assumption of the analysis is that the loop seals in all coolant loops remain plugged with water. If this is not the case, then superheated steam flow in the normal direction around the coolant loops will cause the SG tubes to fail before the HL or surge line. The PIRT considered this a binary parameter: either all loop seals remain water plugged or one-or-more do not. Prior analysis for the Westinghouse plant has indicated that the margin to loop seal clearing is very large; therefore, no sensitivity runs were identified.

A2 Pressurizer Behavior (phase separation, PORV flow, CCFL and draining, spray nozzle venting)

Spray Nozzle Venting Effects

Based on PIRT recommendation, representations of the spray lines and valves were added to the base case model. This model revision was found to result in slightly faster pressurizer draining but no other significant effects. The base case model now better represents the plant configuration and no sensitivity runs related to spray nozzle venting were identified.

Table D.1 Summary of Sensitivity Runs Implementing Variations in the Uncertainty Study Independent Variables

Independent Variable	Notes Regarding Implementing Variations into the Model	Sensitivity Runs Identified to Support the Uncertainty Study
<p>A1 Full loop circulation (loop seal clearing and reactor vessel lower plenum clearing)</p>	<p>An underlying assumption of the analysis is that the loop seals in all four loops will remain plugged with water, setting up circulating flow patterns in the hot leg and SG tube regions. Prior analysis indicates that significant margin to loop seal clearing exists. The uncertainty that the loop seals will not remain plugged is very small.</p>	<p>None</p>
<p>A2 Pressurizer Behavior (phase separation, PORV flow, CCFL & draining, spray nozzle venting)</p>	<p>Spray nozzle venting effects</p> <p>CCFL and draining</p> <p>Phase separation in the tank</p> <p>Relief valve critical flow</p> <p>In the base case run, the pressurizer PORVs and safety relief valves are modeled with flow areas that are sized to deliver the rated flow at the rated upstream pressure condition. Variations in valve flow area account for uncertainties in modeling the critical flow process and in simulating the fluid conditions at the valve inlets.</p>	<p>None</p> <p>None</p> <p>None</p> <p>Run 1A +30% Valve Flow Area</p> <p>Run 1B -30% Valve Flow Area</p>

Table D.1 Summary of Sensitivity Runs Implementing Variations in the Uncertainty Study Independent Variables

Independent Variable	Notes Regarding Implementing Variations into the Model	Sensitivity Runs Identified to Support the Uncertainty Study
<p>A3 Mixing, SG inlet plenum</p>	<p>Variations in the target values for the hot leg discharge coefficient, recirculation ratio and hot/cold mixing fraction will be evaluated.</p> <p>The nominal values for the mixing parameters in the SCDAP/RELAP5 base case run are:</p> <p>Hot Leg $C_D = 0.12$ Recirculation Ratio = 2.0 Hot and Cold Mixing Fraction = 0.85 Hot/Cold Tube Split = 41%/59%</p> <p>The SG inlet plenum flow coefficients will be readjusted so as to attain the desired target value for the parameter that is varied while maintaining the base case target values for the other parameters.</p>	<p>Run 2A Hot Leg $C_D = 0.138$</p> <p>Run 2B Hot Leg $C_D = 0.102$</p> <p>Run 2C Recirculation Ratio = 2.3</p> <p>Run 2D Recirculation Ratio = 1.7</p> <p>Run 2E Mixing Fraction = 0.95</p> <p>Run 2F Mixing Fraction = 0.75</p> <p>Run 2G Hot/Cold Tube Split = 50%/50%</p>
<p>A4 SG tube outer wall heat transfer (SG secondary side heat transfer)</p>	<p>In the sensitivity runs, multipliers are applied to the SG tube outer wall heat transfer coefficient.</p>	<p>Run 3A Tube Outer Wall HTC x 5.0</p> <p>Run 3B Tube Outer Wall HTC x 0.5</p>
<p>A5 Buoyancy-driven flows in SG tubes (ratio of SG tube flow to hot leg flow)</p>	<p>In the model, the calculated recirculation ratio represents the relationship between the SG tube and hot leg flows.</p>	<p>Variations in the target recirculation ratio are evaluated in Sensitivity Runs 2C and 2D (see PIRT Parameter A3 above).</p>

Table D.1 Summary of Sensitivity Runs Implementing Variations in the Uncertainty Study Independent Variables

Independent Variable	Notes Regarding Implementing Variations into the Model	Sensitivity Runs Identified to Support the Uncertainty Study
<p>B1 Core power, especially fuel rod cladding oxidation power</p>	<p>Fission product decay power</p> <p>Oxidation power</p> <p>Implement into model by adding or subtracting heat from the core fluid at rates that are fixed percentages of the code-calculated oxidation power</p>	<p>None</p> <p>Run 4A Oxidation power x 1.2</p> <p>Run 4B Oxidation power x 0.5</p>
<p>B2 Buoyancy-driven flow in vessel (includes effects of vessel internal flow resistances)</p>	<p>Artificial increases and decreases in the input flow losses are made in the axial and crossflow vessel internal junctions to account for uncertainties related to predicting buoyancy-driven flows and friction losses at very low flow rates.</p>	<p>Run 5A 50% decrease in internal vessel flow</p> <p>Run 5B 100% increase in internal vessel flow</p>
<p>B3 Buoyancy-driven flow in hot legs</p>	<p>This parameter is represented in the model by the calculated hot leg discharge coefficient, C_D, which relates the hot leg flow to the densities of the hot and cold fluids.</p>	<p>Variations in the target hot leg discharge coefficient are evaluated in Sensitivity Runs 2A and 2B (see PIRT Parameter A3 above).</p>
<p>B4 RCS heat loss to containment</p>	<p>The base case model assumes a nominal 4 MW heat loss from the RCS to containment at full-power normal operating conditions. The heat loss is implemented by applying a constant heat transfer coefficient on the outer surfaces of the RCS piping and vessel heat structures. For the sensitivity cases the base case heat transfer coefficient is multiplied by 0.5 and 2.0.</p>	<p>Run 6A 2 MW total RCS heat loss at full power conditions</p> <p>Run 6B 8 MW total RCS heat loss at full power conditions</p>
<p>B5 Mixing at the vessel-to-hot leg connection</p>	<p>SCDAP/RELAP5-calculated flow patterns in the region of this connection are physical and consistent with NRC CFD simulations. Therefore, no sensitivity runs are identified.</p>	<p>None</p>

Table D.1 Summary of Sensitivity Runs Implementing Variations in the Uncertainty Study Independent Variables

Independent Variable	Notes Regarding Implementing Variations into the Model	Sensitivity Runs Identified to Support the Uncertainty Study
C1 Operator intervention (event sequence definition item)	Operator intervention involves recognizing the event sequence signature and depressurizing the primary and secondary systems according to procedures. Sensitivity studies evaluating operator intervention were previously performed; no new sensitivity runs are identified.	None
C2 RC pump seal leakage (event sequence definition item)	The base case model includes flow areas for the pump shaft seals that initially pass 21 gpm/pump into the containment. For the sensitivity run, the flow areas are scaled up for the higher assumed leak rate. The uncertainty study assumes a ± 20 gpm simulation uncertainty for pump shaft seal leakage and only a 61 gpm/pump sensitivity case is needed for the generation of statistics for the uncertainty study. Note that sensitivity runs not used for the uncertainty study are identified to investigate other higher pump shaft seal leakage rates, See Table D.2.	<p>Run 7A Leak rate increases to 61 gpm/pump at 2 hours (Interpolation between this run and the base case is used to provide results for a 41 gpm/pump leak rate assumption).</p> <p>Run 7G Leak rate decreases to 1 gpm/pump at 2 hours</p> <p>(Note that discussions of additional pump seal leakage sensitivity runs, unrelated to the uncertainty study, are included in Section D.2.2, see Cases 7B, 7C, 7D, 7E, 7F and 7F2.)</p>
C3 SG tube leakage (event sequence definition item)	Preexisting SG tube leakage conditions were evaluated in a prior sensitivity study. No sensitivity runs are needed to support the uncertainty study. However a tube leakage sensitivity run not used for the uncertainty study is identified, see Table D.2.	<p>None</p> <p>(Note that discussion of an additional SG tube leakage sensitivity run, unrelated to the uncertainty study, is included in Section D.2.2, see Case 8C.)</p>

Table D.1 Summary of Sensitivity Runs Implementing Variations in the Uncertainty Study Independent Variables

Independent Variable	Notes Regarding Implementing Variations into the Model	Sensitivity Runs Identified to Support the Uncertainty Study
C4 Surge line orientation (plant configuration item)	The configuration of the surge line and the location of its hot leg connection are fixed (the connection is made on the side of hot leg). No sensitivity runs are identified to support the uncertainty study. However a sensitivity run, not used for the uncertainty study, which evaluates the effects of relocating the surge line connection to the top of the hot leg is identified, see Table D.2.	None (Note that discussion of an additional surge line configuration sensitivity run, unrelated to the uncertainty study, is included in Section D.2.2, see Case 8A.)
C5 Distribution of metal mass in the plant (plant configuration item)	The distribution of metal mass in a plant is fixed. No sensitivity runs are identified.	None

Table D.2 List of Sensitivity Calculations

Case Number	Sensitivity Calculation Description
Base Case	Nominal: pressurizer relief valve areas, oxidation model, hot leg and surge line inside wall HTCs, SG tube outer wall HTC, vessel internal circulation. No stuck-open SG relief valves or tube leakage. Surge line connects to side of Hot Leg 1. Hot Leg $C_D=0.120$, recirculation ratio=2.0, hot/cold mixing fractions=0.85, hot/cold tube split=41%/59%, RCP seal leakage=21 gpm/pump, steam leak area per SG=0.5 in ² , total RCS heat loss=4 MW.
1A	Pressurizer PORV and SRV valve flow areas increased by 30%
1B	Pressurizer PORV and SRV valve flow areas decreased by 30%
2A	Hot Leg C_D increased to 0.138
2B	Hot Leg C_D decreased to 0.102
2C	Recirculation ratio increased to 2.3
2D	Recirculation ratio decreased to 1.7
2E	Hot and cold mixing fractions increased to 0.95
2F	Hot and cold mixing fractions decreased to 0.75
2G	Hot/cold tube split ratio changed to 50%/50%
3A	SG tube outer wall HTC x 5.0
3B	SG tube outer wall HTC x 0.5
4A	Oxidation power x 1.2

Table D.2 List of Sensitivity Calculations

Case Number*	Sensitivity Calculation Description
4B	Oxidation power x 0.5
5A	50% decrease in reactor vessel internal circulation flow rates
5B	100% increase in reactor vessel internal circulation flow rates
6A	2 MW total RCS heat loss
6B	8 MW total RCS heat loss
7A	RCP shaft seal leak rate increases to 61 gpm/pump at 2 hours
7B*	RCP shaft seal leak rate increases to 300 gpm/pump at 2 hours
7C*	RCP shaft seal leak rate increases to 182 gpm/pump at 2 hours
7D*	RCP shaft seal leak rate increases to 120 gpm/pump at 2 hours
7E*	RCP shaft seal leak rate increases to 90 gpm/pump at 2 hours
7F*	RCP shaft seal leak rate increases to 300 gpm in Loop 1 pump at 2 hours
7F2*	RCP shaft seal leak rate increases to 300 gpm in Loop 2 pump at 2 hours
7G	RCP shaft seal leak rate decreases to 1 gpm/pump at 2 hours
8A*	Pressurizer surge line connection moved to top of hot leg
8B*	Stuck open PORV on SG 1, no leakage from SG secondary in the other 3 SGs
8C*	100 gpm assumed tube leakage in SG 1, Coolant Loop 1 flow parameters adjusted to attain 0.14 hot leg C_D , 1.75 recirculation ratio and 0.75 mixing fractions
8D*	Surge line and hot leg upper section inside wall HTC's x 2.0
8E*	Tubesheet HTC x 2.0
8G*	SG steam leakage flow areas of 0.4, 0.3, 0.2 and 0.1 in ² (one run with different leak area in each SG to determine minimum leak rate needed to depressurize SGs by the time of hot leg failure)

* Runs marked with an asterisk are not used for the statistical evaluation of uncertainties, only for evaluating various other issues.

CCFL and Draining

The PIRT recommended that the effects of CCFL behavior on the pressurizer draining process be evaluated. A previous study investigated variations in CCFL parameters at the tank-to-surge line connection and found that the effects of those variations were small (Reference D.1). The PIRT also recommended that the possibility for CCFL limiting as a result of hydraulic jump conditions forming at elbows between vertical and horizontal sections of the surge line be evaluated. Papers describing this situation were obtained and the SCDAP/RELAP5 calculated surge line conditions were evaluated. It was found that the calculated steam flow from the HL into the surge line is so highly superheated that significant flow of liquid from the pressurizer tank into the HL is prevented. Liquid that enters the surge line from the bottom of the tank is vaporized as it drains into the surge line, creating single-phase steam and droplet flow regimes inside the surge line, depending on whether pressurizer relief valves are open or closed. The vaporization of liquid cools the steam inside the surge line and thereby delays the start of the heat-up of the surge line wall until after the completion of pressurizer draining. These

evaluations indicated that pressurizer draining is controlled by CCFL at the tank-to-surge line connection and that the conditions that could result in hydraulic-jump effects within the surge line are not present. No sensitivity runs related to surge line CCFL effects were identified.

Phase Separation in the Tank

The upward flow of steam through the pressurizer and out the relief valves can support a frothy mixture inside the pressurizer tank. If the froth level is at the top of the tank, then the relief valve flow is a two-phase mixture of water and steam. When the froth level has dropped below the top of the tank, then the relief valve flow is single-phase steam, potentially with entrained liquid droplets. The SCDAP/RELAP5 interphase drag models determine the distribution of steam in the tank and the mixture level. The pressurizer fluid conditions during the pressurizer draining period in the base case calculation were evaluated in order to determine the interphase drag models that are most important for this event sequence. For periods when the pressurizer relief valves are open, slug flow is seen in the bottom of the tank and mist flow is seen in the upper regions of the tank. For periods when the relief valves are closed, vertically-stratified and bubbly flows are seen in the bottom of the tank and mist flow is seen in the upper regions of the tank. Therefore, interphase drag models for the bubbly and slug flow regimes are of most interest for simulating the tank mixture level.

To evaluate the sensitivity of results to variations in the interphase drag models, a check run was made in which the hydraulic diameter for the pressurizer tank was reduced by a factor of 5.0 from the actual tank diameter. For large-diameter vertical tanks, SCDAP/RELAP5 uses the Zuber-Findlay (Reference D.2) and Kataoka and Ishii (Reference D.3) correlations for churn-turbulent bubbly and slug flows. The slip between the phases with the Zuber-Findlay correlation is proportional to the square root of the hydraulic diameter while for the Kataoka and Ishii correlation it is directly proportional to the hydraulic diameter. Therefore, the run with reduced hydraulic diameter effectively implements a reduction in the slip ratio by a factor of between 2.24 and 5.0 and corresponding increases in the interphase drag and the tank mixture level. Compared with the base case, the check run with the reduced tank hydraulic diameter indicated only a small difference in the pressurizer draining process and event sequence timing and no effect on the calculated SG tube failure margins. As a result of this finding, no sensitivity runs related to phase separation in the tank were identified.

Relief Valve Flow

Because the pressurizer pressure remains high in this event sequence, the flow of fluid through the pressurizer PORVs and SRVs is controlled by critical flow processes. The relief valves pass liquid, two-phase fluid and steam over the course of the event sequence. The calculation of critical flow through the valves is subject to uncertainties related to modeling of the critical flow process in general and to uncertainties related to correctly simulating the fluid conditions at the valve inlets. Since the flow of mass and energy out of the primary coolant system by fluid exiting through the pressurizer relief valves is large, it is appropriate to evaluate the sensitivity of calculation results to variations in the relief valve critical flow.

A survey was made of prior assessments of RELAP5 capabilities (Reference D.4) for representing valve and break flows in experiments in the Marviken (References D.5 and D.6), LOFT (References D.7, D.8 and D.9), ROSA-IV (Reference D.10) and MIST (References D.11 and D.12) test facilities. These assessments cover uncertainties related both to critical flow modeling and to adequately representing the fluid conditions upstream of the choking location. Five high-pressure experiments were evaluated, one of which (MIST Test 360499) featured the

behavior for flow through a stuck-open pressurizer PORV. (See Section 3.2.2 for more discussion of the RELAP5 assessment for this test) These assessments include a large range of upstream fluid conditions and indicate that RELAP5 overpredicted and underpredicted the critical flow by up to 27% and 25%, respectively. Based on these assessment findings, sensitivity runs with the pressurizer PORV and SRV valve flow areas varied by $\pm 30\%$ were identified to account for the uncertainties in the relief valve flow.

A3 Mixing, SG Inlet Plenum

Sensitivity calculations were identified for variations in the HL discharge coefficient, recirculation ratio and hot/cold mixing fraction, all of which affect mixing behavior in the SG inlet plenum region. A sensitivity calculation with the assumed hot/cold tube split altered is also identified. The ranges of the variations selected for the sensitivity runs are based on observations of the Westinghouse one-seventh scale experimental data (Reference D.13) and on CFD analyses. In these sensitivity runs, the SG inlet plenum flow coefficients are adjusted so as to attain the revised target value for the parameter that is varied while maintaining the base-case target values for the other mixing parameters.

A4 SG tube outer wall heat transfer (SG secondary side heat transfer)

The base case model uses the maximum heat transfer coefficient among forced, free and laminar convection correlations. The base case model includes a 1.284 multiplier on the heat transfer coefficient (which is needed in order for the model to achieve a satisfactory concurrent match with plant data for the SG secondary pressure, SG secondary fluid mass and the SG heat removal rate during full-power steady state operation). The base case model also includes a physically-based multiplier (which is only applied on the heat transfer coefficient calculated using the Dittus-Boelter forced convection correlation, Reference D.14) that accounts for the effects of flow passing through a tube bundle parallel to the tube axis. However, it is expected that substantial portions of the swirling flows within the actual SG tube bundle will be across the tubes, not in parallel with them. Such crossflows result in still-higher heat transfer coefficients and the extent of this enhancement is not known. During the period when the SG boiler is steam filled, the calculated heat transfer coefficient is very small ($\sim 10 \text{ W/m}^2\text{-K}$).

Sensitivity runs were identified to evaluate +400% and -50% variations in the SG tube outer wall heat transfer coefficient to bound the potential effects of the heat transfer variations described in the previous paragraph.

A5 Buoyancy-driven flows in SG tubes (ratio of SG tube flow to hot leg flow)

The ratio of the SG tube and HL flows is represented in the model by the calculated recirculation ratio. Sensitivity runs evaluating the effect of variations in the target recirculation ratio were identified (see PIRT Parameter A3 above).

B1 Core power, especially fuel rod cladding oxidation power

In the model, the core power is calculated as the sum of fission product decay power and the fuel rod metal-water reaction oxidation power. The fission decay power is based on the nominal ANS1979 standard, Reference D.15. The fission decay power response is relatively stable in time and its uncertainty is relatively small ($\sim 10\%$); placing a multiplier on the fission decay power to represent this uncertainty is expected to only significantly affect the timing of the sequence events (SG dry out, core uncovering, etc.). No sensitivity studies related to fission

decay power were identified. The oxidation power is, however, of particular interest because its response is transient, the peak oxidation power is relatively high (11.2 times the fission decay power in the base case run) and the structural failures of reactor coolant piping and SG tubes occur during the period when the oxidation power is peaking. Therefore, sensitivity runs related to the oxidation process were identified.

In a prior sensitivity study, Reference D.1, the impact of varying the oxidation process modeling was evaluated using a run in which the peak fuel rod linear oxidation heat was limited to 1,000 W/m. That model change limited the peak oxidation rate to 57% of that seen in the base case run and significantly extended the length of the oxidation period. The study indicated only a small reduction in the SG tube failure margin resulted from the change in oxidation modeling. The modeling approach used in the prior study only allows for modeling decreases in the oxidation power (and not increases) so an alternate modeling approach for evaluating variations in the oxidation power is used here.

Sensitivity studies were identified where both increases and decreases in the oxidation power are evaluated by installing artificial heat structures in the core region of the model to add and subtract heat from the core fluid at a rate that is a specified multiple of the oxidation power. Results from a check run made with the artificial structures included in the model but with zero power were compared against the base case calculation to assure that just the presence of the artificial structures does not significantly alter the results. The comparison indicated only slight biases between the output of the two runs, and the sensitivity run results used in the uncertainty calculations are adjusted for those biases.

The SCDAP/RELAP5 manual describes assessments related to reactor core behavior during severe accidents (see Section 3.3). The code performance for predicting fuel rod oxidation behavior was evaluated against test data from nine experiments. The summary finding of the assessments for hydrogen production due to fuel rod oxidation for the nine experiments (Reference D.16, Volume 5, Table 3-1) is that the predicted hydrogen production from fuel rod oxidation ranged from 50% above to 15% below the measured hydrogen production. An additional assessment of the code capabilities for predicting fuel rod oxidation processes against measured/inferred data for the Three Mile Island accident (D.16, Volume 5, Table 4-4) indicates that the code overpredicted oxidation by 22%. Based on these assessment results, sensitivity runs were identified for +20% and -50% variations in the calculated oxidation power.

B2 Buoyancy-driven flow in vessel (includes effects of vessel internal flow resistances)

The PIRT committee suggested that the SCDAP/RELAP5-calculated predictions of vessel circulation rates are "likely within a factor of two" of the physical circulation rates and two sensitivity runs were identified to evaluate the effects of this variation. Modeling uncertainties that could affect the RV internal flow rates were evaluated and it was found that the current model may be understating the friction losses associated with flows that decline into the laminar range. Based on this evaluation, a sensitivity run was identified in which the friction losses are increased so as to reduce the flow rates by 50%. A survey of prior RELAP5 assessments (Reference D.4) for predicting buoyancy-driven flows in vessels uncovered a UPTF assessment case (Reference D.17) in which the code underpredicted the circulating flows by 50%. Therefore, a second sensitivity run was identified in which the friction losses are decreased such that the vessel circulating flow rates are increased by 100%.

B3 Buoyancy-driven flow in hot legs

This parameter is represented in the model by the calculated hot leg discharge coefficient, C_D , which relates the HL flow rate to the densities of the hot and cold fluid streams. Sensitivity runs evaluating the effect of variations in the target hot leg discharge coefficient were identified (see PIRT parameter A3 above).

B4 RCS heat loss to containment

A nominal 4 MW full power operation total heat loss from the outer surfaces of the RCS to containment is included in the base case model. This heat loss rate is based on the capacities of the containment fan coolers, which remove the heat load during normal plant operation. The heat loss is implemented in the model by applying a constant heat transfer coefficient on the outer wall surfaces of the RCS piping, SG and RV structures. A prior sensitivity study (Reference D.1) indicated that the SG tube failure margins are moderately affected by variation in the RCS heat loss. Sensitivity studies were identified with the heat loss reduced to 2 MW and increased to 8 MW. This factor-of-two variation is based on an EPRI report (Reference D.18) that evaluated the causes for plant operating containment temperatures generally exceeding their design values. The report found that many insulating materials did not meet the specified heat loss requirement and that heat losses from vertical components were greater than previously analyzed. To implement the changes into the model, the constant heat transfer coefficient that results in the 4 MW base case heat loss is halved and doubled.

B5 Mixing at the vessel-to-hot leg connection

The PIRT committee discussed that mixing at the connection between the RV and HL is expected to be much less robust than mixing in the SG inlet plenum region. The cool steam returning to the vessel tends to fall downward into the peripheral regions of the core and does not mix with the hot steam that flows into the upper HL sections. Buoyancy effects therefore tend to keep the hot and cold streams apart at the location of this connection.

The SCDAP/RELAP5 base case model is set up to well represent the fluid buoyancy behavior at the RV-to-HL connections and the calculated response is plausible. Within the RV upper plenum region, the code predicts a radially-outward flow of hot steam toward the HLs through the uppermost region of the upper plenum. The flow exiting the RV into the upper HL sections represents only a portion (~30%) of the hot steam carried by that flow. The remainder of the flow turns downward, where it is mixed with the returning cooler steam from the lower HL section, and then turns radially-inward toward the vessel centerline. The SCDAP/RELAP5-calculated behavior in the HL nozzle region results in limited local mixing between the cooler steam entering the RV from the lower HL sections and the hotter steam that flows out of the vessel into the upper HL sections.

NRC CFD simulations also displayed this buoyancy-driven behavior and show only minimal mixing of the hot and cool streams at the RV-to-HL connection. Therefore no SCDAP/RELAP5 sensitivity runs related to fluid mixing at the vessel to HL connection were identified.

C1 Operator intervention (event sequence definition item)

Operator intervention to mitigate the accident was investigated in a prior sensitivity study (Reference D.1). The intervention involves recognizing the event sequence signature and depressurizing the primary and secondary systems according to procedures. The prior studies

demonstrated the effectiveness of the operator intervention for mitigating the accident and the event sequence timing limitations involved. No new sensitivity runs were identified.

C2 RC pump seal leakage (event sequence definition item)

Evaluations of RCP pump shaft seal leakage for SBO accident event sequences have been performed by Brookhaven National Laboratory (Reference D.19). Those evaluations indicate that a leak rate of 1.32 L/s [21 gpm] per pump is likely over the early portion of a SBO accident event sequence. Later during the event sequence a variety of other leak rates are possible, depending on failures of pump seal components.

Sensitivity calculations were identified for a variety of pump seal leakage situations, with the leak rate changing from the 1.32-L/s [21-gpm] rate after two hours. Calculations were identified to investigate a decrease to 0.063 L/s [1 gpm] and increases to 3.83 L/s [61 gpm], 5.66 L/s [90 gpm], 7.54 L/s [120 gpm], 11.4 L/s [182 gpm] and 18.9 L/s [300 gpm] in each of the four RCPs after two hours. Calculations investigating increases to 18.9 L/s [300 gpm] in only one pump were also identified. Most of these calculations address issues relating to the effects of RCP seal leakage variations and, as described below, not for the purpose of the uncertainty evaluation.

Previous sensitivity studies (Reference D.1) were performed with the SCDAP/RELAP5 model to evaluate the effects of various increases in the leak rate after two hours. Those studies indicated that an increase in the leak rate to 3.83 L/s [61 gpm] at two hours moderately decreased the SG tube failure margins and that larger increases in the leak rate led to early core melt and greatly increased SG tube failure margins.

For the purposes of the uncertainty study it is assumed that the event sequence under investigation specifies a 1.32-L/s [21-gpm] leakage rate throughout the event, consistent with the assumption used in the base case calculation. Considerations of lower and higher leak rates are judged to represent separate, distinct event sequences from a PRA view. However, it is acknowledged that (in addition to those considerations) there are uncertainties related simply to the ability of SCDAP/RELAP5 to simulate leak rates in general. Those uncertainties relate to the simulation of the fluid conditions upstream of the leak, the configuration of the leak geometry as well as the ability to predict the critical flow. The uncertainty study assumes that the uncertainty in the SCDAP/RELAP5 simulation for the 1.32 L/s [21 gpm] rate is ± 1.26 L/s [± 20 gpm]. A SCDAP/RELAP5 sensitivity run is made for the 1 gpm assumed leak rate case. For the 2.58-L/s [41-gpm] leak rate assumption, results are obtained by interpolating between the 1.32 L/s [21 gpm] leakage in the SCDAP/RELAP5 base case calculation and a SCDAP/RELAP5 sensitivity case calculation which assumed 3.83-L/s [61-gpm] leakage.

C3 SG tube leakage (event sequence definition item)

The effects of introducing preexisting SG tube primary-to-secondary leakage conditions into the event sequence description were evaluated in a prior sensitivity study (Reference D.1). No new sensitivity runs were identified to address uncertainties in this parameter. However, an additional SG tube primary-to-secondary system leakage sensitivity run (Case 8C), unrelated to the uncertainty study, is discussed in Section D.2.2.

C4 Surge line orientation (plant configuration item)

The configuration of the surge line and the location of its HL connection are fixed (the connection is made on the side of HL). No sensitivity runs were identified to address uncertainties in this parameter. However, an additional surge line configuration sensitivity run evaluating the effects of moving the connection to the top of the HL pipe is discussed in Section D.2.2.

C5 Distribution of metal mass in the plant (plant configuration item)

The distributions of metal mass and materials among the piping and vessels in any plant are fixed. No sensitivity runs were identified.

D.2 Sensitivity Run Results

Section D.2.1 documents the results of the SCDAP/RELAP5 uncertainty evaluation sensitivity case runs. Section D.2.2 documents the results of additional SCDAP/RELAP5 sensitivity runs performed to evaluate various other modeling issues.

D.2.1 Sensitivity Runs Used for the Statistical Evaluations of Uncertainty

Nineteen of the SCDAP/RELAP5 sensitivity runs identified in Table D.2 were used to generate data for the statistical evaluations of uncertainty. The sensitivity runs were performed as variations on the Westinghouse four-loop plant SBO base case calculation described in Section 2.8. With the exception of runs made specifically to evaluate the effect of variations in the SG inlet plenum mixing and flow parameters, the sensitivity runs were performed with the SG inlet plenum region flow coefficients readjusted to retain agreement between the calculated and target mixing and flow parameters of the base case.

The dependent variable output data from the base case and sensitivity calculations used in developing the uncertainty estimates is shown in Tables D.3 and D.4. Other results from the 19 sensitivity runs are summarized as follows:

Pressurizer PORV and SRV Flow Area Variations

The nominal pressurizer PORV and SRV flow areas used in the base case calculation are those needed to provide the rated valve flows at the rated pressures. Two sensitivity runs were performed, Case 1A (with nominal PORV and SRV flow areas increased by 30%) and Case 1B (with nominal PORV and SRV flow areas decreased by 30%).

The mass flow rates through one of the two pressurizer PORVs in the base case, Case 1A and Case 1B are compared in Figure D.1. As expected, during periods when the valve is open the flow rates for Cases 1A and 1B are respectively greater and less than the corresponding base case flow rate. Because the relief valves open as often and as long as needed to control the RCS pressure, the overall results from the three runs are generally not very different, as shown by the comparison of the RCS pressure responses for the three runs in Figure D.2. For the case with the larger valve area the valve opens for shorter periods than in the base case; the opposite is true for the case with the smaller valve area. The SG tube failure margins are only very slightly affected by the variations in the pressurizer relief valve flow areas. Note that the PORVs are not functional after the station batteries are assumed to be depleted at four hours (14,400 s). Afterward, the pressurization of the RCS is limited only by the opening of the pressurizer SRVs.

Table D.3 Comparison of SCDAP/RELAP5-Calculated Results for Failure Times and Margins for the Cases Used in the Uncertainty Analysis

Case Number	First Primary Failure Component	First Primary Failure Time(s)	SG 1 Hottest Tube with 1.0 Multiplier Failure Time – First Primary Failure Time(s)	SG 1 Average Tube Stress Multiplier for Tube Failure Coincident with First Primary Failure
Base Case	Hot Leg 1	13,630	-155	2.10
Case 1A	Hot Leg 1	13,660	-155	2.07
Case 1B	Hot Leg 1	13,685	-150	2.11
Case 2A	Hot Leg 1	13,775	-155	1.92
Case 2B	Hot Leg 1	13,470	-135	2.39
Case 2C	Hot Leg 1	13,765	-170	2.18
Case 2D	Hot Leg 1	13,615	-135	2.02
Case 2E	Hot Leg 1	13,605	-145	2.50
Case 2F	Hot Leg 1	13,740	-160	1.81
Case 2G	Hot Leg 1	13,750	-140	2.21
Case 3A	Hot Leg 1	13,550	-35	2.35
Case 3B	Hot Leg 1	13,650	-160	2.07
Case 4A	Hot Leg 1	13,435	-170	2.16
Case 4B	Hot Leg 1	14,535	-90	1.91
Case 5A	Hot Leg 1	13,355	-260	2.28
Case 5B	Hot Leg 1	14,125	-90	1.97
Case 6A	Hot Leg 1	13,295	-140	2.12
Case 6B	Hot Leg 1	14,385	-255	1.92
Case 7A	Hot Leg 1	13,465	-210	2.33
Case 7B*	Hot Leg 2	14,320	Did Not Fail	7.01
Case 7C*	Hot Leg 2	14,475	Did Not Fail	4.58
Case 7D*	Hot Leg 2	14,300	Did Not Fail	3.30
Case 7E*	Hot Leg 2	13,450	10	2.50
Case 7F*	Hot Leg 2	13,380	Did Not Fail	2.00
Case 7F2*	Hot Leg 1	13,460	-275	2.15**
Case 7G	Hot Leg 1	13,395	-140	2.08

* Runs marked with a single asterisk are not used for the statistical evaluation of uncertainties, only for evaluating various other issues.

** For Case 7F2, the minimum average-tube failure margin shown is calculated in SG 3.

Table D.4 Comparison of SCDAP/RELAP5-Calculated Results for Temperatures and Wall Heat Transfer Coefficients for the Cases Used in the Uncertainty Analysis

Case Number	SG 1 Average Tube Structure Temperature (K)	SG 1 Hottest Tube Structure Temperature (K)	Hot Leg 1 Steam Temperature (K)	Hot Leg 1 Wall HTC (W/m ² -K)	Surge Line Steam Temperature (K)	Surge Line Wall HTC (W/m ² -K)
Base Case	1021.7	1239.6	1776.0	423.13	1373.0	490.86
Case 1A	1023.0	1239.6	1771.9	434.52	1378.3	562.30
Case 1B	1020.9	1238.7	1773.8	412.90	1370.6	454.83
Case 2A	1039.3	1254.1	1744.7	428.99	1360.6	501.09
Case 2B	999.80	1218.4	1744.5	399.42	1346.6	475.78
Case 2C	1014.6	1247.7	1729.4	424.26	1349.2	561.65
Case 2D	1028.6	1217.1	1729.8	404.27	1348.8	470.96
Case 2E	986.70	1226.0	1725.1	407.90	1352.2	517.18
Case 2F	1053.0	1247.1	1780.3	438.17	1369.0	542.98
Case 2G	1013.8	1217.3	1788.3	407.35	1377.0	442.90
Case 3A	1000.7	1173.0	1737.9	413.83	1353.7	499.80
Case 3B	1023.8	1248.5	1751.0	413.18	1355.0	463.99
Case 4A	1018.8	1240.1	1776.8	438.84	1368.1	548.26
Case 4B	1030.9	1189.6	1677.7	297.93	1274.6	243.77
Case 5A	999.20	1157.5	1603.3	380.91	1248.7	468.74
Case 5B	1031.8	1231.3	1800.5	422.80	1405.7	527.39
Case 6A	1017.9	1235.0	1764.1	415.13	1364.8	462.60
Case 6B	1040.7	1250.6	1739.8	419.04	1325.5	490.39
Case 7A	997.80	1180.2	1731.2	364.63	1127.6	279.77
Case 7B	918.10	949.70	1558.3	234.15	623.20	133.41
Case 7C	952.80	989.90	1481.8	247.84	720.10	180.11
Case 7D	960.00	1010.6	1489.1	269.00	741.00	181.79
Case 7E	984.20	1139.9	1719.2	332.79	745.00	284.46
Case 7F	950.10	1049.8	1668.0	334.26	848.20	234.29
Case 7F2	1007.3	1186.1	1668.1	340.33	1004.9	251.34
Case 7G	1023.0	1234.6	1735.3	421.27	1360.7	562.50

* Runs marked with an asterisk are not used for the statistical evaluation of uncertainties, only for evaluating various other issues.

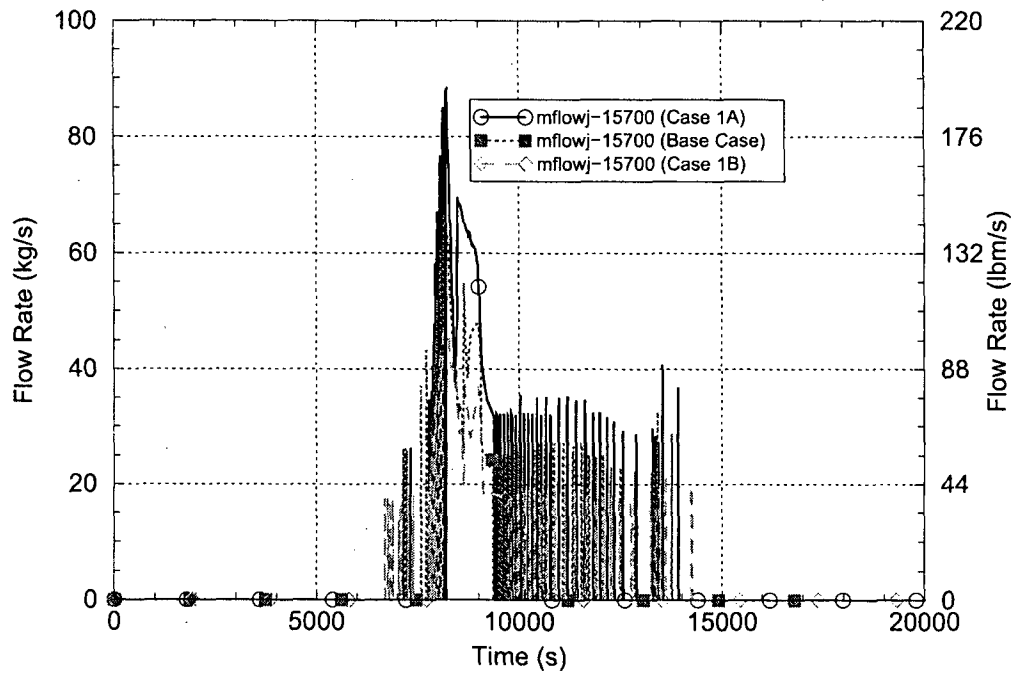


Figure D.1 Mass Flow Rates Through One of the Two Pressurizer PORVs for the Relief Valve Flow Area Sensitivity Cases

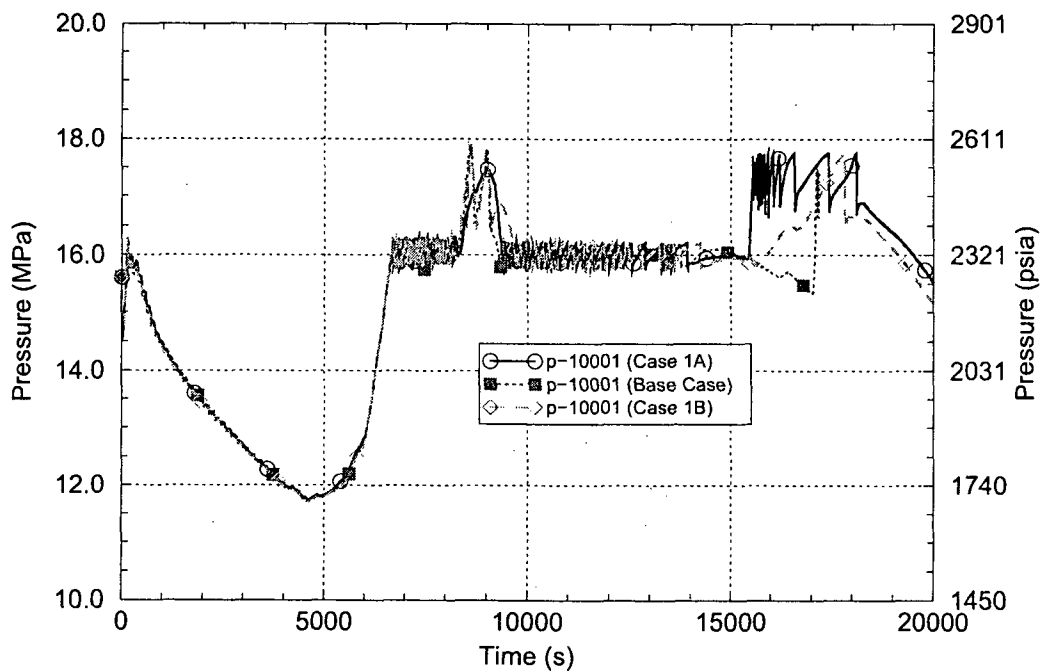


Figure D.2 RCS Pressures for the Relief Valve Flow Area Sensitivity Cases

Hot Leg Discharge Coefficient Variations

The nominal target hot leg discharge coefficient in the base case calculation is 0.12. Two sensitivity runs were performed, Case 2A (with the discharge coefficient increased by 15% to 0.138) and Case 2B (with the discharge coefficient decreased by 15% to 0.102).

The responses of the Hot Leg 1 discharge coefficients for the base case, Case 2A and Case 2B are compared in Figure D.3. The calculated discharge coefficients are in good agreement with the desired target values for all three runs.

Figure D.4 compares the flow rates in the upper section of Hot Leg 1, near the RV, among the three runs. As expected, the HL flow rate is higher when the higher discharge coefficient is used and lower when the lower discharge coefficient is used. Figure D.5 compares the integrated SG 1 power fractions among the three runs. These two figures show the close correlation between the HL flow and the portion of the core heat that is removed to the SGs. The difference in SG heat removal is seen to have a moderate effect on the SG average tube failure margins. Stress multipliers of 1.92, 2.10 and 2.39, respectively are needed for average tube failure to occur coincident with the HL using the increased, nominal and reduced hot leg discharge coefficients. The comparisons also show a small event sequence timing effect, with the lower hot leg discharge coefficient leading to an acceleration of events and the higher discharge coefficient leading to a deceleration of events. This effect results because the reduced SG heat removal associated with a lower hot leg discharge coefficient leads to more frequent and longer opening periods for the pressurizer PORVs, which tends to reduce the RCS fluid inventory more rapidly and accelerate the system heat-up process.

Subsequent to performing Cases 2A and 2B, it was uncovered that the $\pm 15\%$ hot leg discharge coefficient variations assumed in these runs may not fully bound the expected range in the parameter. For that reason, the results from these two runs are extrapolated to effectively incorporate a $\pm 30\%$ hot leg discharge coefficient variation in the uncertainty analysis.

Recirculation Ratio Variations

The nominal target recirculation ratio used in the base case calculation is 2.0. Two sensitivity runs were performed, Case 2C (with the recirculation ratio increased to 2.3) and Case 2D (with the recirculation ratio decreased to 1.7).

The responses of the Loop 1 recirculation ratios for the base case, Case 2C and Case 2D are compared in Figure D.6. The calculated recirculation ratios are in good agreement with the desired target values for all three runs.

Figure D.7 compares the integrated SG 1 power fractions among the three runs. With the other flow and mixing target parameters held constant, an increase in recirculation ratio leads to increased SG heat removal. The difference in SG heat removal is seen to have a small effect on the average tube failure margins. Stress multipliers of 2.02, 2.10 and 2.18, respectively are needed for average tube failure to occur coincident with the HL using the reduced, nominal and increased recirculation ratios. The average tube failure margin increases as the recirculation ratio increases because (with a cold mixing fraction of 0.85) most of the increased cold return tube flow is directed to the mixing plenum, where it lowers the inlet temperature for the hot average tube.

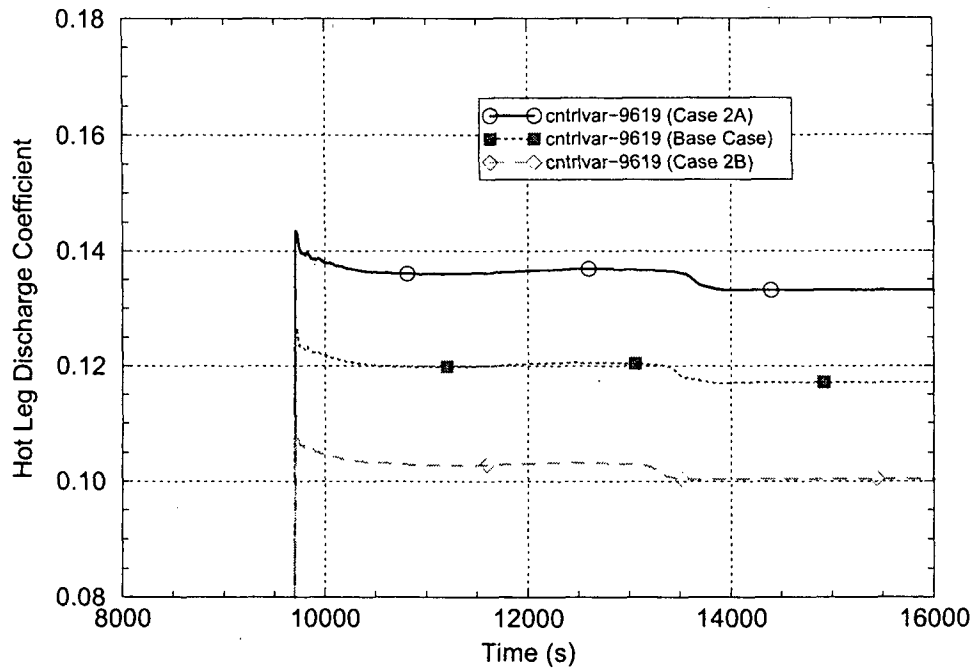


Figure D.3 Hot Leg 1 Discharge Coefficient Responses for the Hot Leg Discharge Coefficient Sensitivity Cases

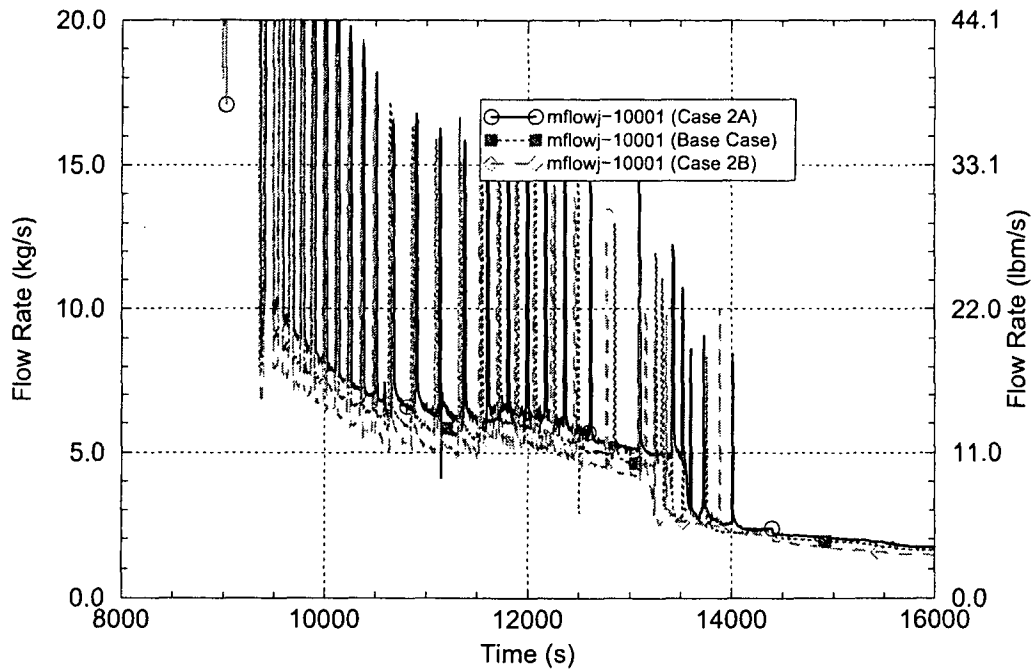


Figure D.4 Hot Leg 1 Upper Section Flow Rates for the Hot Leg Discharge Coefficient Sensitivity Cases

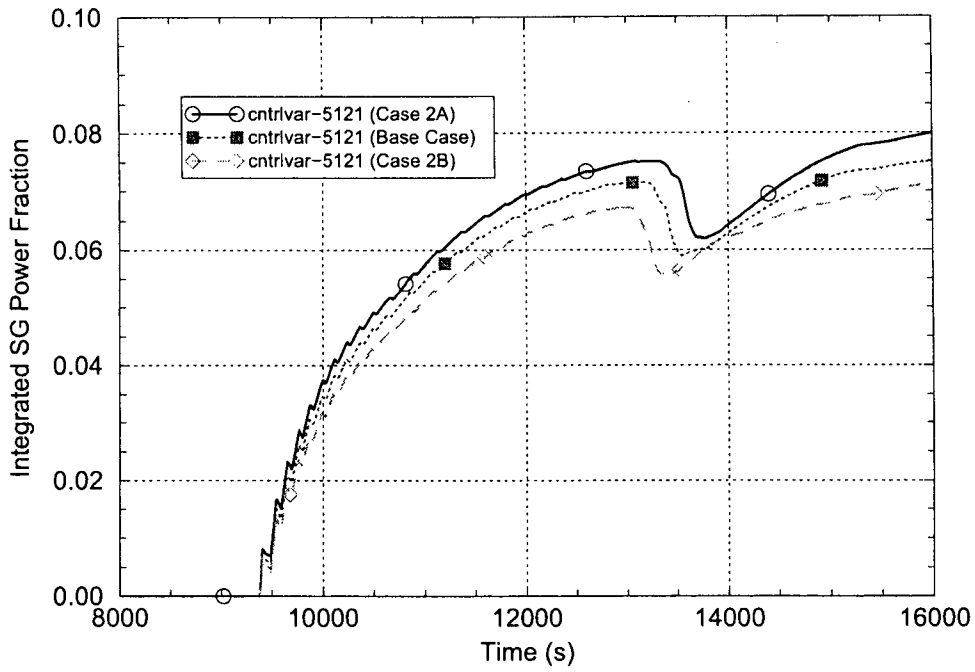


Figure D.5 Integrated SG Power Fractions for the Hot Leg Discharge Coefficient Sensitivity Cases

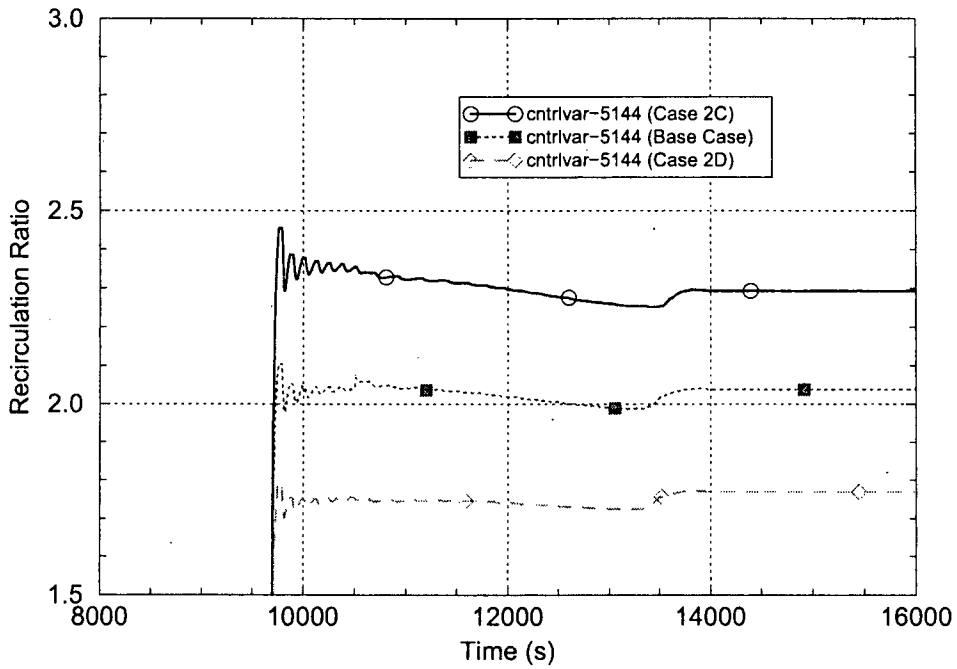


Figure D.6 Loop 1 Recirculation Ratio Responses for the Recirculation Ratio Sensitivity Cases

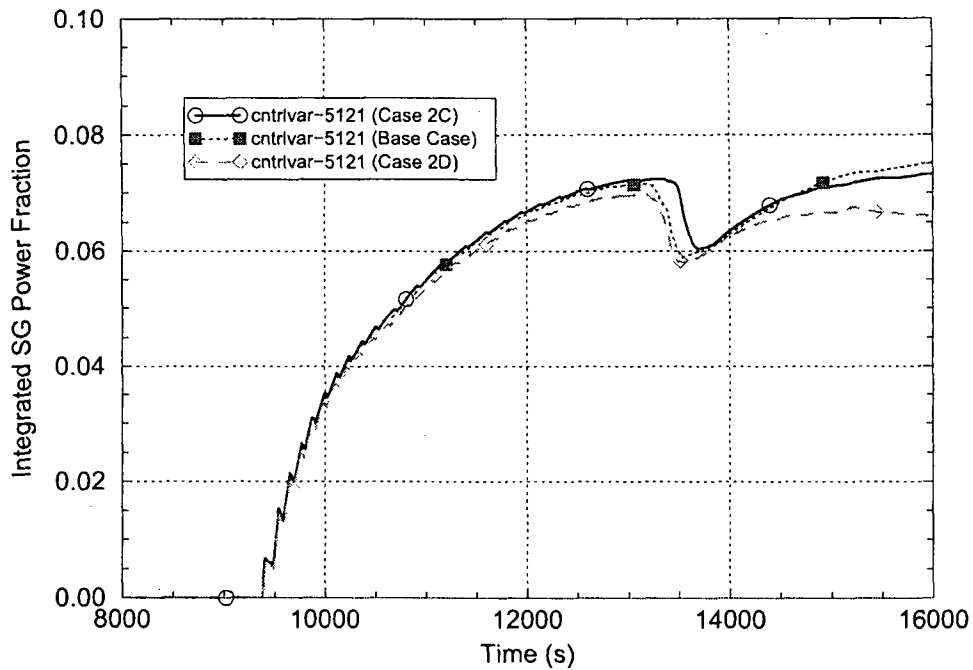


Figure D.7 Loop 1 Integrated SG Power Fractions for the Recirculation Ratio Sensitivity Cases

Unlike the average tube failure margin, the hottest tube failure margin is seen in Table D.3 to decline as the recirculation ratio increases. The reason for this difference is that the modeling which determines the inlet temperatures for the average and hottest tubes is different. For the average tube, the inlet temperature is based on the temperatures in the upper HL section and mixing plenum and on the flow rates from those two into the SG tube. However, for the hottest tube the inlet temperature is based only on the HL upper section temperature and cold tube return temperature (and a constant which defines the hottest tube inlet temperature within the range between the two). So, for an increased recirculation ratio, the average tube benefits, but the hottest tube does not, from the cooling effects of the higher cold return flow rate that passes to the mixing plenum.

The comparisons also show a small event sequence timing effect, with a lower recirculation ratio leading to an acceleration of events and a higher recirculation ratio leading to a deceleration of events. This effect results because the reduced SG heat removal associated with a lower recirculation ratio leads to more frequent and longer opening periods for the pressurizer PORVs, which tends to reduce the RCS fluid inventory more rapidly and accelerate the system heat up process.

Mixing Fraction Variations

The nominal target hot and cold mixing fractions used in the base case calculation are 0.85. Two sensitivity runs were performed, Case 2E (with the mixing fractions increased to 0.95) and Case 2F (with the mixing fractions decreased to 0.75).

The responses of the Loop 1 hot and cold mixing fractions for the base case, Case 2C and Case 2D are compared in Figures D.8 and D.9. The calculated hot and cold mixing fractions are in good agreement with the desired target values for all three runs.

Figure D.10 compares the integrated SG 1 power fractions among the three runs. With the other flow and mixing target parameters held constant, a decrease in the mixing fractions leads to increased SG heat removal. This results because less flow is directed to the SG mixing inlet plenum and more flow is directed to the hot inlet plenum and cold inlet plenum. The difference in SG heat removal is seen to have a moderate effect on the SG average tube failure margins. Stress multipliers of 1.81, 2.10 and 2.50, respectively are needed for average tube failure to occur coincident with the HL using the decreased, nominal and increased mixing fractions.

Hot/Cold Tube Split Variation

The nominal hot/cold tube split assumed in the base case calculation is 41%/59%. A sensitivity run, Case 2G, was performed with the assumed tube split ratio changed to 50%/50%.

The mass flow rates in the SG 1 hot average tube for Case 2G and the base case are virtually the same, as shown in Figure D.11. Changing the partitioning of tubes into the hot and cold sections changes the flow areas of those sections, but the conservation of mass consideration requires that the mass flows through the two sections be the same, regardless of their relative sizes. However, the cross sectional flow area of the hot average tube section is larger (50% of the total) in Case 2G than it is in the base case (where it is 41% of the total). So, although the mass flow rates are the same, the hot average tube fluid velocities are lower in Case 2G than they are in the base case, as shown in Figure D.12.

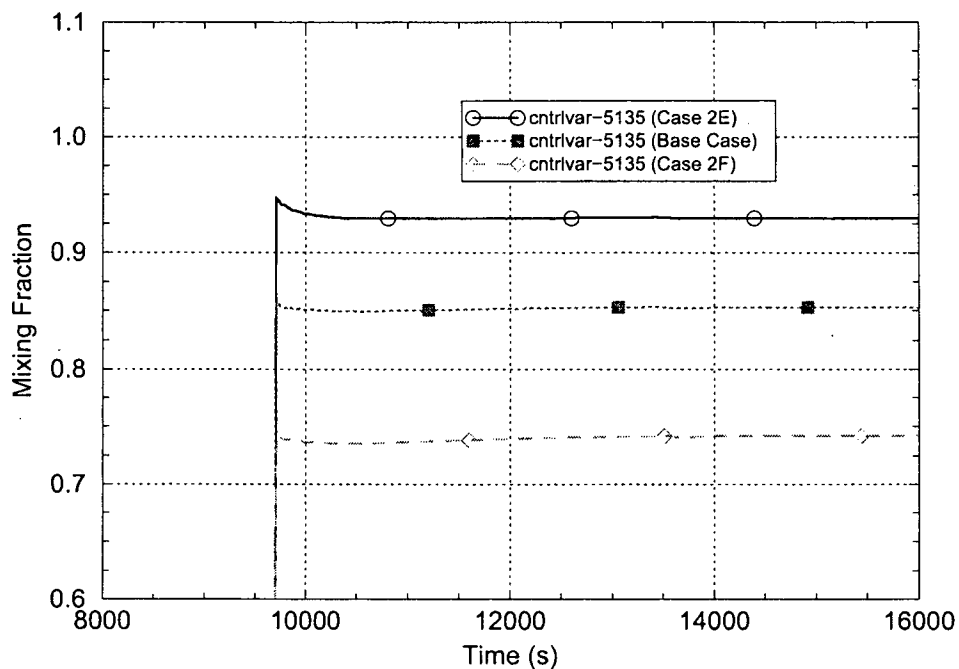


Figure D.8 Loop 1 Hot Mixing Fraction Responses for the Mixing Fraction Sensitivity Cases

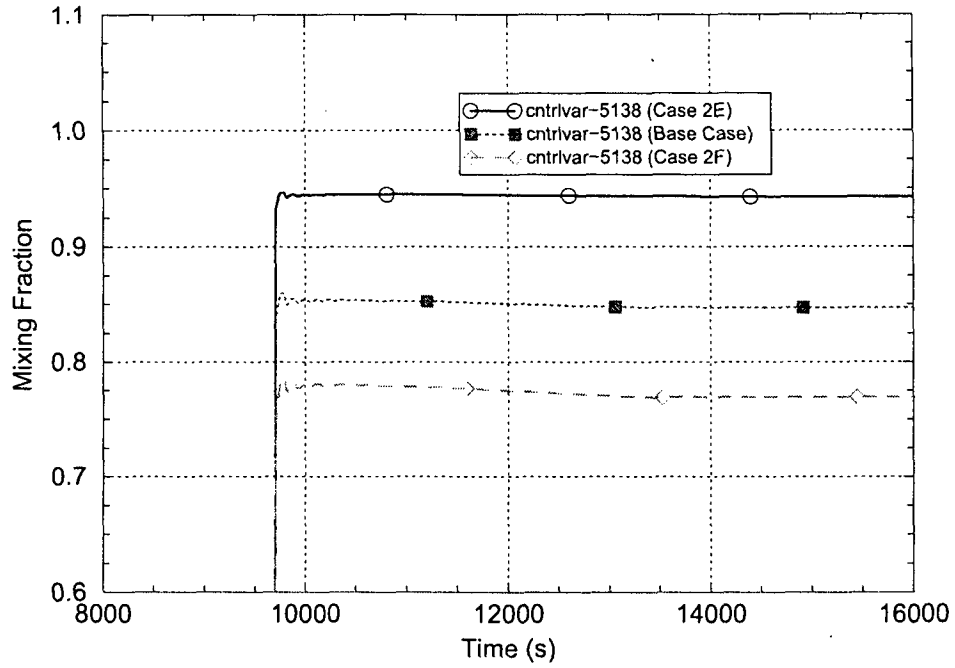


Figure D.9 Loop 1 Cold Mixing Fraction Responses for the Mixing Fraction Sensitivity Cases

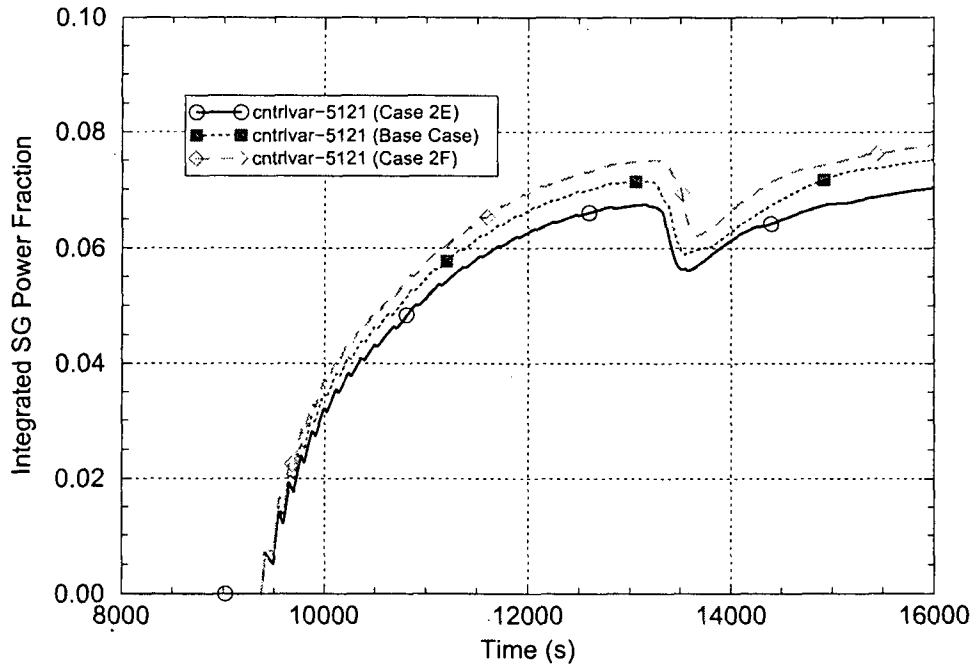


Figure D.10 Integrated SG 1 Power Fractions for the Mixing Fraction Sensitivity Cases

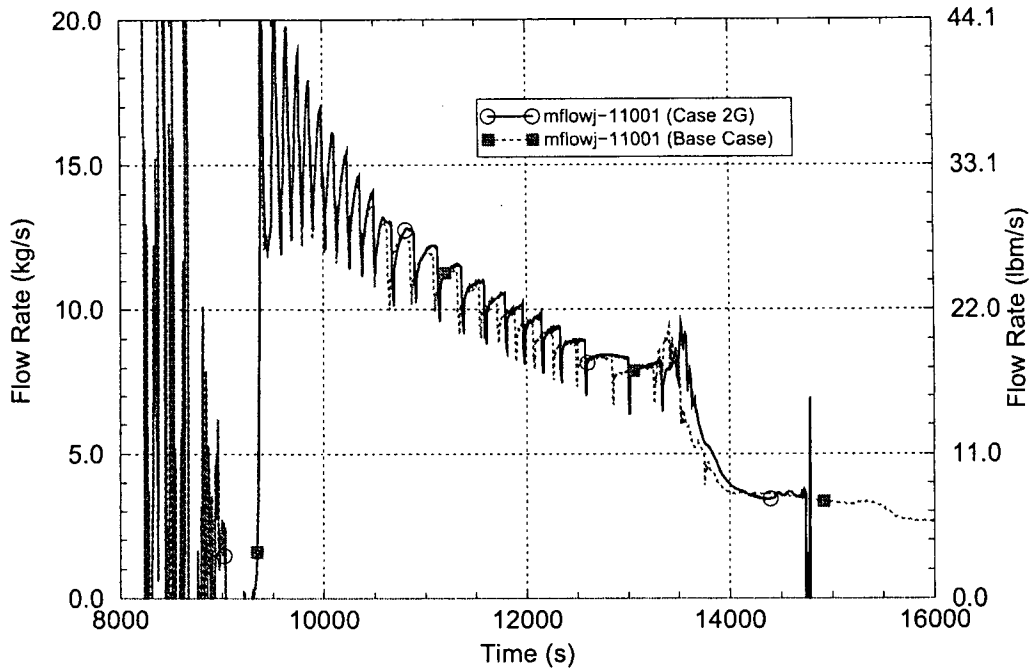


Figure D.11 Mass Flow Rates in SG 1 Hot Average Tube for the Tube Split Sensitivity Cases

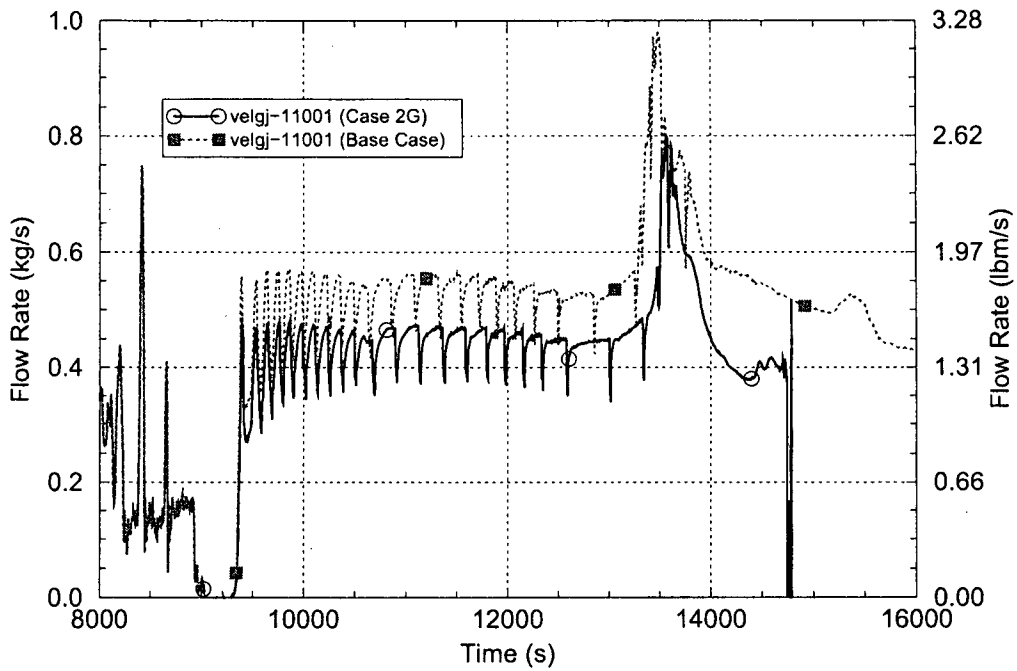


Figure D.12 Fluid Velocities in SG 1 Hot Average Tube for the Tube Split Sensitivity Cases

Lower velocities lead to lower heat transfer coefficients on the inside surfaces of the SG tubes. Figure D.13 shows that the fluid-to-wall heat transfer coefficient for the SG 1 hot average tube section (just above the tubesheet) is lower in Case 2G than in the base case. And the lower wall heat transfer coefficients are seen to result in lower SG 1 tube metal temperatures at that location in Case 2G than in the base case, as shown in Figure D.14.

These differences result in moderately higher SG tube failure margins for Case 2G than for the base case. The SG average tube requires a stress multiplier of 2.21 to fail coincident with the HL in Case 2G, whereas in the base case a stress multiplier of 2.10 is required.

SG Tube Outer-Wall Heat Transfer Coefficient Variations

The base case calculation employs the standard SCDAP/RELAP5 models for wall heat transfer on the outer surfaces of the SG tubes. Two sensitivity runs were performed, Cases 3A and 3B, with 5.0 and 0.5 multipliers respectively applied to the tube outer-surface heat transfer coefficient.

The responses of the SG 1 hot average tube outer-surface heat transfer coefficients for the base case, Case 3A and Case 3B are compared in Figure D.15. The calculated heat transfer coefficients are in good agreement with their expected relative values. Note that the heat transfer coefficient multipliers in the sensitivity case runs were implemented at the time when the core uncovers and the temperature of the steam entering the HLs becomes superheated. The runs were made in this manner because: (1) it is the behavior as the system heats up which is of interest and (2) implementing the multipliers earlier (for example, when the SGs still contain water) would have resulted in significant event sequence timing differences among the runs that would have obscured the desired comparisons.

The difference in the tube outer wall heat transfer coefficients is seen to have a moderate effect on the SG average tube failure margins. Stress multipliers of 2.07, 2.10 and 2.35, respectively are needed for average tube failure to occur coincident with the HL using the reduced, nominal and increased heat transfer coefficients.

The behavior differences among these runs are complex and include many competing effects regarding the temperatures and flow rates among the regions of the primary and secondary coolant systems. The fluid temperatures and velocities in the SG tube primary and SG secondary boiler regions are strong functions of the assumed tube outer-wall heat transfer coefficient. Figure D.16 compares the SG 1 hot average tube wall temperatures (just above the tubesheet) among the three runs for a short time period which includes the HL failure times in all runs (which occur between 13,550 s and 13,650 s). The figure shows that the base case and Case 3B exhibit a similar behavior but that the much higher heat transfer coefficient in Case 3A causes a different behavior. That, coupled with the 100-s difference in the HL failure time, leads to the SG tube failure margin differences among the cases. The competing effects associated with this sensitivity evaluation are discussed in more detail in Reference D.1.

Fuel Rod Cladding Oxidation Variations

The base case calculation employs the standard SCDAP/RELAP5 models for fuel rod cladding oxidation. Two sensitivity runs were performed, Case 4A (with an additional 20% of the calculated oxidation power added to the fluid in the core region) and Case 4B (with 50% of the calculated oxidation power removed from the fluid in the core region).

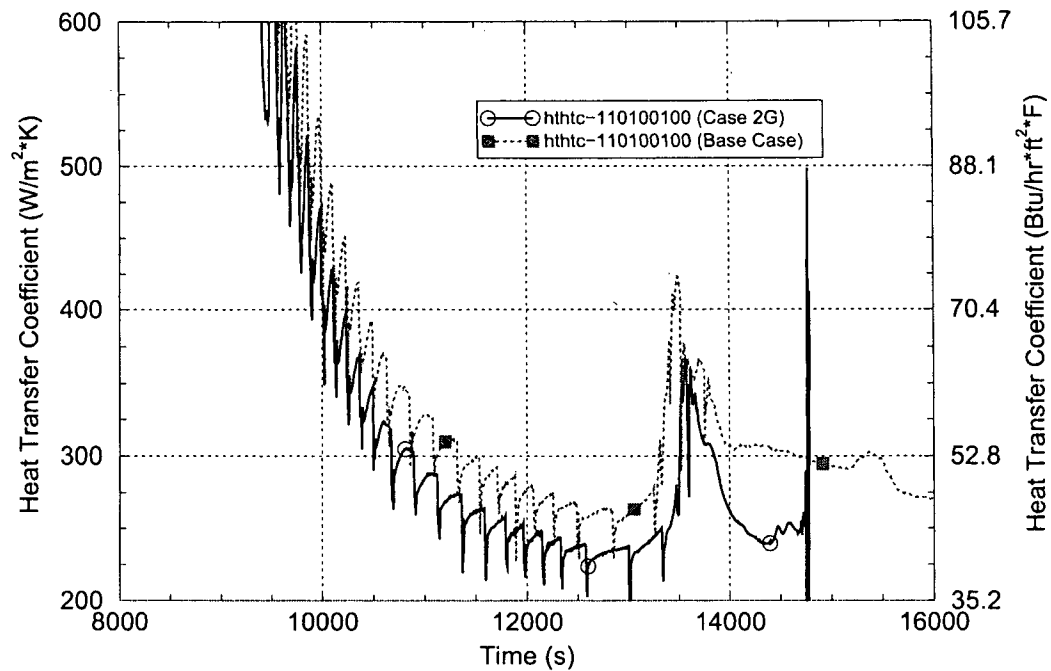


Figure D.13 SG 1 Hot Average Tube Wall Inside Surface Heat Transfer Coefficients for the Tube Split Sensitivity Cases

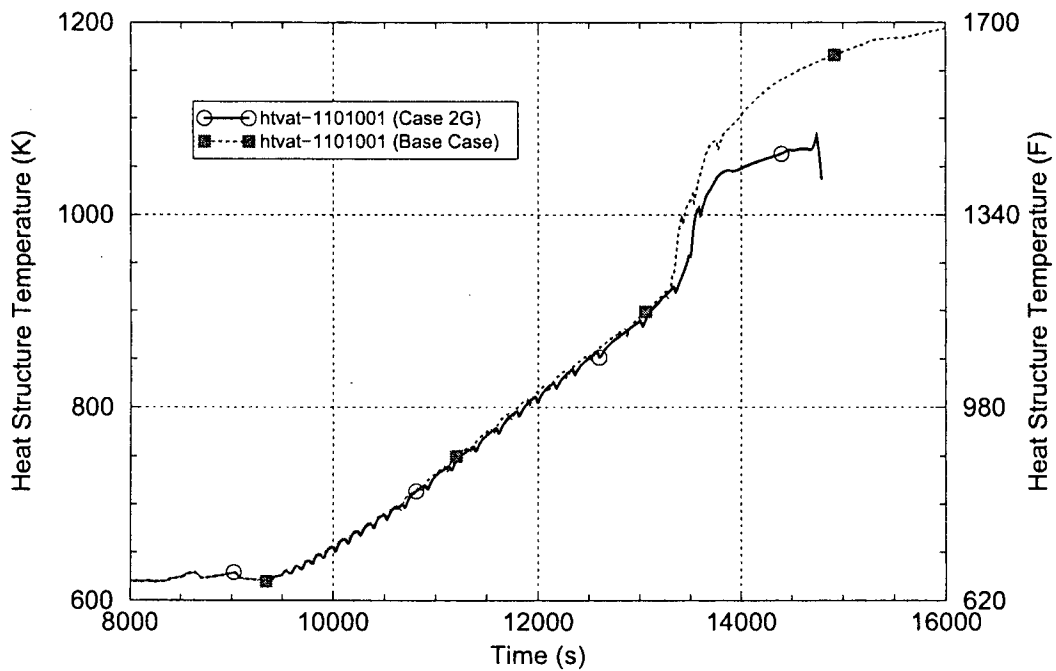


Figure D.14 Tube Wall Temperatures in SG 1 Hot Average Tube for the Tube Split Sensitivity Cases

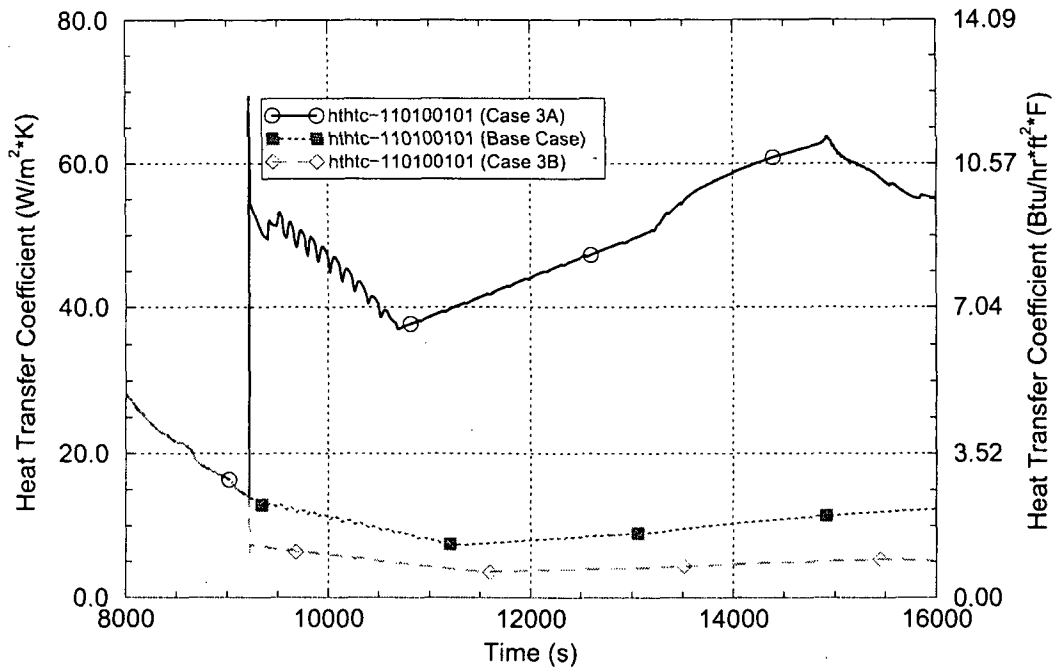


Figure D.15 SG 1 Hot Average Tube Outer Surface Heat Transfer Coefficients for the Tube Outer Wall Heat Transfer Sensitivity Cases

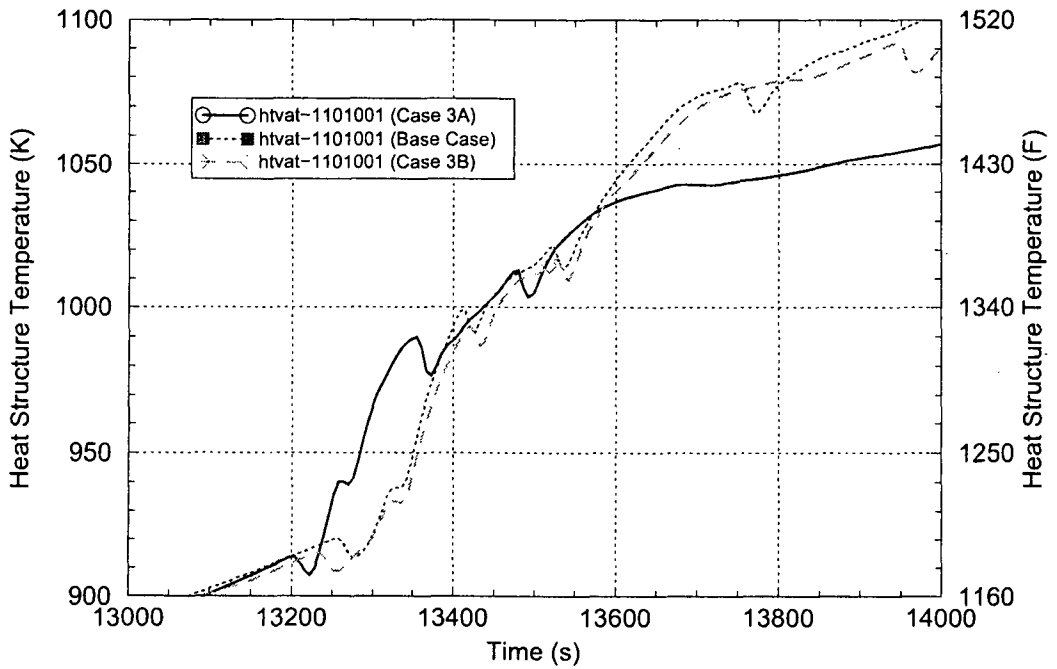


Figure D.16 SG 1 Hot Average Tube Wall Temperatures for the Tube Outer Wall Heat Transfer Sensitivity Cases

The oxidation powers from the base case, Case 4A and Case 4B are compared in Figure D.17. The responses are in good agreement with their expected relative behavior. The event sequence timing and peak oxidation power are significantly affected by the oxidation modeling revisions. In Case 4A, for which supplemental power is added, the peak oxidation power is higher and it occurs earlier than in the base case. In Case 4B, for which supplemental power is removed, the oxidation power peak is much lower and later than in the base case. These differences are as expected because of the positive feedback between oxidation rate and temperature. For example, added power causes the heat-up to become more rapid, and the feedback effect causes the oxidation rate to be higher, which leads to still-higher powers and temperatures.

The difference in the oxidation modeling is seen to have a small effect on the SG average tube failure margins. Stress multipliers of 1.91, 2.10 and 2.16, respectively are needed for average tube failure to occur coincident with the HL using the reduced, nominal and increased oxidation rates. This relationship between the oxidation power and average SG tube failure margin is created mainly because a higher oxidation rate leads to a faster system heat-up and the HLs are located in closer proximity to the reactor core (where the steam is the hottest) than are the SG tubes.

Figure D.18 compares the Hot Leg 1 upper section fluid temperatures near the RV among the three runs. The system heat-up rate for the +20% oxidation case is higher than for the base case and much higher than for the -50% oxidation case. The average tube failure margin for the +20% oxidation case is higher than for the base case because the heat-up rate is faster and the time delay required for the increasingly-hotter steam to migrate out into the SG tubes becomes a more important factor. Conversely, the average tube failure margin for the -50% oxidation case is lower than for the base case because the heat up rate is slower and the migration time delay is no longer as important. In other words, for faster heat-ups the proximity to the core becomes more important, causing the HLs to reach failure temperature preferentially sooner than the SG tubes and for slower heat-ups the proximity to the core becomes less important, causing the SG tubes to reach failure temperature preferentially sooner than the HLs. Unlike the average tube failure margin, the hottest tube failure margin is seen in Table D.3 to decline as the oxidation rate increases. The reason for this difference is the same as described above under "Recirculation Ratio Variations."

Reactor Vessel Internal Circulation Rate Variations

The SCDAP/RELAP5 base case flow circulations within the RV are based on the configuration of the RV fluid regions and internal structures, the fluid conditions and the flow loss coefficients specified in the input model. Two sensitivity runs were performed, Case 5A (with flow loss coefficients increased so as to reduce the vessel internal circulation flow rates by 50%) and Case 5B (with flow loss coefficients decreased so as to increase the vessel internal circulation flow rates by 100%).

The flow rates at the top of the central core channel for the base case, Case 5A and Case 5B are compared in Figure D.19. The relative flow rates among the three calculations are as expected (flow comparisons at other locations within the RV show similar relative behavior).

The changes in the RV internal flow loss modeling are seen to have a small effect on the average tube failure margins. Stress multipliers of 2.28, 2.10 and 1.97, respectively are needed for average tube failure to occur coincident with the HL for the cases representing the reduced, nominal and increased vessel circulation flow rates.

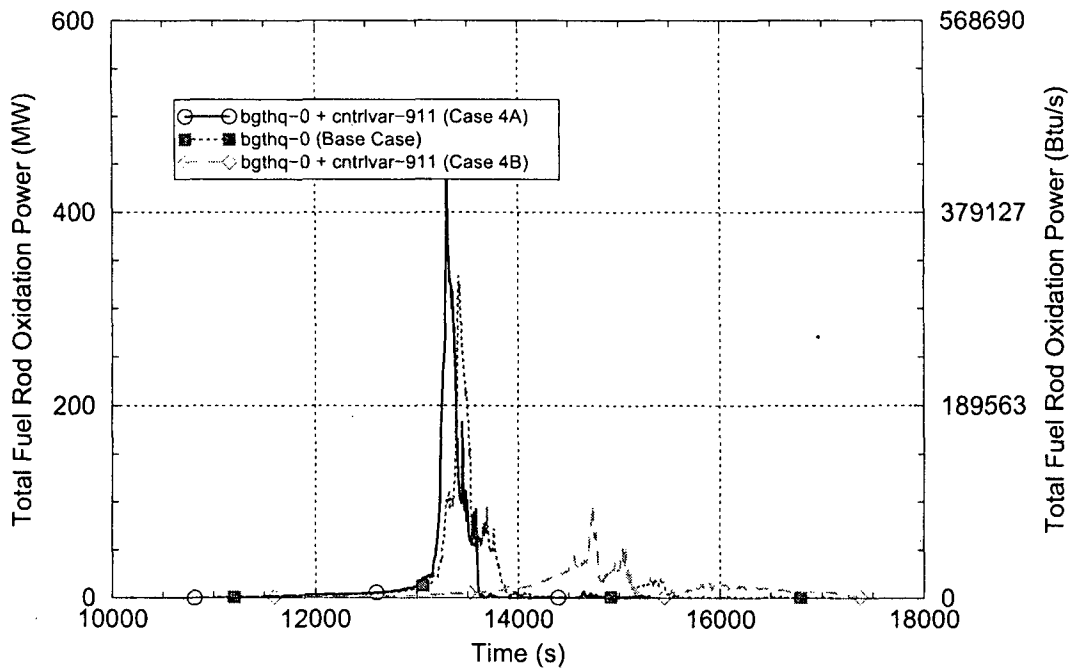


Figure D.17 Fuel Rod Cladding Oxidation Powers for the Oxidation Sensitivity Cases

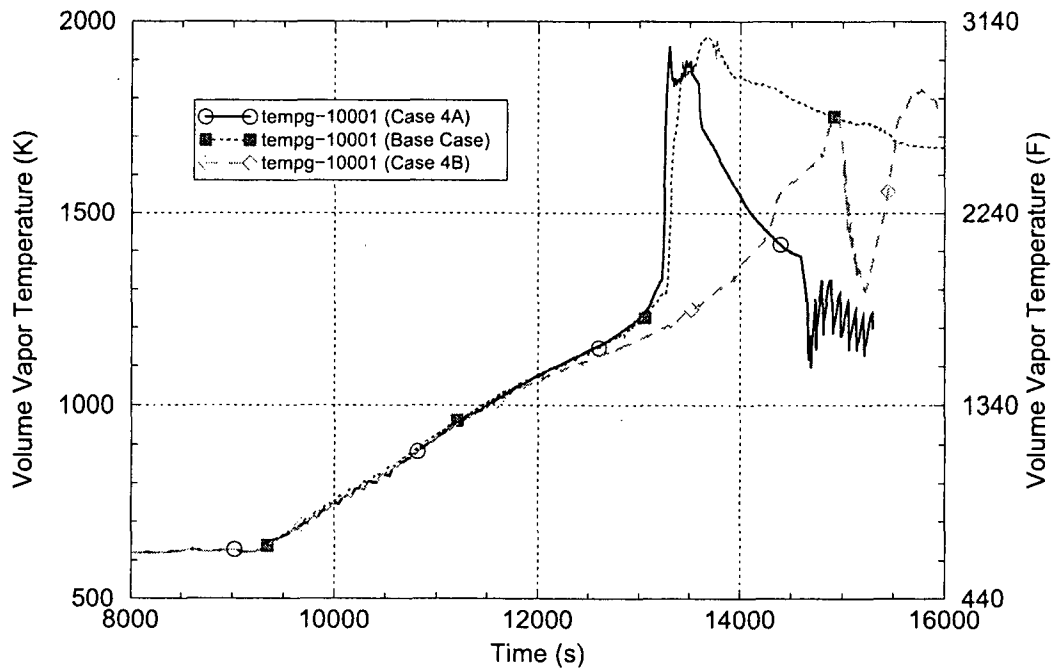


Figure D.18 Hot Leg 1 Upper Section Fluid Temperatures for the Oxidation Sensitivity Cases

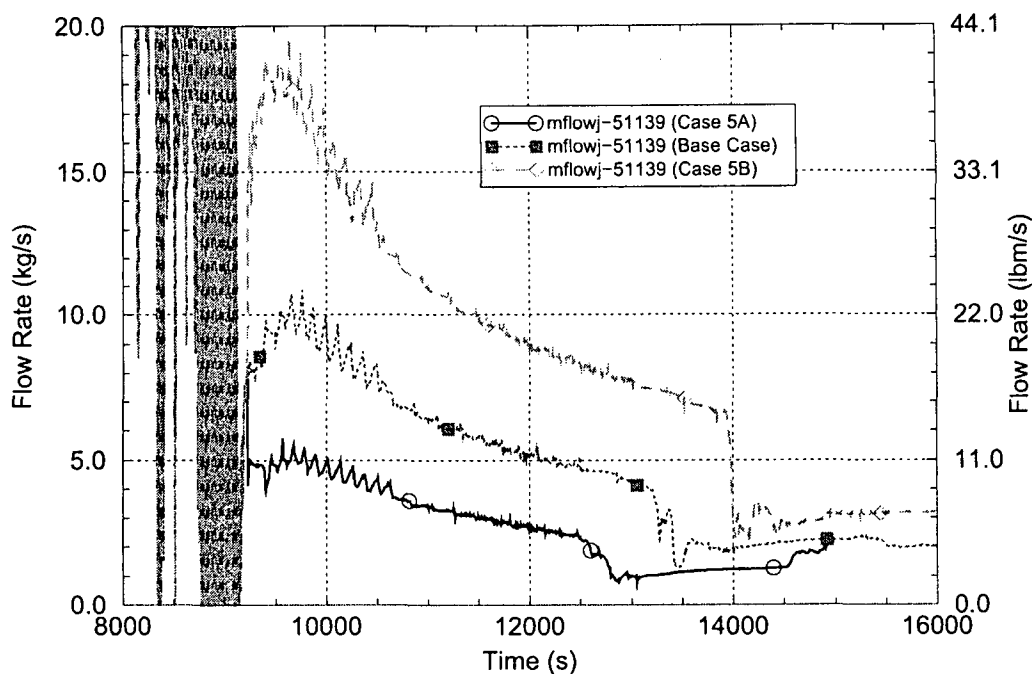


Figure D.19 Flow Rates at Top of Central Core Region for the Vessel Circulation Sensitivity Cases

These margin differences were found to result primarily because the vessel internal circulation rate affects the fuel rod oxidation process. Figure D.20 compares the total fuel rod oxidation power responses for the three cases. The reduced vessel circulation case resulted in a lower and earlier peak oxidation power than the base case. The increased vessel circulation case resulted in a higher and later peak oxidation power than the base case. This difference in oxidation behavior results because, although the vessel internal circulation rates differ widely among the runs, the HL flow rates in all three runs are for the most part the same. Therefore, in the reduced vessel circulation case the cooling afforded by the flow leaving and returning to the vessel becomes a more significant factor, leading to lower core temperatures and lower fuel rod oxidation rates.

The cases with higher vessel internal flow rates and oxidation powers lead to lower average tube failure margins, which is the reverse of the results discussed for the oxidation modeling sensitivity above. This difference appears to result because the peak temperatures achieved were similar in all three of the oxidation power sensitivity runs (see Figure D.18) but the peak temperatures achieved in the three vessel-circulation sensitivity runs are quite different, as shown in Figure D.21. These fluid temperature differences are important because they affect the peak HL wall temperatures (shown in Figure D.22) which directly affect the prediction of the HL failure. A spread of 395 K (711°F) is seen among the peak HL wall temperatures achieved for the three cases.

Unlike the average tube failure margin, the hottest tube failure margin is seen (in Table D.3) to increase as the vessel internal circulation rate increases. The reason for this difference is the same as described above under "Recirculation Ratio Variations."

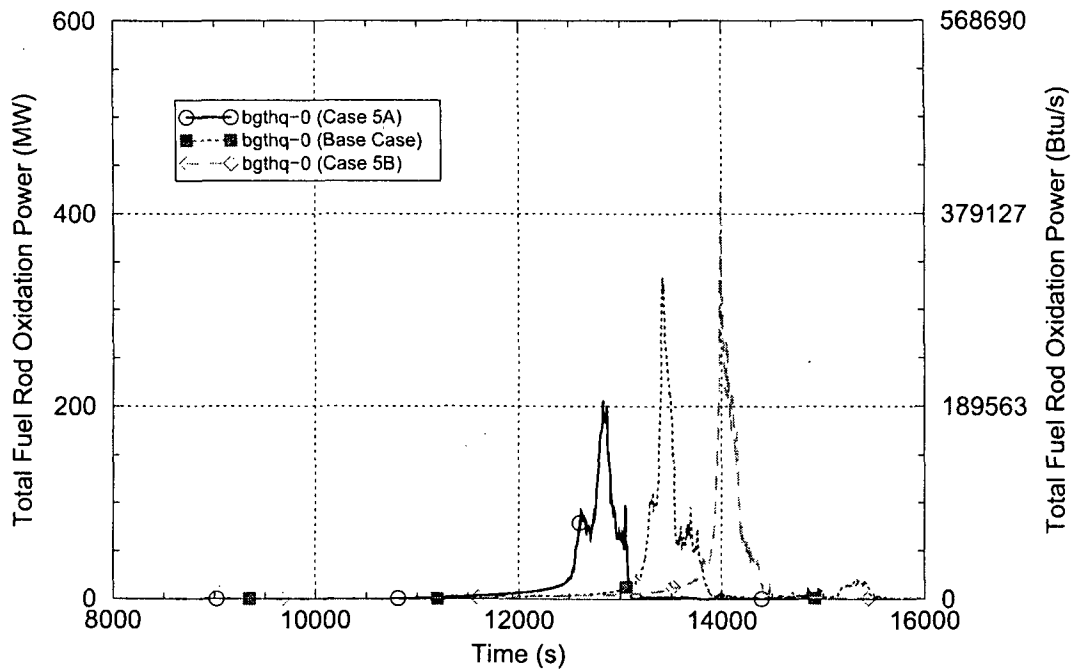


Figure D.20 Total Fuel Rod Cladding Oxidation Power for the Vessel Circulation Sensitivity Cases

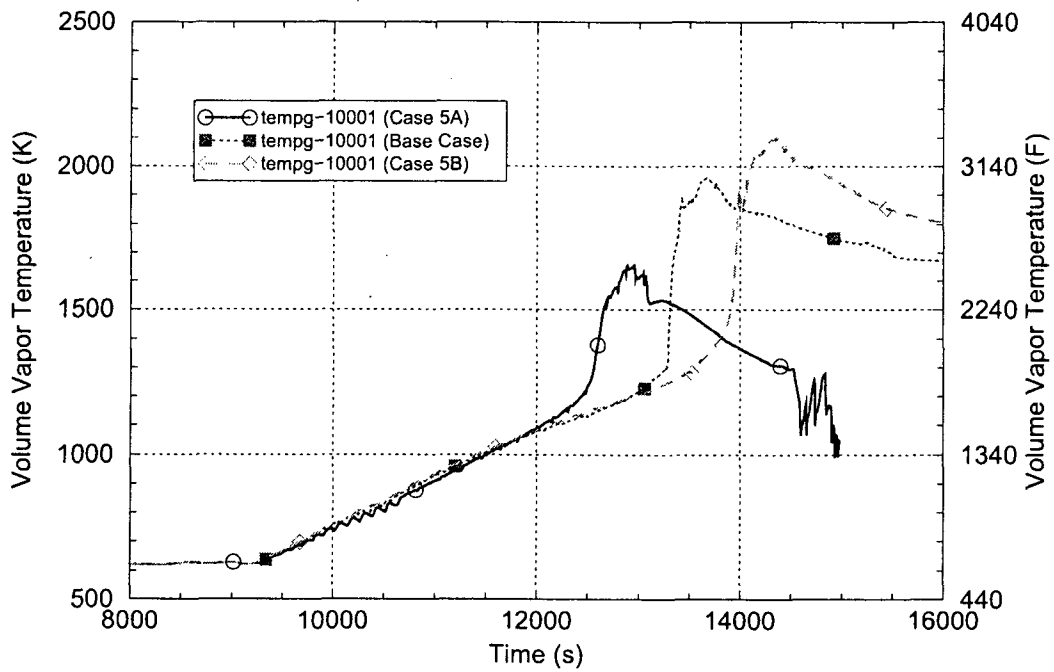


Figure D.21 Hot Leg 1 Upper Section Fluid Temperatures for the Vessel Circulation Sensitivity Cases

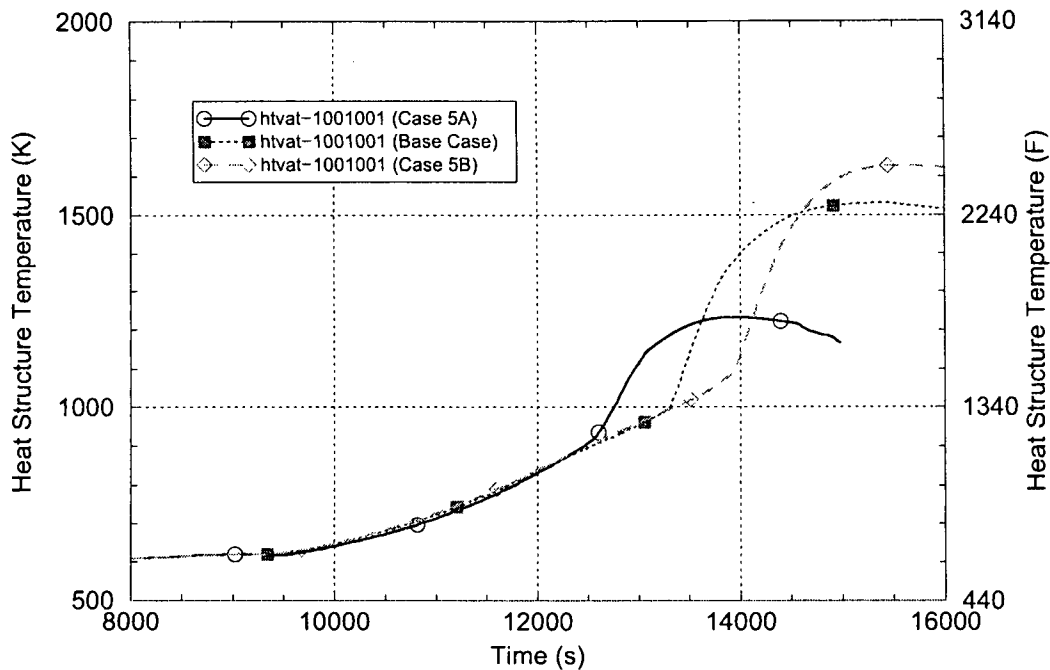


Figure D.22 Hot Leg 1 Upper Section Average Wall Temperatures for the Vessel Circulation Sensitivity Cases

Reactor Coolant System Heat Loss Variations

The base case calculation assumes a 4 MW total heat loss from the outer surfaces of the RCS to the containment. Two sensitivity runs were performed, Case 6A (with the heat loss reduced to 2 MW) and Case 6B (with the heat loss increased to 8 MW).

The heat fluxes from the outer surface of the cylindrical RV wall (at an elevation near the center of the core) for the base case, Case 6A and Case 6B are compared in Figure D.23. The relative heat fluxes among the three calculations are as expected (heat flux comparisons at other RCS locations show similar relative behavior).

The different heat loss modeling is seen to have a small effect on the SG average tube failure margins. Stress multipliers of 2.12, 2.10 and 1.92, respectively are needed for average tube failure to occur coincident with the HL for the cases representing the reduced, nominal and increased RCS heat losses.

These SG tube failure margin differences were found to result primarily from sequence of events timing differences induced by the heat loss assumptions. Lower heat losses tend to accelerate the timing of events while higher heat losses tend to decelerate it. This effect is illustrated in Figure D.24, which shows the pressurizer level comparison among the three cases. The timing differences were found to result from competing effects that differentially affect the heat-up of the HL and surge line relative to the heat-up of the SG tubes (as discussed in Reference D.1)

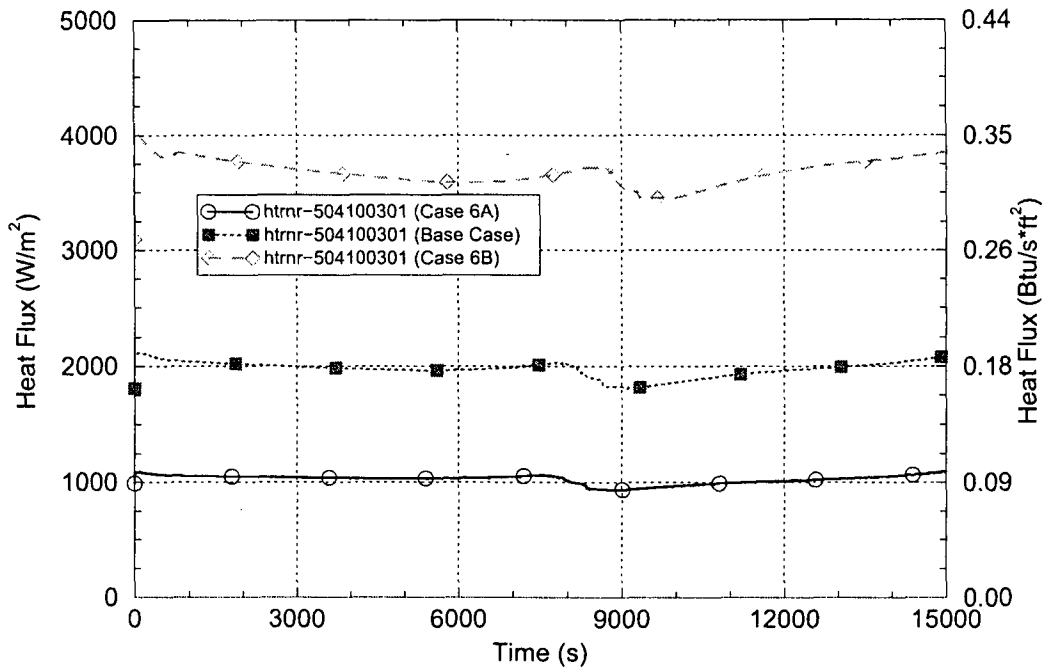


Figure D.23 Heat Fluxes from Outer Surface of Reactor Vessel to Containment for the RCS Heat Loss Sensitivity Cases

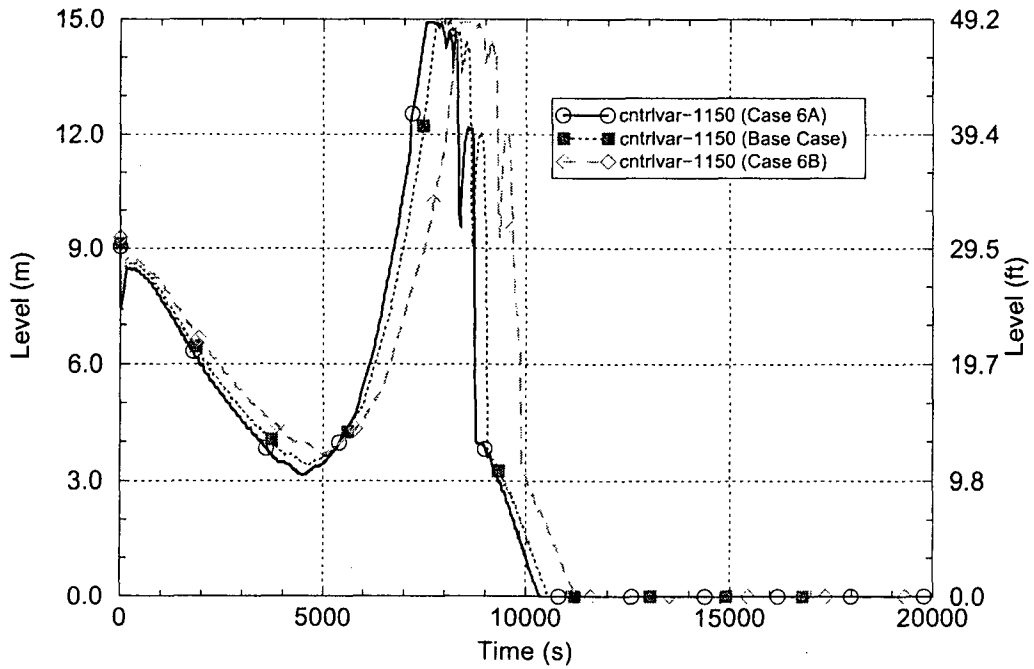


Figure D.24 Pressurizer Level Responses for the RCS Heat Loss Sensitivity Cases

Reactor Coolant Pump Shaft Seal Leakage Variations

The base case calculation simulates shaft seal leakage in all four RCPs based on an initial 1.32 L/s [21 gpm] per pump leak rate at the start of the SBO accident event sequence. Eight sensitivity runs listed in Table D.2 were performed assuming that changes in the leak rate occur two hours following the start of the SBO sequence.

Of these sensitivity runs, only output data from Case 7A (3.83 L/s [61 gpm]) and Case 7G (0.063 L/s [1 gpm]) are used for the purposes of evaluating uncertainties. The uncertainty study considers ± 1.26 -L/s [± 20 -gpm] variations around the 1.32-L/s [21-gpm] nominal leak rate after two hours. The output data from Cases 7A and 7G is used to estimate the effects of those variations, see discussion for PIRT Parameter C2 in Section D.1.2.

The discussion of results for the pump seal leakage sensitivity runs is grouped into symmetric cases (where the same leakage assumption is used in all four pumps) and unsymmetrical cases (where an increased leakage is assumed to occur in only one pump):

Symmetric Cases (Same Leakage in All Four Pumps)

The symmetric cases investigate changes in the leakage rates to 0.063 L/s [1 gpm], 3.83 L/s [61 gpm], 5.66 L/s [90 gpm], 7.54 L/s [120 gpm], 11.4 L/s [182 gpm] and 18.9 L/s [300 gpm] per pump. These are Cases 7G, 7A, 7E, 7D, 7C and 7B, respectively.

Figure D.25 compares the Pump 1 leak rates from these six sensitivity cases with that in the base case. The figure shows that the calculated relative leakage rates among the seven cases are as expected.

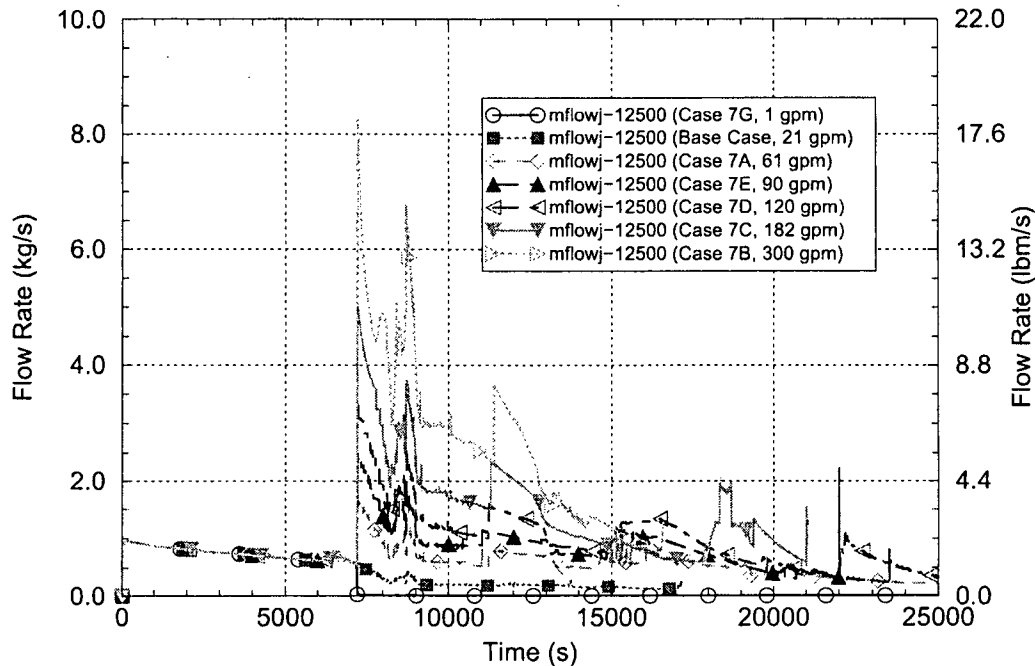


Figure D.25 Pump 1 Leakage Rates for the Symmetric Pump Shaft Seal Leak Sensitivity Cases

Figure D.26 compares the RCS pressure responses among the seven cases. Prior to 10,637 s, when the pressurizer drains, the pressure responses in all runs are virtually the same. While pump leakage provides some added capabilities for reducing RCS pressurization, prior to this time the pressurization load is high and the pump leakage only results in less frequent opening of the pressurizer relief valves. However after the pressurizer drains the RCS steam production rate declines, the pressurization load is reduced and the added pump leakage can succeed in reducing the RCS pressures. The larger the assumed pump shaft seal leakage rate, the greater the RCS pressure relief it provides and the lower the RCS pressures it leads to.

Figure D.27 compares the Hot Leg 1 upper section fluid temperatures among the seven cases. Looking at the period when the heat-up rates are the highest (from about 12,500 s to 13,200 s), the figure shows that the heat-up rate is generally proportional to the assumed pump shaft seal leakage rate. The exception is for the largest assumed leakage rate, 18.9 L/s [300 gpm] in Case 7B, which shows a reduced heat-up rate relative to the next-largest leakage run, Case 7C.

The pump shaft seal leakage modeling is seen to have a large effect on the SG average tube failure margins. For the seven cases (0.063 L/s [1 gpm], 1.32 L/s [21 gpm], 3.83 L/s [61 gpm], 5.66 L/s [90 gpm], 7.54 L/s [120 gpm], 11.4 L/s [182 gpm] and 18.9 L/s [300 gpm]), stress multipliers of 2.08, 2.10, 2.33, 2.50, 3.30, 4.58 and 7.01 respectively are needed for average tube failure to occur coincident with the HL failure. As indicated above, lower RCS pressures and faster RCS heat-ups are seen as the assumed leakage rate increases. Both of these effects promote increased SG tube failure margins. Lower RCS pressures reduce the differential pressure across the SG tubes, reducing the potential for their failure. Higher RCS heat up rates preferentially favor earlier HL failure relative to SG tube failure (see the discussion under "Fuel Rod Cladding Oxidation Variations" above). For 18.9 L/s [300-gpm] Case 7B, the heat-up rate is slower than for 11.48 L/s [182-gpm] Case 7C, but the RCS depressurization effects are much larger, which leads to the very large calculated SG tube failure margin for Run 7B.

Unsymmetrical Cases (Increased Leakage in Only One Pump)

The unsymmetrical cases investigate increased leakage rates of 18.9 L/s [300 gpm] in only one of the four reactor coolant pumps. In Case 7F, the increased leakage is assumed to be in Pump 1 and in Case 7F2 the increased leakage is assumed to be in Pump 2.

Figure D.28 compares the leak rates from these two cases for the pumps which experience the increased leakage. For comparison purposes, the leak rates for these two unsymmetrical cases are compared with the leak rate for the 5.66-L/s [90-gpm] symmetric leakage Case 7E (with a total leak rate of 22.6 L/s [360 gpm]). The figure shows that the relative leakage rates among these three cases are as expected.

Figure D.29 compares the RCS pressure responses among the three cases. As expected, because the total leak rates are about the same for all three cases, the pressure responses are similar. SCDAP/RELAP5 did not predict loop seal clearing in any coolant loop in any of the calculations described in this report.

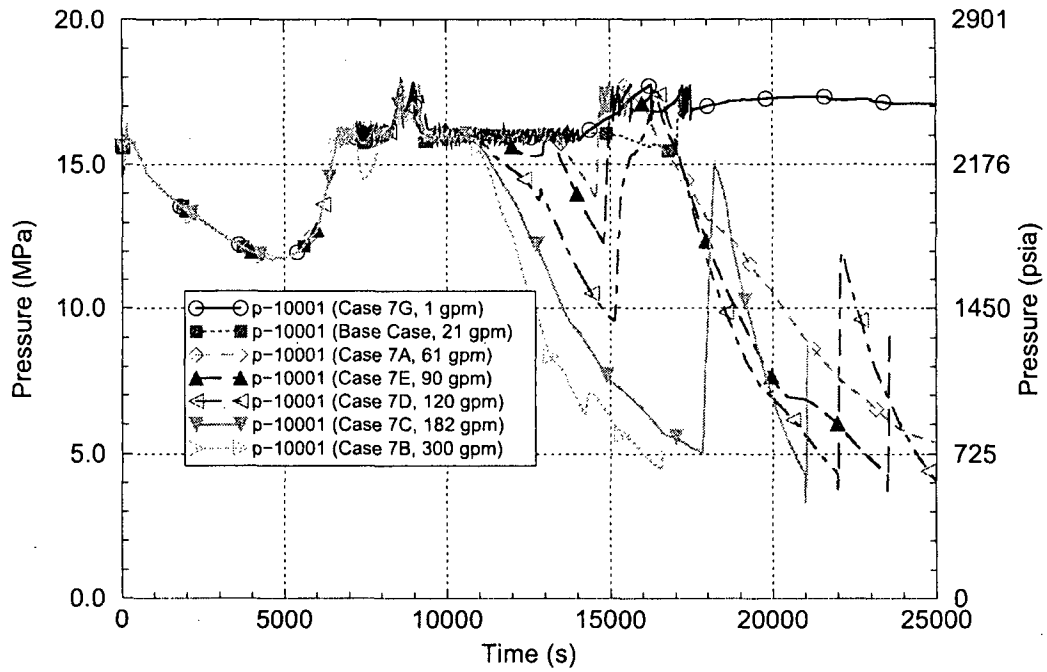


Figure D.26 RCS Pressures for the Symmetric Pump Shaft Seal Leak Sensitivity Cases

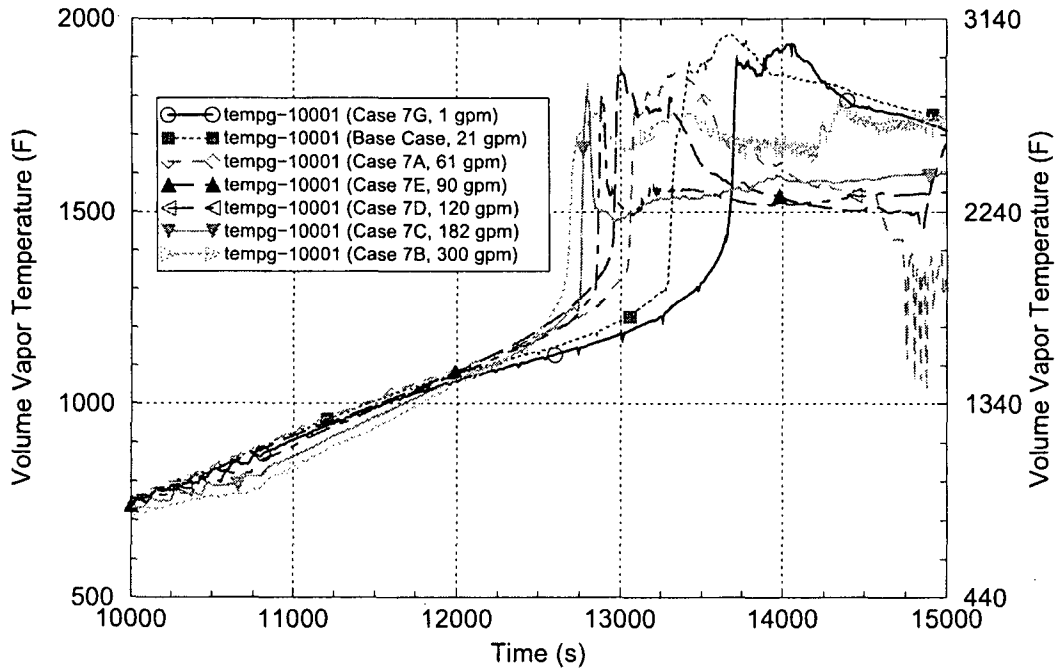


Figure D.27 Hot Leg 1 Fluid Temperatures for the Symmetric Pump Shaft Seal Leak Sensitivity Cases

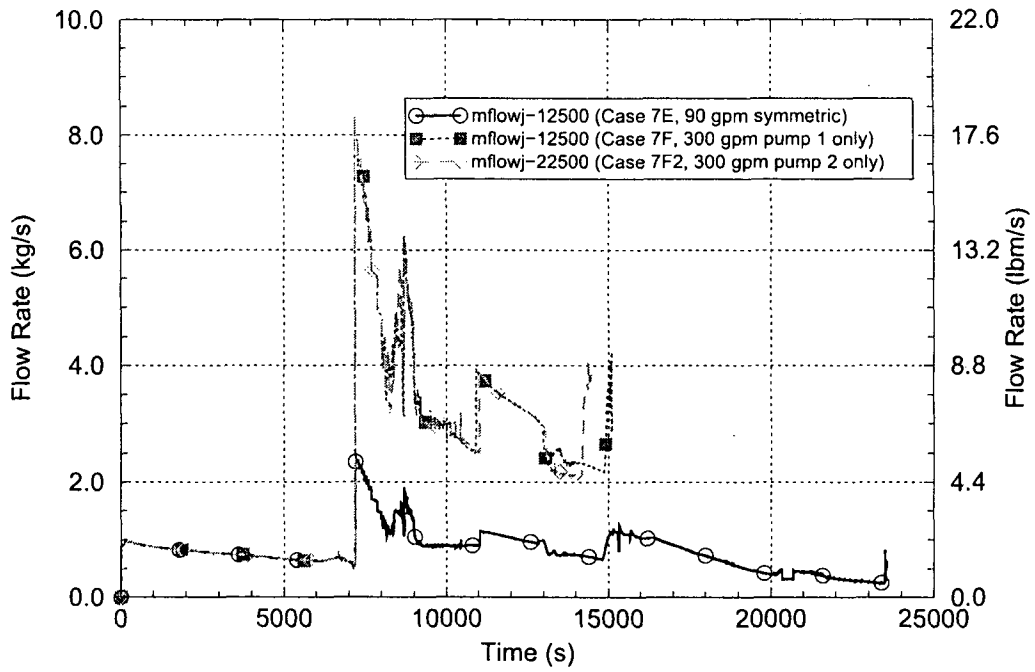


Figure D.28 Single-Pump Leakage Rates for the Unsymmetrical Pump Shaft Seal Leak Sensitivity Cases

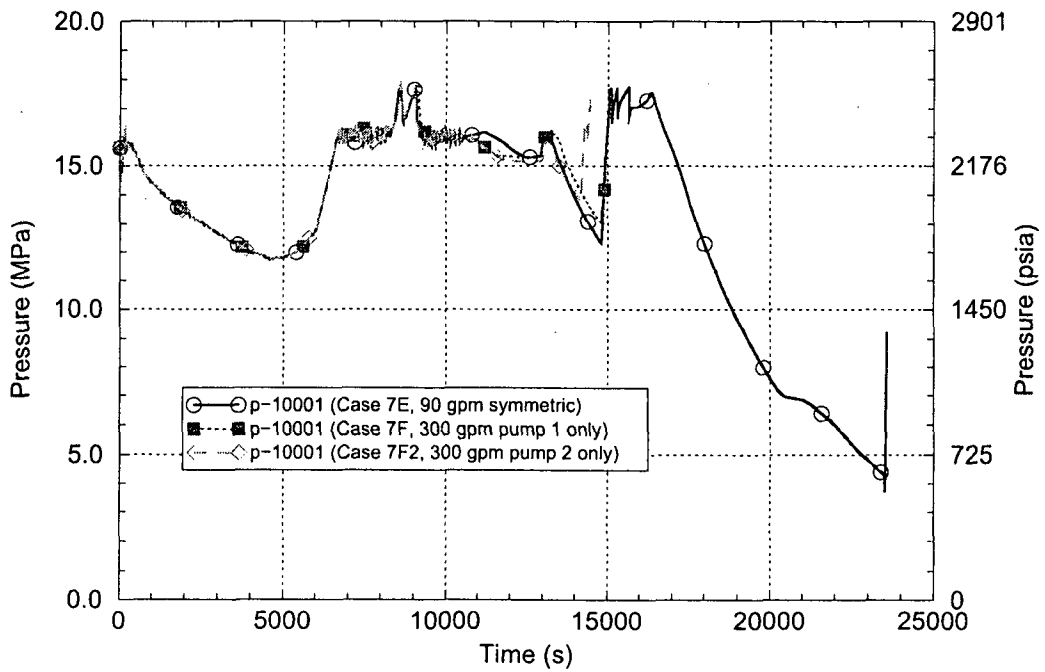


Figure D.29 RCS Pressures for the Unsymmetrical Pump Shaft Seal Leak Sensitivity Cases

Figure D.30 compares the Hot Leg 1 upper section fluid temperatures among the three cases. Looking at the period when the heat-up rates are the highest (from about 12,600 s to 13,000 s), the figure shows that the heat-up rates among the three runs are similar.

The pump shaft seal leakage assumptions for the unsymmetrical cases are seen to have only a small effect on the SG average tube failure margins. For the four cases (the 1.32-L/s [21-gpm] in four pumps base case, the 5.66-L/s [90-gpm] in four pumps Case 7E, the 18.9-L/s [300-gpm] in Pump 1 Case 7F and the 18.9-L/s [300-gpm] in Pump 2 Case 7F2) stress multipliers of 2.10, 2.50, 2.00 and 2.15 respectively are needed for average tube failure to occur coincident with the HL. Therefore the average tube failure margins for these four cases are quite similar. Note that in Case 7F (with the increased leakage in Pump 1) Hot Leg 2 is the first to fail and the same minimum average tube failure margin is calculated in SGs 2, 3 and 4. And, in Case 7F2 (with the increased leakage in Pump 2) note that Hot Leg 1 is the first to fail and that the minimum average tube failure margin is calculated in SG 3.

The average tube failure margins calculated for the unsymmetrical pump seal leakage cases (7F and 7F2) are moderately lower than that calculated for the symmetrical pump seal leakage case with roughly the same total leakage rate (7E). The average tube failure margins for the two unsymmetrical cases show only a small effect of moving the leakage from the pressurizer loop to a non-pressurizer loop. However, as shown in Table D.3, large differences in the hottest tube failure margins are observed among these three cases.

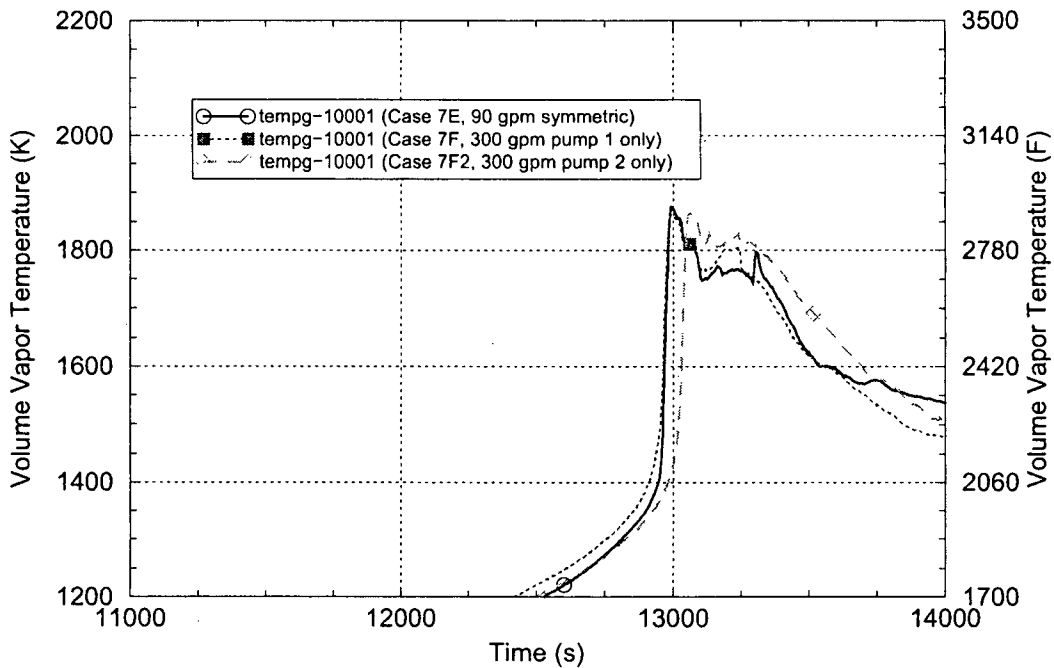


Figure D.30 Hot Leg 1 Fluid Temperatures for the Unsymmetrical Pump Shaft Seal Leak Sensitivity Cases

D.2.2 Additional Sensitivity Runs

Additional sensitivity runs identified with asterisks in Table D.2 are used to investigate various modeling, plant configuration and event-sequence assumption issues which are unrelated to the uncertainty evaluation. The results for these additional sensitivity runs are summarized as follows:

Effect of Configuration of the Hot Leg-to-Surge Line Connection

The base case calculation models the surge line connection on the side of Hot Leg 1, which is consistent the configuration of some Westinghouse plants. A sensitivity run, Case 8A, was performed with the surge line connection moved from the side to the top of Hot Leg 1. This run was made to evaluate the behavior for a top-mounted surge line, which is the connection configuration in other Westinghouse plants.

Figure D.31 compares the pressurizer surge line fluid temperatures (near the HL connection) from Case 8A (with the top-mounted surge line) and the base case (with the side mounted surge line). The figure shows that, as expected, the surge line temperatures are higher when the surge line is connected on the top of the HL.

In the base case the HL failed first, at 13,630 s, followed by the surge line at 13,960 s. However, in Case 8A, the surge line failed first, at 13,660 s, followed by the HL at 13,720 s. Although the time of the first primary piping component failure is about the same in the two runs, the additional extra energy removed from the RCS through the pressurizer relief valves due to the hotter surge line flow in Case 8A reduced the heat-up rate in the rest of the system, including the SGs. The average SG tube failure margin increased slightly from a stress multiplier of 2.10 in the base case run to 2.33 in Case 8A. The consideration of the surge line connection location on the circumference of the HL therefore has a moderate effect on the SG tube failure margin.

Effect of Stuck-Open Steam Generator Relief Valve

The base case calculation models nominal steam leakage from the secondary systems of all four SGs but no stuck-open relief valve on any SG. A sensitivity run, Case 8B, was performed assuming the secondary system PORV on SG 1 sticks open (at the time of its first opening) and no steam leakage in the other three SGs. Case 8B was run for historical comparison purposes, using assumptions consistent with those in the earlier analyses described in Sections 2.3 and 2.4.

The SG secondary pressure responses for Case 8B and the base case are compared in Figure D.32 for SG 1 and in Figure D.33 for SG 2. The SG 1 pressures experienced at the time when the HL failure occurs (14,060 s in Case 8B and 13,630 s in the base case) are not significantly different between the two runs.

Figure D.34 compares the Hot Leg 1 upper section fluid temperatures (near the RV) for Case 8B and the base case. The different SG secondary pressure responses lead to an event timing difference between the two runs, however the figure shows that the heat-up rates at the times when the HL fails are very similar.

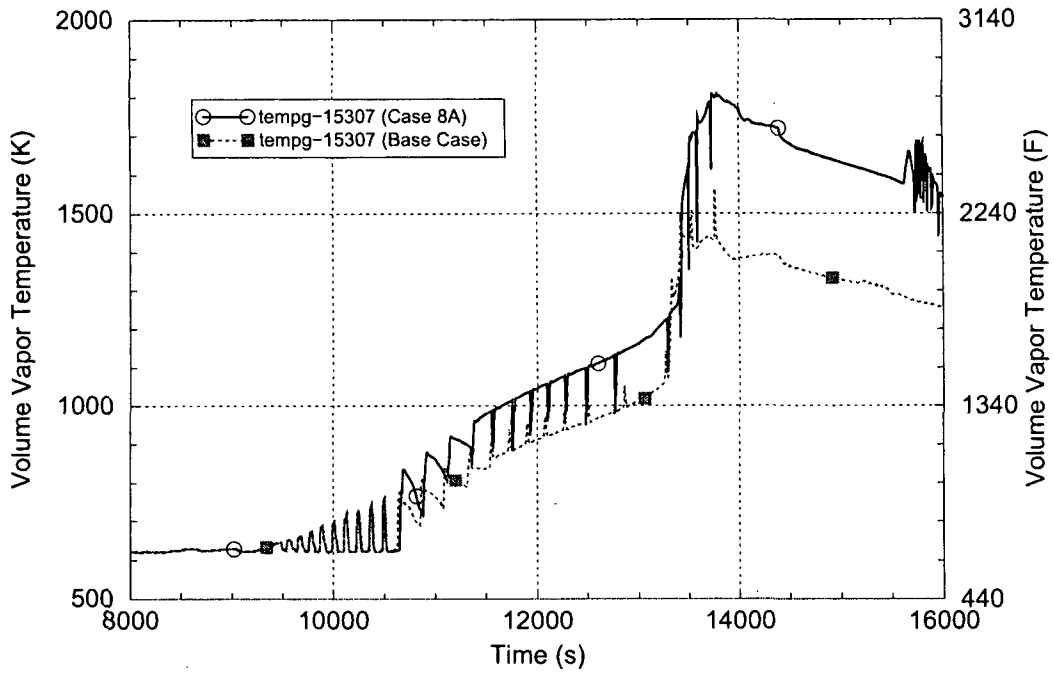


Figure D.31 Pressurizer Surge Line Fluid Temperature for the Top Mounted Surge Line Sensitivity Case

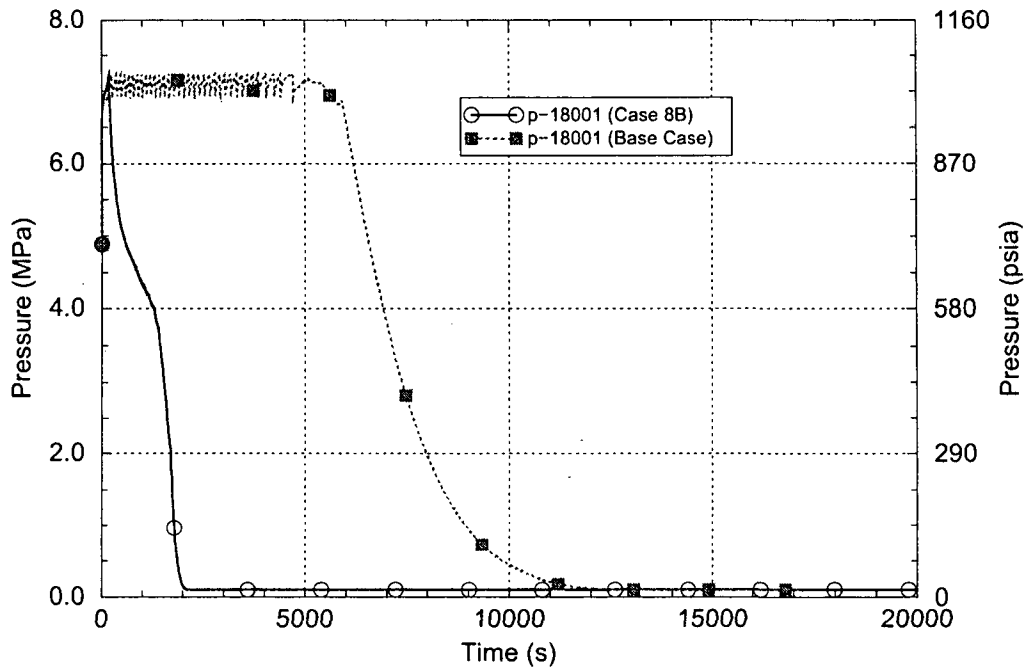


Figure D.32 SG 1 Pressure for the Stuck-Open SG Safety Relief Valve Sensitivity Case

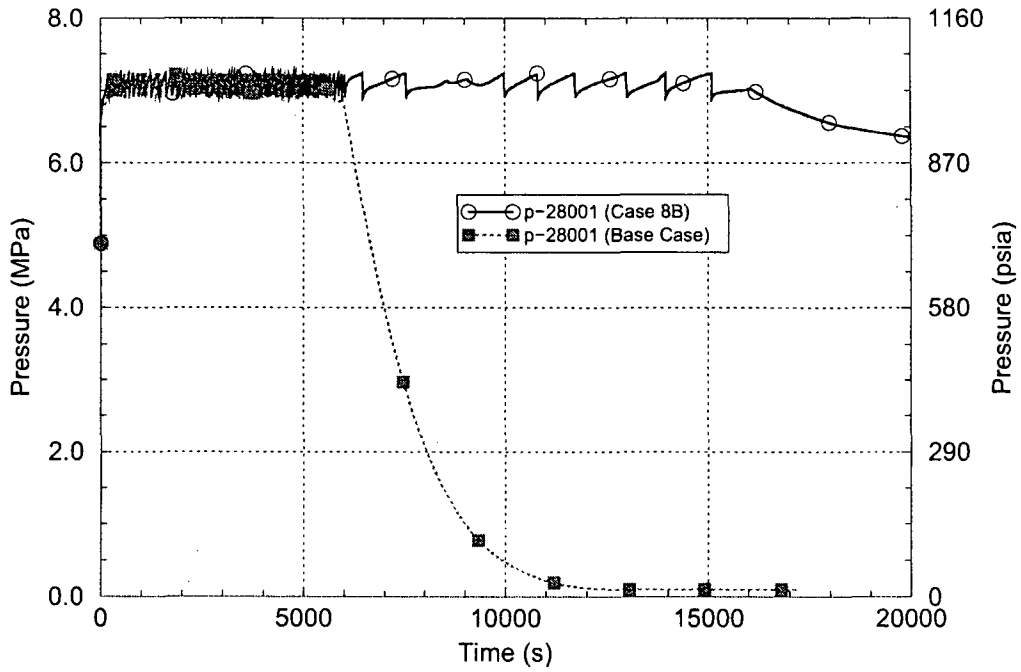


Figure D.33 SG 2 Pressure for the Stuck-Open SG Safety Relief Valve Sensitivity Case

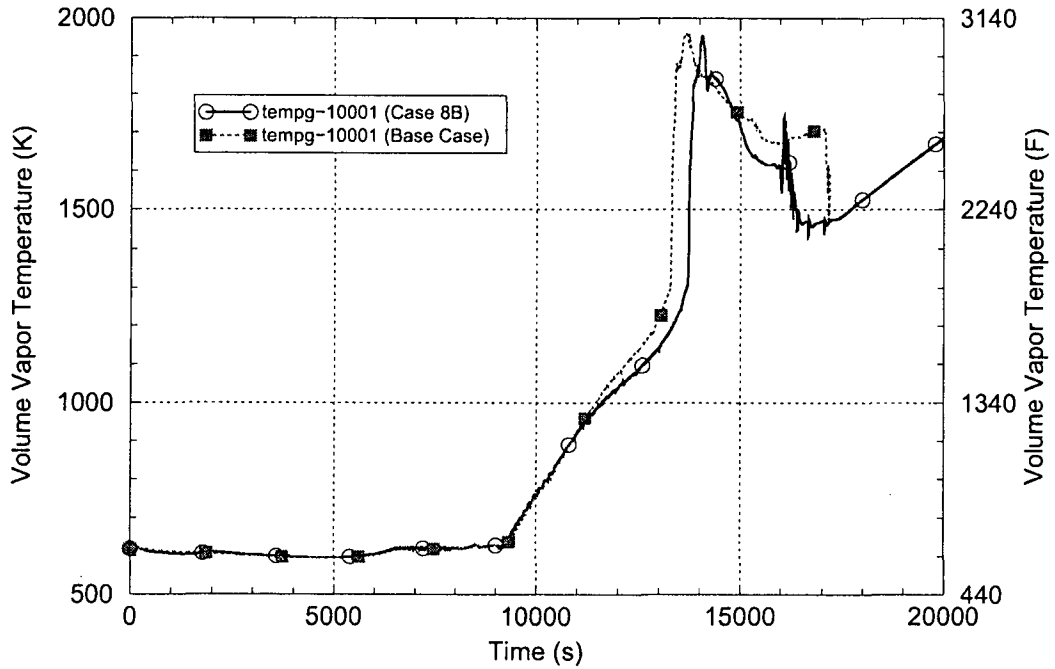


Figure D.34 Hot Leg 1 Fluid Temperature for the Stuck-Open SG Safety Relief Valve Sensitivity Case

Since the temperature and pressure responses of the two runs are similar, little difference is noted in the average SG 1 tube failure margins. The failure margin decreased only slightly from a stress multiplier of 2.10 in the base case to 2.05 in Case 8A. This result occurs because the SG 1 steam leakage rate seen in the base case is sufficient to fully depressurize all of the SGs before the maximum system heat up rate is experienced. See "Effect of Varying SG Secondary Leakage Rate" below for considerations related to the assumed size of the steam leakage path.

Effect of Varying the SG Secondary Leakage Flow Area

A sensitivity run, Case 8G, was performed to evaluate behavior using different assumptions for the SG steam leakage flow area. For this run, a different steam leakage flow area was used in each of the four SGs. Flow areas representing 80%, 60%, 40% and 20% of the 3.23-cm² [0.5-in²] per SG leak flow area assumed in the base case calculation were used in SGs 1 through 4, respectively.

Figure D.35 compares the SG secondary pressure responses for the SGs from Case 8G with 0.65-cm² [0.1-in²], 1.29-cm² [0.2-in²], 1.94-cm² [0.3-in²], and 2.58-cm² [0.4-in²] leak flow areas in their secondary systems with the base case SG pressure. As expected the SG depressurization rate is proportional to the size of the assumed leak flow area.

The average-tube failure margins from Case 8G are compared with the base case margins in Table D.5 (note that in the base case run the minimum margin is in the pressurizer loop SG and margins are slightly higher in the non-pressurizer loop SGs). The results indicate that the SG tube failure margin increases gradually as the leak flow area is decreased from 3.23 cm² [0.5 in²] to 1.94 cm² [0.3 in²], and then increases significantly faster as the flow area falls below 1.94 cm² [0.3 in²].

Surge Line and Hot Leg Wall Inside Surface Heat Transfer Coefficient Variation

A sensitivity run, Case 8D, was performed to simulate increased heat transfer from the fluid to the inside surfaces of the surge line and HL upper section walls. A multiplier of 2.0 was placed on the heat transfer coefficients employed in the base case for the combination of convection and steam-to-wall radiation heat transfer. No change was made in the HL wall-to-wall radiation heat transfer modeling.

Figure D.36 compares the heat transfer coefficient on the inside surface of the upper section of Hot Leg 1 (near the RV) for Case 8D and the base case. The increase in the heat transfer coefficient in Case 8D is as expected (the comparisons at other locations within the upper HL sections and the pressurizer surge line are similar).

The heat transfer modeling revisions in Case 8D are seen to result in a moderate increase in the SG average tube failure margin. Stress multipliers of 2.96 and 2.10, respectively, are needed for average tube failure to occur coincident with the HL using the increased and nominal HL and pressurizer surge line heat transfer coefficients.

This margin improvement results because the increased heat transfer coefficient leads to faster heat-up of the HL wall (and earlier HL failure) and slower heat-up of the SG tubes (and later SG tube failure). Figure D.37 compares the Hot Leg 1 upper section wall temperatures for the two cases and Figure D.38 compares the SG 1 hot average tube wall temperatures for the two cases.

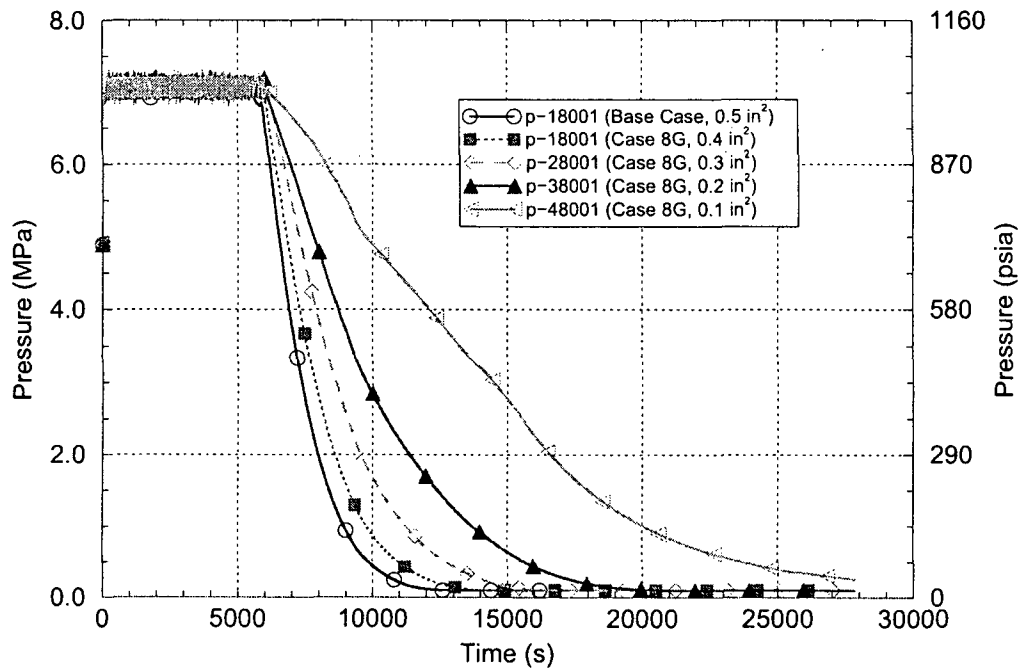


Figure D.35 SG Secondary Pressures for the SG Secondary Leakage Sensitivity Cases

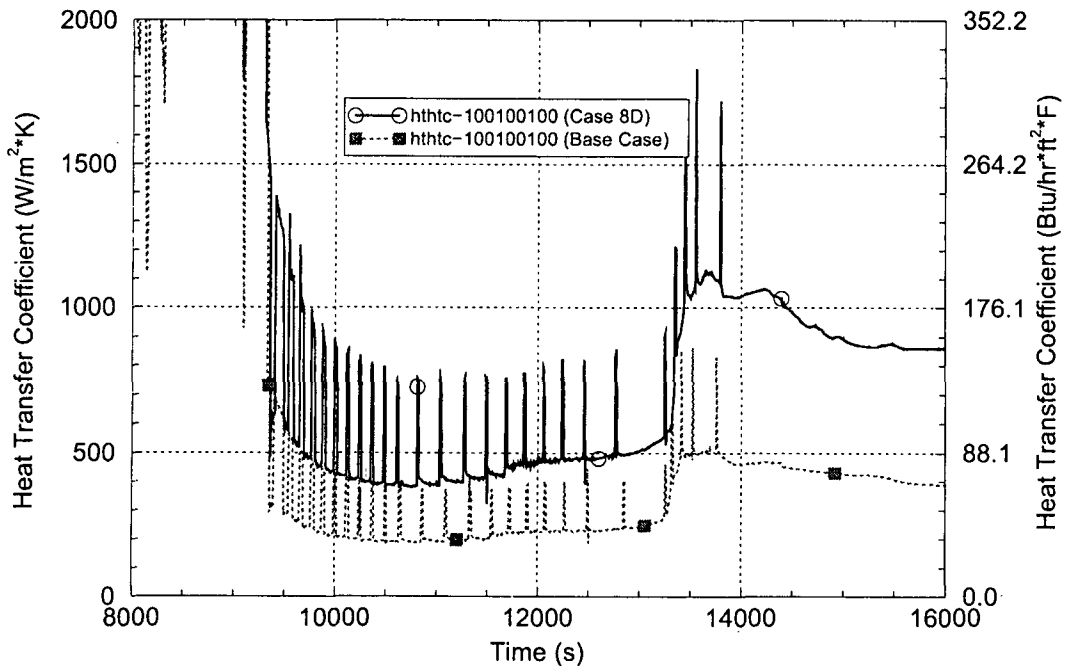


Figure D.36 Hot Leg 1 Inside Surface Heat Transfer Coefficient for the Hot Leg and Surge Line Heat Transfer Sensitivity Cases

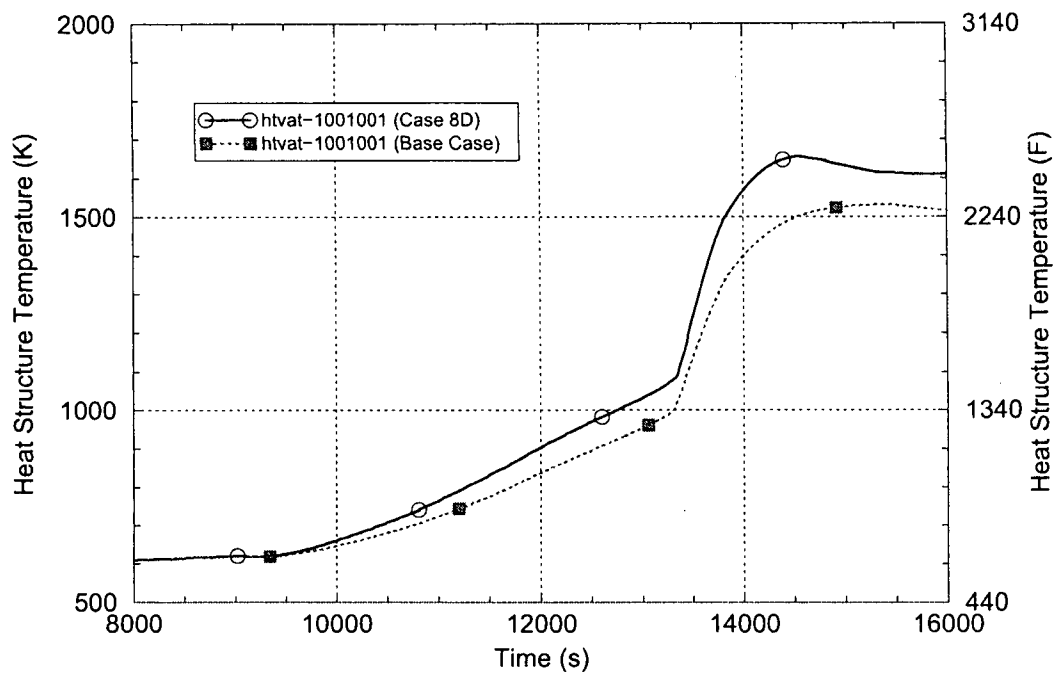


Figure D.37 Hot Leg 1 Wall Temperature for the Hot Leg and Surge Line Heat Transfer Sensitivity Cases

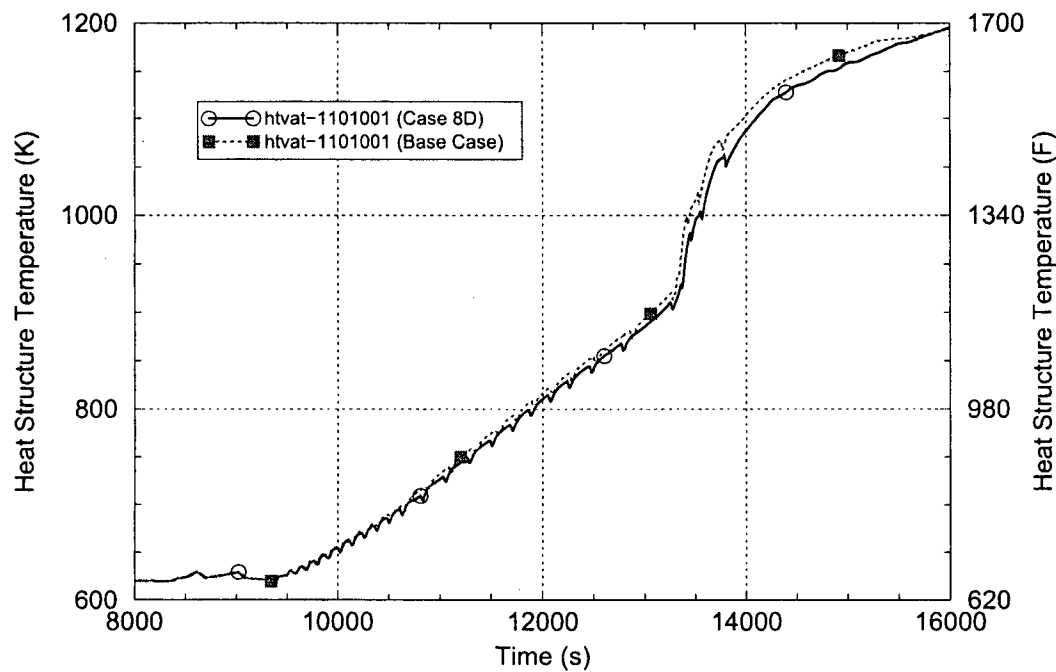


Figure D.38 SG 1 Hot Average Tube Wall Temperature for the Hot Leg and Surge Line Heat Transfer Sensitivity Cases

Table D.5 SCDAP/RELAP5-Calculated Results for Case 8G, Evaluating Sensitivity to SG Secondary Steam Leak Flow Area Assumptions

SG Number	Case	Leak Flow Area (in ²)	Average SG Tube Failure Margin (Stress Multiplier for Tube Failure Coincident with Hot Leg Failure)
1	Base	3.23 cm ² [0.5 in ²]	2.100
1	8G	2.58 cm ² [0.4 in ²]	2.076
2	Base	3.23 cm ² [0.5 in ²]	2.150
2	8G	1.94 cm ² [0.3 in ²]	2.303
3	Base	3.23 cm ² [0.5 in ²]	2.133
3	8G	1.29 cm ² [0.2 in ²]	2.679
4	Base	3.23 cm ² [0.5 in ²]	2.150
4	8G	0.65 cm ² [0.1 in ²]	2.909

Tubesheet Wall Inside Surface Heat Transfer Coefficient Variation

A sensitivity run, Case 8E, was performed to simulate increased heat transfer from the fluid to the SG tubesheet structures. A multiplier of 2.0 was placed on the heat transfer coefficients employed in the base case for the combination of convection and steam-to-wall radiation heat transfer.

Figure D.39 compares the heat transfer coefficient on the SG 1 tubesheet (near the SG inlet plenum) for Case 8E and the base case. The increase in the heat transfer coefficient in Case 8E is as expected at this location (the comparisons at other tubesheet locations are similar).

The heat transfer modeling revisions in Case 8E are seen to result in a small increase in the SG average tube failure margin. Stress multipliers of 2.20 and 2.10, respectively, are needed for average tube failure to occur coincident with the HL using the increased and nominal tubesheet heat transfer coefficients.

This margin improvement results because the increased heat transfer coefficient leads to a faster heat-up of the tubesheet wall and a slower heat-up of the SG tubes (and later SG tube failure). Figure D.40 compares the SG 1 tubesheet wall temperatures for the two cases and Figure D.41 compares the SG 1 hot average tube wall temperatures for the two cases.

Effect of Pre-Existing Steam Generator Tube Leakage

The base case calculation assumes no SG tube leakage exists. A sensitivity run, Case 8C, was performed assuming that a tube leakage path with an initial flow rate of 6.29 L/s [100 gpm] in SG 1 exists at the start of the SBO accident event sequence. The leak is assumed to be located midway between the tubesheet and the top of the U-bend in the hot average tube. To implement the tube leakage into the model, a valve with a flow area of 0.5972 cm² [0.0006428 ft²] was added to the model at the start of the transient event sequence calculation.

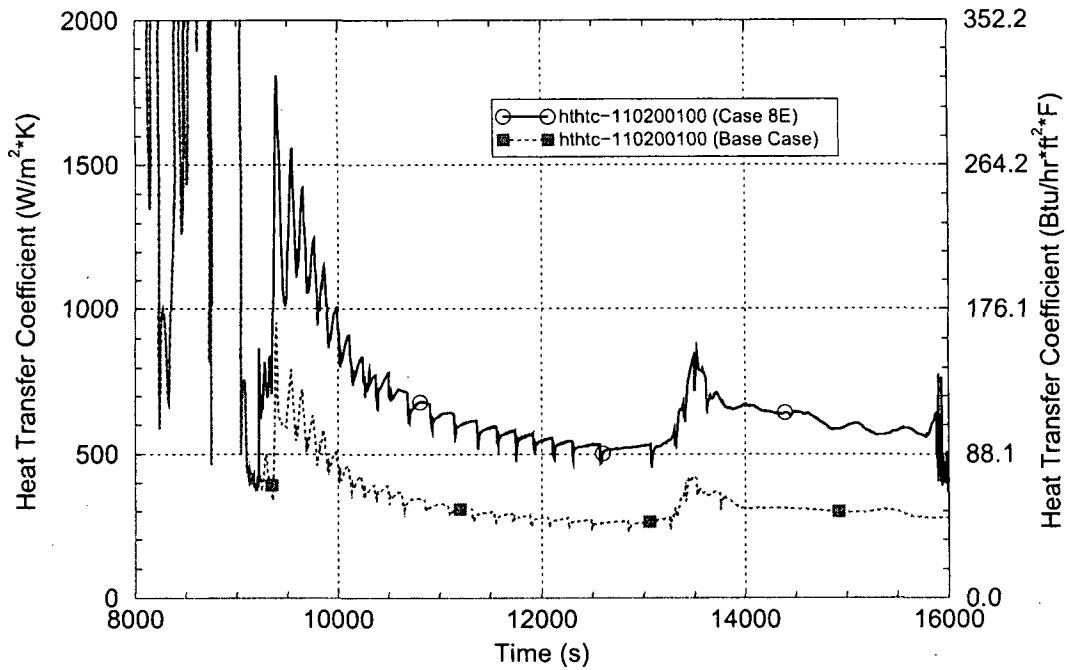


Figure D.39 SG 1 Tubesheet Heat Transfer Coefficient for the Tubesheet Heat Transfer Sensitivity Cases

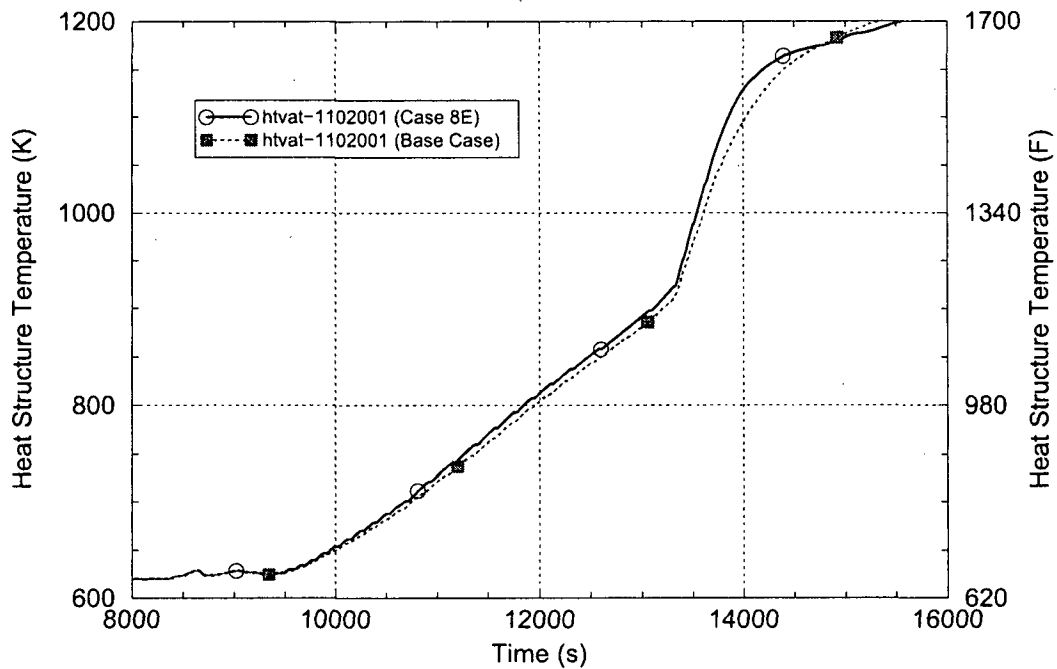


Figure D.40 SG 1 Tubesheet Wall Temperature for the Tubesheet Heat Transfer Sensitivity Cases

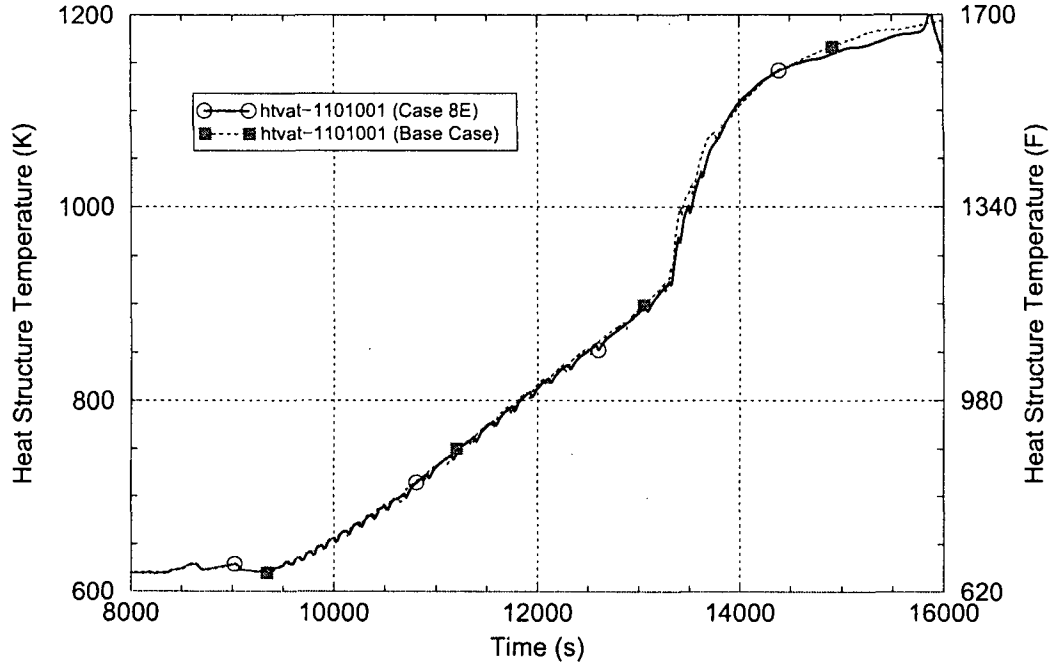


Figure D.41 SG 1 Hot Average Tube Wall Temperature for the Tubesheet Heat Transfer Sensitivity Cases

This flow area represents a circular hole with a diameter of 0.871 cm [0.343 in]; therefore the leak flow area is less than the equivalent flow area of a single SG tube.

The SG 1 inlet plenum flow losses were adjusted to attain the following revised set of target values for the mixing and flow parameters: hot leg discharge coefficient 0.14 (versus 0.12 in the base case), recirculation ratio 1.75 (versus 2.0 in the base case) and hot and cold mixing fractions 0.75 (versus 0.85 in the base case). These revised target values resulted from CFD evaluations of the fluid conditions expected in a coolant loop with a leaking SG tube. No changes were made to the SG inlet plenum flow losses in the other three SGs.

The tube leakage mass flow rate from Case 8C is shown in Figure D.42. The flow rate is erratic due to the changing transient conditions in the RCS and SG secondary, but it generally trends downward as the leaking fluid changes from water at the beginning of the event sequence to saturated steam and then to superheated steam.

Relative to the base case, the results for Case 8C indicate improved SG tube failure margins for both the hottest tube in SG 1 and the average tube in SG 1. The hottest SG 1 tube fails 2,235 s after the HL fails in Case 8C, while in the base case it failed 155 s earlier than the HL. The SG 1 average tube stress multiplier required for tube failure coincident with HL failure rose from 2.10 in the base case to 2.94 in Case 8C as a result of the relative changes in the HL and SG 1 average tube failure times.

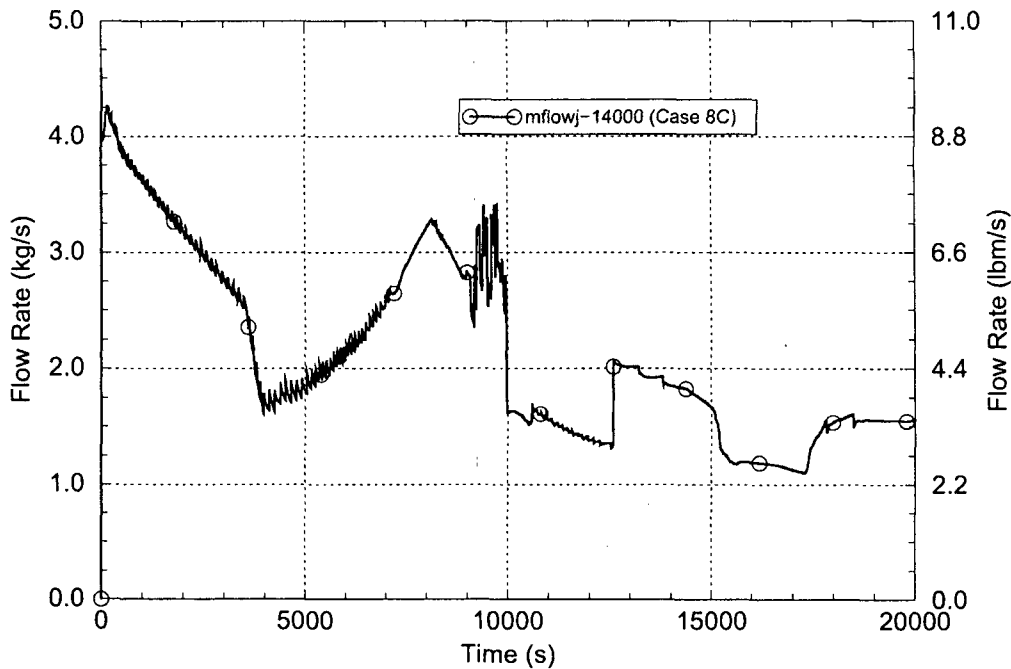


Figure D.42 Tube Leak Rate for the SG Tube Leakage Sensitivity Case

Figures D.43 and D.44, respectively, compare the Hot Leg 1 upper section and SG 1 average tube wall temperatures from the two runs. From the base case calculation to the Case 8C calculation, comparable changes are seen in the times when the HL and tube temperatures rise rapidly. Therefore, the improved SG tube failure margins in Case 8C do not result from changes in the relative timing of structure heat-up.

Figures D.45 and D.46, respectively, compare the Hot Leg 1 and SG 1 secondary pressures from the two runs. On the primary side, the tube leakage leads to moderately more depressurization than seen in the base case. Less frequent pressurizer PORV opening is seen in Case 8C; however the peak RCS pressures and the behavior of the RCS pressure during the period when structure failures occur are nearly the same for the two cases. On the SG 1 secondary side, the tube leakage causes the pressure to be significantly higher in Case 8C than in the base case. The differential pressure from primary to secondary in Case 8C is therefore much less than seen in the base case, and this is the explanation for the increased SG 1 failure margins.

The tube failure margin improvements for the SG 1 tubes are not shared by the tubes in the other three SGs. The tube leakage in SG 1 does not affect the secondary pressures in SGs 2, 3 and 4 and no readjustments of SG inlet plenum flow losses are made in SGs 2, 3 and 4. As a result, for Case 8C the limiting tube failure moves from SG 1 to SG 3. The increase in the SG 3, 2.0-multiplier average tube failure time from the base case to Case 8C is virtually identical to that seen for the HL failure time. Therefore, only a small improvement is seen in the limiting average tube failure margin (a stress multiplier for tube failure coincident with HL failure of 2.21 for the SG-3 tube in Case 8C, versus 2.10 for the SG-1 tube in the base case). The conclusion is therefore that the effect of pre-existing SG tube leakage in a single SG does not significantly affect the overall outcome of the analysis.

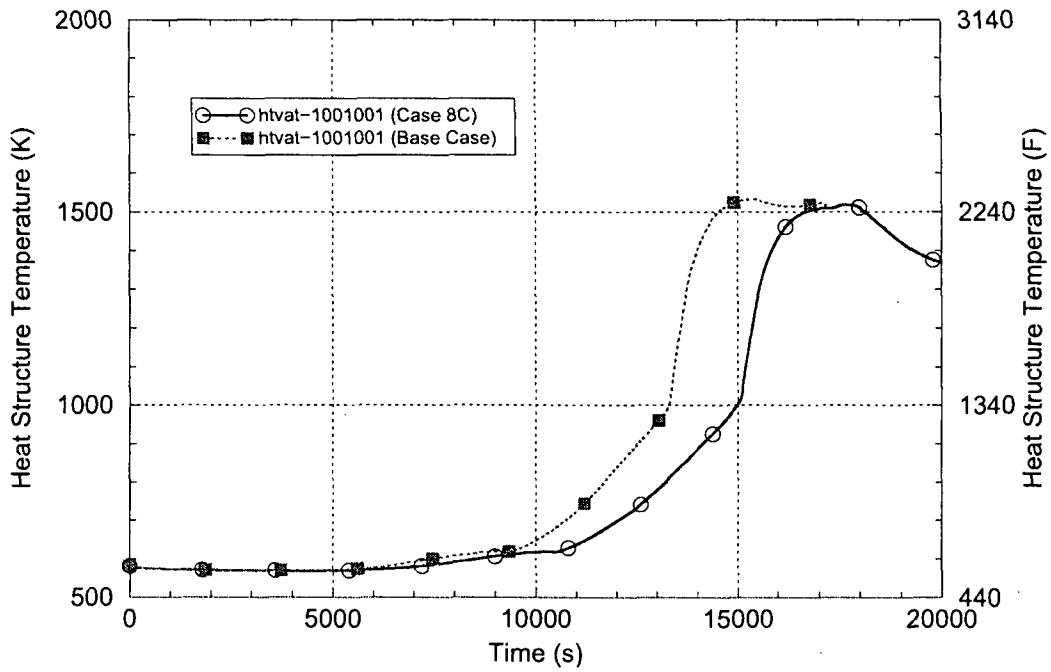


Figure D.43 Hot Leg 1 Upper Section Wall Temperature for the SG Tube Leakage Sensitivity Case

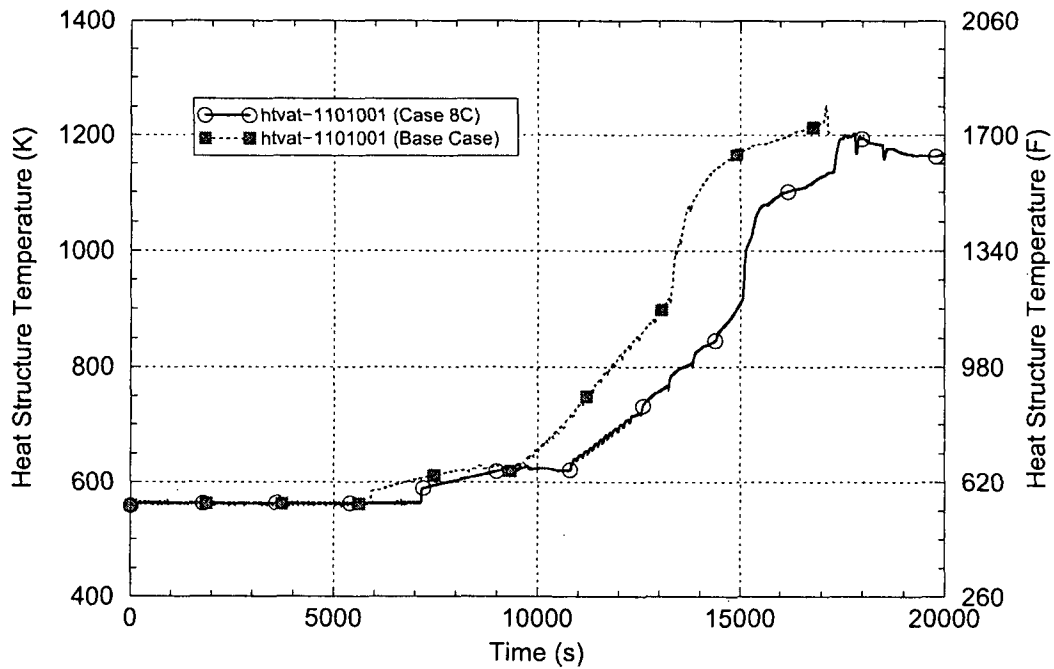


Figure D.44 SG 1 Average Tube Wall Temperature for the SG Tube Leakage Sensitivity Case

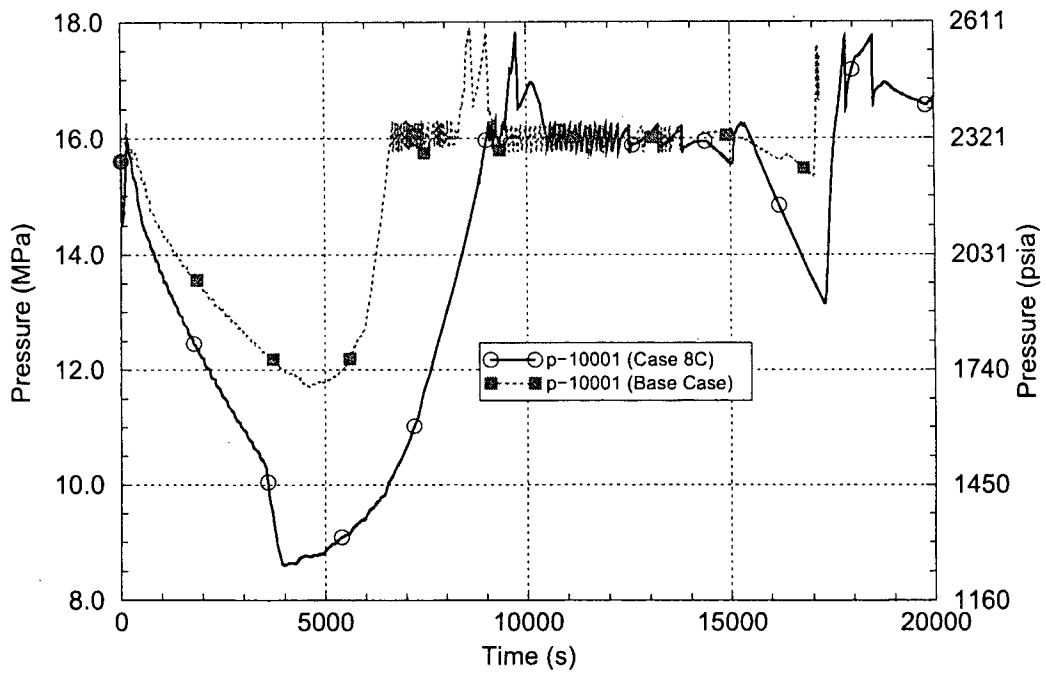


Figure D.45 Hot Leg Pressure for the SG Tube Leakage Sensitivity Case

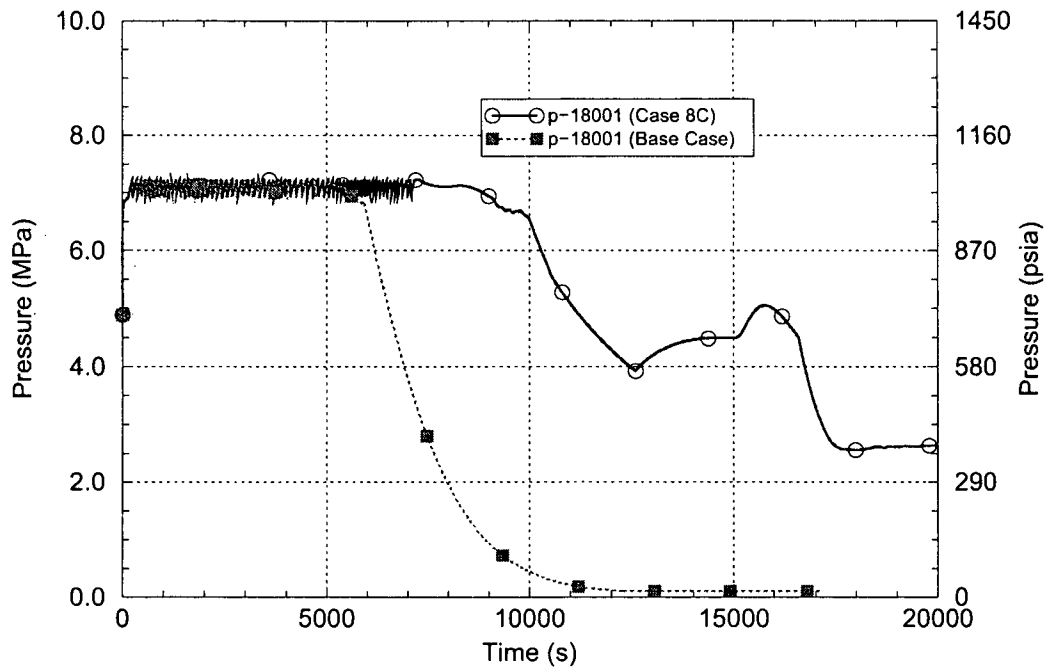


Figure D.46 SG 1 Secondary Pressure for the SG Tube Leakage Sensitivity Case

It is noted, however, that the Case 8C event sequence evaluated here does not include rapid depressurization of the SG secondary systems that could result, for example, from a stuck-open relief valve or main steam line break. The analysis results may be different for a case where the pre-existing SG tube leakage resides in a rapidly-depressurizing SG.

D.3 Estimates of Uncertainties in the SCDAP/RELAP5 Calculation Output

Section D.3.1 describes the method used to estimate the uncertainties in the SCDAP/RELAP5-calculated responses for the key output parameters, the dependent variables. The method compares the output from the SCDAP/RELAP5 base case calculation and sensitivity calculations performed to evaluate the changes in the dependent variables resulting from variations in the independent variables (which are parameters deemed by the PIRT evaluation to be important for the simulation of the dependent variables). The uncertainty evaluation results are described in Section D.3.2

D.3.1 Methods for Estimating Uncertainties

The eight dependent variables for the uncertainty study are the key parameters used by the project stress analysts and PRA analysts (see Section 2.7.2):

- Failure margin for average SG tube
- Failure margin for hottest SG tube
- Average SG tube metal temperature
- Hottest SG tube metal temperature
- HL steam temperature
- HL piping wall inner surface heat transfer coefficient
- Pressurizer surge line steam temperature
- Pressurizer surge line piping wall inner surface heat transfer coefficient

The exact descriptions (location, evaluation time, smoothing process, etc.) selected for each of the dependent variables are provided in Section D.1.1.

The PIRT identified 15 parameters important for the plant thermal-hydraulic response; these are the independent variables for the uncertainty study (see Section 2.7.3). For each PIRT parameter, the thermal-hydraulic phenomena, the event sequence assumptions and progression, the current SCDAP/RELAP5 modeling, experience from prior sensitivity analyses and prior SCDAP/RELAP5 assessments were evaluated. From these evaluations, the list of 19 sensitivity runs in Table D.2 was developed to generate statistics needed for the uncertainty evaluation. The sensitivity runs incorporate variations into the model that cover the expected ranges of the important PIRT parameters. The sensitivity run output for the temperatures, heat transfer coefficients and SG tube failure margins is then compared against the corresponding output from the base case calculation and the differences are used to estimate the uncertainties in the dependent variables.

A paper by Macdonald, Clark and Strachan (Reference D.20) describes methods for assessing the uncertainty in simulation of building energy and environmental responses. The situation described in the paper is analogous in many respects to the subject analysis of this report. A model of the physical building is assembled (similar to the SCDAP/RELAP5 plant model) consistent with the geometry, materials, and initial and boundary conditions. To characterize the building performance, the model is run using simulation software (similar to the

SCDAP/RELAP5 computer code) to represent the physical processes, such as flow of heat and moisture.

Reference D.20 indicates that the traditional and most widely-used methods for assessing uncertainty are based on sensitivity analysis. Sensitivity analysis allows assessing the relationship between variations in input parameters and resulting variations in the output predictions. The sources of uncertainty affecting the model need to be identified and quantified, which for this application has been accomplished through the PIRT and subsequent evaluations related to the PIRT parameters. Reference D.20 describes a differential sensitivity analysis method which is adopted here. This method requires a base case simulation in which the input parameters are set to represent their best-estimate conditions. The simulation is then repeated with one input parameter varied to represent its expected extreme variation in one direction and the effect on the output variables are noted. The method assumes linearity, which means that variation of the input parameter in the opposite direction results in corresponding opposite variations in the output variables.

A differential sensitivity analysis is not optimized for the number of simulations required and does not identify parameter interactions, for which factorial designs could be used. In this analysis, the number of uncertain parameters is ten and 19 sensitivity runs have been performed in addition to the base case run. A full factorial analysis for ten parameters would require 1,024 SCDAP/RELAP5 runs, although fractional factorial design approaches could reduce the number of runs somewhat. An alternate approach for addressing parameter interactions using Bayesian Networks (also involving additional sensitivity runs) could be used.

Given the complexity of performing SCDAP/RELAP5 runs, it was judged for this project that expanding the number of runs past 20 cannot be justified at this time for economic reasons. Instead, maximum use is made of the 19 sensitivity runs to determine rough estimates for the uncertainties in the temperatures, heat transfer coefficients and SG tube failure margins. These rough uncertainty estimates will be provided to the stress and probabilistic risk analysts. Should it later be found that the uncertainties in the thermal-hydraulic results dominate the uncertainties in the overall project results, then the additional effort to use a fractional factorial or Bayesian Network approach for addressing the interactions among the parameters may be justified.

It is assumed that the set of sensitivity runs is normally distributed (i.e., based on a Gaussian distribution with the shape of the "bell curve") around the base case run.

Reference D.21 provides the following formula for the standard deviation, σ_x , of N readings of parameter x around a mean value, m:

$$\sigma_x = \left\{ \left[1.0 / (N - 1.0) \right] \sum_{i=1}^N (x_i - m)^2 \right\}^{0.5}$$

For this application, N (the number of sensitivity runs) is 19, the x_i are the values for the dependent variable output variables from the sensitivity runs and m is the corresponding values for the dependent variables from the output of the base case run. The primary results from the uncertainty study are the values for σ_x , representing rough estimates for the standard deviations of the SCDAP/RELAP5 calculated results, for the eight dependent variables (the SG tube failure margins, temperatures and wall heat transfer coefficients). For this report, the standard deviations in the dependent variables are reported first using the above approach.

Next, for some of the x_i parameters, there are indications that the distribution around the base case values may not be symmetric. For example, plant operating experience suggests that it is more likely that our base case calculation is underpredicting, rather than overpredicting, the heat loss from the RCS into the containment. The effects of modifying the standard deviation calculation in the following manner, which introduces weighting factors, w_i , to account for known unsymmetrical behavior, are evaluated:

$$\sigma_x = \left\{ \left[1.0 / (N - 1.0) \right] \sum_{i=1}^N [w_i (x_i - m)^2] \right\}^{0.5}$$

This weighting-factor approach introduces, in a simplistic way, the concept of distributions in the independent variables, such as featured in factorial, response surface approaches to uncertainty evaluation. In this report the standard deviations in the dependent variables are also reported using this second, weighting-factor approach.

Finally, consideration is added that the 20 runs (base case and 19 sensitivity cases) collectively, rather than the base case alone, represent the true mean. With this approach, the total uncertainty includes the effects of uncertainty in the mean itself, not just an uncertainty due to distribution around the mean. From Reference D.21 the uncertainty in the mean σ_m is given by:

$$\sigma_m = \sigma_x / N^{0.5}$$

For the purposes here a revised total standard deviation, σ , is developed by combining the uncertainty in the mean with the uncertainty of the distribution around that mean:

$$\sigma = \left[\sigma_m^2 + \sigma_x^2 \right]^{0.5} = \sigma_x \left[(1.0 / N^{0.5})^2 + 1.0^2 \right]^{0.5}$$

For $N = 20$, this becomes: $\sigma = 1.025 \sigma_x$

The standard deviations provided in this report are therefore calculated using both unweighted and weighted approaches, with and without application of a multiplier that considers the uncertainty in the mean.

D.3.2 Uncertainty Estimate Results

The SCDAP/RELAP5-calculated results for the eight dependent variables (temperatures, heat transfer coefficients and SG tube failure margins) for the SBO base case run and the 19 sensitivity runs are shown in Tables D.4 and D.5. For each sensitivity run, the differences between the results for the sensitivity and base case runs are taken for each dependent variable. Tables D.6 and D.7 compile the differences between the sensitivity and base case run results. The differences are calculated by subtracting the base case dependent variable values from the corresponding sensitivity run dependent variable values.

As identified in the tables, the differences listed for certain runs reflect adjustments made to the output data from the SCDAP/RELAP5 sensitivity case calculations. The runs for Cases 2A and 2B were performed to consider $\pm 15\%$ variations in the hot leg discharge coefficient. It was subsequently judged that larger variations are needed to bound the expected ranges for that parameter. The differences shown for Cases 2A and 2B represent twice the differences calculated between those runs and the base case run, thereby effectively representing $\pm 30\%$ variations in the hot leg discharge coefficient. The differences shown for Cases 4A and 4B

(variations in the fuel rod oxidation power) were adjusted to account for slight changes seen in the calculated response as a result of implementing the model features needed to perform the sensitivity runs (see discussion for PIRT Parameter B1 in Section D.1.2). The differences shown for Case 7A (3.83-L/s [61-gpm] per pump shaft seal leakage after two hours) reflect adjustments, based on interpolation of results, to represent a 41-gpm RCP shaft seal leakage rate assumption (see discussion for PIRT Parameter C2 in Section D.1.2).

For each of the dependent variables, the relative magnitudes of the differences associated with the sensitivity cases in Tables D.6 and D.7 reflect their influence on the overall uncertainty. For three of the dependent variables (average SG tube failure margin, average SG tube wall temperature and hottest SG tube wall temperature), the uncertainties from many independent variables contribute relatively-equally to the overall uncertainty. For the other five dependent variables, the overall uncertainty is dominated by the contributions from only a few of the independent variables. When the number of dependent variables for which the individual contributions are considered dominant are counted, the following cases are seen to have the most important effect on the overall uncertainties (in decreasing order of importance): Case 5A (50% decrease in RV internal circulation rate), Case 4B (50 % decrease in fuel rod oxidation power) and Case 7A (RCP shaft seal leakage increased to 2.50 L/s [41 gpm] per pump at two hours).

Standard deviations were calculated for each of the eight dependent variables using the methods described in Section D.3.1. The standard deviation results shown in Table D.8 were calculated with four different approaches: using equal-weighting and biased-weighting of the independent-variable terms and with and without considering the effects of uncertainty in the mean.

The biased-weighting approach takes advantage of information, where available, regarding the likelihoods of the variation of a parameter in one direction versus the other direction. Pertinent information may be available from plant operating experience, the assessment of SCDAP models against specific severe accident experiments and the assessment of RELAP5 models against a much larger set of general reactor safety-related thermal-hydraulic experiments. The scheme by which biased weighting was applied in this analysis is described as follows.

For most of the independent variables, there was no known basis supporting the weighting of variations in one direction differently than those in the other direction. For the cases in this category (1A, 1B, 2A through 2G, 3A and 3B), weighting factors of 1.0 were used.

For the fuel rod oxidation power sensitivity cases, there are pertinent prior assessments of SCDAP/RELAP5 capabilities for predicting hydrogen generation in nine tests and five experimental facilities (see Section 3.2.2). In these assessments, the code underpredicted hydrogen generation in seven tests and overpredicted it in two tests. To account for this underprediction bias, the results for Case 4A (oxidation rate x 1.2) are weighted by $(2 \times 7 / 9 =) 1.556$ and the results for Case 4B (oxidation rate x 0.5) are weighted by $(2 \times 2 / 9 =) 0.444$.

For the vessel internal circulation sensitivity, years of general RELAP5 assessment background suggests that, due to numerical difficulties, the code is much more likely to overpredict circulation rates than to underpredict them. To account for this overprediction bias, the results for Case 5A (50% decrease in vessel circulation rate) are weighted by $(2 \times 2 / 3 =) 1.333$ and the results for Case 5B (100% increase in vessel circulation rate) are weighted by $(2 \times 1 / 3 =) 0.667$.

Table D.6 Compilation of Differences Between the SCDAP/RELAP5-Calculated Results from the Sensitivity and Base Case Runs for the SG Tube Failure Margin and SG Tube Temperature Dependent Variables

Case Number and Description of the Variation	Difference in SG 1 Hottest Tube with 1.0 Multiplier Failure Time – First Primary Failure Time(s)	Difference in SG 1 Average Tube Stress Multiplier for Tube Failure Coincident with First Primary Failure (-)	Difference in SG 1 Average Tube Structure Temperature (K)	Difference in SG 1 Hottest Tube Structure Temperature (K)
Case 1A, Pressurizer PORV and SRV flow areas x 1.3	0.02	-0.03	1.33	-0.08
Case 1B, Pressurizer PORV and SRV flow areas x 0.7	4.99	0.01	-0.78	-0.91
Case 2A (adjusted), Hot Leg Discharge Coefficient x 1.3	0.04	-0.37	35.32	28.98
Case 2B (adjusted), Hot Leg Discharge Coefficient x 0.7	40.00	0.57	-43.71	-42.46
Case 2C, recirculation ratio = 2.3	-14.99	0.08	-7.10	8.02
Case 2D, recirculation ratio = 1.7	19.98	-0.08	6.88	-22.54
Case 2E, mixing fractions = 0.95	9.99	0.40	-34.95	-13.62
Case 2F, mixing fractions = 0.75	-4.98	-0.29	31.31	7.49
Case 2G, assumed hot/cold tube split = 50%/50%	15.00	0.11	-7.84	-22.32
Case 3A, SG tube wall outside surface HTC x 5.0	120.02	0.25	-20.96	-66.66
Case 3B, SG tube wall outside surface HTC x 0.5	-5.02	-0.03	2.07	8.87
Case 4A (adjusted), fuel rod oxidation power x 1.2	-14.98	0.06	-3.23	0.47
Case 4B (adjusted), fuel rod oxidation power x 0.5	64.94	-0.19	9.26	-50.06
Case 5A, vessel internal circulation rate x 0.5	-104.98	0.18	-22.49	-82.11
Case 5B, vessel internal circulation rate x 2.0	65.01	-0.13	10.10	-8.30
Case 6A, 2 MW total RCS heat loss	14.97	0.02	-3.74	-4.65
Case 6B, 8 MW total RCS heat loss	-99.98	-0.18	19.04	11.01
Case 7A (adjusted), 41 gpm pump seal leakage after 2 hours	-27.50	0.11	-11.93	-29.73
Case 7G, 1 gpm pump leakage after 2 hours	15.00	-0.02	1.32	-5.04

Table D.7 Compilation of Differences Between the SCDAP/RELAP5-Calculated Results from the Sensitivity and Base Case Runs for the Hot Leg and Surge Line Temperature and Heat Transfer Coefficient Dependent Variables

Case Number and Description of the Variation	Difference in Hot Leg 1 Steam Temperature (K)	Difference in Hot Leg 1 Wall Inside Surface HTC (W/m ² -K)	Difference in Surge Line Steam Temperature (K)	Difference in Surge Line Wall Inside Surface HTC (W/m ² -K)
Case 1A, Pressurizer PORV and SRV flow areas x 1.3	-4.12	11.40	5.25	71.44
Case 1B, Pressurizer PORV and SRV flow areas x 0.7	-2.23	-10.23	-2.45	-36.03
Case 2A (adjusted), Hot Leg Discharge Coefficient x 1.3	-62.60	11.71	-24.78	20.45
Case 2B (adjusted), Hot Leg Discharge Coefficient x 0.7	-63.00	-47.42	-52.80	-30.15
Case 2C, recirculation ratio = 2.3	-46.67	1.13	-23.86	70.79
Case 2D, recirculation ratio = 1.7	-46.23	-18.86	-24.19	-19.90
Case 2E, mixing fractions = 0.95	-50.94	-15.23	-20.80	26.32
Case 2F, mixing fractions = 0.75	4.27	15.04	-4.04	52.12
Case 2G, assumed hot/cold tube split = 50%/50%	12.30	-15.78	3.98	-47.96
Case 3A, SG tube wall outside surface HTC x 5.0	-38.13	-9.30	-19.28	8.94
Case 3B, SG tube wall outside surface HTC x 0.5	-25.01	-9.95	-18.03	-26.87
Case 4A (adjusted), fuel rod oxidation power x 1.2	-9.26	15.71	-4.89	57.40
Case 4B (adjusted), fuel rod oxidation power x 0.5	-98.33	-125.20	-98.42	-247.09
Case 5A, vessel internal circulation rate x 0.5	-172.77	-42.22	-124.27	-22.12
Case 5B, vessel internal circulation rate x 2.0	24.48	-0.33	32.69	36.53
Case 6A, 2 MW total RCS heat loss	-11.97	-8.00	-8.23	-28.26
Case 6B, 8 MW total RCS heat loss	-36.20	-4.09	-47.52	-0.46
Case 7A (adjusted), 41 gpm pump seal leakage after 2 hours	-22.41	-29.25	-122.72	-105.55
Case 7G, 1 gpm pump leakage after 2 hours	-40.73	-1.86	-12.28	71.64

For the heat loss sensitivity, an EPRI report (Reference D.18) indicates that vessel and piping insulation installed in plants is in general performing more poorly than designed. This suggests that a higher RCS heat loss is more likely than a lower RCS heat loss. To account for this bias, the results for Case 6A (2 MW total RCS heat loss) are weighted by $(1 \times 2 / 3 =) 0.667$ and the results for Case 6B (8 MW total RCS heat loss) are weighted by $(2 \times 3 / 3 =) 1.333$.

Finally, for the RCP shaft seal leak sensitivity, ± 1.262 L/s [± 20 gpm] variations around the nominal 1.325 L/s [21 gpm] per pump leakage are assumed. This uncertainty accounts for several factors related to: (1) predicting the correct conditions upstream of the leak, (2) adequately representing the complex geometry of the pump shaft seal configuration and (3) general considerations regarding the prediction capabilities of the RELAP5 critical flow model. Case 7G (1 gpm leakage per pump after two hours) considers that the code might underpredict the leak flow by a factor of $(21 / 1 =) 21.0$. Case 7A (adjusted for 41 gpm leakage per pump after two hours) considers that the code might overpredict the flow by a factor of $(41 / 21 =) 1.95$. Since RELAP5 code assessment experience shows no general bias for the code either underpredicting or overpredicting critical flows, the results for these two cases are weighted $(90\% \times 2 =) 1.8$ for Case 7A (adjusted for 41 gpm) and $(10\% \times 2 =) 0.2$ for Case 7G (1 gpm).

The results for the standard deviations calculated with equal weighting and biased weighting of the sensitivity case results were seen to generally be similar. For only three of the dependent variables (HL wall inside surface heat transfer coefficient, pressurizer surge line steam temperature and pressurizer surge line wall inside surface heat transfer coefficient) were the differences in the standard deviations obtained with equal-weighting and biased-weighting greater than 10%. The greatest difference was only 22%. Since the weighted approach provides results which take advantage of various additional assessment, modeling and plant operation experiences, the use of the standard deviations calculated using the weighted approach was selected.

Finally, the total number of cases is only 20, so the approach which applies a 1.025 multiplier to consider effects related to the uncertainties in the dependent variable mean values was selected.

The recommended results for the standard deviations in the eight dependent variables are shown in the right-hand column of Table D.8.

D.4 Summary of Uncertainty Estimates

Standard deviations were developed for the uncertainties in eight important output parameters (the dependent variables, which are SG tube failure margins, temperatures and heat transfer coefficients) for SCDAP/RELAP5 simulations of SBO severe accident events in a Westinghouse four-loop PWR. The standard deviations were obtained using a sensitivity-study method employing 19 sensitivity runs in addition to the base-case run.

Table D.8 Standard Deviations for the Dependent Variables Calculated Using Four Methods

Parameter and Units	Standard Deviations Approach 1 Equal Weighting Base Case = Mean	Standard Deviations Approach 2 Equal Weighting Uncertainty in the Mean Effects Included	Standard Deviations Approach 3 Biased Weighting Base Case = Mean	Recommended Standard Deviations Approach 4 Biased Weighting Uncertainty in the Mean Effects Included
1.0-Multiplier Hottest Tube Failure Margin [Hottest Tube Failure Time – First Primary Piping Failure Time] (s)	51.60	52.87	53.57	54.89
Average Tube Failure Margin [Stress Multiplier for Tube Failure Coincident with First Primary Failure]	0.227	0.233	0.228	0.234
Average SG Tube Wall Temperature (K)	19.98	20.47	20.43	20.93
Hottest SG Tube Wall Temperature (K)	32.36	33.16	33.67	34.50
Hot Leg Steam Temperature (K)	58.16	59.60	60.00	61.48
Hot Leg Wall Inside Surface Heat Transfer Coefficient (W/m ² -K)	35.37	36.24	29.06	29.78
Pressurizer Surge Line Steam Temperature (K)	52.45	53.75	58.50	59.94
Pressurizer Surge Line Wall Inside Surface Heat Transfer Coefficient (W/m ² -K)	75.61	77.48	64.56	66.15

Standard deviations were calculated through four different approaches, using equal-weighting and biased-weighting of the independent-variable contributions to uncertainty, and with and without consideration of the uncertainties in the means. Since a weighted approach provides results which take advantage of various additional assessment, modeling and plant operation experiences, the use of the standard deviations calculated using the weighted approach were selected. Since the total number of cases is only 20, the calculation approach which applies a 1.025 multiplier in order to include the consideration that there is an uncertainty in the mean values for the dependent variables was also selected.

The base-case values, the evaluation times and the recommended standard deviations for the eight dependent variables are listed in Table D.9.

Table D.9 Base Case Values and Recommended Standard Deviations for the Dependent Variables

Parameter and Units	Evaluation Time for Base Case Value(s)	Base Case Value	Recommended Standard Deviation
Hottest SG Tube Failure Margin [1.0 Stress Multiplier Hottest Tube Failure Time – First Primary Piping Failure Time], s	Not Applicable	-155	54.89
Average SG Tube Failure Margin [Stress Multiplier for Tube Failure Coincident with First Primary Piping Failure], dimensionless	Not Applicable	2.10	0.234
Average SG Tube Wall Temperature, K	13,630	1021.7	20.93
Hottest SG Tube Wall Temperature, K	13,630	1239.6	34.50
Hot Leg Steam Temperature, K	13,517	1776.0	61.48
Hot Leg Wall Inside-Surface Heat Transfer Coefficient, W/m ² -K	13,517	423.1	29.78
Pressurizer Surge Line Steam Temperature, K	13,517	1373.0	59.94
Pressurizer Surge Line Wall Inside-Surface Heat Transfer Coefficient, W/m ² -K	13,517	490.9	66.15

D.5 References for Appendix D

- D.1 C. D. Fletcher, R. M. Beaton and W. C. Arcieri, *SCDAP/RELAP5 Sensitivity Evaluations for a Zion TMLB' Station Blackout Event*, Information Systems Laboratories, Inc., ISL-NSAD-TR-04-05, March 2004.
- D.2 N. Zuber and J. Findlay, "Average Volumetric Concentrations in Two-Phase Flow Systems," *Journal of Heat Transfer*, Vol. 87, 1965, pp. 453-568.
- D.3 I. Kataoka and M. Ishii, "Drift Flux Model for Large Diameter Pipe and New Correlations for Pool Void Fraction," *International Journal of Heat and Mass Transfer*, Vol. 30, 1987, pp. 1927-1939.
- D.4 C. D. Fletcher, D. A. Prelewicz and W. C. Arcieri, "RELAP5/MOD3.2.2Gamma Assessment for Pressurized Thermal Shock Applications," NUREG/CR-6857, Information Systems Laboratories, Inc., October 2004.
- D.5 L. Erickson, et al., "The Marviken Full-Scale Critical Flow Tests Interim Report: Results from Test 22," MXC222, March 1979.
- D.6 Erickson, et al., "The Marviken Full-Scale Critical Flow Tests Interim Report: Results from Test 24," MXC224, May 1979.
- D.7 D. L. Gills and J. M. Carpenter, "Experimental Data Report for LOFT Nuclear Small Break Experiment L3-7," Idaho National Engineering Laboratory, EG&G Idaho, Inc., NUREG/CR-1570, August 1980.
- D.8 P. D. Bayless and J. M. Devine, "Experiment Data Report for LOFT Large Break Loss of Coolant Experiment L2-5," Idaho National Engineering Laboratory, NUREG/CR-2826, EGG-2210, August 1982.
- D.9 P. D. Bayless, J. B. Marlow and R. H. Averill, "Experiment Data Report for LOFT Nuclear Small Break Experiment L3-1," Idaho National Engineering Laboratory, NUREG/CR-1145, EGG-2007, January, 1980.
- D.10 ISP-26, OECD/NEA/CSNI International Standard Problem No. 26, ROSA-IV LSTF Cold-Leg Small-Break LOCA Experiment, Comparison Report, OECD Nuclear Energy Agency, NEA/CSNI/R(91)13, February 1992.
- D.11 T. F. Habib, et al., "Multiloop Integral System Test (MIST): MIST Facility Functional Specification," NUREG/ CR-5670, April, 1991.
- D.12 J. A. Klingenfus and M. V. Parece, "Multiloop Integral Systems Test, Final Report," NUREG/CR-5395, December 1989.
- D.13 W. A. Stewart, et al., *Natural Circulation Experiments for PWR High Pressure Accidents*, EPRI Project No. RP2177-5, Westinghouse Electric Corp., December 1992.
- D.14 F. W. Dittus and L. M. K. Boelter, "Heat Transfer in Automobile Radiators of the Tubular Type," *Publications in Engineering*, Vol. 2, University of California, Berkeley, 1930, pp. 443-461.

- D.15 American National Standard For Decay Heat Power in Light Water Reactors," ANSI-5.1-1979, American Nuclear Society, 1979.
- D.16 L. J. Siefken et al., *SCDAP/RELAP5/MOD3.3 Code Manual*, NUREG/CR-6150, INEL-96/0422, Revision 2, Idaho National Engineering and Environmental Laboratory, January 2001.
- D.17 Kraftwerk Union AG, "Upper Plenum Test Facility, Test No. 1, Fluid-Fluid Mixing Test," R515/87/09, April 1987.
- D.18 EPRI Report NP-2694, Research Project No. 1730-1, "Control of Containment Air Temperature: An Industry Survey and Insulation Test," Final Report, October 1982.
- D.19 C. Ruger, J. Higgins and G. Martinez-Guridi, "Evaluation of RCP Seal Models Used for the Zion SBO Core Damage Scenario," Brookhaven National Laboratory (Draft), April 14, 2004.
- D.20 I. A. Macdonald, J. A. Clarke and P. A. Strachan, "Assessing Uncertainty in Building Simulation," *Proceedings of Building Simulation '99*, Kyoto, Japan, September 13-15, 1999, Vol. 2, pp. 683-690.
- D.21 L. Riley, "Random or Statistical Uncertainties, Estimating Uncertainties," <http://webpages.ursinus.edu/lriley/ref/unc/unc.html>, Ursinus College, Collegeville, Pennsylvania, January 10, 2006.

APPENDIX E – EFFECT OF MODELING REACTOR VESSEL OUTLET NOZZLE CARBON STEEL SAFE END

The SCDAP/RELAP5 analyses described in this report are based on a model that employs solid stainless steel HL structures. The stainless steel HLs are welded to the carbon-steel RV at the safe ends of the RV outlet nozzles. The nozzle safe ends are carbon steel structures with stainless-steel cladding. As described in Section 2.10, EPRI indicated that in their analysis the weakest point in the HL for creep rupture failure was found to be the carbon steel safe end rather than the HL itself.

SCDAP/RELAP5 lacks the multi-dimensional heat structure and creep rupture modeling capabilities to fully analyze creep rupture behavior within the complex RV nozzle configuration. However, for the purpose of estimating the effects on the SG tube failure margins that would result from considering a carbon steel nozzle safe end material, a SCDAP/RELAP5 sensitivity calculation was performed with the HLs modeled as being fabricated entirely from carbon steel. The SCDAP/RELAP5 Westinghouse four-loop plant SBO base case calculation described in Section 4 was repeated with the materials specified for the upper and lower HL structures in the four coolant loops revised from stainless steel to carbon steel. The HL creep rupture modeling was also changed from stainless steel to carbon steel, but the HL wall emissivity was not changed since the inside surfaces of the carbon steel HLs are clad with stainless-steel.

A change in HL material is expected to affect the distribution and absorption of heat and the timing of the heat-up of the system components in many different ways. The calculation results indicate that the HLs fail 135 s to 140 s earlier in the sensitivity run than in the base case run. In the sensitivity run, the average-tube predicted failure margin (the stress multiplier indicating strength degradation) for tube failure to occur coincident with HL failure is 3.34, as compared with 2.74 in the base case run. In the sensitivity run, the hottest-tube predicted failure margin is 2.26, as compared with 1.68 in the base case run, and the non-degraded (1.0 stress multiplier) hottest tube is predicted to fail 450 s after the HL, compared with 360 s in the base case run.

In summary, the sensitivity evaluation indicates that the SCDAP/RELAP5-calculated SG tube failure margins, based on solid stainless steel HLs, are expected to be conservative compared with the outcome that is likely to be obtained using more detailed HL creep rupture failure analyses of the RV outlet nozzle configuration.

BIBLIOGRAPHIC DATA SHEET

(See instructions on the reverse)

NUREG-CR-6995

2. TITLE AND SUBTITLE

SCDAP/RELAP5 Thermal-Hydraulic Evaluations of the Potential for Containment Bypass During Extended Station Blackout Severe Accident Sequences in a Westinghouse Four-Loop PWR

3. DATE REPORT PUBLISHED

MONTH	YEAR
March	2010

4. FIN OR GRANT NUMBER

5. AUTHOR(S)

C. D. Fletcher
R. M. Beaton
V. V. Palazov
D. L. Caraher
R. W. Shumway (Consultant)

6. TYPE OF REPORT

Technical

7. PERIOD COVERED (Inclusive Dates)

8. PERFORMING ORGANIZATION - NAME AND ADDRESS (If NRC, provide Division, Office or Region, U.S. Nuclear Regulatory Commission, and mailing address; if contractor, provide name and mailing address.)

Division of System Analysis
Office of Nuclear Regulatory Research
U.S. Nuclear Regulatory Commission
Washington, DC 20555-0001

Information System Laboratories
10070 Barnes Canyon Rd
San Diego, CA 92121

9. SPONSORING ORGANIZATION - NAME AND ADDRESS (If NRC, type "Same as above"; if contractor, provide NRC Division, Office or Region, U.S. Nuclear Regulatory Commission, and mailing address.)

Same as above

10. SUPPLEMENTARY NOTES

11. ABSTRACT (200 words or less)

The U.S. Nuclear Regulatory Commission has been conducting studies to evaluate the risk associated with steam generator tube failure during low probability severe accidents in pressurized-water reactors (PWRs) employing U-tube-type steam generators as part of the agency's Steam Generator Action Plan (ML 011300073). The evaluations focus on station blackout events that include a series of unlikely events and conditions that result in a "high-dry-low" plant condition.

This report summarizes thermal-hydraulic evaluations performed using the SCDAP/RELAP5 systems analysis code and a model representing a Westinghouse four-loop PWR. An assessment is made of the SCDAP/RELAP5 capabilities for predicting the phenomena and behavior important for this application. The plant model has benefitted from (1) extensive iterative comparisons with evaluations of natural circulation flows and turbulent mixing using a computational fluid dynamics code and (2) from comparison with experimental data for pertinent fluid-mixing behavior. This report documents the recent history of SCDAP/RELAP5 model improvements for this application, numerous sensitivity evaluations, estimates of the uncertainties in the calculated results, analyses of extended station blackout accident event sequences in a Westinghouse four-loop PWR, and a categorization of those event sequences based on containment bypass outcome.

12. KEY WORDS/DESCRIPTORS (List words or phrases that will assist researchers in locating the report.)

steam generator tube failure
containment bypass
induced rupture
severe accident
station blackout

13. AVAILABILITY STATEMENT

unlimited

14. SECURITY CLASSIFICATION

(This Page)

unclassified

(This Report)

unclassified

15. NUMBER OF PAGES

16. PRICE



Federal Recycling Program

NUREG/CR-6995

**SCDAP/RELAP5 Thermal-Hydraulic Evaluations of the Potential for
Containment Bypass During Extended Station Blackout
Severe Accident Sequences in a Westinghouse Four-Loop PWR**

March 2010



UNITED STATES
NUCLEAR REGULATORY COMMISSION
WASHINGTON, DC 20555-0001

OFFICIAL BUSINESS